UNIVERSITY OF SOUTHERN CALIFORNIA
DEPARTMENT OF CIVIL ENGINEERING

INVESTIGATION OF EARTHQUAKE RESPONSE OF LONG BUILDINGS

by

Marija I. Todorovska, V. W. Lee and M. D. Trifunac

Report No. 88-02

February 1988

TABLE OF CONTENTS

ABSTRACT

In this work the physical phenomena associated with the wave passage under long buildings have been studied. Two-dimensional, continuous models have been used to represent the building vibration. Buildings without major discontinuities, with shear walls at the ends, with a central core and with a soft first floor have been considered. Analytical, closed form solutions have been obtained for the response to incident monochromatic, plane SH waves. The soil-structure interaction has been neglected.

Response of a building to a translational and rotational excitation has been calculated also, as an approximation when the ratio between the length of the building and the apparent wave length of the ground wave in the horizontal direction is very small.

Methods for computation of the response to realistic ground motion have been suggested, for different forms of incident waves and in terms of Fourier synthesis.

CHAPTER I

INTRODUCTION

1.1 General Introduction

It is customary in the typical analyses of the response of buildings to strong earthquake ground motion to neglect the propagating character of the wave motion in the ground. Detailed three dimensional models, involving non-linear analyses are used but the spatial dependence of excitation is usually oversimplified. It is assumed, for example, that the seismic waves arrive with the same phase delay at various points of the base of the building. This corresponds either to vertical incidence, i.e. to infinite phase velocity in the horizontal direction, or to waves with angle of incidence other than zero, but with very large wavelengths compared to the size of the base of the building. However, in general, the seismic waves arrive at the building foundation with incident angles other than vertical, and may have wavelengths comparable with the horizontal dimensions of the building, resulting in phased excitation at its base. The above mentioned oversimplification of the character of the excitation may lead to underestimation of the seismic forces that act upon the building during seismic response and therefore it is important that these effects be studied carefully.

The effect of traveling seismic waves on extended structures was studied, for example, for long bridges. Werner, et al. (1977) presented a detailed review of the subject up to 1977, and Kashefi and Trifunac (1986) updated this review up to 1986.

The effect of traveling seismic waves on buildings has been studied very little so far. Tzenov and Boncheva (1979) and Tzenov (1981) noted the need for the two-dimensional models of "long in plan buildings" to account for the phase difference between the excitation at different points of the base of the building. However, they did not consider

the excitation to be a propagating wave. In their approximate analysis, they introduced factors into the calculation of the mode participation factors for the first symmetric and antisymmetric modes of vibration. The factor corresponding to the first symmetric mode has been calculated assuming a symmetric non-propagating wave under the building of frequency equal to the natural frequency of the building and associated with that mode. Similarly, the factor for the first torsional mode has been calculated assuming an antisymmetric non-propagating wave of frequency equal to the natural frequency of the building and corresponding to that mode. These factors depend on the ratio of the length of the building ℓ and the wavelength in the soil λ. Three methods for superposition of the contributions of these modes to the overall seismic forces in the building have been suggested by Tzenov and Boncheva (1979): simple summation, square root of the sum of the squares and an arithmetic average. The contributions of the higher modes of vibration have been neglected.

The wave nature of the seismic energy transfer from the ground into the foundation of a building as well as the transport of energy within the building itself, has been discussed recently in the publication by the Soviet Academy of Sciences (1987) on the "Wave Processes in Structures During Seismic Interactions." In Chapter 2 the authors discuss modeling of buildings and suggest methods for calculating the equivalent P and S wave velocities of the equivalent continuous model. In the same chapter they discuss the dependence of the interaction on the incident angle of P and S waves. In Chapter 3 of the same publication the authors discuss the propagating seismic waves under structures, and suggest a scheme for resolving a propagating wave into a symmetric and an antisymmetric standing waves.

The focus of this work will be to understand the physical phenomena associated with the passage of seismic waves under extended buildings. Simple models which allow

analytical, closed form solutions will be considered. The models studied will be two-dimensional, isotropic, perfectly elastic plates, placed over the elastic halfspace. A linear stress-strain relationship will be assumed, the soil-structure interaction will be neglected and only incident SH-waves will be considered. Such oversimplifications and idealizations of the real problem are necessary for the fulfillment of one of the aims of this work, that is providing analytical solutions of the problem.

The first model analyzed in this work is a homogeneous plate placed over a uniform elastic halfspace. The second and the third models are also plates placed over the homogeneous half-space but have vertical and horizontal discontinuities, respectively, in their material properties. This analysis is aimed to help in understanding the wave phenomena in buildings with a stiff shear elements at the ends, with stiff central core and with a soft first floor. The fourth model will again be a homogeneous plate, but this time the soil will have a vertical discontinuity in its material properties. The purpose of analyzing this model will be to illustrate the phenomena associated with long buildings placed on inhomogeneous soil. The model of the soil is simple enough to allow a closed form solution for the displacement of the plate but at the same time possesses the main features of the displacements in the inhomogeneous soil.

The displacements of the four models will be calculated for incident monochromatic waves, representing the transfer function of the system. The ways of synthesizing the response to polychromatic motion will be suggested, for different types of excitation.

The models analyzed in this work cannot be considered as real buildings, but as equivalent structures whose response to propagating waves will display the same phenomena which are expected to occur in the response of real buildings. The main objective of this work is qualitative analysis and recognizing and understanding of the new physical

phenomena, rather than precise quantiative or engineering design analyses. The simplicity of these models eliminates many details in realistic buildings, but abounds in the physical phenomena. More realistic analyses involving more complicated geometries, anisotrophy and nonlinear stress-strain relationships are left for future work.

1.2 Organization of this Work

The material in this work has been presented in six chapters and in several appendices.

Chapter I is the introduction. Chapter II presents general discussion on modeling of buildings and a method for estimation of the equivalent material properties of continuous models. In Chapter III, the theory of the homogeneous model and of the models with vertical and horizontal discontinuities, placed over the homogeneous halfspace will be presented. Also, the displacement response of the homogeneous model will be derived to pure translation and rotation at the base. In Chapter IV the theory of the Fourier synthesis of the displacement of the building to dispersed and non-dispersed wave motion, the effects of the inhomogeneous soil and the response of the building to random ground motion will be discussed. In the same chapter, the displacement response of the homogeneous model will be derived when it is excited by the displacement on the surface of the half-space with a vertical discontinuity in the material properties and for incident plane SH waves. Chapter V contains the discussion and the supporting results on the following phenomena associated with the wave passage under "long" buildings: transfer of the seismic wave energy into the building, excitation of symmetric and antisymmetric modes of vibration, the influence of the inhomogeneities within the building on its response, and the influence of the inhomogeneities in the soil on the building response. Chapter VI presents the conclusions.

CHAPTER II

WAVES IN STRUCTURES

2.1 Discretization of Structural Models

In common practice the structures as buildings, bridges, dams, etc., are modeled by discrete models, for example, by lumped mass or by finite element models.

The simplest lumped mass model of a building is the one-dimensional one. It assumes that the mass of one floor level has been lumped at a point. The masses corresponding to each floor are usually connected by massless springs representing the stiffness of the structural elements connecting the floor levels (Meirovitch, 1975). The dash-pots are added to represent the damping of the system. In Figure 2.1.1 a one-dimensional lumped mass model of an n-story building has been drawn where m_i, k_i and C_i are the mass, stiffness and the damping coefficient of the i-th level.

There are two and three-dimensional lumped mass models with translational and rotational degrees of freedom that can give accurate representation of the mass and stiffness distribution of the structure. The equations of motion written in matrix form are:

$$[M]\{\ddot{v}(t)\} + [C]\{\dot{v}(t)\} + [K]\{v(t)\} = \{F(t)\} \tag{2.1.1}$$

where: $[M], [C]$ and $[K]$ are the mass, damping and the stiffness matrices, $\{v(t)\}$ is the displacement vector and$\{F(t)\}$ is the force vector. This equation of motion can be solved by various numerical techniques.

The finite element method discretizes the structure into small, but finite elements. The displacements at certain selected points of the finite elements, called nodes, become

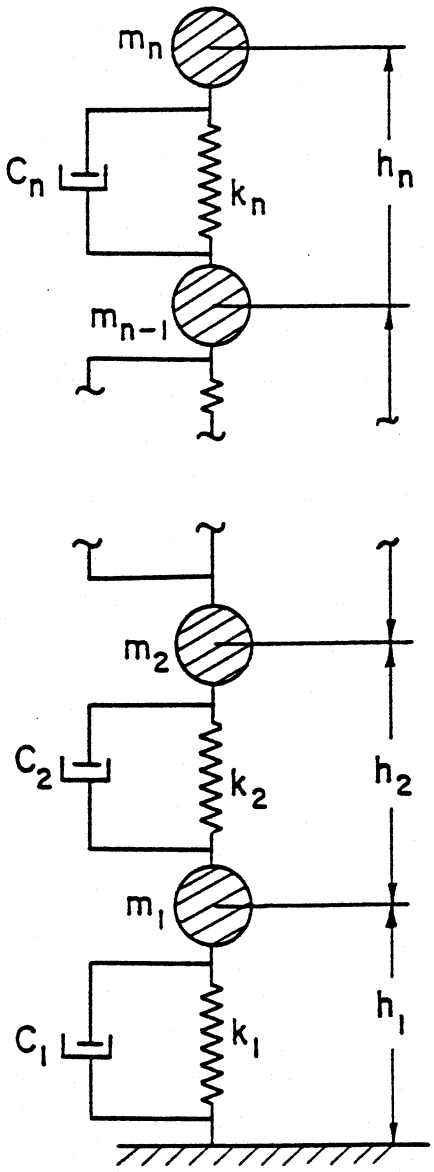

Figure 2.1.1 Lumped mass model of an n story building. m_i, k_i and ℓ_i are the mass, stiffness and damping of the i-th floor. h_i is the equivalent story height between the $(i-1)$-st and the i-th floors.

the degrees of freedom of the system. The finite element models can be two and three-dimensional and can include translational as well as rotational degrees of freedom. The resulting equations of motion are usually solved numerically.

Both the lumped-mass and the finite element methods give only approximate solutions of the problem, but their advantage over the analytical models, is that they can be used for a structure of arbitrary shape. On the other hand, the geometry of the structures that can be modeled by an analytical model has to be simple, thus limiting the number of practical applications. The availability of electronic computers permits the number of degrees of freedom to be increased, thus increasing the accuracy of the method. At the same time, the finite arithmetics used by the electronic machines limits the number of the degrees of freedom that can be used, because the accumulated round-off error, from a large number of calculations, can also produce considerable errors in the final solution.

2.2. Continuous Representation and its Advantages

An example of a simple continuous representation of a building is a one- dimensional beam of length L, stress-free at the top and cantilevered at the bottom (Figure 2.2.1a), with shear wave velocity β and shear modulus μ. It can be a good representation for vibration of a tall building with the in-plan dimensions smaller than its height.

For long structures two-dimensional models may be used. The building can be represented by a rectangular plate of length L and height H, with physical parameters β_x and μ_x, in the horizontal direction and β_z and μ_z in the vertical direction. These represent the shear wave velocities and the shear moduli of the building (Figure 2.2.1b).

An example of a three-dimensional continuous model of a building is a rectangular solid with in-plan lengths L_1 and L_2 and height H (Figure 2.2.1c). The physical parameters

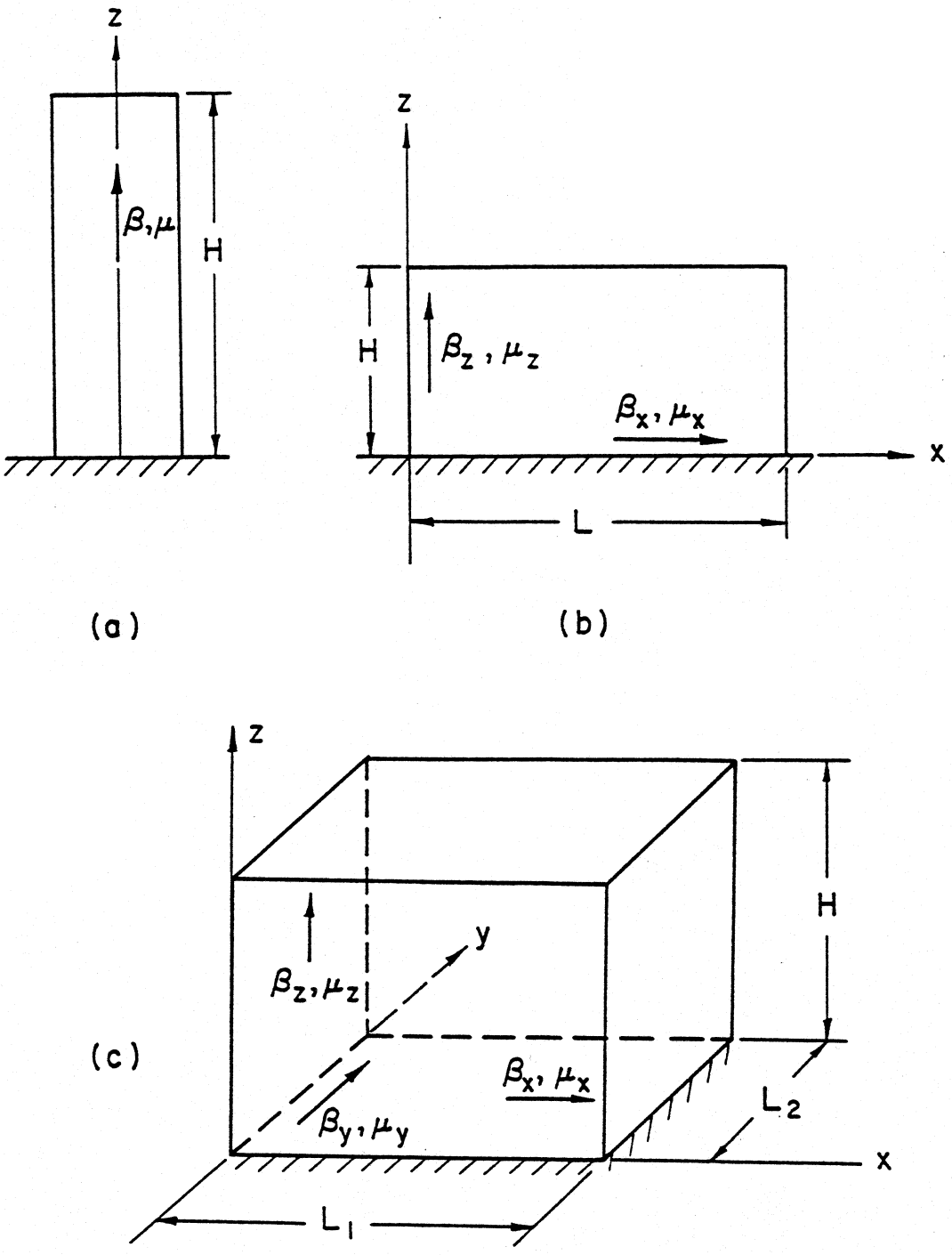

Figure 2.2.1 Continuous models of buildings. a) one-dimensional model: β and μ are the shear wave velocity and the shear modulus. b) two-dimensional model: β_x and μ_x, and β_z and μ_z are the shear wave velocities and the shear moduli in the x and in the z-directions, respectively. c) three-dimensional model: β_x and μ_x, β_y and μ_y, and β_z and μ_z are the shear wave velocities and the shear moduli in the x, y and z-directions, respectively.

$\beta_x, \mu_x, \beta_y, \mu_y$ and β_z and μ_z for the three coordinate directions now represent the respective velocities and rigidities in the respective coordinate directions. This representation may be required where $L_1 \approx L_2 \approx H$.

For example, the displacement of the continuous model in Figure 2.2.1b, associated with shear waves only, has to satisfy the differential equation of motion

$$\mu_x \frac{\partial^2 v}{\partial x^2} + \mu_z \frac{\partial^2 v}{\partial z^2} = \rho \frac{\partial^2 v}{\partial t^2} \qquad (2.2.1a)$$

where:

$$v(x,z): \text{ displacement in } y \text{ direction} \qquad (2.2.2a)$$

$$x, z: \text{ spatial coordinates} \qquad (2.2.2b)$$

$$t: \text{ time variable} \qquad (2.2.2c)$$

$$\rho: \text{ density.} \qquad (2.2.2d)$$

When devided by ρ, equation (2.2.1a) can be written in the following form

$$\beta_x^2 \frac{\partial^2 v}{\partial x^2} + \beta_z^2 \frac{\partial^2 v}{\partial z^2} = \frac{\partial^2 v}{\partial t^2} \quad , \qquad (2.2.3)$$

where $\beta_x^2 = \mu_x/\rho$ and $\beta_z^2 = \mu_z/\rho$. For certain boundary conditions and simple excitations it is possible to solve the equation of motion exactly.

The exact analytical solutions of the wave propagation and vibrational problems are desirable because those are convenient to study the physics of the problem. The analytical expressions of the solution directly involve the physical parameters of the system and make it easy to change them and to study their effects. The possibility of getting an analytical form of the solution is very advantageous also because the exact solutions can provide a basis for the testing of the approximate methods. The biggest disadvantage of

the continuous models is that only a limited number of problems, with simple geometrical features, can be solved analytically.

2.3 Equivalent Physical Constants

A simple method to estimate the equivalent shear wave velocity in continuous modeling of buildings will be presented in this section. For this rough estimate it can be assumed that only the frame of the structure, consisting of reinforced concrete columns and of horizontal concrete panels transmits the seismic waves. Schematic representations of the horizontal and vertical plans of a moment resisting frame of a reinforced concrete building are shown in Figures 2.3.1a and 2.3.1b. The lengths of the frame in the x and y- directions are L and D, and H is the height of the frame. The distance between the columns is A in the x-direction and B in the y-direction, and h is the average height between the floors. The reinforced concrete columns have rectangular cross-section with size a in the x-direction and b in the y-direction.

2.3.1 Equivalent Shear Wave Velocity in the Vertical Direction

To find the equivalent shear wave veloity in the vertical direction, the equivalent shear modulus $\mu_{eq}^{(z)}$ and the equivalent density $\rho_{eq}^{(z)}$ for this direction need to be known. From the definition, the equivalent shear wave velocity in the z-direction will be

$$\beta_{eq}^{(z)} = \sqrt{\frac{\mu_{eq}^{(z)}}{\rho_{eq}^{(z)}}} \quad . \tag{2.3.1}$$

A shear wave with displacement in the y-direction is being transmitted vertically through the frame mainly by the elastic deformation of the columns in the y-direction. The space in between the columns of one floor level can be evenly divided between the columns

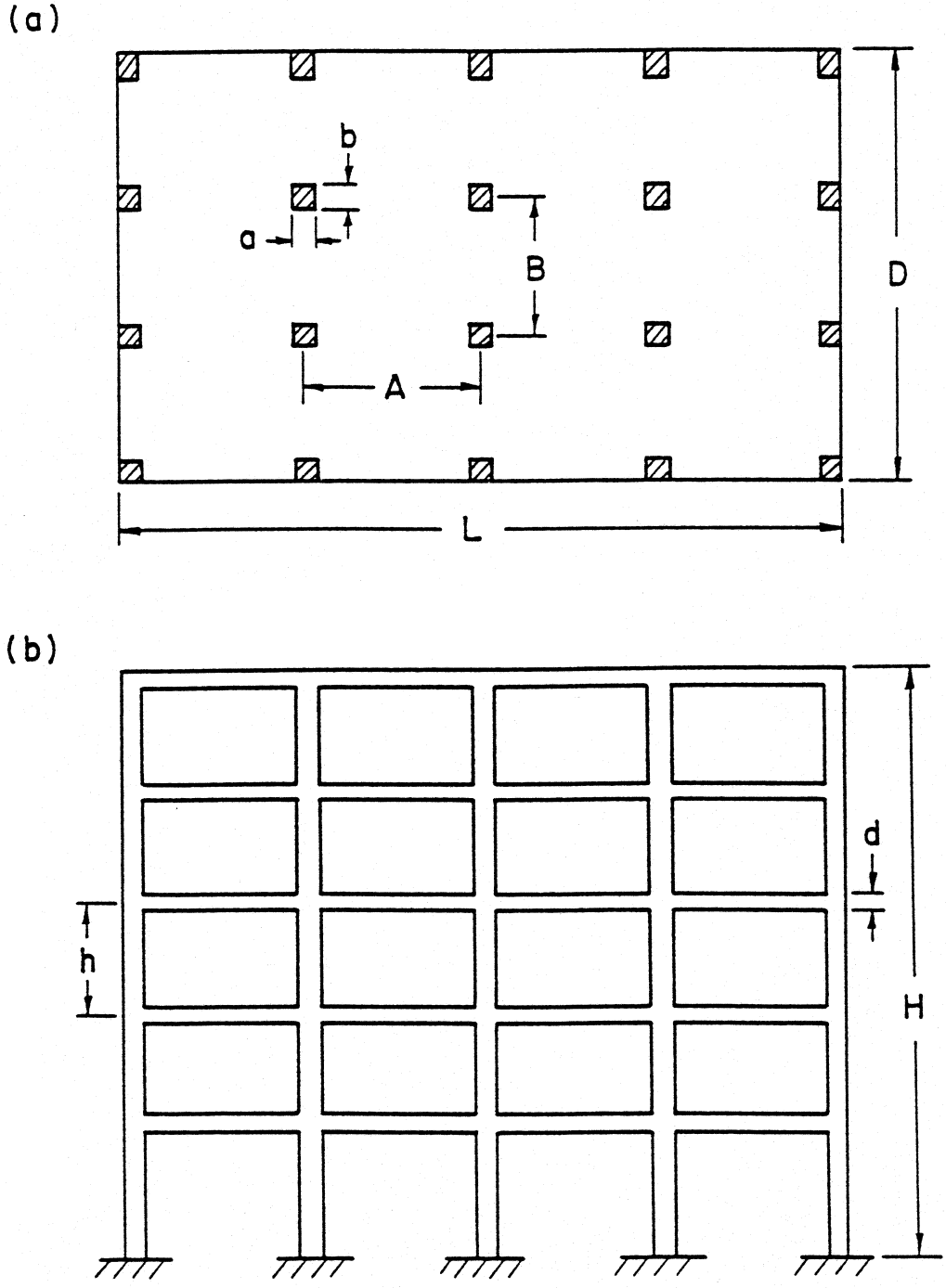

Figure 2.3.1 Moment resistant frame of a building. a) horizontal cross-section. b) vertical cross-section.

so that the equivalent shear modulus and the equivalent density of a typical element, shown in Figure 2.3.2a and Figure 2.3.2b, will be the equivalent shear modulus and the equivalent density for the whole frame.

If the element in Figure 2.3.2b is given a displacement Δ in the y-direction, the column will deform in the double curvature, as shown in Figure 2.3.3a, and the shear force Q at each support will be

$$Q = k\Delta \tag{2.3.2}$$

where k is the stiffness of the column in the y-direction. If the column were made of concrete only, the stiffness k would be

$$k = \frac{12E_cI_y}{h^3} \tag{2.3.3a}$$

where E_c is the Young's modulus of elasticity for the concrete and $I_y = \frac{ab^3}{12}$ is the area moment of inertia of the section in the y-direction. Because of the steel reinforcement,

$$k = f\frac{12E_cI_y}{h^3} \quad , \tag{2.3.3b}$$

where, $f > 1$, is a factor depending on the percentage of steel in the cross-section. A method of calculating the factor f is described in the Appendix A.

If the element in Figure 2.3.2b were made of homogeneous material (with shear modulus $\mu_{eq}^{(z)}$), deforming in shear only, the shear force Q at the top of the element and corresponding to the displacement Δ at the top (Figure 2.3.3b) would be

$$\begin{aligned} Q = \tau(A \cdot B) &= \left(\mu_{eq}^{(z)} \frac{\partial \tau}{\partial z}\bigg|_{z=h} \right)(A \cdot B) \\ &= \mu_{eq}^{(z)} \frac{\Delta}{h}(A \cdot B) \end{aligned} \tag{2.3.4}$$

where τ is the stress at the top of the element.

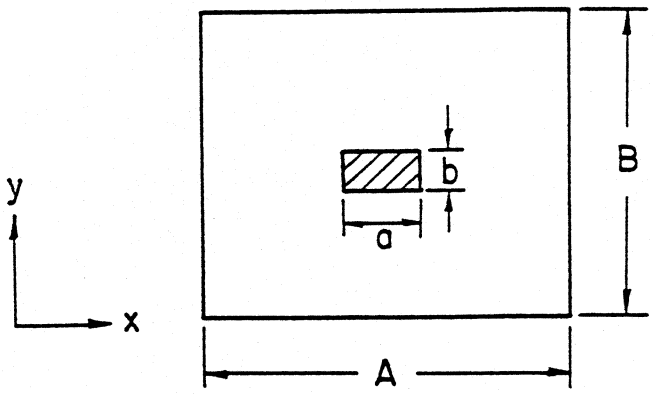

(a)

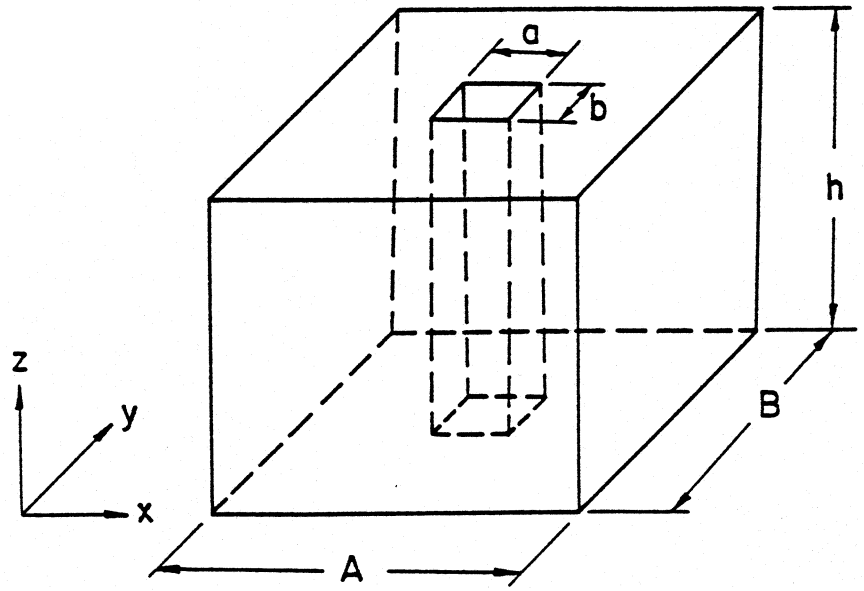

(b)

Figure 2.3.2 An element of the moment resisting frame in Figure 2.3.1, used to calculate the equivalent shear wave velocity in the z-direction for continuous building models shown in Figure 2.2.1. a) horizontal cross-section. b) vertical cross section.

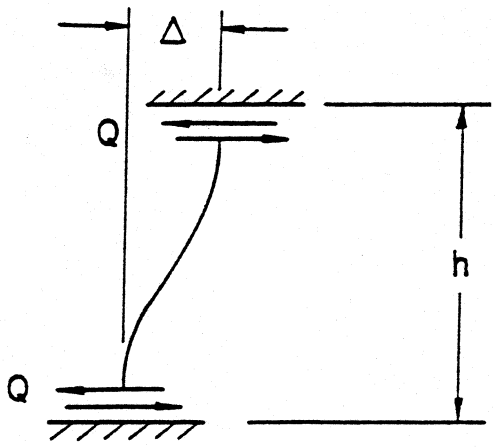

(a)

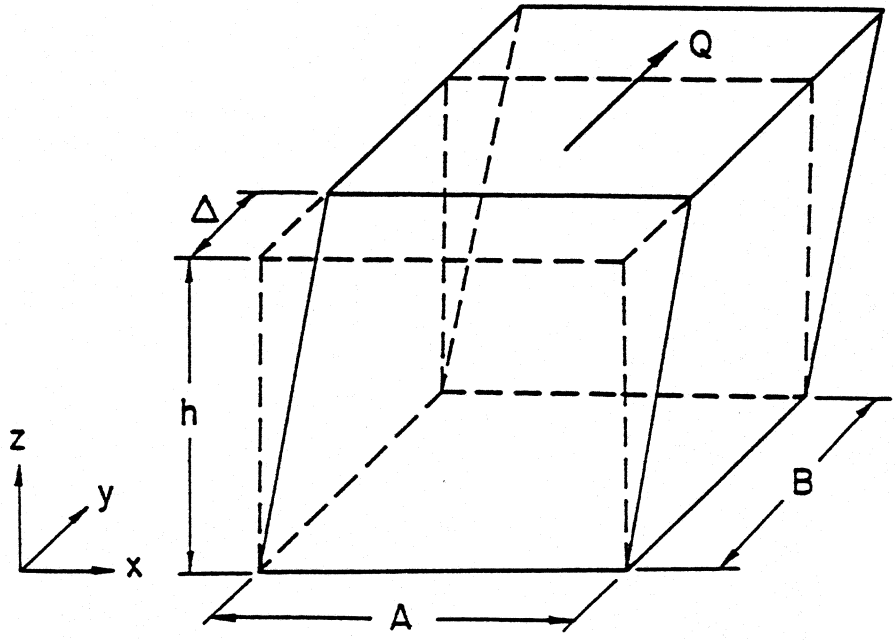

(b)

Figure 2.3.3 a) Shear deformation of the column in the element shown in Figure 2.3.2. b) Shear deformation of an element of the continuous equivalent building model shown in Figure 2.3.2.

Equating equations (2.3.4) and (2.3.2) the equivalent shear modulus $\mu_{eq}^{(z)}$ is:

$$\begin{aligned}\mu_{eq}^{(z)} &= \frac{h}{AB} \cdot k = \frac{h}{AB} f \frac{12 E_c I_y}{h^3} \\ &= \frac{h}{AB} f \frac{12 E_c \frac{ab^3}{12}}{h^3}\end{aligned} \tag{2.3.5a}$$

The equivalent density $\rho_{eq}^{(z)}$ of the element shown in Figure 2.3.2b can be calculated if the total mass of the concrete column is divided by the volume of the element. The result is:

$$\rho_{eq}^{(z)} = \frac{\text{mass of the column}}{h \cdot A \cdot B} = \frac{\rho_c a \cdot b \cdot h}{h \cdot A \cdot B} = \rho_c \frac{ab}{AB} \tag{2.3.5b}$$

where ρ_c is the density of the concrete. (The difference between the densities of the steel and of the concrete has been neglected here.)

Substituting equations (2.3.5a) and (2.3.5b) into equation (2.3.1), the equivalent shear wave velocity for the vertical direction is

$$\beta_{eq}^{(z)} = \sqrt{\frac{\mu_{eq}^{(z)}}{\rho_{eq}^{(z)}}} = \sqrt{\frac{f \cdot E_c b^2}{h^2 \rho_c}} \tag{2.3.6}$$

2.3.2 Equivalent Shear Wave Velocity in the Horizontal Direction

The equivalent shear wave velocity in the x-direction can be calcualted similarly, i.e. by separating the frame into elements whose equivalent shear wave velocity will be the equivalent shear wave velocity for the whole frame.

A wave traveling in the x-direction is carried through the frame mainly by the concrete floor slabs. This suggests partitioning the frame by passing horizontal planes

halving the space in between the two floor levels. A typical element is shown in Figure 2.3.4a. The equivalent shear wave velocity in the x-direction $\beta_{eq}^{(x)}$ will, by definition be

$$\beta_{eq}^{(x)} = \sqrt{\frac{\mu_{eq}^{(x)}}{\rho_{eq}^{(x)}}} \tag{2.3.7}$$

where $\mu_{eq}^{(x)}$ and $\rho_{eq}^{(x)}$ are the equivalent shear modulus and the equivalent density for the element in Figure 2.3.4a.

When a shear wave passes through the floor slabs, they deform in shear and bending. For simplicity, the equivalent shear modulus $\mu_{eq}^{(x)}$ will be calculated assuming pure shear deformation of the floor slabs.

If the element in Figure 2.3.4a is given lateral displacement Δ in the y-direction at one of the lateral surfaces, as shown in Figure 2.3.4b, the floor slabs will deform as shear beams, with shear stress τ_{xy} at the cross-section equal to

$$\begin{aligned} \tau_{xy} &= \mu_c \cdot \text{strain} \\ &= \mu_c \cdot \frac{\Delta}{L} \end{aligned} \tag{2.3.8}$$

where μ_c is the shear modulus of the concrete. The total shear force Q acting on the lateral surface of the typical element will be equal to the shear stress in the concrete slabs times the area of the surface in concrete, i.e.

$$Q = \tau_{xy} \cdot (D \cdot d) \quad , \tag{2.3.9}$$

since the rest of the element consists of the empty space. Combining equations (2.3.8) and (2.3.9), the shear force Q is:

$$Q = \mu_c \frac{\Delta}{L} D \cdot d \quad . \tag{2.3.10}$$

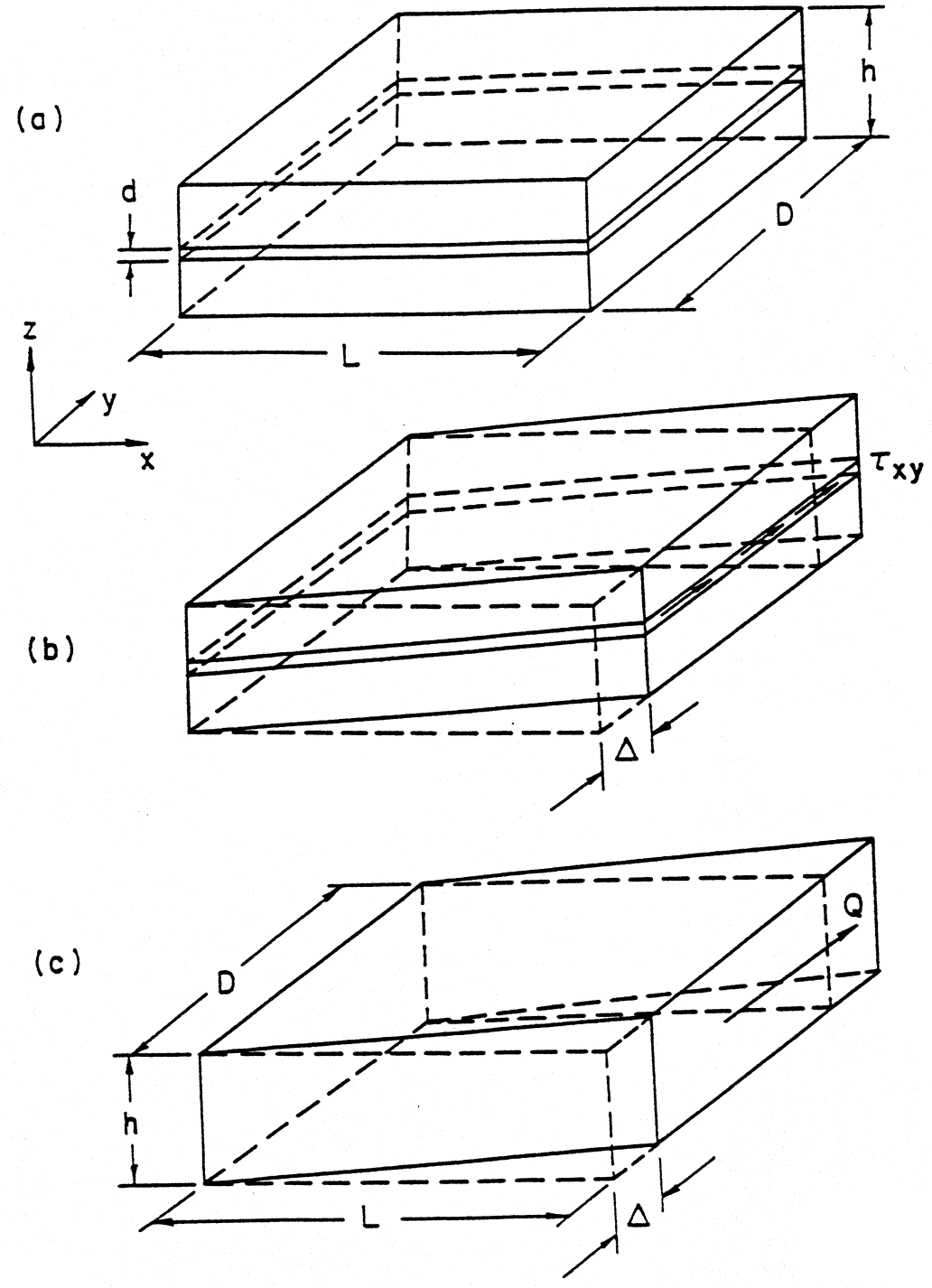

Figure 2.3.4 a) Typical element of the frame in Figure 2.3.1 used to calculate the equivalent shear wave velocity in the x-direction. b) The element in part a) of this figure deformed in shear. c) Continuous equivalent of the element shown in part a) of this figure.

If the typical element were made of homogeneous material with shear modulus $\mu_{eq}^{(x)}$, the shear force Q would have been (Figure 2.3.4c)

$$Q = \mu_{eq}^{(x)} \frac{\Delta}{L} D \cdot h \quad . \tag{2.3.11}$$

From the equations (2.3.10) and (2.3.11) it follows that

$$\mu_{eq}^{(x)} = \mu_c \frac{d}{h} \quad . \tag{2.3.12}$$

Using similar analysis as in section 2.3.1, the equivalent density $\rho_{eq}^{(x)}$ for the typical element will be

$$\rho_{eq}^{(x)} = \rho_c \frac{d}{h} \tag{2.3.13}$$

where ρ_c is the density of the concrete.

Substituting equations (2.3.12) and (2.3.13) into equation (2.3.7), the equivalent shear wave velocity in the x-direction will be found to be the same as the shear wave velocity for the concrete, i.e.

$$\beta_{eq}^{(x)} = \sqrt{\frac{\mu_c}{\rho_c}} = \beta_c \quad . \tag{2.3.14}$$

2.3.3 Example: The Equivalent Shear Wave Velocities for the Imperial County Services Building in El Centro

In the following section the methods for estimation of the equivalent shear wave velocity of a continuous model, described in sections 2.3.1 and 2.3.2, will be applied to an example of a real building, the Imperial County Services Building in El Centro, California (Kojić et al., 1984). Figure 2.3.5 and Figure 2.3.6 represent a West-East longitudinal section and a typical floor layout of the building, respectively.

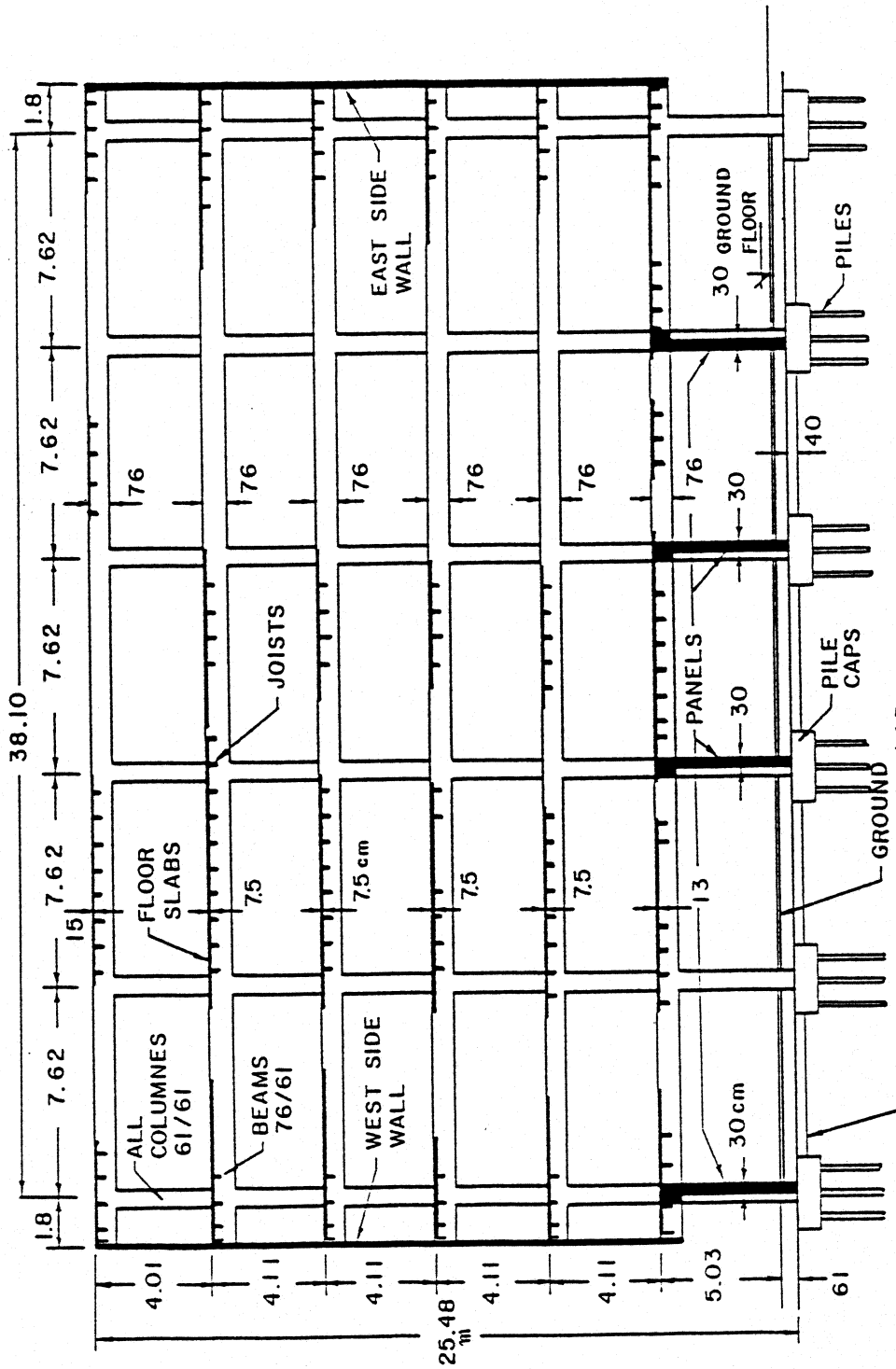

Figure 2.3.5 West-East longitudinal section of the Imperial County Services Building in El Centro, after Kojić et al. (1984).

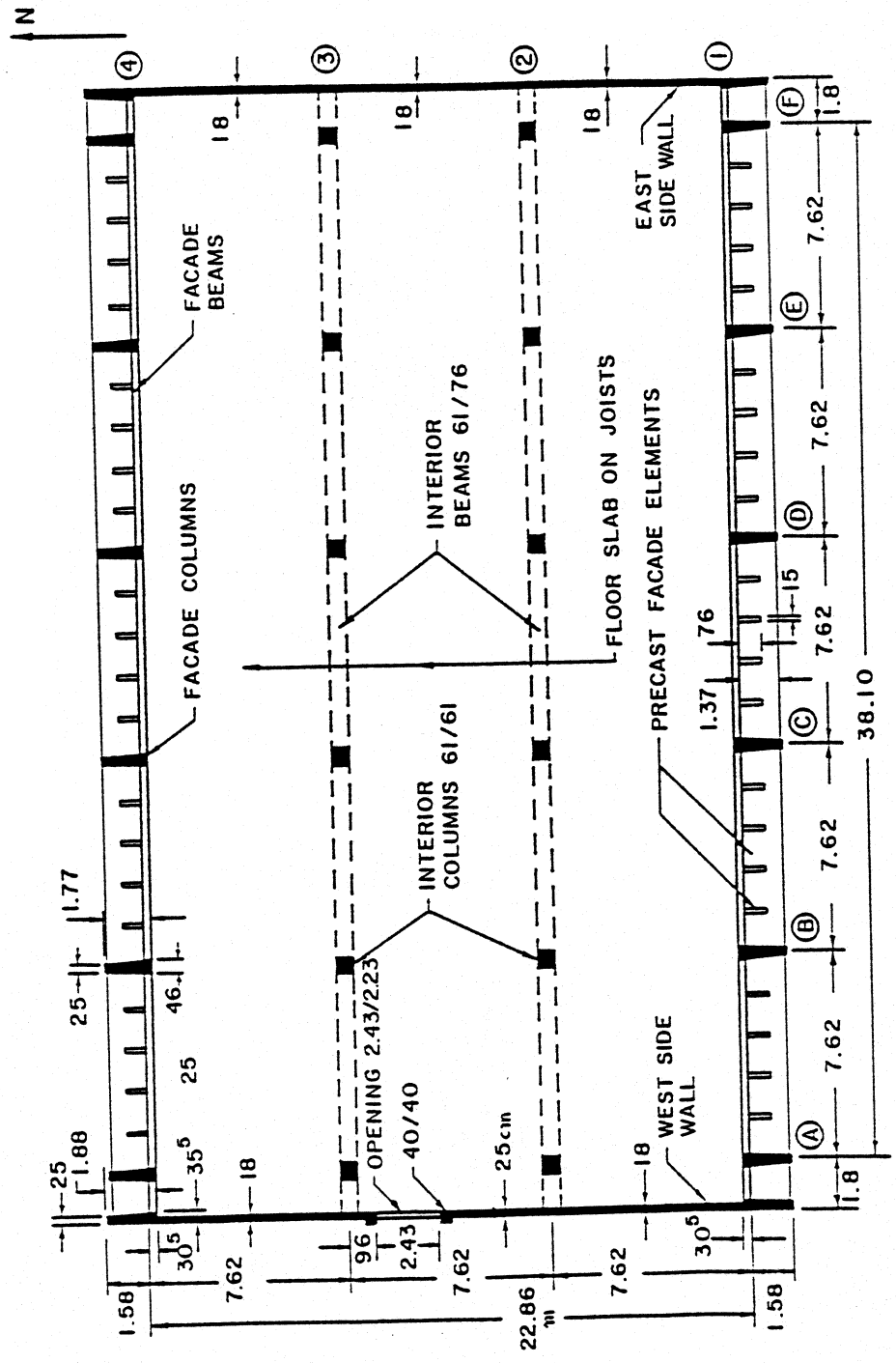

Figure 2.3.6 Typical floor layout of the Imperial County Services Building in El Centro, after Kojić et al. (1984).

The building was a six story reinforced concrete structure, with a base $4170m$ (136 feet 10 inches) by $26.02m$ (85 feet 4 inches) and height of $25.48m$ (83 feet 7 inches). The columns had rectangular cross-sections 61 by $61cm$ (24 by 24 inches), with the area of compression steel A_s equal to the area of the tension steel A'_s, such that $A_s = A'_s = 0.4-1$ percent of the total cross-sectional area. The ratio between the Young's moduli of elasticity of the steel E_s and of the concrete is $E_s/E_c = 8$. The distance between the columns in both the longitudinal and the transverse directions is 7.62 m (25 feet). The building has two lateral shear walls, consisting of 18 cm (7 inches) thick panels, increasing the stiffness of the building in the transverse (North) direction (Figure 2.3.6). The concrete floor slabs have thickness of $7.5cm$ (3 1/8 inches) and the distance between the floors is $4.11m$ (13.5 feet). The building has been described in more detail by Kojić et al. (1984) from where the Figure 2.3.5 and Figure 2.3.6 have been reproduced.

For the percentage of steel in the cross-section, the factor f in the equation (2.3.6) has values between 1.1 and 1.3. The Young's modulus of the concrete is $E_c = 3 \cdot 10^6 \#/in^2$, the shear modulus is $G_c = 1.3 \cdot 10^6 \#/in^2$ $(= \mu_c)$. If an average value for $f = 1.2$ is taken, the shear wave velocity in the vertical and in the longitudinal directions in the inside of the building will be

$$\begin{aligned} \beta_{eq}^{(z)} &\approx 420\text{m/s} \approx 1400.\text{ft/s} \\ \beta_{eq}^{(z)} &\approx 1950\text{m/s} \approx 6400.\text{ft/s} \quad . \end{aligned} \tag{2.3.15}$$

2.3.4 Discussion

The values for the equivalent shear wave velocities in the vertical and in the longitudinal directions obtained from equations (2.3.6) and (2.3.14) are only approximate and are meant to be used in the further analysis only to estimate the order of their magnitude. If the shear walls at the ends of the building were included in the analysis

(Figure 2.3.5 and 2.3.6), the value of the shear wave velocity in the vertical direction would have been larger (because the stiffness would have increased). Also, if the contributions of the non-structural elements were included into the analysis, the values for $\beta_{eq}^{(z)}$ and $\beta_{eq}^{(x)}$ would have increased.

The Soviet engineers (Soviet Academy of Sciences, 1987) have found the equivalent shear wave velocities for six different types of buildings to be in the range $300 - 1800 m/s$ (1000-5900 feet/sec). The calculated value for the equivalent shear wave velocity in the vertical direction for the El Centro building is within this range, while the value of the shear wave velocity for the longitudinal direction is slightly above the upper limit.

The anisotropy is thus evident for the El Centro building and it must be considered in the continuous modeling. The degree of anisotropy depends on the type of the structure. For a structure with strong masonary non-structural elements, the degree of anisotropy will be smaller during linear vibrations, while for a building with light non-structural elements (e.g. glass, plastic) the degree of the anisotropy may be high.

In this work only isotropic continuous models will be analyzed, because the main purpose of this work is qualitative analysis of the physical phenomena of the waves propagating through the buildings.

CHAPTER III

SHEAR WAVES IN CONTINUOUS STRUCTURAL MODELS

In this chapter, two-dimensional models of long buildings excited by the propagating, monochromatic SH-waves will be considered. These models will account for the time and space dependent character of the excitation, and their simplicity will allow exact, analytical form of the solution. The solution can be interpreted as a transfer function of the system.

3.1 General Discription of the Models

A simple continous model of a long building can be represented by a two-dimensional plate, placed over the homogeneous half-space. A slice of the plate of thickness 1 has been shown in Figure 3.1.1. Let L and H represent the length and the height of the plate and $\beta(x,z)$ and $\mu(x,z)$, where x and z are the spatial coordinates, the shear wave velocity and the shear modulus in the plate. Let β_s and μ_s denote the shear wave velocity and the shear modulus of the homogeneous half-space. When an incident, plane SH-wave, with angle of incidence θ, reflects from the surface of the half-space, with the structure placed over it, the time dependent displacement of the plate $v(x,z,t)$ and of the half-space $v_s(x,z,t)$, where t is the time coordinate, have to satisfy the stress free condition at their outer boundaries and the continuity of stresses and displacements condition at the interface between the plate and the half-space. The solution of this problem requires numerical solution of the governing system of equations and must consider all the details the of the soil-structure interaction problem with wave energy propagating in and out of the structure, and with the scattered wave field being transmitted into the half-space.

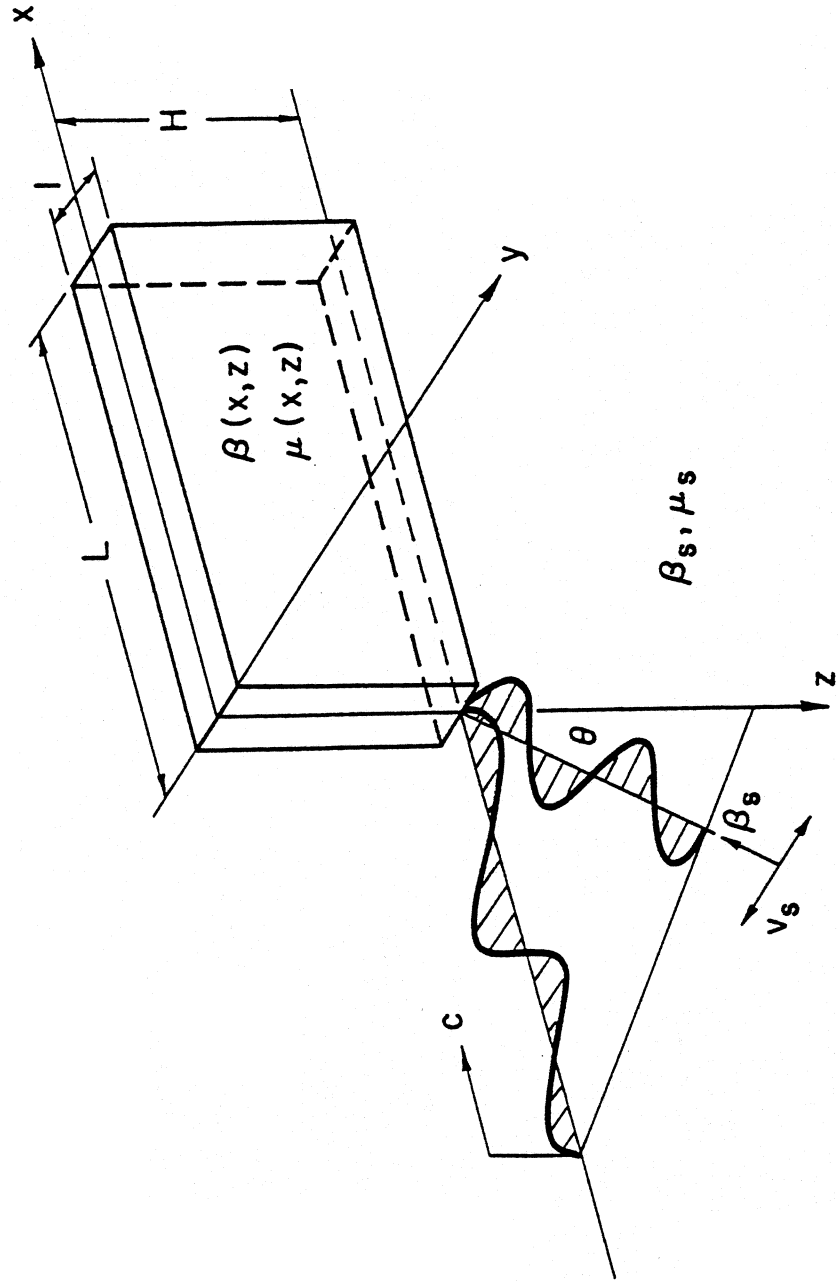

Figure 3.1.1 Two-dimensional model of a building, placed over the homogeneous half-space and excited by incident SH-waves. The angle of incidence is θ.

In this work the soil-structure interaction will not be considered and it will be assumed that the presence of the building does not change the motion of the elastic half-space. Assuming the linear stress-strain relationship in the building and requiring only the continuity of the displacements at $z = H$ it is possible to obtain an analytical solution. Such assumptions are justified in the case of a building having much smaller stiffness than the half-space, so that the presence of the plate has no effect on the motion in the half-space. Then, the mathematical model of the building may be represented by a piece of length H of a semi-infinite plate in the z-direction, with width L, stress-free boundaries at $z = 0, x = 0$ and $x = L$ and with prescribed displacements at $z = H$, equal to the free-field displacement of the half-space. A slice of thickness 1 of the two-dimensional semi-infinite plate is shown in Figure 3.1.2. In case of an incident plane SH-wave of frequency ω, traveling with velocity β_s through the homogeneous half-space and with an angle of incidence θ (Figure 3.1.1) the motion of the half-space can be expressed as (Achenbach, 1973)

$$v_s(x,z,t) = 2\cos\frac{\omega(z-H)}{c_z^{(s)}} \cdot e^{i\omega\left(t-\frac{x}{c_x^{(s)}}\right)} \tag{3.1.1}$$

where

$$c_x^{(s)} = \frac{\beta_s}{\sin\theta} \tag{3.1.2a}$$

and

$$c_z^{(s)} = \frac{\beta_s}{\cos\theta} \tag{3.1.2b}$$

are the phase velocities of the wave in the x and in the z-direction, respectively. Therefore, the free field displacement at the surface of the half-space will be

$$v_s(x,H,t) = 2e^{i\omega\left(t-\frac{x}{c_x^{(s)}}\right)} \quad . \tag{3.1.3}$$

Three models of this type will be analyzed in the present chapter. All three models have isotropic material constants $\beta(x,z)$ and $\mu(x,z)$. The first model considered, Figure

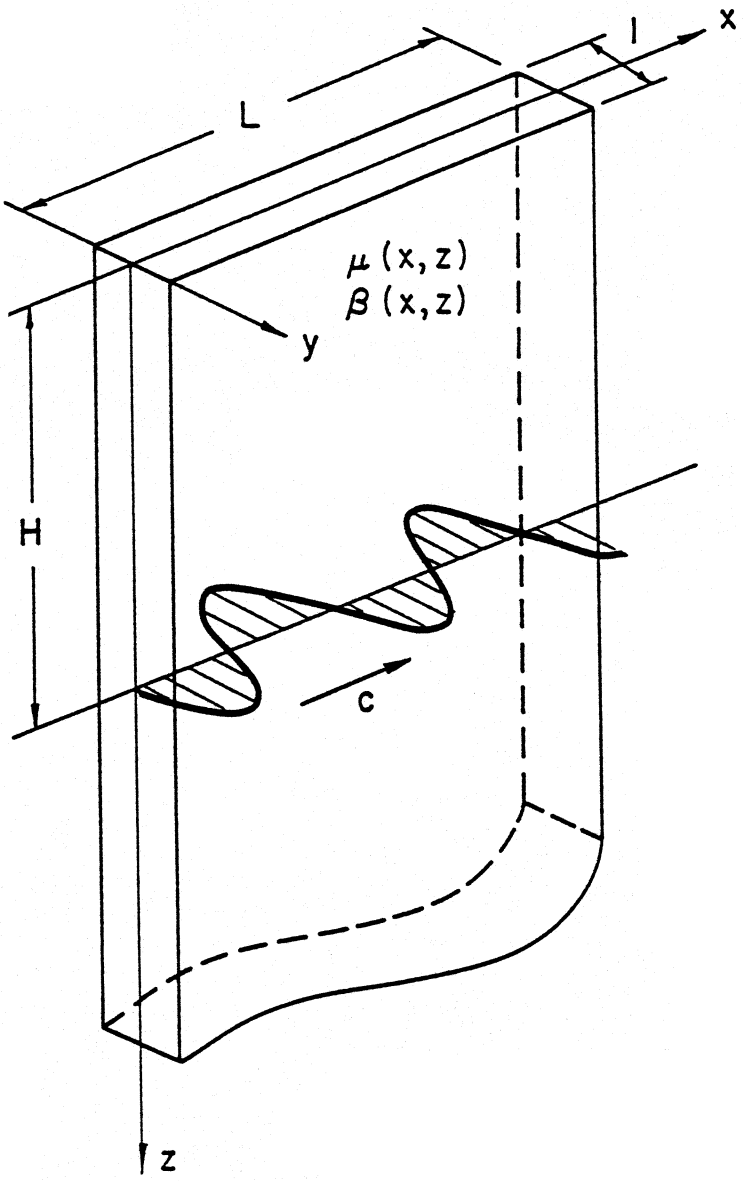

Figure 3.1.2 Two-dimensional continuous model of a building of length L and height H. Soil-structure interaction is neglected. $\mu(x,z)$ and $\beta(x,z)$ are the equivalent shear modulus and shear wave velocity of the continuous building model. The building is excited at $z = H$ by the free-field displacement on the surface of the half-space.

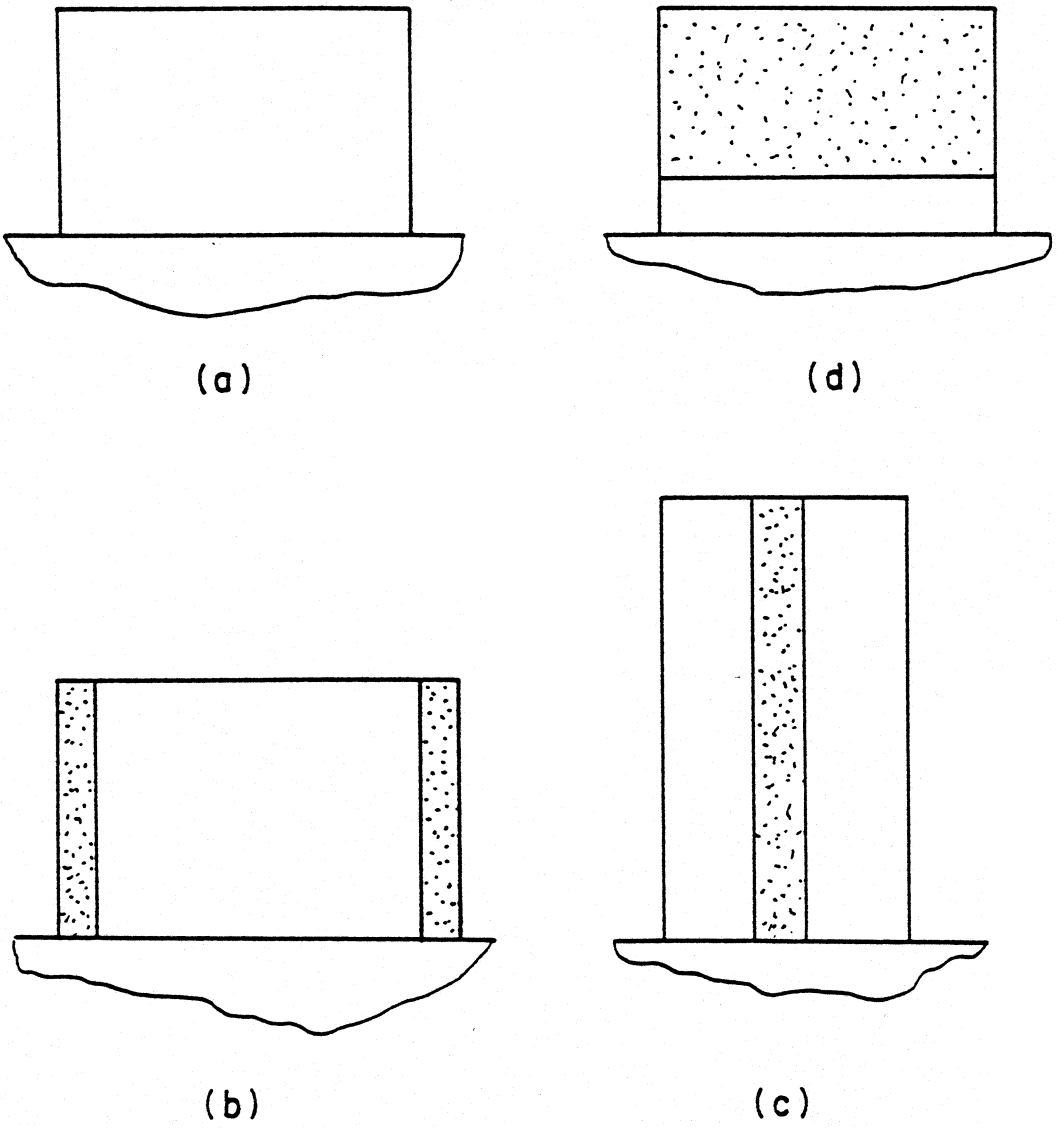

Figure 3.1.3 a) A building without major discontinuities. b) A building with two shear walls at the ends. c) A building with a central core. d) A building with "soft" first floor.

3.1.3a, has constant values of the shear wave velocity and the shear modulus, and will be presented in section 3.2. The second model is piecewise homogeneous, having vertical discontinuities in the material properties and will be discussed in the third section of this chapter. It corresponds to a building with stiff shear elements at the ends (Figure 3.1.3b), or to a building having a stiff central core (Figure 3.1.3c), for example, an elevator core. The third model, that will be presented in section 3.4, is piecewise and homogeneous, but having horizontal discontinuities in the material properties. Of interest in this work is a plate made of two horizontal layers, with the lower being "softer" than the upper one. This model corresponds to a building with a "soft" first floor (Figure 3.1.3d).

The two-dimensional wave equation, which is the governing equation of motion, will be solved by the method of separation of variables, and eigenfunction expansion of the solution will be used to derive the displacement response of the plate to input base motion $e^{i\omega\left(t-\frac{x}{c}\right)}$, where c is the horizontal phase velocity of the motion in the soil for given circular frequency ω. This solution will also represent the transfer function of the system, so that the response to any enforced displacement at the base can be calculated by using the Fourier synthesis, discussed in the next chapter. Thus, without a loss in generality, in this work the emphasis will be placed on finding and interpreting the response to the periodic wave excitation only.

3.2 The Homogeneous Model

3.2.1 Formulation and Solution of the Problem

The mathematical model that will be considered in this section is the two-dimensional, isotropic, semi-infinite, elastic plate of width L, shown in Figure 3.2.1, having constant μ and β, the shear modulus and the shear wave velocity, for $0 \leq z \leq H$, and whose displacement at $z = H$ has to be equal to $e^{i\omega\left(t-\frac{x}{c}\right)}$. Of interest are the displacements

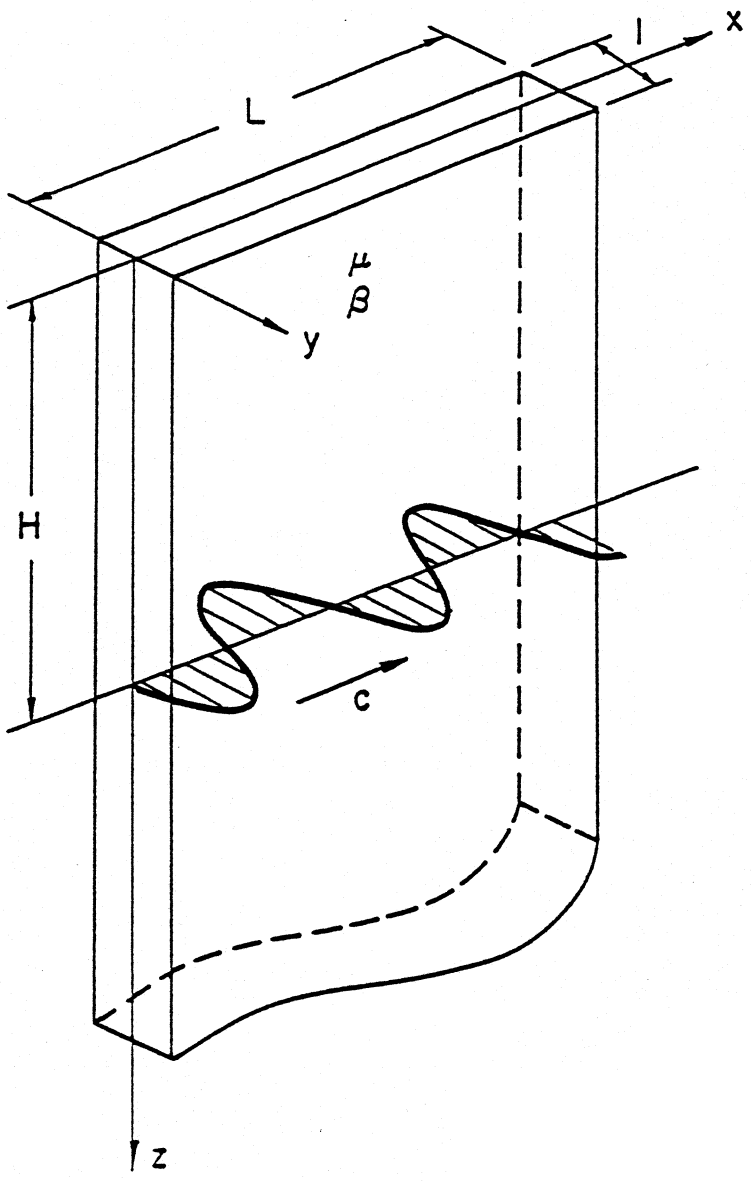

Figure 3.2.1 Homogeneous model of a building of length L and height H, and excited at the base by a wave of amplitude 1, frequency ω and propagating with phase velocity c in the positive x-direction. The soil-structure interaction is neglected.

of the plate for $0 \leq z \leq H$ that will correspond to the displacements of a building with equivalent shear wave velocity β and shear modulus μ placed over the elastic half-space and excited by a wave motion $e^{i\omega\left(t-\frac{z}{c}\right)}$ at its base.

The governing equation of motion for the anti-plane displacement of the plate $v(x,z,t)$ is the two-dimensional, linear wave equation

$$\frac{\partial^2 v(x,z,t)}{\partial x^2} + \frac{\partial^2 v(x,z,t)}{\partial z^2} = \frac{1}{\beta^2}\frac{\partial^2 v(x,z,t)}{\partial t^2} \tag{3.2.1}$$

where x and z are the spatial coordinates, t is the time coordinate and β is the shear wave velocity of the plate. The conditions that the displacement $v(x,z,t)$ has to satisfy are the following boundary conditions

$$\tau_{xy} = 0 \quad \text{at} \quad x = 0 \quad , \quad 0 \leq z < \infty \tag{3.2.2a}$$

$$\tau_{xy} = 0 \quad \text{at} \quad x = L \quad , \quad 0 \leq z < \infty \tag{3.2.2b}$$

$$\tau_{zy} = 0 \quad \text{at} \quad z = 0 \quad , \quad 0 \leq x \leq L \tag{3.2.2c}$$

and the displacement condition

$$v = e^{i\omega\left(t-\frac{z}{c}\right)} \quad \text{at} \quad z = H \quad , \quad 0 \leq x \leq L \quad , \tag{3.2.3}$$

where $\tau_{xy} = \mu\partial v/\partial x$ and $\tau_{zy} = \mu\partial v/\partial z$ are the shear stresses in the plate and ω and c are the circular frequency and the phase velocity in the x-direction of the motion at $z = H$.

The differential equation (3.2.1) and the boundary conditions (3.2.2a,b and c) define a boundary value problem (also called a Sturm-Liouville problem) and the functions that satisfy the differential equation and the imposed boundary conditions are called the eigen-functions of the problem. The set of all the eigen-functions of a Sturm-Liouville problem is a complete orthogonal set, (Courant and Hilbert, 1953), that may serve as a

basis in the representation of any solution of the problem. The differential equation (3.2.1) is variable separable, implying that every eigenfunction can be represented as a product of a function of x, a function of z and a function of t. The following representation of any solution of the boundary value problem results from the facts mentioned:

$$v(x,z,t) = \sum_j C_j^* X_j(x) Z_j(z) T(t) \tag{3.2.4}$$

where $X_j(x)$ and $Z_j(z)$ are the eigenfunctions for the x and the z-direction, $T(t)$ is the time dependent part of the solution, and C_j^* are the Fourier coefficients of the orthogonal expansion.

The eigenfunctions $X_j(x)$ and $Z_j(z)$ that satisfy the boundary conditions (3.2.2a,b and c) are the following

$$X_j(x) = \cos k_{x,j} x \tag{3.2.5}$$

$$Z_j(z) = \cos k_{z,j} z \tag{3.2.6}$$

where $k_{x,j}$ and $k_{z,j}$ are the wave numbers in the x and in the z-direction, corresponding to the j-th eigenfunction. The time dependent function $T(t)$ matching the displacement condition (3.2.3) is

$$T(t) = e^{i\omega t} \tag{3.2.7}$$

The wave numbers $k_{x,j}$ and $k_{z,j}$ together with the wave number $k = \omega/\beta$ in the plate appear as constants in the separation of the variables and are related by the following equation

$$k_{z,j} = \sqrt{k^2 - k_{x,j}^2} \tag{3.2.8}$$

The wave numbers $k_{x,j}$ can have only certain allowable values, specified by the frequency equation

$$k_{x,j} = \frac{j\pi}{L} \qquad j = 0, 1, 2, \ldots, \tag{3.2.9}$$

that follows directly from the boundary condition (3.2.2b). It follows from the frequency equation that the eigenfunctions of the problem form an infinite set.

The eigenfunctions $X_j, j = 0,1,2,\ldots$ are orthogonal with respect to the inner product $(\cdot,\cdot)$ defined as

$$(f,g) = \int_0^L f(x)\bar{g}(x)dx \quad , \tag{3.2.10}$$

where f and g are continuous functions on the interval $[0,L]$, and $\bar{g}(x)$ indicates the complex conjugate of $g(x)$. When an inner product is taken of an eigenfunction X with the left and the right hand side of the equation (3.2.3), after substituting the expression (3.2.4) for v and the value H for z, the equation

$$C_n^* Z_n(H)(X_n, X_n) = (e^{i\omega\frac{x}{c}}, X_n) \tag{3.2.11}$$

follows. From there, the Fourier coefficients C_n^* are

$$C_n^* = \frac{C_n}{Z_n(H)} \quad , n = 0,1,2,\ldots \tag{3.2.12}$$

where

$$C_n = \frac{(e^{i\omega\frac{x}{c}}, X_n)}{(X_n, X_n)} \quad , n = 0,1,2,\ldots \quad . \tag{3.2.13}$$

The coefficients $C_n, n = 0,1,\ldots$ can be calculated analytically by performing direct integration of the required functions, and their values are

$$C_o = \frac{1}{\frac{\omega L}{c}}\left[\sin\frac{\omega L}{c} + i\left(\cos\frac{\omega L}{c} - 1\right)\right] \tag{3.2.14a}$$

$$C_n = \frac{2}{L}\frac{\frac{\omega}{c}}{\left(\frac{\omega}{c}\right)^2 - \left(\frac{n\pi}{L}\right)^2}\left[(-1)^n \sin\frac{\omega L}{c} + i\left((-1)^n\cos\frac{\omega L}{c} - 1\right)\right] \quad , n \geq 1 \tag{3.2.14b}$$

when $\omega/c \neq m\pi/L$ for any $m = 1,2,3,\ldots$, and

$$C_o = \frac{i}{m\pi}\left[(-1)^m - 1\right] = \begin{cases} 0, & \text{m even} \\ \frac{-2i}{m\pi}, & \text{m odd} \end{cases} \tag{3.2.15a}$$

$$C_n = \frac{2}{L}\frac{i\frac{m\pi}{L}}{\frac{(m^2-n^2)\pi^2}{L^2}}\left[(-1)^{n+m}-1\right] = \begin{cases} 0, & (n+m) \text{ even}, \; n \neq m \\ \frac{-4im\pi}{(m^2-n^2)\pi^2}, & (n+m) \text{ odd}, \; n \geq 1 \end{cases} \qquad (3.2.15b)$$

$$C_m = 1 \qquad (3.2.15c)$$

if $\omega/c = m\pi/L$ for some integer m. In the limiting case when $\omega/c \to 0$, the coefficients C_n become

$$C_o = 1 \qquad (3.2.16a)$$

and

$$C_n = 0, \quad n \geq 1 \quad . \qquad (3.2.16b)$$

3.2.2 Discussion of the Solution

The wave numbers in the x-direction k_x can take on only real values in order for the boundary conditions to be satisfied, and these values are determined by the frequency equation (3.2.9). Consequently, the allowable values of the wave numbers in the z-direction k_z are

$$k_{z,n} = \sqrt{\frac{\omega^2}{\beta^2} - \frac{n^2\pi^2}{L^2}} \quad , \quad n = 0, 1, 2, \ldots, \qquad (3.2.17)$$

and are real only for finite number of modes, whose index n satisfies the inequality

$$\frac{\omega}{\beta} \geq \frac{n\pi}{L} \quad . \qquad (3.2.18)$$

For the rest of the modes, the wave numbers $k_{z,n}$ are pure imaginary, and therefore, the corresponding shape functions $Z_n(z)$ are hyperbolic functions of a real argument. Knowing

these facts, the displacement of the plate can be written as follows

$$v(x,z,t) = \left[\sum_{n=0}^{N} C_n \cos\frac{n\pi x}{L} \frac{\cos\sqrt{\frac{\omega^2}{\beta^2} - \frac{n^2\pi^2}{L^2}}z}{\cos\sqrt{\frac{\omega^2}{\beta^2} - \frac{n^2\pi^2}{L^2}}H} + \sum_{n=N+1}^{\infty} C_n \cos\frac{n\pi x}{L} \frac{\cosh\sqrt{\left(\frac{n\pi}{L}\right)^2 - \left(\frac{\omega}{\beta}\right)^2}z}{\cosh\sqrt{\left(\frac{n\pi}{L}\right)^2 - \left(\frac{\omega}{\beta}\right)^2}H} \right] e^{i\omega t} \quad , \tag{3.2.19}$$

where N is the largest integer n that satisfies the inequality (3.2.18), and all the arguments of the functions involved are real.

Some important properties of the behavior of $v(x,z,t)$ can be concluded by analyzing the analytical expression (3.2.19), and without doing any actual numerical calculations.

The coefficients $C_n, n = 0,1,2,\ldots$ have always finite values, even when the input base motion has the same wave number in the horizontal direction as one of the eigenfunctions in the x-direction $X_n(x), n = 1,2,\ldots$, as can be seen from equations (3.2.14a and b), (3.2.15a,b and c) and (3.2.16a and b). The shape functions

$$\cos\frac{n\pi x}{L} \qquad \text{and} \qquad \cos\sqrt{\frac{\omega^2}{\beta^2} - \frac{n^2\pi^2}{L^2}}z, \quad n = 0,1,\ldots \quad ,$$

are also bounded.

The cosine-hyperbolic function is an increasing function when its argument takes real and positive values. Therefore, the term

$$\cosh\sqrt{\frac{n^2\pi^2}{L^2} - \frac{\omega^2}{c^2}}z \Big/ \cosh\sqrt{\frac{n^2\pi^2}{L^2} - \frac{\omega^2}{c^2}}H$$

will have the maximum value equal to 1 at $z = H$ and will rapidly decrease towards the top of the plate. This simply means that the displacement of the plate resulting from the

modes corresponding to $n > N$ will be small at the top of the plate ($z = 0$), will increase with increasing z and at $z = H$ will be large enough so that the total displacement can follow the imposed displacement there. As a result, no energy is being transmitted into the plate by the modes that are hyperbolic functions in the vertical direction.

On the other hand, the displacement inside the plate, resulting from the modes that are harmonic functions in the vertical direction, can be very large and become unbounded when the following condition is satisfied

$$\sqrt{\frac{\omega^2}{\beta^2} - \frac{n^2\pi^2}{L^2}}H = \left(k + \frac{1}{2}\right)\pi, \quad \begin{matrix} k = 0, 1, 2, \ldots \\ n = 0, 1, 2, \ldots, N \end{matrix} \quad . \tag{3.2.20}$$

The frequencies ω_{nk} that satisfy this condition are called the resonant frequencies of the building. For the first mode ($n = 0$) they are the same as the resonant frequencies for a cantilevered shear beam, and for the higher modes ($n \geq 1$), the same as the resonant frequencies of a two dimensional shear plate, rigidly fixed at one side.

When the input wave number ω/β becomes smaller, the number of the modes having a harmonic shape function in the vertical direction decreases. However, even when the wave number in the plate ω/β is so small that zero is the largest integer satisfying the inequality (3.2.18), there is a mode that has a harmonic shape function in the vertical direction, the zero-th mode, through which energy can be transmitted into the interior of the plate and whose Fourier coefficient $C_o^* = C_o/\cos(\omega H/\beta)$ may have unbounded values.

The shape functions in the horizontal direction $X_n(x), n = 0, 1, \ldots$ represent standing waves, that result from the constructive interference between the waves reflected from the ends of plates at $x = 0$ and $x = L$. For even n $X_n(x)$ are symmetric and for odd n they are antisymmetric functions with respect to $x = L/2$.

The expressions (3.2.14a,b), (3.2.15a,b) and (3.2.16a,b) for the Fourier coefficients of the eigenfunction expansion of the displacement response tell about the contribution of the particular modes to the overall displacement. The equations (3.2.14a,b) show that in general all the Fourier coefficients are nonzero, meaning that all the modes of vibration are excited.

The equations (3.2.15a,b) imply that in the special case when the wave number in the x-direction of the input motion equals the wave number in the x-direction of one of the higher modes, i.e. $\omega/c = m\pi/L$ for some $m \geq 1$, the m-th coefficient has some value and the rest of the coefficients are either zero, or pure imaginary, with absolute value less than 1. If m is even, all the other even coefficients are zero, and the odd ones are nonzero. If m is odd, all the other odd coefficients are zero, while the even ones are nonzero. Even in this spacial case both symmetric and anti-symmetric modes are excited.

It is interesting to examine the behavior of the function $v(x,z,t)$, given by the equation (3.2.19), in the limiting case when the wave number of the input motion $\omega/c = 0$. Then, the input motion at $z = H$

$$v(x,H,t) = e^{i\omega t} \tag{3.2.21}$$

becomes a function of time only. In the previous section it was shown that in this limiting case all the coefficients C_n are zero except C_o, which is equal to 1, meaning that only the first symmetric mode contributes to the total displacement $v(x,z,t)$, and that no antisymmetric modes can be excited.

3.2.3 The Dimensionless Parameters of the Model and Discussion of the Frequency Equation

To make the problem more general, it is convenient to set up the problem and to

carry out the analysis of the solution in terms of dimensionless parameters. The four basic parameters can be defined as follows

$$\eta = \frac{L}{cT} : \quad \text{dimensionless length,} \tag{3.2.22}$$

$$\Omega = \frac{\omega L}{\beta} : \quad \text{dimensionless circular frequency,} \tag{3.2.23}$$

$$\frac{c_x}{\beta} : \quad \text{dimensionless horizontal phase velocity in the plate,} \tag{3.2.24}$$

and

$$\frac{c}{\beta} : \quad \text{dimensionless horizontal phase velocity of the input motion,} \tag{3.2.25}$$

where $T = 2\pi/\omega$ is the period of the input motion and $c_x = \omega/k_x$ is the phase velocity in the x-direction. The above parameters are related by the following equation

$$\Omega = 2\pi\eta\frac{c}{\beta} \quad . \tag{3.2.26}$$

The wave numbers k, k_x, k_z and the wave number of the input motion ω/c, expressed in terms of the dimensionless parameters will have the following form

$$k = \frac{\omega}{\beta} = \frac{\omega L}{\beta}\frac{1}{L} = \frac{\Omega}{L} \tag{3.2.27}$$

$$k_x = \frac{\omega}{c_x} = \frac{\omega L}{\beta}\frac{\beta}{c_x} = \frac{\Omega}{L}\left(\frac{c_x}{\beta}\right)^{-1} \tag{3.2.28}$$

$$k_z = \sqrt{k^2 - k_x^2} = \frac{\Omega}{L}\sqrt{1 - \left(\frac{c_x}{\beta}\right)^{-2}} \tag{3.2.29}$$

$$\frac{\omega}{c} = \frac{\Omega}{L}\left(\frac{c}{\beta}\right)^{-1} \quad . \tag{3.2.30}$$

The frequency equation (3.2.9) in terms of the dimensionless parameters will become

$$\frac{c_x}{\beta} = \frac{1}{n\pi}\Omega, \quad n = 0, 1, 2, \ldots, \tag{3.2.31}$$

showing that the horizontal phase velocities in the plate are linear functions of the dimensionless circular frequency Ω. The dispersion curves $c_x/\beta = f(\Omega)$ for the homogeneous plate are straight lines, with slope $1/n\pi$ and passing through zero. For given frequency Ω_o, the allowable horizontal phase velocities in the plate c_x/β are the points where the vertical line $\Omega = \Omega_o$ intersects the dispersion curves. The intersection with the dispersion curve corresponding to $n = 0$, and which has vertical slope, will be at c_x/β equal to infinity.

The resonance condition (3.2.20) in terms of the dimensionless parameters will have the following form

$$\sqrt{\Omega^2 - n^2\pi^2}\frac{H}{L} = \left(k + \frac{1}{2}\right)\pi, \quad \begin{matrix} k = 0, 1, 2, \ldots \\ n = 0, 1, \ldots N \end{matrix} \tag{3.2.32}$$

where N is the largest integer n such that $n\pi \leq \Omega$.

3.3 Plate Having Vertical Discontinuities in the Material Properties

3.3.1 Formulation and Solution of the Problem

The mathematical model discussed in this section is a two dimensional, semi-infinite, elastic plate of length L that has been made up of three layers of different material properties and perfectly bonded to each other. The layers are isotropic and homogeneous and with ℓ_i, β_i and $\mu_i, i = 1, 2, 3$ representing their widths, shear wave velocities and shear muduli (Figure 3.3.1). The displacement response of the plate to the imposed SH wave motion $e^{i\omega\left(t - \frac{x}{c}\right)}$ at $z = H$ will be derived, again by using the method of separation of variables and eigenfunction expansion of the solution. Similarly as in the previous section, the displacements of the plate for $0 \leq z \leq H$ will correspond to the displacement of a

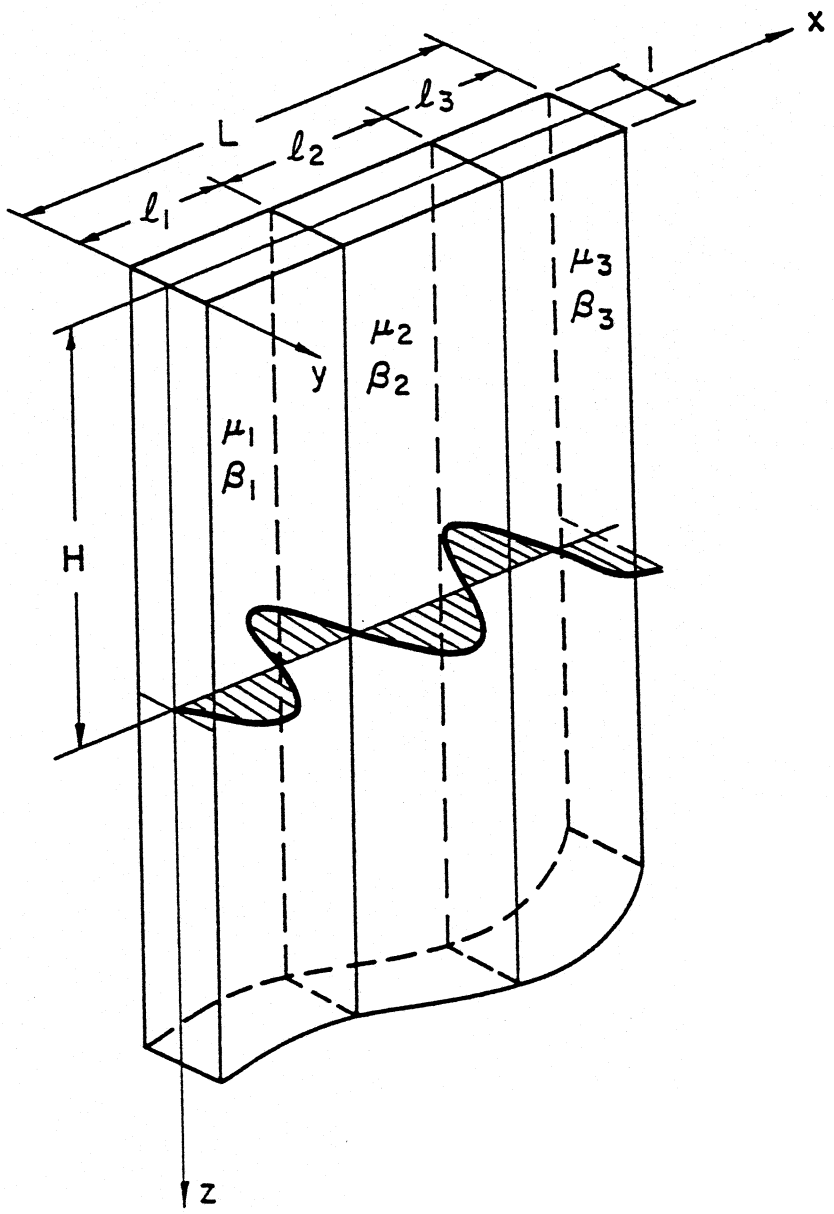

Figure 3.3.1 Model of a building of length L and height H with two vertical discontinuities in the material properties. It is excited at the base by a wave of amplitude 1, frequency ω and propagating with phase velocity c in the positive x-direction. The soil structure interaction is neglected.

building of length L and height H placed over the homogeneous half-space and excited by the same propagating SH wave motion at the base.

The displacement in the plate $v(x,z,t)$ can have the following representation

$$v(x,z,t) = \begin{cases} v^{(1)}(x,z,t) & , \quad 0 \le x \le \ell_1 \\ v^{(2)}(x,z,t) & , \quad \ell_1 < x \le \ell_1 + \ell_2 \\ v^{(3)}(x,z,t) & , \quad \ell_1 + \ell_2 < x \le L \end{cases} \tag{3.3.1}$$

Each of the displacements $v^{(i)}(x,z,t), i = 1,2,3$ has to satisfy the two-dimensional wave equation (3.2.1) with the corresponding value of the shear wave velocity β. The displacement $v(x,z,t)$ has to satisfy the same boundary conditions (3.2.2a,b and c) and the same displacement condition at $z = H$ (3.2.3) as the homogeneous plate. It also has to meet the following conditions requiring continuity of stresses and displacements

$$v^{(1)}(\ell_1,z,t) = v^{(2)}(\ell_1,z,t) \tag{3.3.2a}$$

$$\tau_{xy}^{(1)}(\ell_1,z,t) = \tau_{xy}^{(2)}(\ell_1,z,t) \tag{3.3.2b}$$

$$v^{(2)}(\ell_1+\ell_2,z,t) = v^{(3)}(\ell_1+\ell_2,z,t) \tag{3.3.3a}$$

and

$$\tau_{xy}^{(2)}(\ell_1+\ell_2,z,t) = \tau_{xy}^{(3)}(\ell_1+\ell_2,z,t) \quad , \tag{3.3.3b}$$

where

$$\tau_{xy}^{(i)}(x,z,t) = \mu_i \frac{\partial v^{(i)}(x,z,t)}{\partial x} \quad , i = 1,2,3 \tag{3.3.4}$$

are the shear stresses in the layers.

Using the method of separation of variables and the eigenfunction expansion of the solution, the displacement $v(x,z,t)$ can be represented as in equation (3.2.4), where the

time dependent function $T(t)$ and the eigenfunctions in the vertical direction $Z_j(z), j = 1,2,\ldots$ are the same as for the homogeneous model and are given by the equations (3.2.6) and (3.2.7). The eigenfunctions for the horizontal direction $X_j(x), j = 0,1,\ldots$ that satisfy the imposed boundary conditions can be represented as follows

$$X_j(x) = \begin{cases} \cos k_{x,j}^{(1)} x, & 0 \le x \le \ell_1 \\ A_j^{(2)} \cos k_{x,j}^{(2)} x + B_j^{(2)} \sin k_{x,j}^{(2)} x, & \ell_1 < x \le \ell_1 + \ell_2 \\ A_j^{(3)} \cos k_{x,j}^{(3)} (L - x), & \ell_1 + \ell_2 < x \le L \end{cases} \tag{3.3.5}$$

where $k_{x,j}^{(i)}$ is the wave number in the x-direction in the i-th layer and corresponding to the j-th mode of vibration.

The wave number in the vertical direction, $k_{z,j}$, corresponding to the j-th mode of vibration, is the same in all the layers because of the continuity conditions, and is related to the corresponding wave numbers in the horizontal direction by the following equation

$$k_{x,j}^{(i)} = \sqrt{k_i^2 - k_{z,j}^2} \quad , \quad i = 1,2,3 \quad , \tag{3.3.6}$$

where $k_i = \frac{\omega}{\beta_i}$ is the wave number in the i-th layer.

The continuity conditions (3.3.2a,b) and (3.3.3a) imply the following form of the coefficients $A_j^{(2)}$, $B_j^{(2)}$ and $A_j^{(3)}$ that appear in the equation (3.3.5)

$$A_j^{(2)} = \cos k_{x,j}^{(1)} \ell_1 \cdot \cos k_{x,j}^{(2)} \ell_1 + \frac{\mu_1}{\mu_2} \frac{k_{x,j}^{(1)}}{k_{x,j}^{(2)}} \sin k_{x,j}^{(1)} \ell_1 \cdot \sin k_{x,j}^{(2)} \ell_1 \quad , \tag{3.3.7a}$$

$$B_j^{(2)} = \sin k_{x,j}^{(1)} \ell_1 \cdot \cos k_{x,j}^{(2)} \ell_1 + \frac{\mu_1}{\mu_2} \frac{k_{x,j}^{(1)}}{k_{x,j}^{(2)}} \sin k_{x,j}^{(1)} \ell_1 \cdot \cos k_{x,j}^{(2)} \ell_1 \tag{3.3.7b}$$

and

$$A_j^{(3)} = \frac{1}{\cos k_{x,j}^{(3)} \ell_3} \left[A^{(2)} \cos k_{x,j}^{(2)} (\ell_1 + \ell_2) + B^{(2)} \sin k_{x,j}^{(2)} (\ell_1 + \ell_2) \right] . \tag{3.3.7c}$$

The continuity condition (3.3.3b) leads to the frequency equation for the system

$$\frac{\mu_2}{\mu_3}\frac{k_{x,j}^{(2)}}{k_{x,j}^{(3)}}\left[-A_j^{(2)}\sin k_{x,j}^{(2)}(\ell_1+\ell_2)+B_j^{(2)}\cos k_{x,j}^{(2)}(\ell_1+\ell_2)\right]=-A_j^{(3)}\sin k_{x,j}^{(3)}\ell_3 \quad . \tag{3.3.8}$$

After applying the relationship among the wave numbers (3.3.6), the frequency equation (3.3.8) will have only one unknown and its solutions can be evaluated numerically.

It can be proved (Appendix B) that the eigenfunctions $X_j(x)$ are orthogonal with respect to the weighted inner product $(\cdot,\cdot)_w$ defined as follows

$$(f,g)_w=\int_0^L f(x)\bar{g}(x)w(x)dx \tag{3.3.9}$$

where the weighting function $w(x)$ is

$$w(x)=\begin{cases}\mu_1, & 0\le x\le \ell_1\\ \mu_2, & \ell_1<x\le \ell_1+\ell_2\\ \mu_3, & \ell_1+\ell_2<x\le L\end{cases} \quad , \tag{3.3.10}$$

f and g are continuous functions of x and the bar over $g(x)$ indicates the complex conjugate of $g(x)$.

Following the procedure that was used in the previous section, the Fourier coefficients C_n^* for this model have the representation (3.2.12) where

$$C_n=\frac{\left(e^{-i\frac{\omega}{c}x},X_n(x)\right)_w}{\left(X_n(x),X_n(x)\right)_w} \quad ,n=0,1,\ldots \quad . \tag{3.3.11a}$$

Since the eigenfunctions $X_n(x)$ and the function $e^{i\frac{\omega}{c}x}$, can be differentiated and integrated analytically, the coefficients $C_n, n=0,1,\ldots$ can be expressed in an analytical form (Appendix C).

When $\omega/c\to 0$, i.e. when the motion at $z=H$ becomes $\Delta e^{i\omega t}$, the coefficients C_n can be calculated as follows

$$C_n=\frac{(1,X_n(x))_w}{\left(X_n(x),X_n(x)\right)_w} \quad , \quad n=0,1,\ldots \quad , \tag{3.3.11b}$$

and will be non-zero only for even n.

3.3.2 The Dimensilonless Parameters of the Model

The dimensionless length η for this model is defined in the same way as for the homogeneous model, equation (3.2.22). The other dimensionless parameters are defined in a similar way

$$\Omega = \frac{\omega L}{\beta_i} : \quad \text{dimensionless circular frequency,} \tag{3.3.12}$$

$$\frac{c}{\beta_i} : \quad \text{dimensionless } x - \text{phase velocity of the input motion,} \tag{3.3.13}$$

and

$$\frac{c_x^{(i)}}{\beta_i} : \quad \text{dimensionless } x - \text{phase velocity in the } i - th \text{ layer.} \tag{3.3.14}$$

The first three of the dimensionless parameters are related by the following equation

$$\Omega = 2\pi\eta\frac{c}{\beta_i} \quad . \tag{3.3.15}$$

The wave numbers in terms of these parameters will be

$$k_j = \frac{\Omega}{L}\frac{\beta_j}{\beta_i} \quad , \tag{3.3.16a}$$

$$k_i = \Omega/L \quad , \tag{3.3.16b}$$

$$k_x^{(j)} = \frac{\Omega}{L}\sqrt{\left(\frac{\beta_i}{\beta_j}\right)^2 - 1 + \left(\frac{c_x^{(i)}}{\beta_i}\right)^{-2}} \qquad j \neq i \quad , \tag{3.3.17a}$$

$$k_x^{(i)} = \frac{\Omega}{L}\left(\frac{c_x^{(i)}}{\beta_i}\right)^{-1} \tag{3.3.17b}$$

and

$$k_z = \frac{\Omega}{L}\sqrt{1 - \left(\frac{c_x^{(i)}}{\beta_i}\right)^{-2}} \tag{3.3.18}$$

3.3.3 Discussion of the Frequency Equation

The horizontal wave numbers in the "softest" layer are always real (the proof is contained in the Appendix D), while in the other two layers they may be real or imaginary. Because the numerical searching for real roots only is more convenient than searching for roots that may be real or imaginary, all the wave numbers that appear in the frequency equation (3.3.8) will be expressed in terms of the wave number in the x-direction, $k_x^{(i)}$, where i is the index of the layer which has the smallest value of the shear wave velocity. Because of the same reason the dimensionless parameters have been defined relative to the "softest" layer.

In Figure 3.3.2 the normalized phase velocities $c_x^{(2)}/\beta_2 = f(\omega L/\beta_2)$ have been drawn, for a plate with thin and stiff outside layers (i.e. $\ell_1/L = \ell_3/L = 0.1$ and $\beta_1/\beta_2 = \beta_3/\beta_2 = 4$). The same material density has been assumed in all the layers and therefore $\mu_1/\mu_2 = \sqrt{\beta_1/\beta_2} = 2$ and $\mu_3/\mu_2 = \sqrt{\beta_3/\beta_2} = 2$. The first impression from this figure is that there is wave dispersion in the solution of this problem, for all the modes. (In the case of the homogeneous plate there was no dispersion of c_x/β for $n = 0$). All the phase velocities in Figure 3.3.2 asymptotically approach straight lines for large $\omega L/\beta_2$. For small $\omega L/\beta_2$ the curve for $n = 0$ approaches a constant value as $\omega L/\beta_2 \to 0$ while the curves for $n \geq 1$ approach zero, as straight lines, when $\omega L/\beta_2 \to 0$.

For a given $\omega L/\beta_2$, the allowable phase velocities $c_x^{(2)}/\beta_2$ can be determined from intersection points of the line $\omega L/\beta_2 =$ constant with the dispersion curves, as shown in

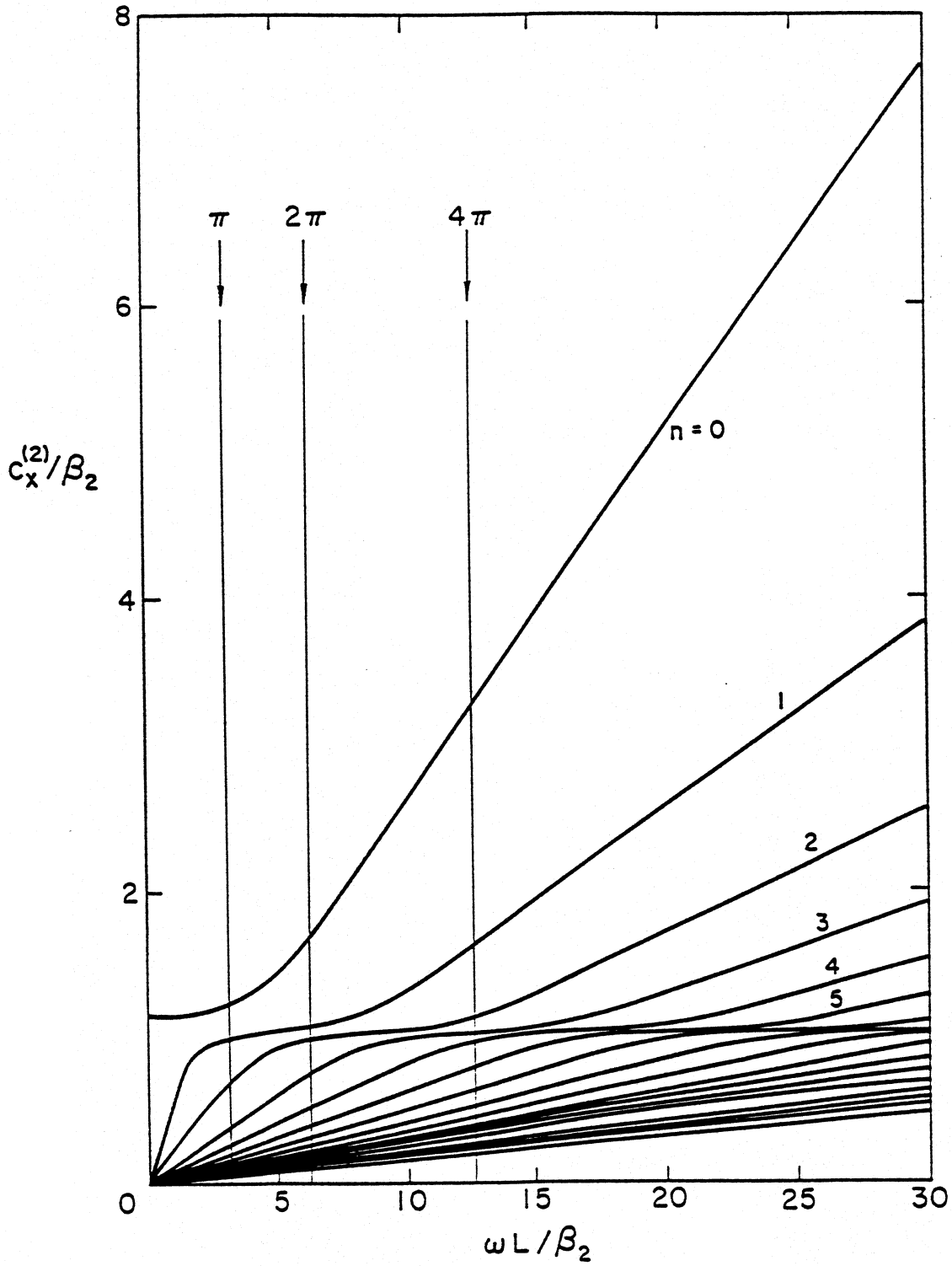

Figure 3.3.2 Dispersion curves $c_x^{(2)}/\beta_2 = f(\omega L/\beta_2)$ for the model with thin and stiff shear walls. $\ell_1/L = \ell_3/L = 0.1$ and $\beta_1/\beta_2 = \beta_3/\beta_2 = 4$ (see Figure 3.3.1). $c_x^{(2)}$ is the x-phase velocity in the central layer.

Figure 3.3.2. In Figures 3.3.3a, b and c the first five mode-shapes ($n = 0, 1, 2, 3$ and 4) for the x-direction are shown, for $\omega L/\beta_2 = \pi, 2\pi$ and 4π, respectively. The mode-shapes corresponding to $n = 0, 2, \ldots$ are symmetric, while those that correspond to $n = 1, 3, \ldots$ are anti-symmetric.

The characteristics of the dispersion curves and of the mode-shapes are closely related and the asymptotic behavior of the curves is reflected in the appearance of the mode-shapes. For example, for large $\omega L/\beta_2$, the dispersion curves asymptotically approach the dispersion curves of a homogeneous plate of width ℓ_2 (which is the width of the soft layer of the layered plate) and fixed at $x = 0$ and $x = \ell_2$. The shape functions for the plate fixed at both sides are

$$X_n(x) = \sin k_{x,n} x \tag{3.3.19a}$$

and the allowable wave numbers are

$$k_{x,n} = \frac{n\pi}{\ell_2}, \quad n = 1, 2, 3 \ldots \quad . \tag{3.3.19b}$$

($k_x = 0$ is not an eigenvalue, because the corresponding eigenfunction would be identically equal to zero, and by definition the eigenfunctions cannot be identically equal to zero). The shape functions of the layered plate for large $\omega L/\beta_2$ instead behave like $\sin \frac{m\pi}{L} x$ for large $\omega L/\beta_2$, which can be seen in Figure 3.3.3c. The shape function for $n = 0$ in this figure resembles a half wavelength of a sine wave, the mode-shape for $n = 1$ contains one wavelength of a sine wave, the one for $n = 1$ contains $3/2$ wave lengths of a sine wave etc. From this behavior of the mode-shapes it can be concluded that for the waves with large frequencies, i.e. small wave lengths, the stiff layers act as stiff barriers so that the waves will propagate only through the central soft layer.

Comparing parts "a", "b" and "c" of Figures 3.3.3 one can see that as $\omega L/\beta_2 \to 0$ the mode-shapes have longer wavelengths. For small $\omega L/\beta_2$ (e.g. $\omega L/\beta_2 = \pi$, Figure

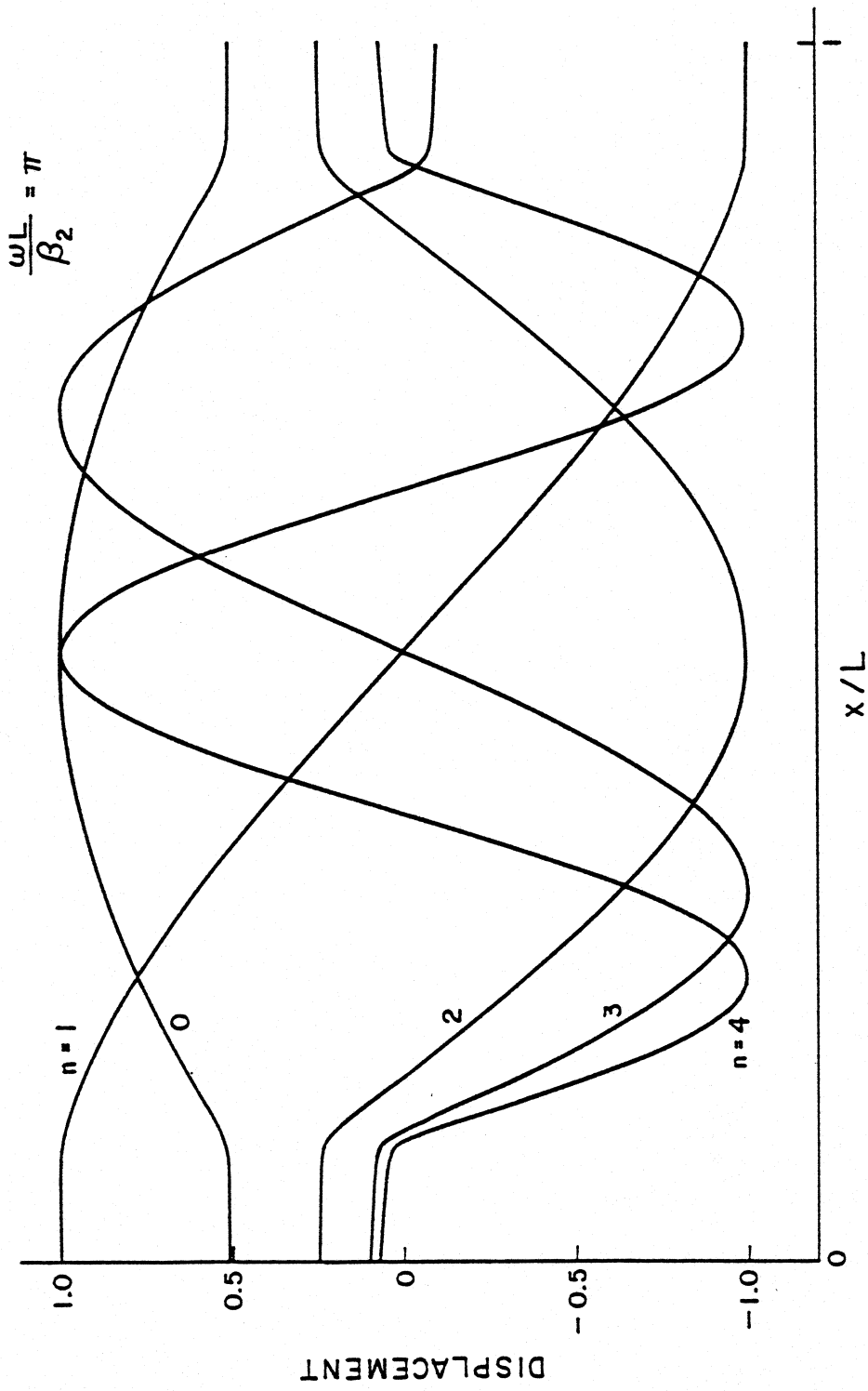

Figure 3.3.3a The first five mode-shapes in the x-direction for the model with thin and stiff shear walls. $\ell_1/L = \ell_3/L = 0.1$ and $\beta_1/\beta_2 = \beta_3/\beta_2 = 4$ (see Figure 3.3.1). The dimensionless frequency is $\omega L/\beta_2 = \pi$.

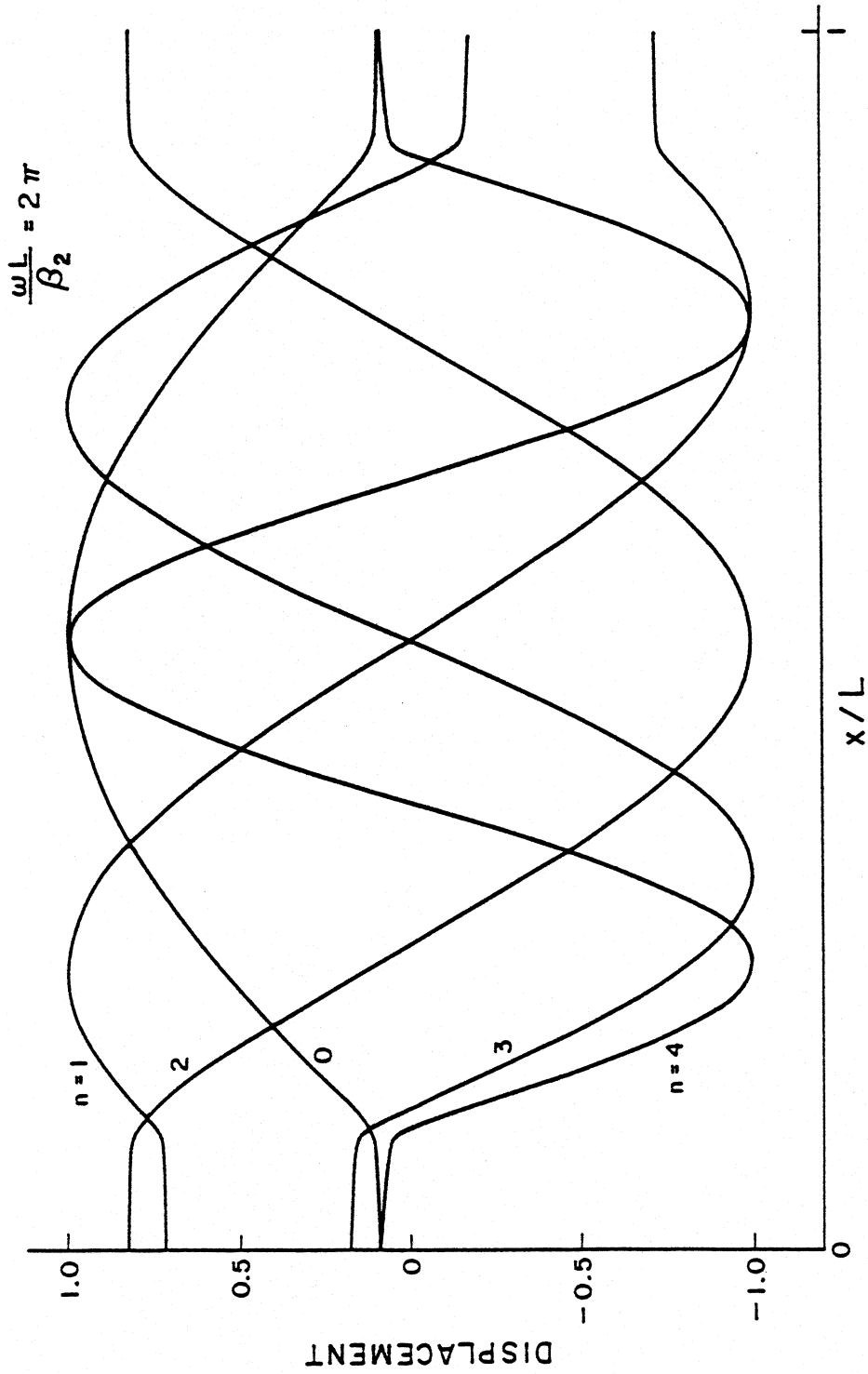

Figure 3.3.3b The first five mode-shapes in the x-direction for the model with thin and stiff shear walls. $\ell_1/L = \ell_3/L = 0.1$ and $\beta_1/\beta_2 = \beta_3/\beta_2 = 4$ (see Figure 3.3.1). The dimensionless frequency is $\omega L/\beta_2 = 2\pi$.

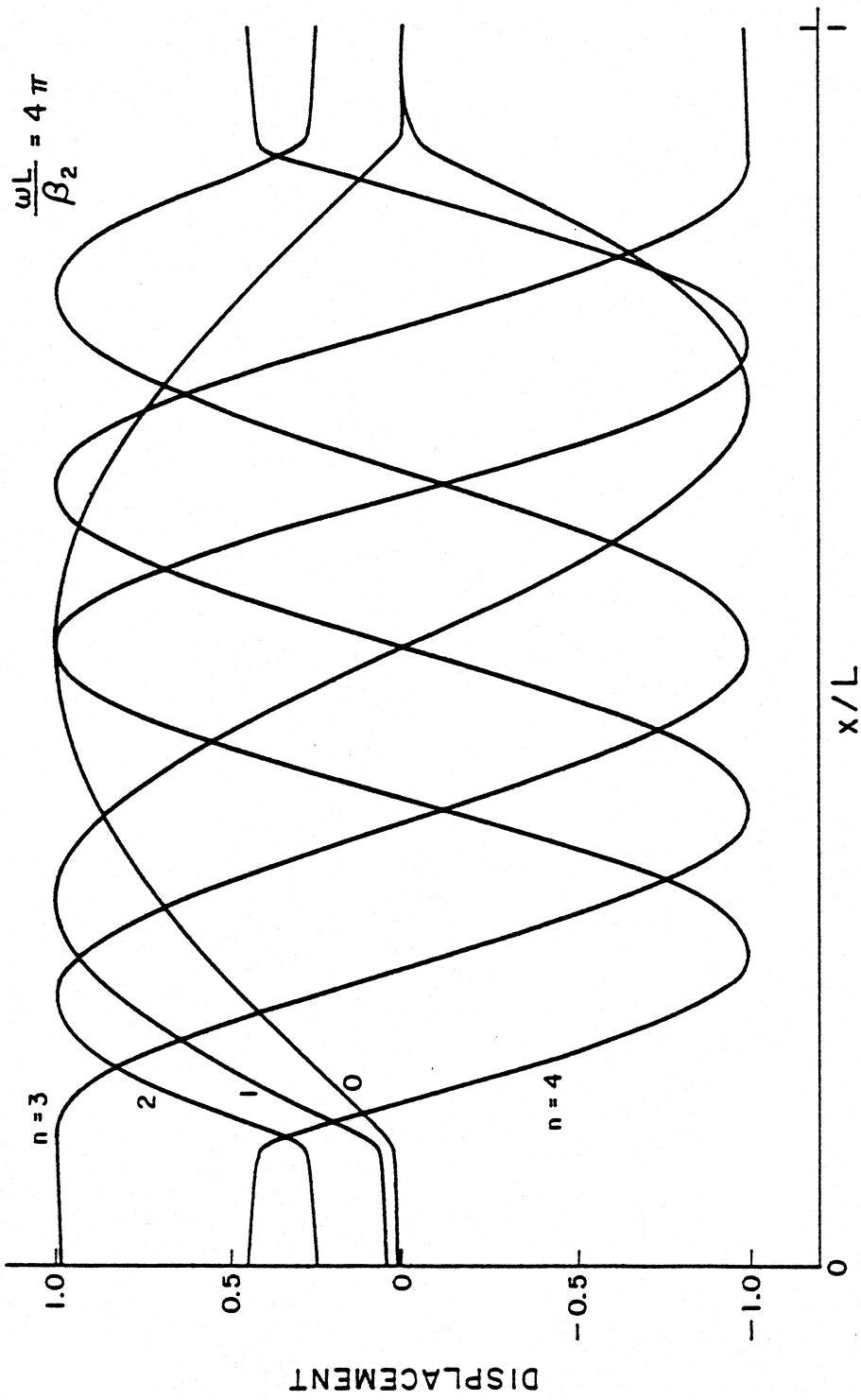

Figure 3.3.3c The first five mode-shapes in the x-direction for the model with thin and stiff shear walls. $\ell_1/L = \ell_3/L = 0.1$ and $\beta_1/\beta_2 = \beta_3/\beta_2 = 4$ (see Figure 3.3.1). The dimensionless frequency is $\omega L/\beta_2 = 4\pi$.

3.3.3a), the mode-shape for $n = 0$ approaches a straight line, and the mode shape for $n = 1$ looks almost like a $\cos \pi x/L$. In other words, these modes start to look like the shape functions of a homogeneous plate with stress free boundaries at $x = 0$ and $x = L$. This means that the first two modes, and corresponding to the waves with small phase velocities for this frequency, do not "see" the discontinuities at the ends of the plate. The higher modes for this frequency still look like the modes for a building with fixed ends. This means that the waves with shorter wave lengths will still "see" the thin "harder" layers at the two ends as a barrier.

Another feature of the asymptotic behavior of the dispersion curves in Figure 3.3.2 is that for small frequencies as $\omega \to 0$ the dispersion curves for $n \geq 2$ have the same slope as the dispersion curves for $n-2$ at high frequencies. For example, the curve for $n = 2$, for small $\omega L/\beta_2$, has almost the same slope as the curve for $n = 0$ for higher frequencies, the curve $n = 3$ for large $\omega L/\beta_2$ has the same slope as the curve for $n = 1$ when $\omega L/\beta_2 \to 0$, etc. The curves with similar slope will have similar wave numbers k_x and therefore the corresponding mode shapes will contain almost the same number of wave lengths. Even though the lower order modes at higher frequencies may look like higher modes at lower frequency, the number of zero crossings, which is equal to the order of the mode, is not changed.

In Figure 3.3.4 the dispersion curves $c_x^{(1)}/\beta_1 = f(\omega L/\beta_1)$ have been illustrated for a layered plate with one stiff central layer ($\ell_2 = 0.2L$, $\ell_1 = \ell_3 = 0.4L$, $\beta_1/\beta_2 = \beta_3/\beta_2 = 1/4$). The first five mode-shapes for $\omega L/\beta_1 = \pi, 2\pi$ and 4π are illustrated in Figures 3.3.5a, b and c.

For large freqeuncies the phase velocities for $n = 0$ and $n = 1, n = 2$ and $n = 3, n = 4$ and $n = 5$, etc. asymptotically approach the phase velocities for a homogeneous plate,

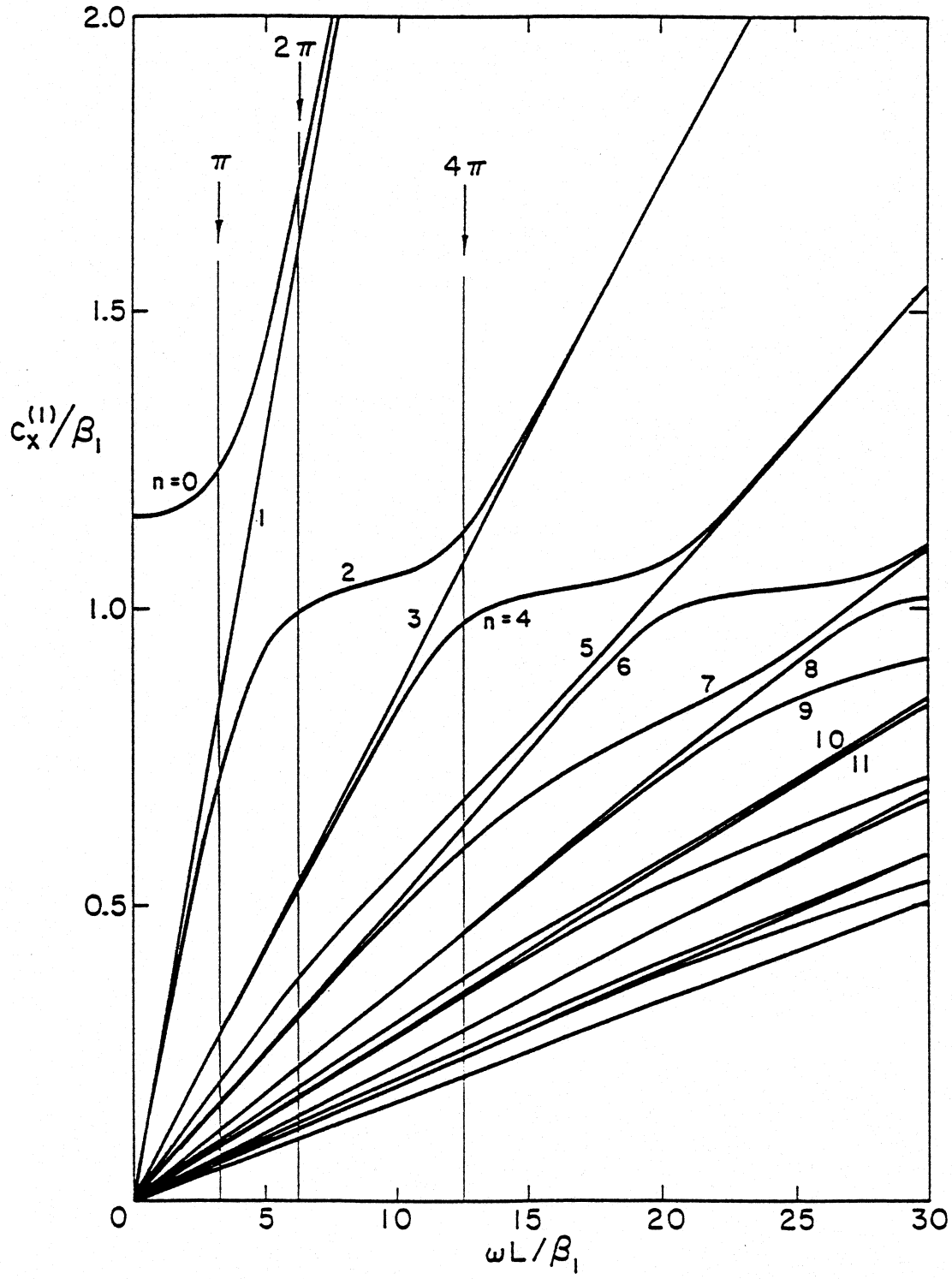

Figure 3.3.4 Dispersion curves $c_x^{(1)}/\beta_1 = f(\omega L/\beta_1)$ for the model with stiff central layer (central core), with $\ell_1/L = \ell_3/L = 0.4$ and $\beta_2/\beta_1 = \beta_2/\beta_3 = 4$ (see Figure 3.3.1). $c_x^{(1)}$ is the x-phase velocity in the outside layers.

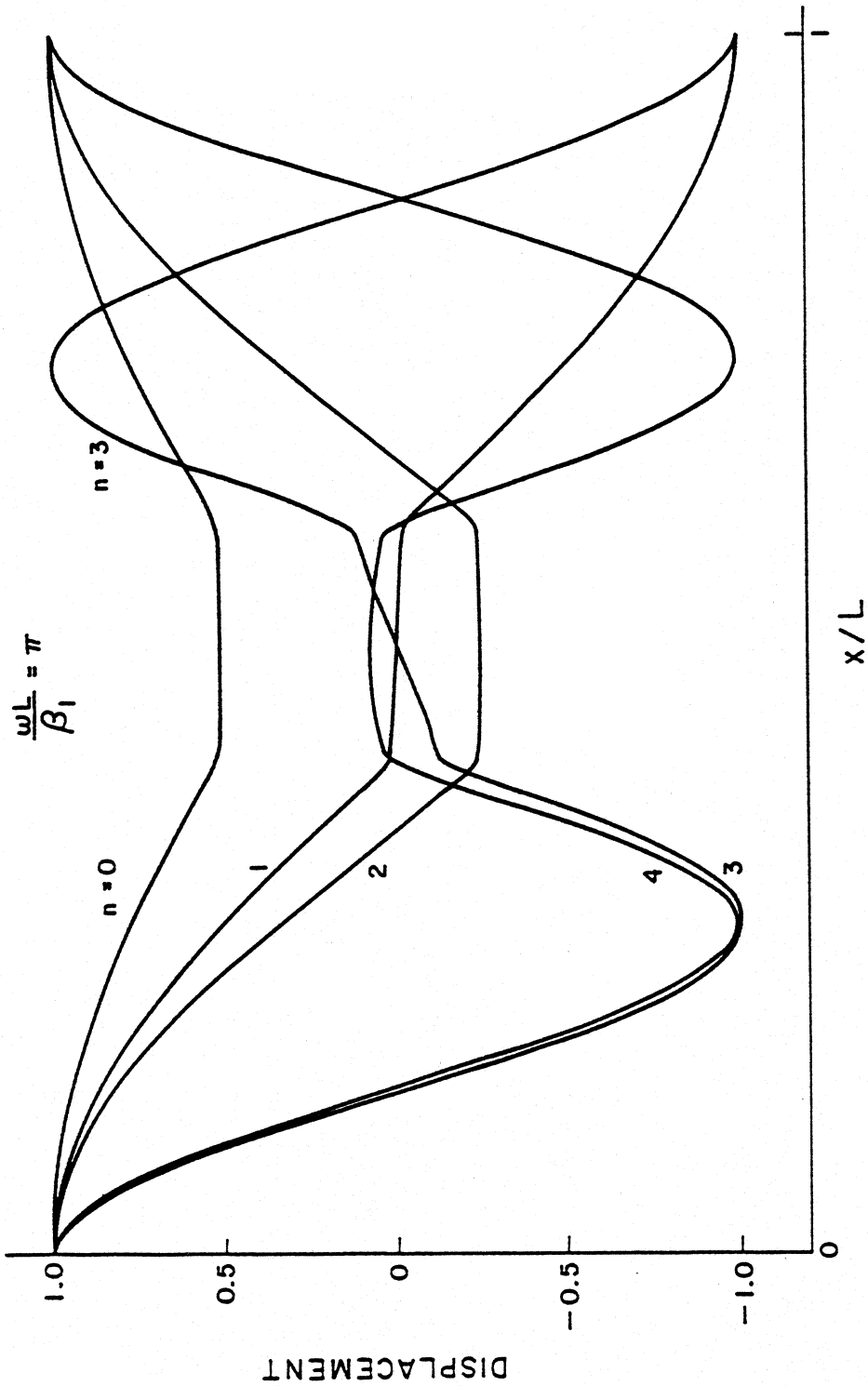

Figure 3.3.5a Mode-shapes in x-direction for the model with stiff central layer. $\ell_1/L = \ell_3/L = 0.4$ and $\beta_2/\beta_1 = \beta_2/\beta_3 = 4$ (see Figure 3.3.1). The dimensionless frequency is $\omega L/\beta_1 = \pi$.

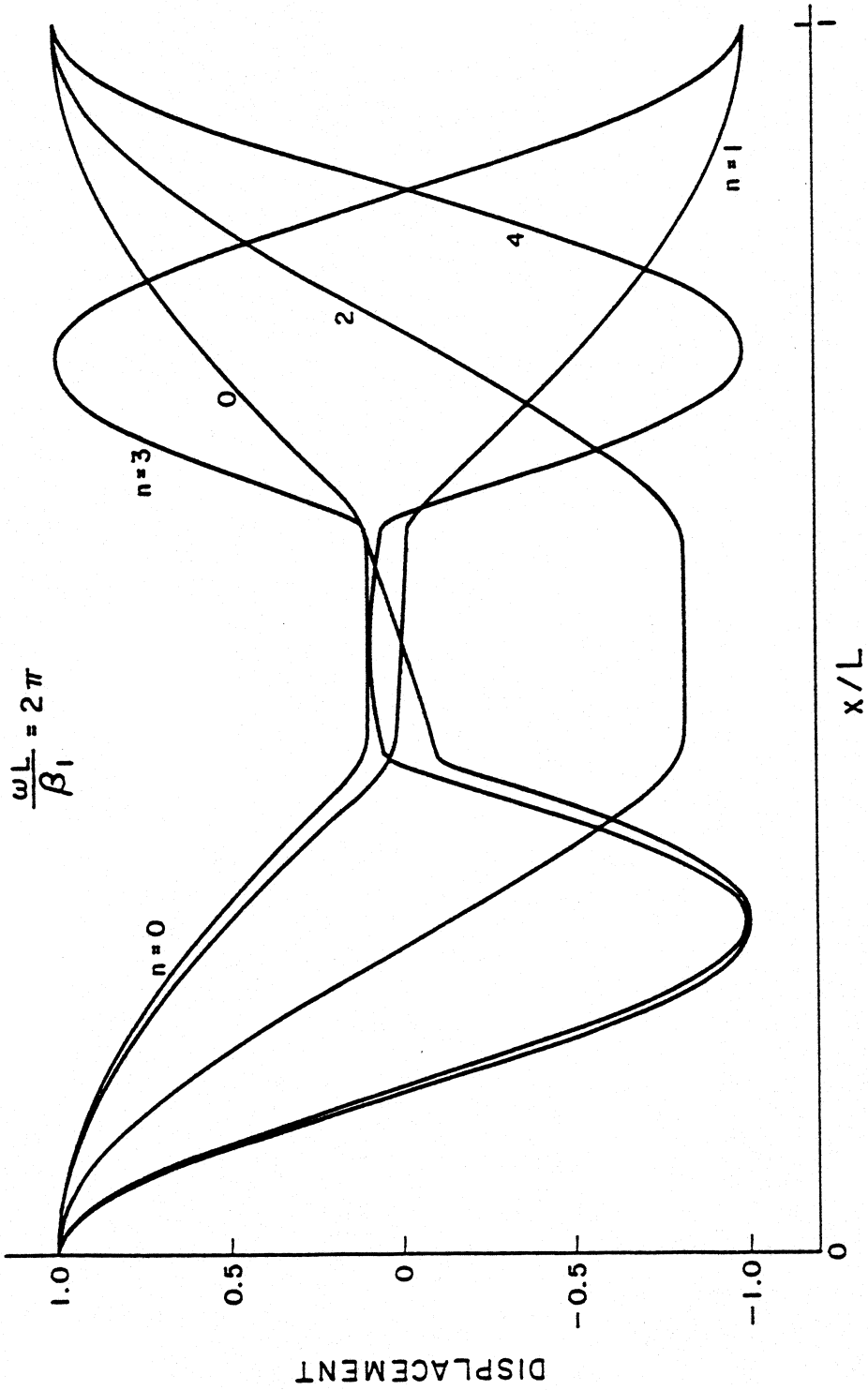

Figure 3.3.5b Mode-shapes in x-direction for the model with stiff central layer. $\ell_1/L = \ell_3/L = 0.4$ and $\beta_2/\beta_1 = \beta_2/\beta_3 = 4$ (see Figure 3.3.1). The dimensionless frequency is $\omega L/\beta_1 = 2\pi$.

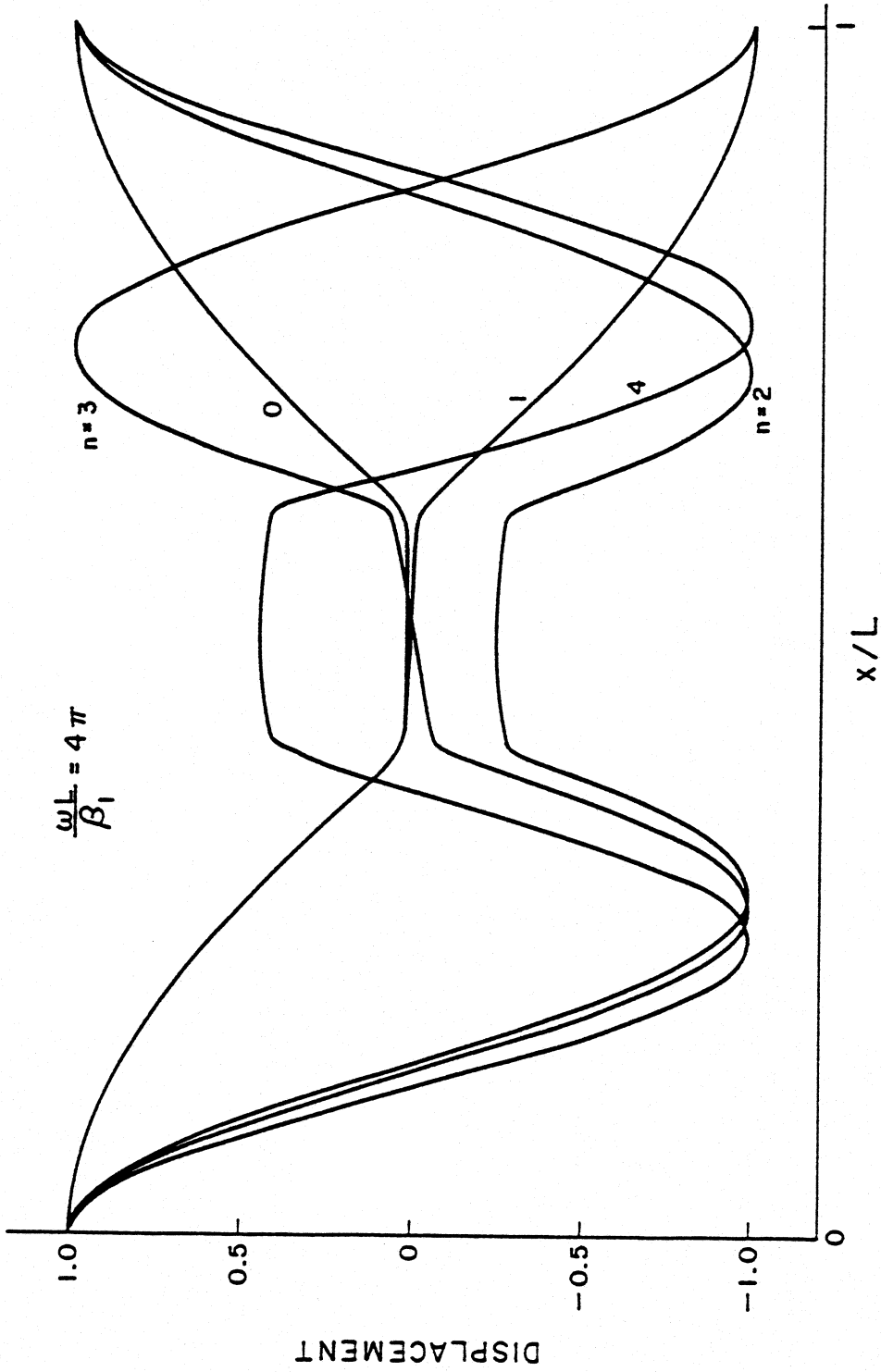

Figure 3.3.5c Mode-shapes in x-direction for the model with stiff central layer. $\ell_1/L = \ell_3/L = 0.4$ and $\beta_2/\beta_1 = \beta_2/\beta_3 = 4$ (see Figure 3.3.1). The dimensionless frequency is $\omega L/\beta_1 = 4\pi$.

with width and material properties the same as the width and the material properties of the soft layer, and fixed at $x = \ell_1$. The eigenfunctions for such a plate are

$$X_n(x) = \cos k_{x,n} x \tag{3.3.20a}$$

where

$$k_{x,n} = \left(n + \frac{1}{2}\right)\frac{\pi}{\ell_1} \quad n = 0, 1, \ldots \quad . \tag{3.3.20b}$$

This means that for large frequencies the above pairs of modes will have almost the same wave numbers and therefore will contain the same number of wavelengths. This can be observed for the mode-shapes in Figure 3.3.5c. In this figure ($\omega L/\beta_1 = 4\pi$) the modes for $n = 0$ and $n = 3$ have almost the same value of the wave number k_x. The only significant difference in the mode shapes is that one of them is symmetric and the other one is antisymmetric with respect to $x = L/2$. Both pairs of those mode-shapes in the first layer look like $\cos(n + 1/2)\pi x/\ell_1$, for $n = 0$ and 1, respectively, which would be the mode shapes of the first layer if it were fixed at $x = \ell_1$. Physically, this means that for higher frequencies the central layer acts as a barrier for the waves, and that the soft layers will vibrate "independently" of each other. With $\omega L/\beta_1 \to 0$, the mode shapes become more flat and the mode shape for $n = 0$ approaches a constant.

For small and for high frequencies, the anti-symmetric mode-shapes are not very different from the anti-symemtric mode-shapes of a homogeneous plate. It can be expected, therefore, that the central core will not change appreciably the anti-symmetric displacements of the plate, but that it will change the symmetric ones.

3.4 Plate with Horizontal Discontinuities in the Material Properties

3.4.1 Formulation and Solution of the Problem

The model considered in this section is a two-dimensional, semi-infinite plate of

width L, composed of horizontal layers with different material properties, perfectly bonded to each other. The material of which the layers have been made is assumed to be homogeneous, isotropic and perfectly elastic. The model is shown on Figure 3.4.1, where h_i, β_i and $\mu_i, i = 1, 2, \ldots M$ represent the height, shear wave velocity and shear modulus of the i-th layer and M is the total number of layers. h_i, $i = 1, \ldots, M-1$ represent the thickness of the layers and h_M represents the distance between the top of the semi-infinite bottom layer and the line $z = H$. Again, an analytical expression for the displacement response of the plate to the imposed SH wave motion $e^{i\omega\left(t-\frac{x}{c}\right)}$ at $z = H$ will be derived by using the method of separation of variables and the eigenfunction expansion of the solution.

Let $v^{(i)}(x, z, t)$ represent the displacement in the i-th layer. Then, the displacement of the plate may be written as follows

$$v(x,z,t) = \begin{cases} v^{(1)}(x,z,t) & 0 \le x < h_1^* \\ v^{(2)}(x,z,t) & h_1^* \le x < h_2^* \\ \vdots & \\ v^{(i)}(x,z,t) & h_{i-1}^* \le x < h_i^* \\ \vdots & \\ v^{(M)}(x,z,t) & h_{M-1}^* \le x < \infty \end{cases} \tag{3.4.1}$$

where $h_i^* = \sum_{j=1}^{i} h_j$. The displacements in the layers $v^{(i)}(x, z, t)$ have to satisfy the two-dimensional wave equation (3.2.1) with the constant β equal to the corresponding shear wave velocity in the layer. The boundary conditions that the displacements $v(x, z, t)$ satisfy are expressed in the equations (3.2.2a,b and c), where $\tau_{xy} = \mu\frac{\partial v}{\partial x}$ and $\tau_{zy} = \mu\frac{\partial v}{\partial z}$ are the shear stresses in the plate, and

$$\mu = \begin{cases} \mu_1, & 0 \le x < h_1^* \\ \vdots & \\ \mu_i, & h_{i-1}^* \le x < h_i^* \\ \vdots & \\ \mu_M, & h_{M-1}^* \le x < \infty \end{cases} \tag{3.4.2}$$

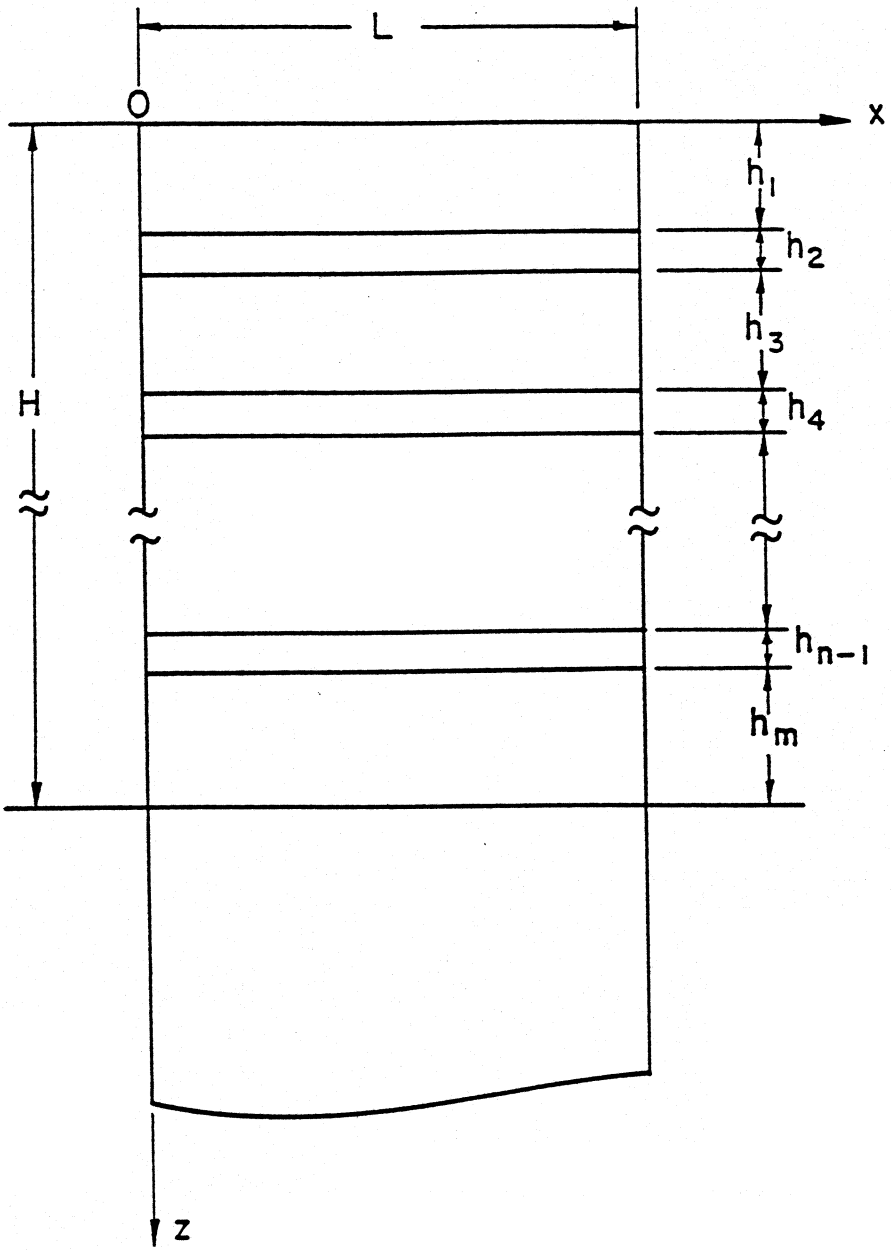

Figure 3.4.1 Two-dimensional, continuous model of a building of length L and height H having horizontal discontinuities in the material properties. The soil-structure interaction is neglected, and the building is forced to vibrate by the free field displacements on the surface of the half-space.

At the interfaces between the different media, the following continuity conditions have to be satisfied

$$v^{(i)}(x,h_i^*,t) = v^{(i+1)}(x,h_i^*,t) \quad ,i = 1,\ldots,M-1 \tag{3.4.3a}$$

$$\tau_{xz}^{(i)}(x,h_i^*,t) = \tau_{xz}^{i+1}(x,h_i^*,t) \quad ,i = 1,\ldots,M-1 \tag{3.4.3b}$$

where $\tau_{xz}^{(i)} = \mu_i \frac{\partial v^{(i)}}{\partial z}$ is the shear stress in the i-th layer. The displacement condition at $z = H$ is the same as for the previous models and is given by the equation (3.2.3).

By applying the same methods that have been used in solving the previous two problems, the displacement $v(x,z,t)$ may have the representation as in the equation (3.2.4), where the time dependent function $T(t)$ and the eigenfunctions in the x-direction $X_j(x), j = 0,1,2,\ldots$ are the same as in the equations (3.2.7) and (3.2.5), respectively.

The frequency equation results from the requirement that the allowable wave numbers in the x-direction $k_{x,j}, j = 0,1,\ldots$ must satisfy is the equation (3.2.9), same as for the homogeneous model. The allowable wave numbers in the z-direction have different values in different layers, and can be calculated from the following relationship between the wave numbers

$$k_{z,j}^{(i)} = \sqrt{k_i^2 - k_{x,j}^2} \qquad \begin{matrix} i = 1,\ldots,M \\ j = 0,1,\ldots \end{matrix} \quad . \tag{3.4.4}$$

The eigenfunctions for the vertical direction and satisfying the boundary condition (3.2.2c) and the continuity conditions (3.4.3a and b) can be represented in the following form

$$Z_j(z) = \begin{cases} \cos k_{z,j}^{(1)} z, & 0 \le x < h_1^* \\ A_j^{(2)} \cos k_{z,j}^{(2)} z + B_j^{(2)} \sin k_{z,j}^{(2)} z, & h_1^* \le x < h_2^* \\ \vdots & \vdots \\ A_j^{(i)} \cos k_{z,j}^{(i)} z + B_j^{(i)} \sin k_{z,j}^{(i)} z, & h_{i-1}^* \le x < h_i^* \\ \vdots & \vdots \\ A_j^{(M)} \cos k_{z,j}^{(M)} z + B_j^{(M)} \sin k_{z,j}^{(M)} z, & h_{M-1}^* \le x < \infty \end{cases} \tag{3.4.5}$$

where the coefficients $A_j^{(i)}$ and $B_j^{(i)}$ can be calculated by the use of the following recursive equations

$$\begin{aligned} A_j^{(i)} = A_j^{(i-1)} \Bigg[& \cos k_{z,j}^{(i-1)} h_{i-1}^* \cos k_{z,j}^{(i)} h_{i-1}^* \\ & + \frac{\mu_{i-1}}{\mu_i} \frac{k_{z,j}^{(i-1)}}{k_{z,j}^{(i)}} \sin k_{z,j}^{(i-1)} h_{i-1}^* \sin k_{z,j}^{(i)} h_{i-1}^* \Bigg] \\ + B_j^{(i-1)} \Bigg[& \sin k_{z,j}^{(i-1)} h_{i-1}^* \cos k_{z,j}^{(i)} h_{i-1}^* \\ & + \frac{\mu_{i-1}}{\mu_i} \frac{k_{z,j}^{(i-1)}}{k_{z,j}^{(i)}} \cos k_{z,j}^{(i-1)} h_{i-1}^* \sin k_{z,j}^{(i)} h_{i-1}^* \Bigg] \end{aligned} \tag{3.4.6a}$$

$$\begin{aligned} B_j^{(i)} = A_j^{(i-1)} \Bigg[& \cos k_{z,j}^{(i-1)} h_{i-1}^* \sin k_{z,j}^{(i)} h_{i-1}^* \\ & + \frac{\mu_{i-1}}{\mu_i} \frac{k_{z,j}^{(i-1)}}{k_{z,j}^{(i)}} \sin k_{z,j}^{(i-1)} h_{i-1}^* \cos k_{z,j}^{(i)} h_{i-1}^* \Bigg] \\ + B_j^{(i-1)} \Bigg[& \sin k_{z,j}^{(i-1)} h_{i-1}^* \sin k_{z,j}^{(i)} h_{i-1}^* \\ & + \frac{\mu_{i-1}}{\mu_i} \frac{k_{z,j}^{(i-1)}}{k_{z,j}^{(i)}} \cos k_{z,j}^{(i-1)} h_{i-1}^* \cos k_{z,j}^{(i)} h_{i-1}^* \Bigg] \end{aligned} \tag{3.4.6b}$$

for $i = 2, 3, \ldots, M$, and $A_j^{(1)} = 1$ and $B_j^{(1)} = 0$.

The Fourier coefficients C_n^* that satisfy the displacement condition at $z = H$ have the representation as in the equation (3.2.12), where

$$Z_n(H) = A_n^{(M)} \cos k_{z,n}^{(M)} H + B_n^{(M)} \sin k_{z,n}^{(M)} H \quad , \tag{3.4.7}$$

and the coefficients $C_n, n = 0, 1, \ldots$ are the same as the corresponding coefficients for the homogeneous model (equations (3.2.14a,b), (3.2.15a,b) and (3.2.16a,b)).

3.4.2 The Dimensionless Parameters of the Model

The dimensionless length η, again is defined in the same way as for the homogeneous model in section 3.2.3. The other dimensionless parameters for this model are defined as follows

$$\Omega = \frac{\omega L}{\beta_M} : \quad \text{dimensionless circular frequency,} \tag{3.4.8}$$

$$\frac{c_x}{\beta_M} : \quad \text{dimensionless phase velocity in the } x\text{-direction in the lowest layer,} \tag{3.4.9}$$

and

$$\frac{c}{\beta_M} : \quad \text{dimensionless phase velocity of the input motion in } x - \text{direction.} \tag{3.4.10}$$

The wave numbers expressed in terms of the dimensionless parameters are

$$k_i = \frac{\Omega}{L}\frac{\beta_M}{\beta_i} \tag{3.4.11}$$

$$k_z^{(i)} = \sqrt{\Omega^2 \left(\frac{\beta_M}{\beta_i}\right)^2 - (n\pi)^2} \quad \frac{1}{L} \tag{3.4.12}$$

and

$$\frac{\omega}{c} = \frac{\Omega}{L}\left(\frac{c}{\beta_M}\right)^{-1} \quad . \tag{3.4.13}$$

3.4.3 Discussion of the Solution

Because of the same form of the frequency equation as for the homogeneous plate problem, the dispersion curves $c_x/\beta_M = f(\Omega)$ and the shape function $X_n(x)$ will remain the same as before. However, the shape functions $Z_n(z)$ will be different.

Of interest in this work is the case when the number of layers is equal to two, and when the upper layer is "harder" than the lower layer (Figure 3.4.2). Such a model will be used to represent a building with a soft first floor. The wave numbers in the vertical direction for this model will be

$$k_{z,n}^{(1)} = \sqrt{\left(\frac{\omega}{\beta_1}\right)^2 - \left(\frac{n\pi}{L}\right)^2} \quad , n = 0, 1, \ldots \tag{3.4.14a}$$

$$k_{z,n}^{(2)} = \sqrt{\left(\frac{\omega}{\beta_2}\right)^2 - \left(\frac{n\pi}{L}\right)^2} \quad , n = 0, 1, \ldots \quad . \tag{3.4.14b}$$

From the above equations it can be seen that for the first mode ($n = 0$) both wave numbers are always real, meaning that the shape function $Z_o(x)$ will always be composed of harmonic functions. The higher modes may be harmonic, or hyperbolic functions, depending on the frequency ω and on the values of the shear wave velocities β_1 and β_2. The number of modes that have real wave numbers in the z-direction in both layers is finite. Let N_i be the total number of the modes with real wave numbers in the vertical direction in the i-th layer. Then N_i is the largest integer n for which

$$\frac{\omega}{\beta_i} \geq \frac{n\pi}{L} \quad . \tag{3.4.15}$$

Since the upper layer is "harder" than the lower one $N_1 \geq N_2$.

Real wave numbers $k_{z,n}^{(i)}$ correspond to modes that are harmonic functions in the i-th layer and imaginary $k_{z,n}^{(i)}$ correspond to hyperbolic functions in the i-layer. If the upper layer is much "harder" than the lower one, then $N_1 < N_2$ and there will be more modes that are harmonic functions in the lower layer, continuing as hyperbolic functions in the "upper" layer. These modes will be associated with propagation of energy into the lower layer only. The upper part will have displacements that decay exponentially towards the top of the plate.

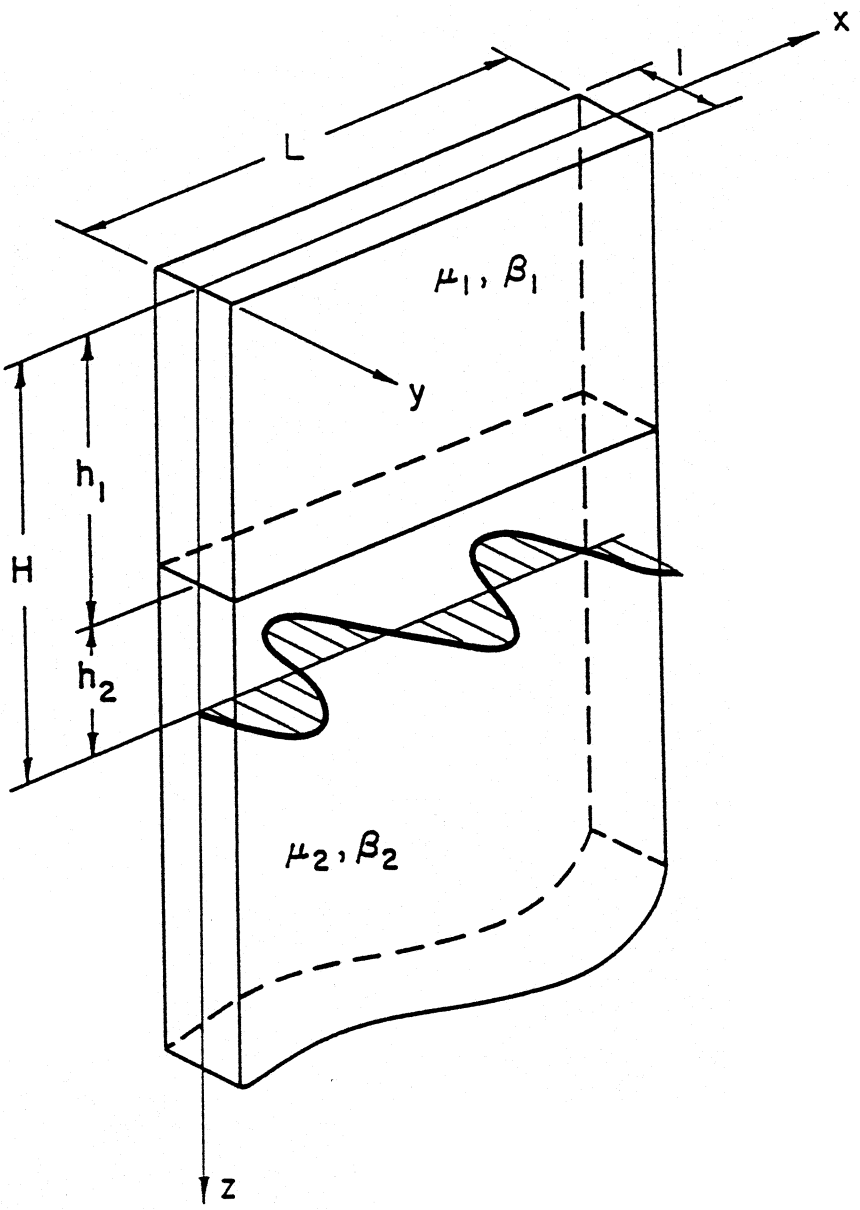

Figure 3.4.2 Two-dimensional, continuous model of a building with soft first floor. The soil-structure interaction is neglected and the model is excited to vibrate by the imposed displacement $e^{i\omega\left(t-\frac{x}{c}\right)}$ at $z = H$.

The Fourier coefficients C_n^* will become infinitely large when

$$A_n^{(2)} \cos k_{x,n}^{(2)} + B_n^{(2)} \sin k_{x,n}^{(2)} \to 0 \quad . \tag{3.4.16}$$

The frequencies ω for which this happens are called the resonant frequencies of the plate. During resonance an infinite amount of energy is being transferred into the plate and its displacements become unbounded. Realistic models have damping and during resonance their displacements are finite, but may be large.

When $\eta \to 0$, for the input motion $\omega/c \to 0$ and the excitation becomes $\Delta e^{i\omega t}$, with Δ =constant. Similarly, as in the case of the homogeneous plate, only the 0-th mode will contribute to the displacement, and the displacement of the plate will be symmetric with respect to $x = L/2$.

3.5 Response of Buildings to Rotational Excitation

3.5.1 The Rotational Excitation

For small values of the dimensionless length η, the effects of the wave passage may be considered approximately by representing the motion at the base of the building as a translation $\Delta e^{i\omega t}$ of the end $x = 0$, plus a rotation $\phi_o e^{i\omega t}$ about the same end.

For the two-dimensional problem when the seismic waves propagate in the x-direction under the building, the torsional excitation $\Phi_s(x,t)$ can be defined as follows

$$\Phi_s(x,t) = \frac{\partial v_s(x,t)}{\partial x} \quad , \tag{3.5.1}$$

where $v_s(s,t)$ is the displacement at the surface of the halfspace.

When the SH-wave displacement at the surface of the halfspace is a propagating wave with wave number ω/c in the x-direction, i.e.

$$v_s(x,t) = e^{i\omega(t-x/c)} \tag{3.5.2}$$

then, the torsional excitation will be:

$$\Phi_s(x,t) = -\frac{i\omega}{c} e^{i\omega(t-\frac{x}{c})} \quad , \tag{3.5.3}$$

having a phase delay of $\pi/2$ relative to $v_s(x,t)$. For small values of the dimensionless length of the building η, i.e. for $L << cT$, where T is the period of the wave, the displacement under the building is nearly a straight line, implying that all the points at the base of the building will have nearly the same amplitude of the torsional excitation, and can be expressed as

$$\Phi_s(t) = \Phi_o e^{i\omega t} \quad , \tag{3.5.4}$$

where the amplitude Φ_o is

$$\Phi_o = -\frac{i\omega}{c} \quad . \tag{3.5.5}$$

The amplitude Δ of the translational excitation for the base motion (3.2.2) will be:

$$\Delta = 1 \quad . \tag{3.5.6}$$

Figure 3.5.1 represents an in-plan view of a building excited by a "long" wave, and illustrates the translational and rotational excitations.

The synthesis of torsional accelerograms out of the translational ones was studied by Lee and Trifunac (1985) and further details about this topic can be found in their work.

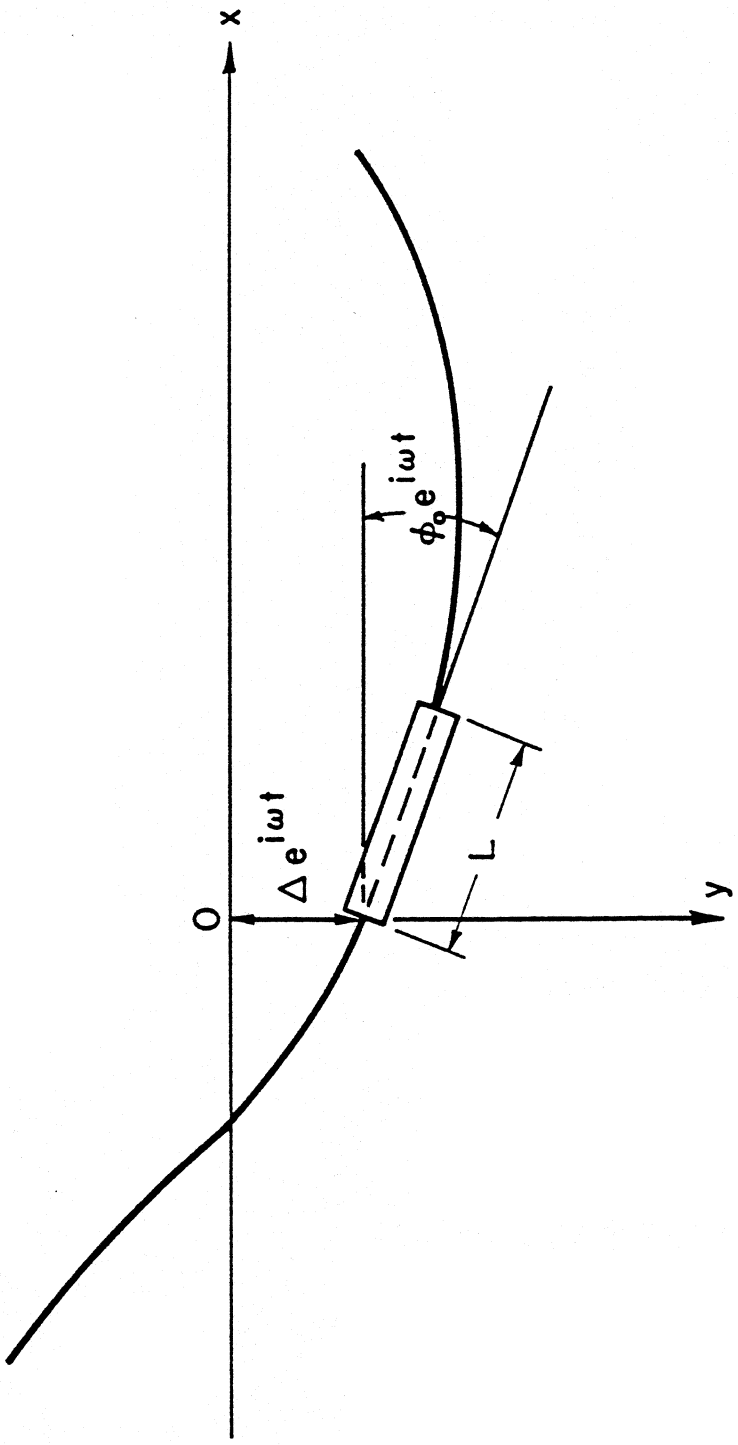

Figure 3.5.1 Plan view of a building "riding" on a wave with long wave length in x-direction. The base motion can be approximated by translation $\Delta e^{i\omega t}$ and rotation $\phi_o e^{i\omega t}$.

3.5.2 The Response of the Building

The displacement response of the building v, for small values of η, can be represented as a summation of the responses to the translational v_{tran} and rotational v_{rot} excitations separately, i.e.

$$v = v_{tran} + v_{rot} \quad . \tag{3.5.7}$$

If the excitation is same as in equation (3.5.2) and the building is represented by the homogeneous model, the response to the translational part of excitation $v_{s,tran}(t)$ will be:

$$v_{tran} = Z_o(z)e^{i\omega t} \quad , \tag{3.5.8}$$

and follows from the analysis in section 3.2.2. The response to the rotational part excitation $\Phi_s(t)$ can be expanded in terms of the eigenfunctions of the model as follows:

$$v_{rot} = \sum_{n=0}^{\infty} \tilde{C}_n^* X_n(x) Z_n(z) e^{i\omega t} \quad . \tag{3.5.9}$$

Similarly, as in the previous sections, the Fourier coefficients are:

$$\tilde{C}_n^* = \tilde{C}_n / Z_n(H) \tag{3.5.10}$$

where

$$\tilde{C}_o = -\frac{i}{2}\frac{\omega}{c}L \tag{3.5.11a}$$

and

$$\tilde{C}_n = \begin{cases} 0 & \text{, n even} \\ \frac{4}{L} i \frac{\omega}{c} \left(\frac{L}{n\pi}\right)^2 & \text{, n odd} \end{cases} \tag{3.5.11b}$$

The total displacement v expanded in terms of the eigenfunctions will have coefficients C_n^* as follows:

$$C_n^* = C_n / Z_n(H) \tag{3.5.12}$$

where

$$C_o = 1 - \frac{i}{2}\frac{\omega L}{c} \tag{3.5.13a}$$

and

$$C_n = \begin{cases} 0 & , n \text{ even} \\ \frac{4}{L} i \frac{\omega}{c} \left(\frac{L}{n\pi}\right)^2 & , n \text{ odd} \end{cases} \tag{3.1.13b}$$

It can be shown that the corresponding coefficients C_n given by equations (3.2.14) approach C_o and C_n above, when η is small (see Appendix E). Thus for small η the response of extended structures to propagating wave motion can be approximated by the translational, $\Delta e^{i\omega t}$, and torsional $\Phi_o e^{i\omega t}$ excitations only.

CHAPTER IV

RESPONSE OF THE BUILDING TO GENERAL GROUND MOTION

In reality, the buildings are subjected to arbitrary excitation and not to the periodic sinusoidal motion as discussed in the previous chapters. The actual excitation contains a wide range of frequencies and the direction from which it comes as well as the spectral amplitudes are known in advance only with certain level of confidence. The soil inhomogeneities increase the degree of complexity. For example, dispersed waves result from horizontal discontinuities and standing wave patterns may be present in soil with vertical and near vertical discontinuities. Inside and near alluvium valleys, focusing and complicated interference patterns of the incident motion are present (Trifunac, 1971a; Wong, 1979).

The Fourier synthesis of the response of the building to: nondispersed and dispersed propagating waves, nondispersed propagating together with nonpropagating waves, and nondispersed waves of random amplitude and coming from a random direction will be discussed in this chapter.

4.1 Fourier Synthesis of the Response of the Building to Nondispersed Propagating Waves

Many seismic waves coming from a distant source and propagating through the homogeneous halfspace can be approximated by plane waves. The Fourier spectrum of the motion

$$F(\omega) = \int_0^\infty f(t) e^{i\omega t} dt \quad , \tag{4.1.1}$$

where $f(t)$ is the time history of the incident ground displacement, has amplitudes $|F(\omega)|$ significantly greater than zero, for ω between zero and up to $\sim 50 Hz$.

The resultant wave motion caused by the interference of an incident plane, monochromatic, SH wave of frequency ω, and of unit amplitude and angle of incidence θ, with the analogous wave, refracted from the stress-free surface of the half-space is (Achenbach (1973)):

$$v_s^{inc+ref}(x', z', \omega, \theta) = 2\cos\frac{\omega}{c_{z'}} z' \cdot e^{i\omega(t-\frac{x'}{c})} \tag{4.1.2}$$

where

$$c = \frac{\beta_s}{\sin\theta} : \quad \text{phase velocity in the } x'\text{-direction} \tag{4.1.3a}$$

$$_z' = \frac{\beta_s}{\cos\theta} : \quad \text{phase velocity in the } z'\text{-direction} \tag{4.1.3b}$$

$$\omega : \quad \text{circular frequency} \tag{4.1.4a}$$

$$x', z' : \quad \text{spatial coordinates} \tag{4.1.4b}$$

$$\beta_s : \quad \text{shear wave velocity in the half-space} \tag{4.1.4c}$$

$$t : \quad \text{time coordinate,} \tag{4.1.4d}$$

as shown in Figure 4.1.1. It represents a wave propagating in the x'-direction with velocity c, and having amplitude that is a cosine function of the depth. It is an undispersed wave because the phase velocities c and $c_{z'}$ do not depend on the frequency ω. The resultant displacement at the surface of the half-space due to this wave only is

$$v_s^{inc+ref}(x', 0, \omega, \theta) = 2e^{i\omega(t-\frac{x'}{c})} \quad , \tag{4.1.5}$$

and due to a general incident wave motion will be

$$v_s(x', 0, t) = \int_0^\infty 2F(\omega)e^{i\omega(t-\frac{x}{c})}d\omega \quad , \tag{4.1.6}$$

where $F(\omega)$ is the Fourier spectrum of the incident motion.

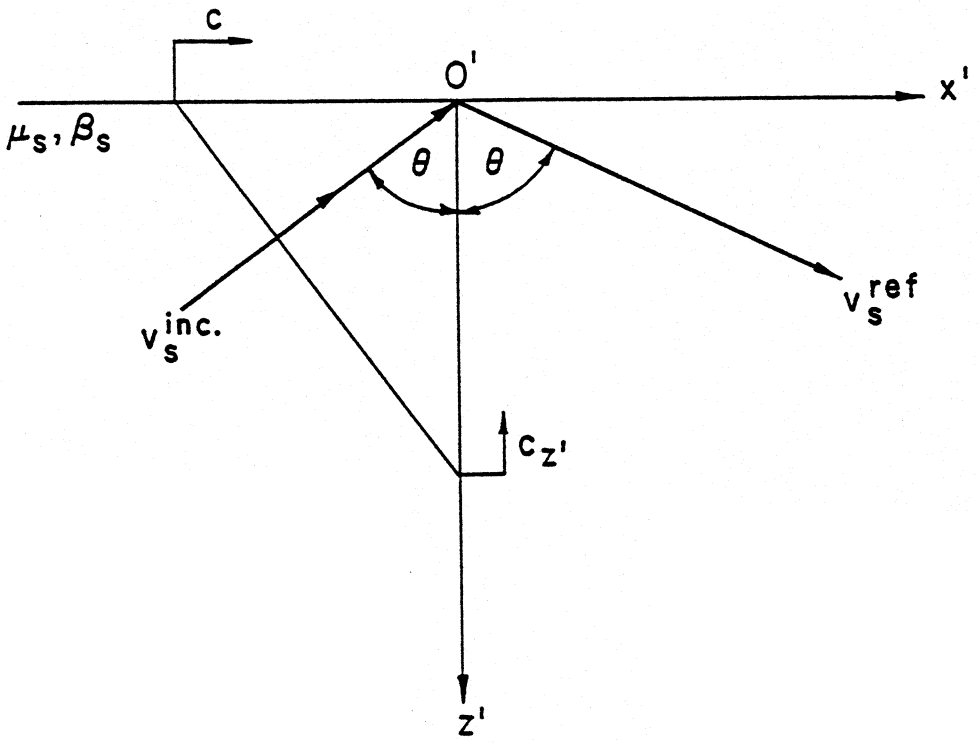

Figure 4.1.1 Homogeneous half-space with an incident SH-wave with amplitude 1 and incident angle θ. c and c'_z are the phase velocities of the wave in the x' and in the z'-directions, respectively.

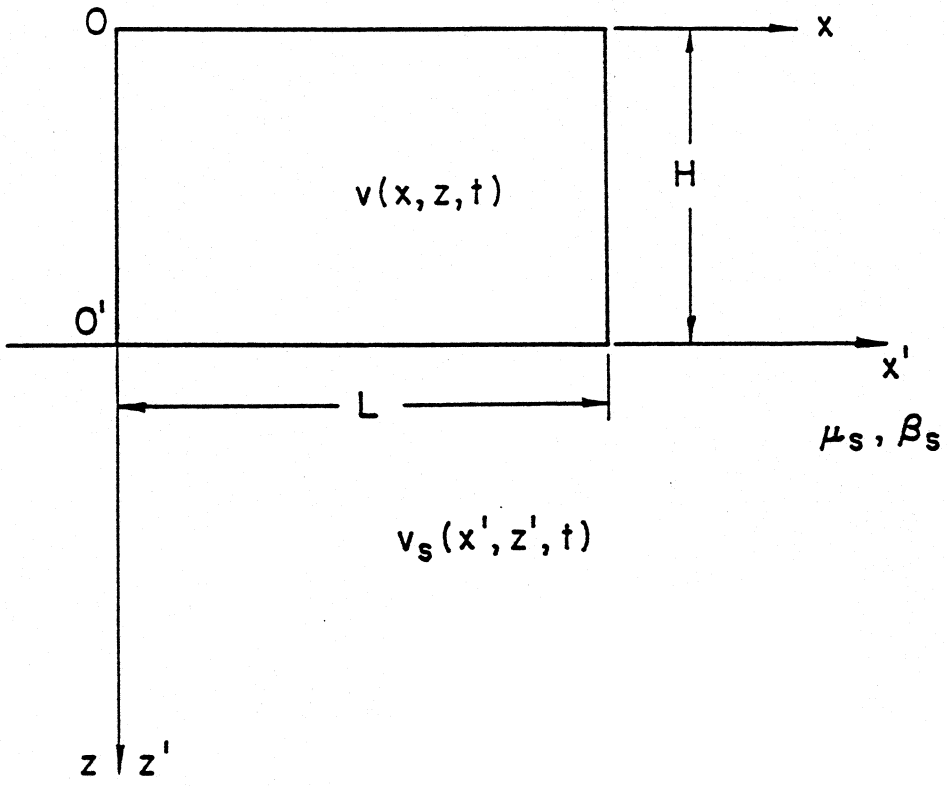

Figure 4.1.2 Two-dimensional model of a building placed onto the homogeneous half-space. The figure illustrates the relationship between the coordinate systems of the building $(x, 0, z)$ and of the half-space $(x', 0', z')$.

Let $H(x,z,\omega,\theta)$ be the response of the building to the wave motion $e^{i\omega(t-\frac{x}{c})}$ at its base. Then, according to the transfer function theory (Meirovitch, 1975), the response to the general wave motion described by equation (4.1.4) will be

$$v(x,z,t,\theta) = \frac{1}{2\pi}\int_0^\infty 2F(\omega)H(x,z,\omega,\theta)d\omega \quad , \tag{4.1.7}$$

where the relationship between the coordinate system used for the soil $(x',0',y')$ and for the building $(x,0,y)$ is shown in Figure 4.1.2.

4.2 Fourier Synthesis of the Response of the Building to General Dispersed Wave Motion

The synthesis of the response of the building to a dispersed excitation will be illustrated here for an example of Love waves in a soft, elastic layer placed over the homogeneous, elastic half-space, as shown in Figure 4.2.1a.

The Love waves result from interference of plane SH waves and can exist in the layered half-space. They represent a solution of the two-dimensional wave equation (3.2.1) that satisfies the following conditions: zero stress at the upper surface of the top layer, continuity of stresses and displacements at the interface between the different media and exponentially decreasing amplitudes with increasing depth in the half-space. For the case of a single layer over the half-space and the coordinate system as in Figure 4.2.1a, the displacement in the layer $v^{(L)}$ and in the half-space $v^{(HS)}$ will have the following form,

$$v^{(L)} = A\cos qz' \cdot e^{-bz'} \tag{4.2.1}$$

$$v^{(HS)} = Be^{-i\omega(t-\frac{z'}{c})} \cdot e^{-bz'} \tag{4.2.2}$$

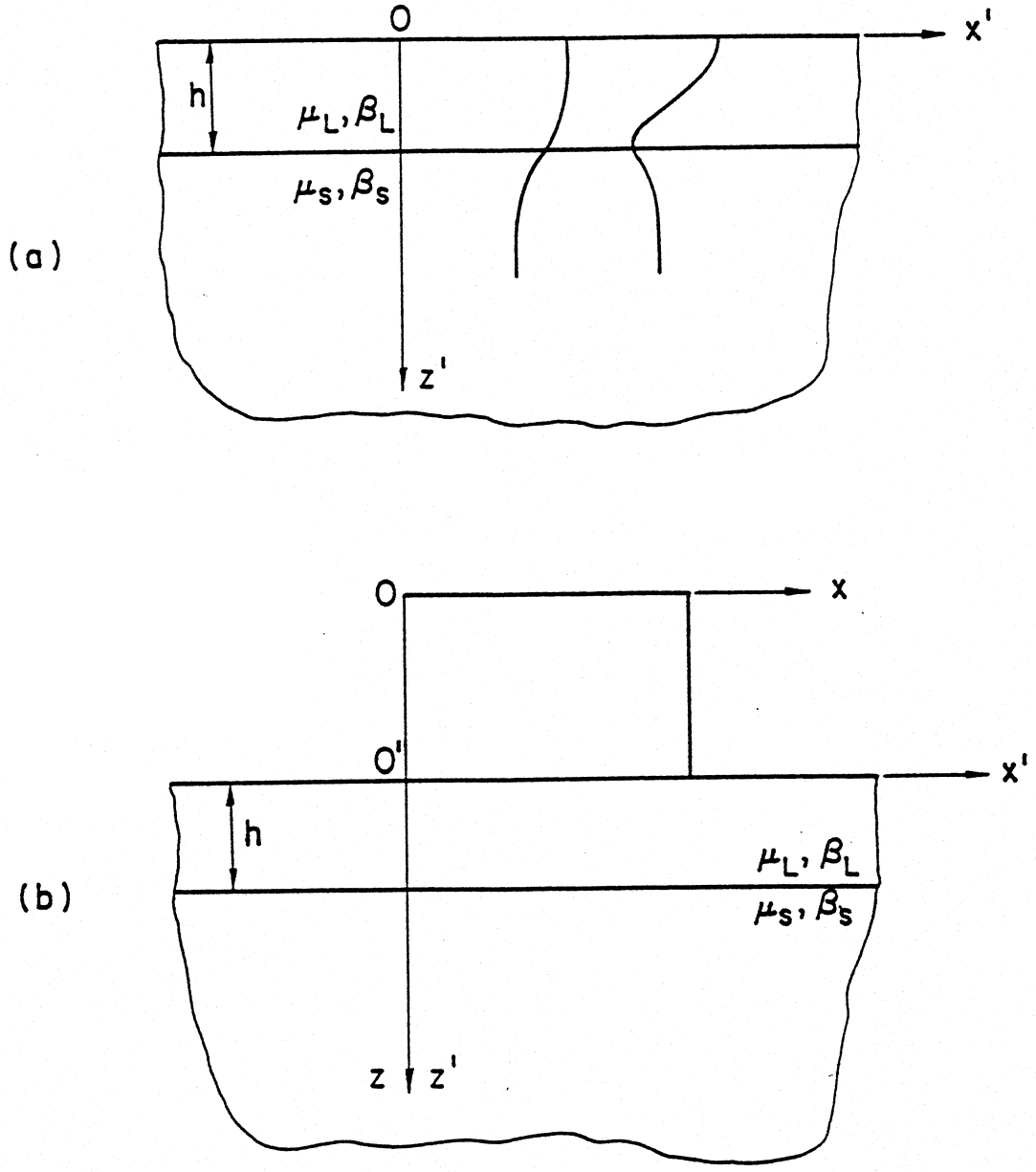

Figure 4.2.1 a) Homogeneous half-space with one soft surface layer of thickness h. The first two Love wave mode shapes are illustrated. b) A building placed over the layered half-space.

where q and b are defined as,

$$q = \frac{\omega}{c}\left[\left(\frac{c}{\beta_L}\right)^2 - 1\right]^{1/2} \tag{4.2.3}$$

$$b = \frac{\omega}{c}\left[1 - \left(\frac{c}{\beta_{HS}}\right)^2\right]^{1/2} \tag{4.2.4}$$

and

$$\begin{aligned} c &: \text{ the phase velocity in the horizontal direction} \\ \omega &: \text{ the circular frequency} \\ \beta_L &: \text{ shear wave velocity in the layer} \\ \beta_{HS} &: \text{ shear wave velocity in the half-space} \\ x', z' &: \text{ spatial coordinates} \\ t &: \text{ time coordinate} \quad . \end{aligned} \tag{4.2.5}$$

The constants A and B have to satisfy the following equation:

$$\begin{bmatrix} \cos qh & -e^{-bh} \\ \sin qh & -\frac{\mu_{HS} b}{\mu_L q} e^{-bh} \end{bmatrix} \begin{bmatrix} A \\ B \end{bmatrix} = \begin{bmatrix} 0 \\ 0 \end{bmatrix} \tag{4.2.6}$$

where h is the thickness of the layer, and the frequency ω has to satisfy the following frequency equation (Achenbach (1973))

$$\frac{\mu_{HS}\left[1 - \left(\frac{c}{\beta_{HS}}\right)\right]^{1/2}}{\mu_L\left[\left(\frac{c}{\beta_L}\right)^2 - 1\right]^{1/2}} = \tan\left\{\left[\left(\frac{c}{\beta_L}\right)^2 - 1\right]^{1/2} \frac{\omega h}{c}\right\} \tag{4.2.7}$$

where μ_L and μ_{HS} are the shear moduli in the layer and in the half-space, respectively. Figure 4.2.2 redrawn from Lee and Trifunac (1985) illustrates Love- and Rayleigh-wave phase velocity dispersion curves for a realistic site geology.

For a given frequency ω there is a finite number of roots $c_n(\omega), n = 1, \ldots, N(\omega)$ satisfying the frequency equation. To each root corresponds a Love mode shape $\psi(z, \omega)$,

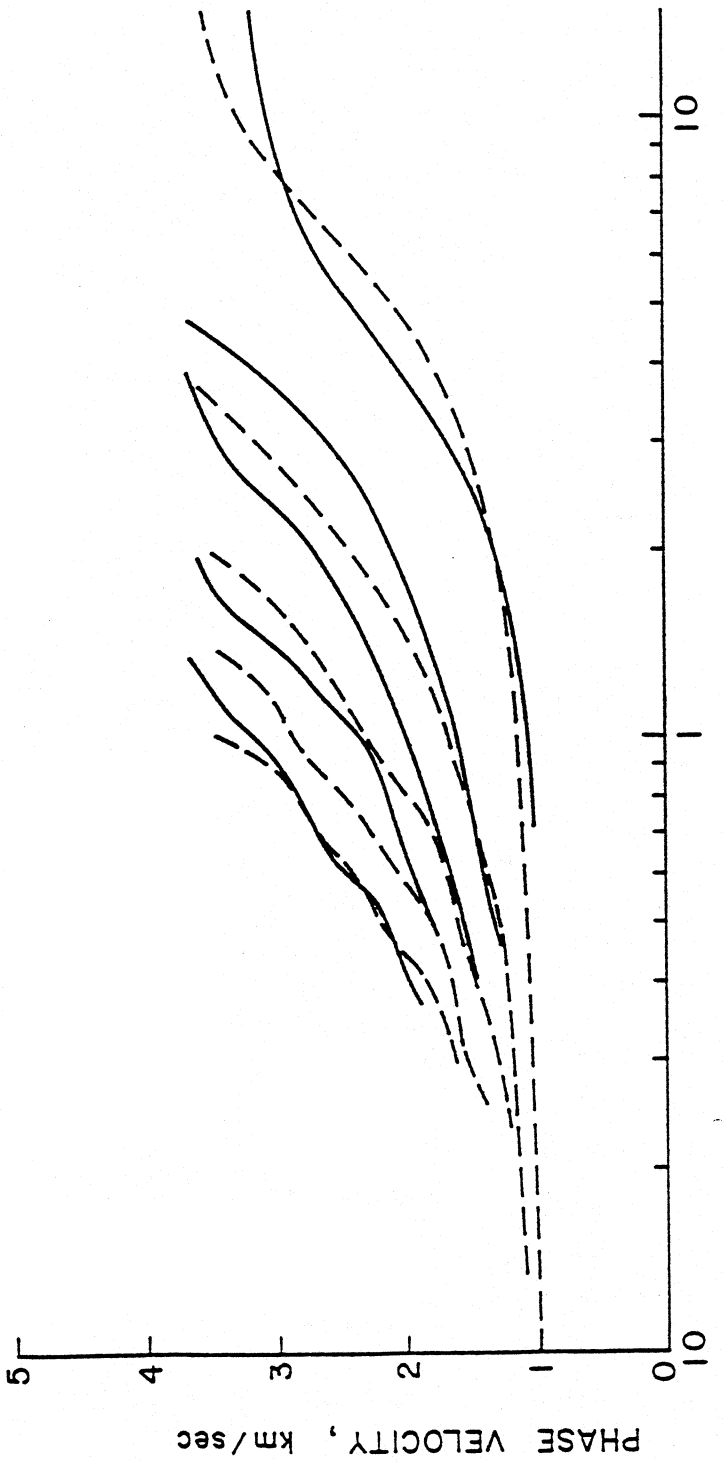

Figure 4.2.2 First five Love (dashed lines) and Rayleigh (full lines) wave phase velocity curves for El Centro site, California (after Lee and Trifunac, 1985).

that propagates with the phase velocity $c_n(\omega)$. All these modes form a basis and any Love wave motion of frequency ω has a unique representation of the form

$$v_s(x',z',\omega) = \sum_{n=1}^{N(\omega)} D_n(\omega)\psi_n(z',\omega)e^{i\omega\left(t-\frac{x'}{c_n(\omega)}\right)} \quad , \tag{4.2.8}$$

where

$$\psi_n(z',\omega) = \begin{cases} \cos(q_n(\omega)z') \quad , & 0 \le z' \le h \\ \cos(q_n(\omega)h)\cdot e^{b_n(\omega)(h-z')} \quad , & h < z' < \infty \end{cases} \tag{4.2.9}$$

and q_n and b_n are the values of q and b in equations (4.2.3) and (4.2.4), when $c = c_n(\omega)$.

In the time domain, the Love wave motion $v_s(x,z,t)$ can be represented by an integral over all the frequencies,

$$v_s(x',z',t) = \frac{1}{2\pi}\int_0^\infty F(\omega)\sum_{n=1}^{N(\omega)} D_n(\omega)\psi_n(z',\omega)e^{i\omega\left(t-\frac{x'}{c_n(\omega)}\right)}d\omega \quad , \tag{4.2.10}$$

where $F(\omega)$ as in section 4.1, is a Fourier transform of the time dependent part of the Love wave motion. At the free-surface all the mode shapes ψ_n have amplitudes equal to 1 and the displacement becomes

$$v_s(x',0,t) = \frac{1}{2\pi}\int_0^\infty F(\omega)\sum_{n=1}^{N(\omega)} D_n(\omega)e^{i\omega\left(t-\frac{x'}{c_n(\omega)}\right)}d\omega \quad . \tag{4.2.11}$$

Let a building be placed over the surface of the layer, and let the coordinate systems of the building be $(x,0,y)$ and of the soil $(x',0',y')$, as shown in Figure 4.2.1b. If the response of the building to the motion $e^{i\omega\left(t-\frac{z}{c_n(\omega)}\right)}$ at its base is denoted by $H(x,z,\omega,c_n(\omega))$, according to the transfer function theory, the response $v(x,z,t)$ to the general Love wave motion, given by equation (4.2.11), will be

$$v(x,z,t) = \frac{1}{2\pi}\int_0^\infty F(\omega)\sum_{n=1}^{N(\omega)} D_n(\omega)H\left(x,z,\omega,c_n(\omega)\right)d\omega \quad . \tag{4.2.12}$$

Again, in this case, the assumption of continuity of displacement only at the interface between the structure and the soil has been made.

Comparing the expressions for the response of the building for the general nondispersed and dispersed ground motion, the degree of complexity that the dispersion introduces into the problem becomes evident. Equation (4.2.9) is very impractical to solve numerically. However, it is the exact solution of the problem, under the assumptions stated above.

4.3 The Response of a Building Placed Over Inhomogeneous Soil

Investigations have shown (Trifunac, 1971a; Wong, 1979; Moeen-Vaziri and Trifunac, l986 1986) that the inhomogeneities in the soil may considerably influence the displacement of the ground motion on the surface of the earth. For example, inside alluvial deposits vibrational characteristics of the motion are present, as a result of the interference of the incoming waves with the waves reflected from the interfaces between the different media. For nearly horizontal incidence, both standing waves and propagating waves are present in front of alluvial valleys, while a shadow zone may be created behind them. Figure 4.3.2, redrawn from Moeen-Vaziri and Trifunac (1986), illustrates this phenomenon. It represents the displacement pattern, for incident plane SH-waves along the surface of an alluvium valley of irregular shape, shown in Figure 4.3.1 which is representative for the Los Angeles basin. In these two figures a_1 represents half of the width of the layer, μ, α, β and κ and μ_1, β_1, α_1 and κ_1 represent the shear moduli, P-wave velocities, shear-wave velocities and wave numbers in the half-space and in the layer, respectively. γ is the incident angle of the waves measured from the horizontal and η is the ratio between the width of the layer $(2a_1)$ and the wave length, λ, of the incident wave.

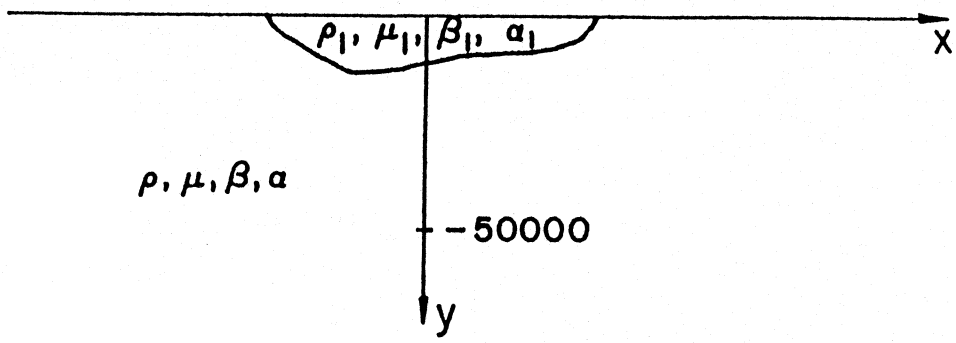

Figure 4.3.1 Typical cross-section of sedimentary layer in the Los Angeles basin (after Moeen-Vaziri and Trifunac, 1986).

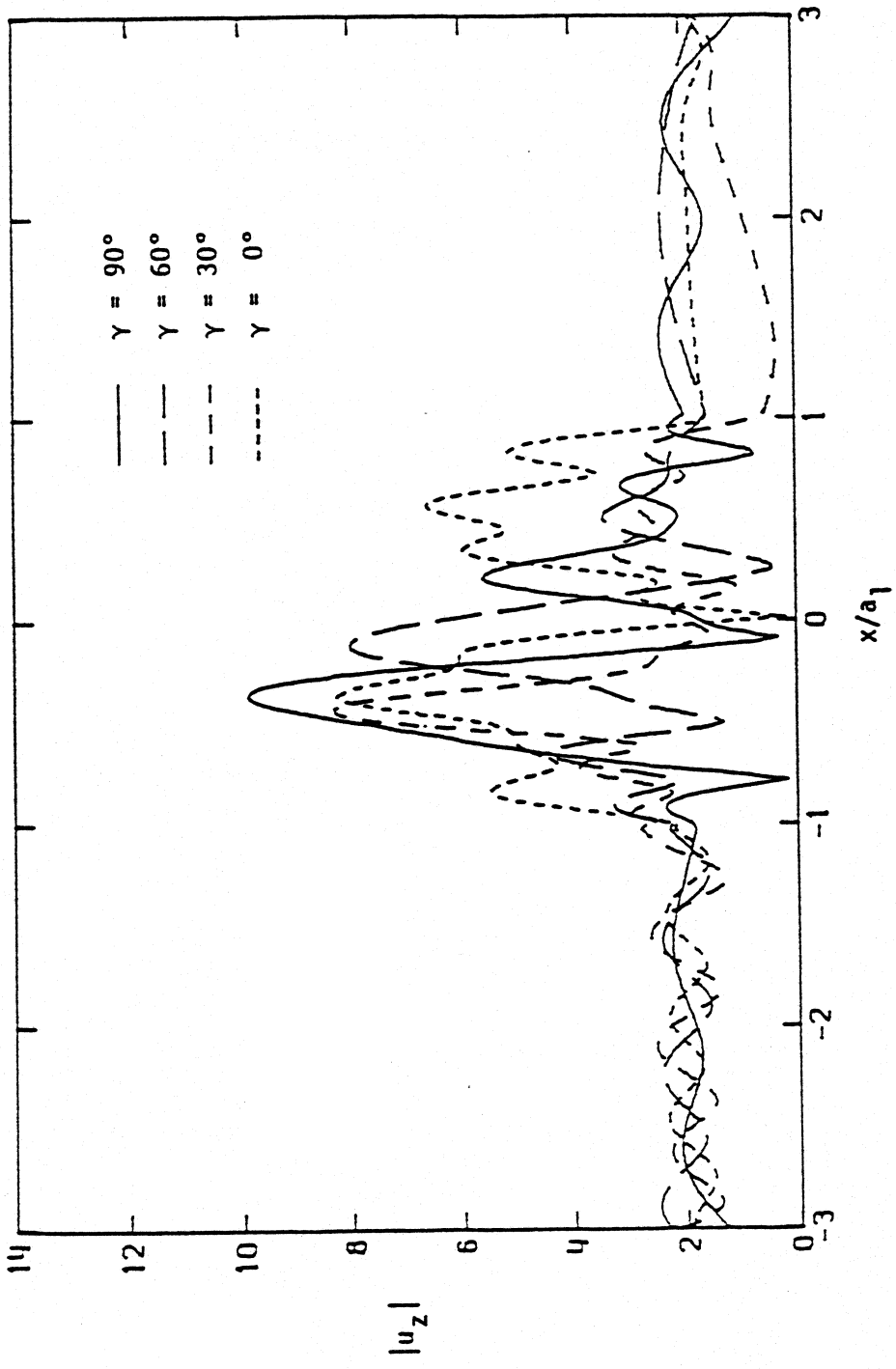

Figure 4.3.2 Surface displacement amplitudes, u_z, for surface layer shown in figure 4.3.1, for incident SH waves ($\eta = 2.0, \kappa_1/\kappa = 2.3, \mu_1/\mu = 0.144$). (After Moeen-Vaziri and Trifunac, 1986).

In this section a simple model of two quarter spaces with different material properties will be used to illustrate the nearly standing waves and the possible shadow zones of the ground displacement under the structure. The simplicity of this soil model will allow analytical form of the solution for the displacement of the building, modeled as in Chapter III.

4.3.1 The Displacement in the Half-Space Having a Vertical Discontinuity for Incident Plane SH Waves

The model consisting of two homogeneous, isotropic and perfectly bonded quarter spaces is shown in Figure 4.3.3. The shear modulus and the shear wave velocities in the media on the left and on the right of the discontinuity are μ_L, β_L and μ_R and β_R respectively. For an incident plane SH wave with angle of incidence γ the steady state displacement in the left medium v_L and in the medium on the right v_R satisfying the continuity of stresses and displacements at $x' = d$ can be expressed as

$$v_L = \left[A_o e^{i\omega\left(t-\frac{x'}{c_L}\right)} + A_1 e^{i\omega\left(t+\frac{x'}{c_L}\right)}\right] \cos\frac{\omega}{c_{z'}} z' \tag{4.3.1}$$

and

$$v_R = A_2 e^{i\omega\left(t-\frac{x'}{c_R}\right)} \cos\frac{\omega}{c'_z} z' \quad , \tag{4.3.2}$$

where

$$c_L = \frac{\beta_L}{\sin\gamma} \tag{4.3.3}$$

is the phase velocity in the x'-direction in the medium on the left and c_R is the phase velocity in the x'-direction in the medium on the right. $c_{z'}$ is the phase velocity in the z'-direction, and here for simplicity it is assumed to be the same for both media, implying the following relationship between c_L and c_R

$$\left(\frac{\omega}{\beta_L}\right)^2 - \left(\frac{\omega}{c_L}\right)^2 = \left(\frac{\omega}{\beta_R}\right)^2 - \left(\frac{\omega}{c_R}\right)^2 \quad . \tag{4.3.4}$$

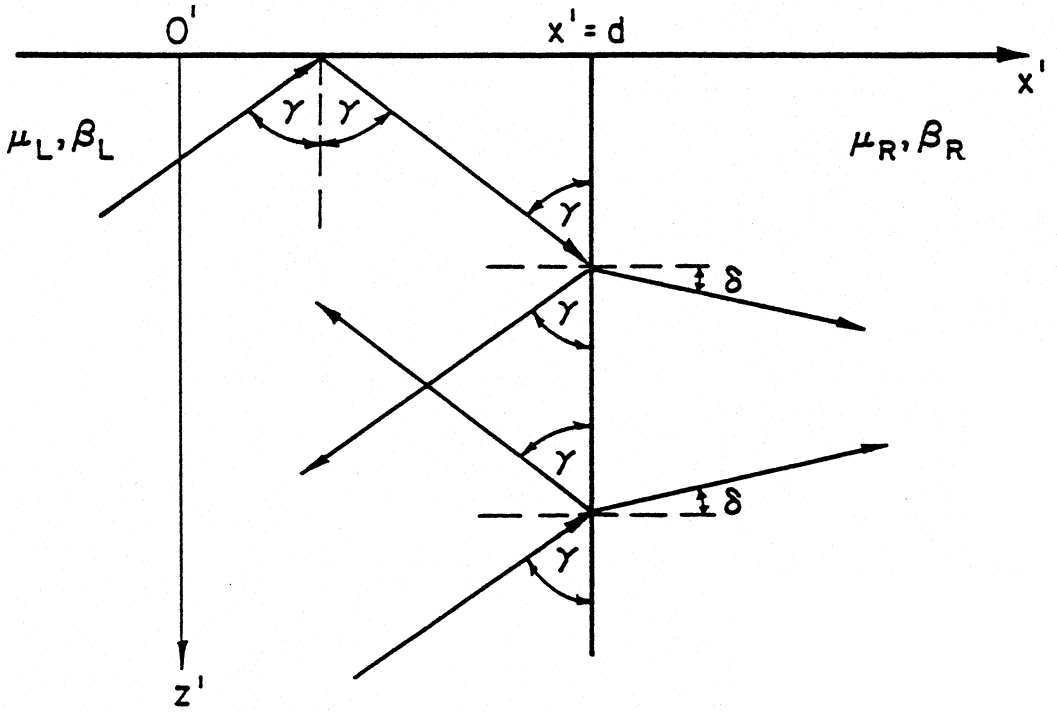

Figure 4.3.3 Half-space with vertical discontinuity at $x' = d$, and an incident plane SH-wave, propagating from left towards the discontinuity.

When the medium on the right hand side of the discontinuity is "harder" than the one of the left, i.e. $\beta_R > \beta_L$, the wave number $\frac{\omega}{c_R}$ in the medium on the right may be real or imaginary, depending on the incident angle γ. For real $\frac{\omega}{c_R}$

$$\frac{\omega}{c_R} = +\sqrt{\left(\frac{\omega}{\beta_R}\right)^2 - \left(\frac{\omega}{\beta_L}\right)^2 + \left(\frac{\omega}{c_L}\right)^2} \quad , \tag{4.3.5}$$

so that in the second medium there is a wave propagating to the right. If $\frac{\omega}{c_R}$ is imaginary,

$$\frac{\omega}{c_R} = -i\sqrt{\left|\left(\frac{\omega}{\beta_R}\right)^2 - \left(\frac{\omega}{\beta_L}\right)^2 + \left(\frac{\omega}{c_L}\right)^2\right|} \quad . \tag{4.3.6}$$

The continuity of stress and displacements at $x = d$ implies that

$$A_1 = A_0 e^{-2i\frac{\omega}{c_L}d} \frac{\frac{\mu_L}{\mu_R}\frac{\omega/c_L}{\omega/c_R} - 1}{\frac{\mu_L}{\mu_R}\frac{\omega/c_L}{\omega/c_R} + 1} \tag{4.3.7}$$

and

$$A_2 = A_0 e^{-i\left(\frac{\omega}{c_L} - \frac{\omega}{c_R}\right)d} \left(1 + \frac{\frac{\mu_L}{\mu_R}\frac{\omega/c_L}{\omega/c_R} - 1}{\frac{\mu_L}{\mu_R}\frac{\omega/c_L}{\omega/c_R} + 1}\right) \quad . \tag{4.3.8}$$

The resulting motion in the medium on the left is a standing wave together with a wave propagating in the positive x-direction, while the motion in the medium on the right is a wave propagating to the right, or a vibrating motion with exponentially decreasing amplitude in the positive x-direction. The displacement on the free surface may be written as

$$\begin{aligned} v_L\Big|_{z=0} &= 2A_o e^{2i\frac{\omega}{c_L}d} \frac{\frac{\mu_L}{\mu_R}\frac{\omega/c_L}{\omega/c_R} - 1}{\frac{\mu_L}{\mu_R}\frac{\omega/c_L}{\omega/c_R} + 1} \cos\frac{\omega x'}{c_L} \cdot e^{i\omega t} \\ &\quad + A_o \left(1 - e^{2i\frac{\omega}{c_L}d} \frac{\frac{\mu_L}{\mu_R}\frac{\omega/c_L}{\omega/c_R} - 1}{\frac{\mu_L}{\mu_R}\frac{\omega/c_L}{\omega/c_R} + 1}\right) e^{i\omega\left(t - \frac{x'}{c_L}\right)} \end{aligned} \tag{4.3.9}$$

and

$$v_R\Big|_{z=0} = \begin{cases} A_2 e^{i\omega\left(t - \frac{x'}{c_R}\right)} & \text{if } \frac{\omega}{c_R} \text{ real} \\ A_2 e^{-\left|\frac{\omega}{c_R}\right| x'} e^{i\omega t} & \text{if } \frac{\omega}{c_R} \text{ imag.} \end{cases} \tag{4.3.10}$$

where

$$A_2 = \begin{cases} A_o e^{-i\left(\frac{\omega}{c_L} - \frac{\omega}{c_R}\right)d} & \left(1 + \frac{\frac{\mu_L}{\mu_R}\frac{\omega/c_L}{\omega/c_R} - 1}{\frac{\mu_L}{\mu_R}\frac{\omega/c_L}{\omega/c_R} + 1}\right) \quad \text{if } \frac{\omega}{c_R} \text{ real} \\ A_o e^{-i\frac{\omega}{c_L}d} e^{\left|\frac{\omega}{c_R}\right|d} & \left(1 + \frac{\frac{\mu_L}{\mu_R}\frac{\omega/c_L}{\omega/c_R} - 1}{\frac{\mu_L}{\mu_R}\frac{\omega/c_L}{\omega/c_R} + 1}\right) \quad \text{if } \frac{\omega}{c_R} \text{ imag.} \end{cases} \tag{4.3.11}$$

A similar problem for Love waves hitting a vertical discontinuity in the half-space was studied by Sato (1961).

4.3.2 The Response of the Building

Let the building, represented by the homogeneous model, be placed over the half-space as shown in Figure 4.3.4. Using the same method and the models as in Chapter III (i.e. neglecting the continuity of stresses, the displacement in the building will be

$$v(x,z,t) = \sum_{n=0}^{\infty} C_n^* X_n(x) Z_n(z) e^{i\omega t} \tag{4.3.12}$$

where $X_n(x)$ and $Z_n(z), n = 0, 1, \ldots$ are the eigen-functions for the x and the z direction respectively, and the coefficients of the expansion C_n^*'s are

$$C_n^* = C_n / Z_n(H) \quad , \tag{4.3.13a}$$

where

$$C_n = \frac{(f(x), X_n(x))}{(X_n(x), X_n(x))} \quad , \tag{4.3.13b}$$

with the inner product $(\cdot, \cdot)$ defined as in Chapter III, and where $f(x)$ is the displacement at the base of the building. If the building is entirely situated over the soft medium, Figure 4.3.4a, i.e. $L < d$, and $d > 0$ then

$$f(x) = A_o e^{-i\frac{\omega}{c_L}x} + A_1 e^{i\frac{\omega}{c_L}x} \tag{4.3.14}$$

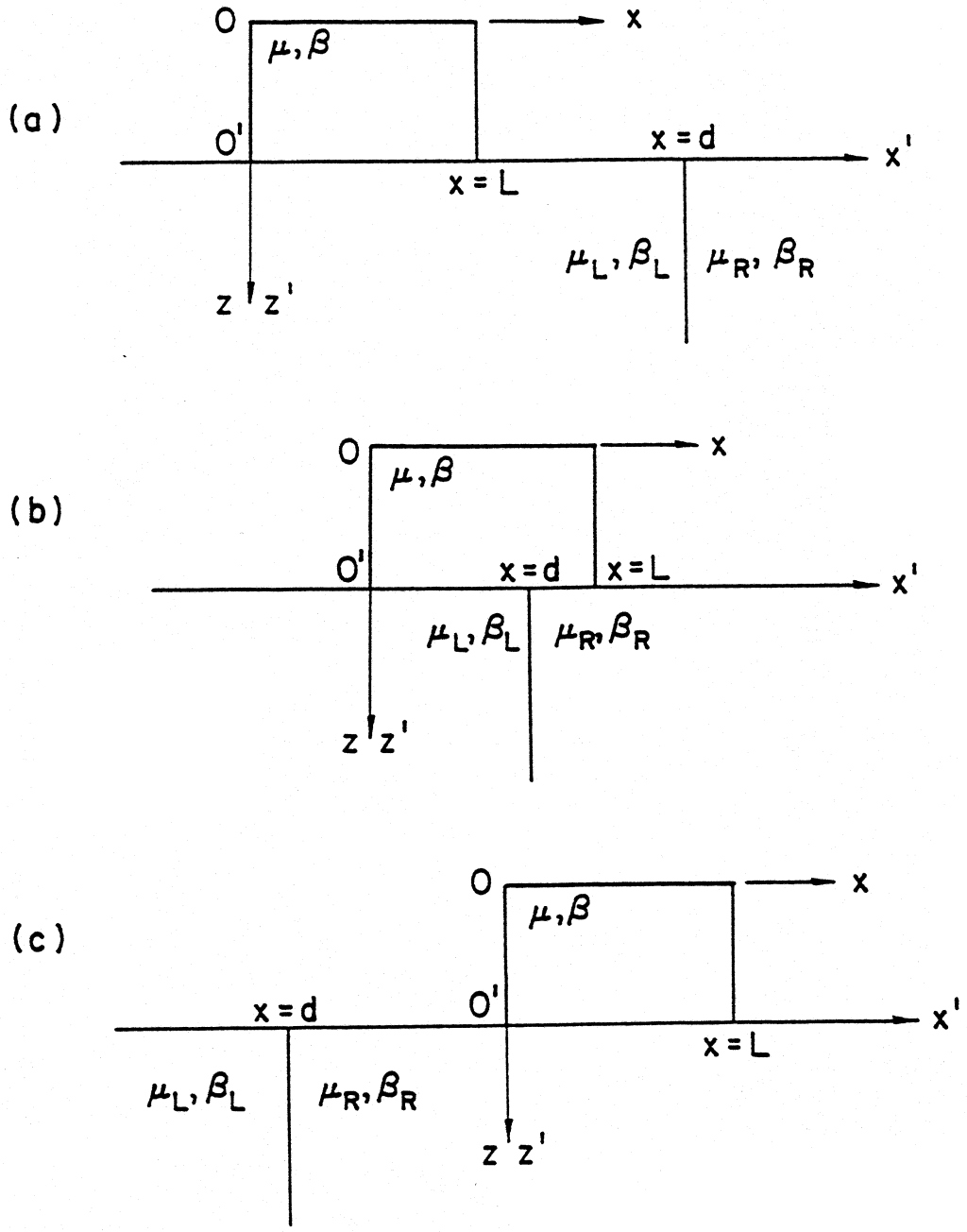

Figure 4.3.4 Half-space with vertical discontinuity and a building located: a) in front of the discontinuity, b) on the discontinuity, and c) behind the discontinuity.

If the building is partially situated on soft medium, i.e., $L \geq d > 0$, then

$$f(x) = \begin{cases} A_o e^{-i\frac{\omega}{c_L}x} + A_1 e^{i\frac{\omega}{c_L}x} & 0 \leq x \leq d \\ A_2 e^{-i\frac{\omega}{c_R}x} & d \leq x \leq L \end{cases} \tag{4.3.15}$$

If the building is entirely over the hard medium, as shown in Figure 4.3.4c, i.e. $d \leq 0$,

$$f(x) = A_2 e^{-i\frac{\omega}{c_R}x} \quad . \tag{4.3.16}$$

With this simple form of $f(x)$ the coefficients can be evaluated analytically (see Appendix F).

4.4 Response of the Building to Random Ground Motion

If the ground motion is assumed to be represented by a random process and the direction from which the waves come, as well as the spectral amplitudes are known only in terms of their statistical parameters, let

$$F(\tilde{c}, \tilde{A}) = P\{c \leq \tilde{c}, A \leq \tilde{A}\} \tag{4.4.1a}$$

and

$$f(c, A) = \frac{\partial^2}{\partial c \partial A} F(c, A) \tag{4.4.1b}$$

where

$$c = \frac{\beta_s}{\sin\gamma} \quad , \tag{4.4.2}$$

be the joint cummulative and density probability functions, respectively, of the phase velocity c in the x-direction and the amplitude A, of a plane monochromatic wave of frequency ω, hitting the homogeneous isotropic half-space (Figure 4.1.1), characterized by the shear wave velocity β_s. Then, if for a fixed ω the displacement response of the building v is given, as in Chapter III, by

$$v = A \sum_{n=0}^{\infty} C_n X_n(x) Z_n(z) e^{i\omega t} \tag{4.4.3}$$

by the Law of the Unconscious Statistician, (Grimmet and Stirzaker, 1985), the expected value (if it exists), of the response at a point in the building with coordinates x and z will be

$$\begin{aligned} E[v] &= \int_{-\infty}^{\infty}\int_{-\infty}^{\infty} A\sum_{n=0}^{\infty} C_n(\omega,c)X_n(x)Z_n(z) \\ &\qquad \cdot f\,(c,A)\,dcdA \\ &= \sum_{n=0}^{\infty}\left[\int_{-\infty}^{\infty}\int_{-\infty}^{\infty} AC_n(\omega,c)f\,(c,A)\,dcdA\right] \\ &\qquad \cdot X_n(x)Z_n(z)e^{i\omega t} \quad . \end{aligned} \tag{4.4.4}$$

If the spectral amplitude A is independent of the direction from which the waves are coming (i.e. independent of the phase velocity c), then (Grimmet and Stirzaker, 1985)

$$f\,(c,A) = f_c(c)\cdot f_A\,(A) \tag{4.4.5}$$

where $f_c(c)$ and $f_A\,(A)$ are the distribution density functions for c and A. In this case the expected value of the displacement of the building will be

$$\begin{aligned} E\,[v] &= \int_{-\infty}^{\infty} Af_A\,(A)\,dA \\ &\cdot\left[\sum_{n=0}^{\infty}\int_{-\infty}^{\infty} C_n(\omega,c)f_c(c)dc\right] X_n(x)Z_n(z)e^{i\omega t} \end{aligned} \tag{4.4.6}$$

and the variance of the spectral amplitude and of the phase velocity c will be

$$Var[A] = E[A^2] - (E[A])^2 \tag{4.4.7a}$$

$$Var[c] = E[c^2] - (E[c])^2 \tag{4.4.7b}$$

respectively, where

$$E[A^2] = \int_{-\infty}^{\infty} A^2 f_A\,(A)\,dA \tag{4.4.8a}$$

$$E[c^2] = \int_{-\infty}^{\infty} c^2 f_c(c)dc \tag{4.4.8b}$$

are the second moments (Grimmet and Stirzaker, 1985) of A and c.

CHAPTER V

RESULTS AND DISCUSSION

5.1 The Nature of Strong Ground Motion

Investigations have shown that most earthquakes in California are shallow, with the earthquake source lying not deeper than about 25 km. The region around the epicenter where the buildings are most threatened has a radius up to about 100-150 km for large damaging eathquakes. This means that if there are no major discontinuities in the earth's crust in the region between the source and the building, the earthquake energy can arrive at the site of the building in the form of body waves at angles θ (θ is the angle between the direction of propagation of the incident wave and the vertical) varying from zero, which happens when the building is directly above the source, up to very large angles, when the source is shallow and the building is far from the epicenter (Figure 5.1.1a). If there are soft layers near the earth's surface, and the building is not situated directly above the source, the seismic energy will be transmitted to the building site mainly in the form of surface waves (Figure 5.1.1b). Trifunac (1971b) has shown that from 70 percent to 90 percent of the seismic energy arriving at the building sites in California can come through the surface waves. In the figures mentioned, D is the distance between the epicenter and the building, d is the depth of the source and h is the thickness of the soft layer in the layered half-space.

The phase velocity in the horizontal direction c, can become infinite only in two cases, (1) when the earthquake waves arrive nearly vertically at the building site, which is possible if the source is deep under the building, or (2) when it is far from the building so that the first body waves arrive almost vertically because of the progressive bending of the rays up towards the vertical. This can result from the presence of low velocity surface layers. In the above two cases, the earthquake waves arrive at all points of the base of the building with the same phase. In all the other instances the phase velocities of the

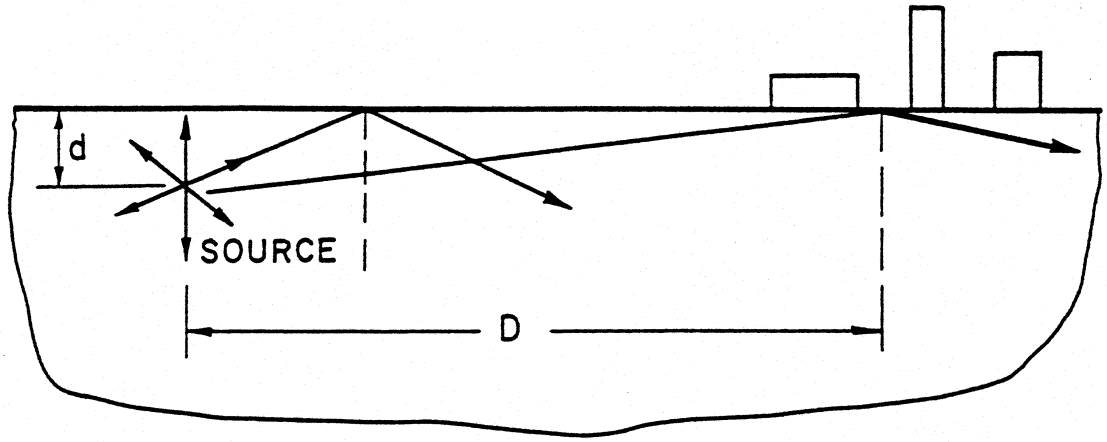

(a)

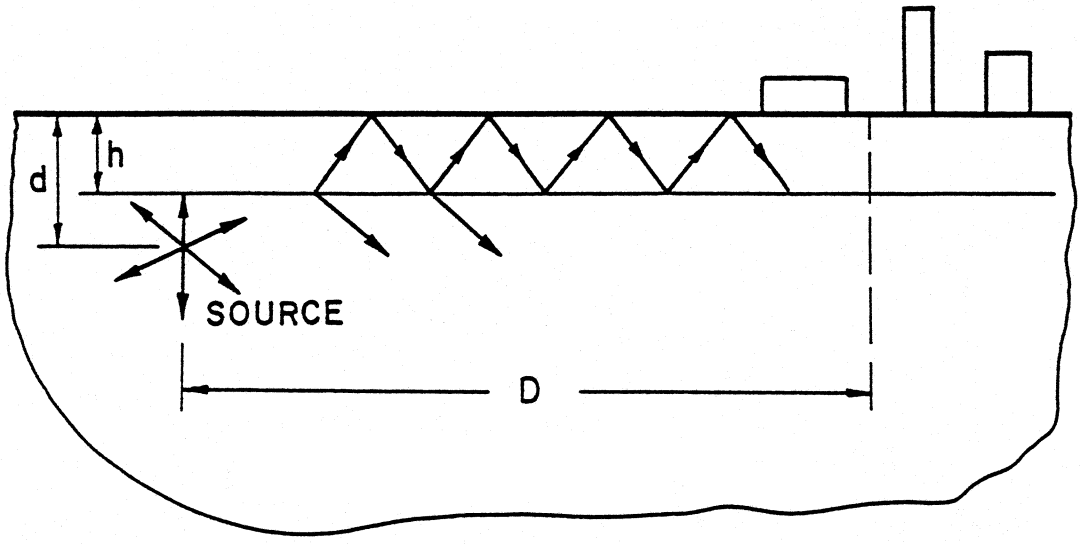

(b)

Figure 5.1.1 An illustration of the relative positions of the earthquake source and the building sites for typical earthquakes in California, considering: a) homogeneous half-space and b) layered half-space.

earthquake motion under the building will be finite and there will be phase difference in the motion at different points of the base. This fact, that the earthquake energy arrives the building sites with finite phase velocities in the horizontal direction, calls for the investigation of the various phenomena associated with the response of buildings to phased excitation at the base.

5.2 The Range of the Dimensionless Parameters

The phase velocity in the horizontal direction, c, was defined in Chapter III as the ratio between the shear wave velocity of the soil β_s and the sine of the incident angle θ. The minimum value of the shear wave velocity in the soil is about $\beta_{s,min} = 50$ m/s and the maximum value of $\sin\theta = 1$. This gives the minimum value of the phase velocity in the soil to be $c_{min} = 50$ m/s. The maximum value is $c_{max} = \infty$, and corresponds to the vertical incidence of seismic waves. The equivalent shear wave velocity in the building is in the range $500m/s \leq \beta \leq 1800$ m/s (Soviet Academy of Sciences (1986)). The analysis of 57 modern tall buildings in the Los Angeles area, Moslem and Trifunac (1987), for example, shows that the maximum length for most buildings in that area is $L_{max} = 80 - 100$ m.

Considering all the above facts and taking the value of 40 Hz to be the maximum frequency of interest in the spectrum of the earthquake waves, the range of the dimensionless length η, (defined in Chapter III, Section 3.2.3), becomes $0 \leq \eta \leq 60$.

In the calculations considered in this work the maximum value of η is 4. No higher values of η were needed, because all physical phenomena associated with the wave passage under the building are evident even for $\eta = 2$.

The values of the dimensionless phase velocity c/β, (defined in Section 3.2.3), are in the range $0.03 \leq c/\beta < \infty$. The following values: $c/\beta = 0.05, 1, 20$ were used in the

calculations. The value of the dimensionless phase velocity c/β will play an important role in connection with the transfer of energy from the ground into the building. This will be shown in Section 5.3.

The range of the height-to-length ratio for long buildings, that are of interest in this investigation, can be roughly estimated to be $.25 \leq H/L \leq 3$. The values $H/L = 0.25$, 1 and 2 were used in the calculations.

5.3 The Transfer of the Energy of Ground Motion into Continuous Structural Systems

Let a building be represented by a two-dimensional elastic plate of length L and height H placed over the homogeneous half-space. When an incident SH wave hits the interface between the two different media, it will be partially reflected back into the half-space and partially transmitted into the other medium. The incident angle γ and the refracted angle α (Figure 5.3.1) have to satisfy the Snell's law (Achenbach (1973))

$$\frac{\sin\alpha}{\sin\gamma} = \frac{\beta}{\beta_s} \tag{5.3.1}$$

where β and β_s are the shear wave velocities of the plate and of the half-space, respectively. Having in mind that the ratio $\beta_s/\sin\gamma$ is equal to the phase velocity in the horizontal direction, the Snell's law can be written in the following form:

$$\sin\alpha = \frac{\beta}{c} \quad . \tag{5.3.2}$$

From the above equation it can be seen that the refracted angle α is real only if $\beta \leq c$. If $\beta > c$, α takes on imaginary values and the wave in the plate will be inhomogeneous instead of progressive, having exponentially decreasing amplitude towards the top of the plate, meaning that no energy will be transferred into the plate. Hudson (1961) has proved

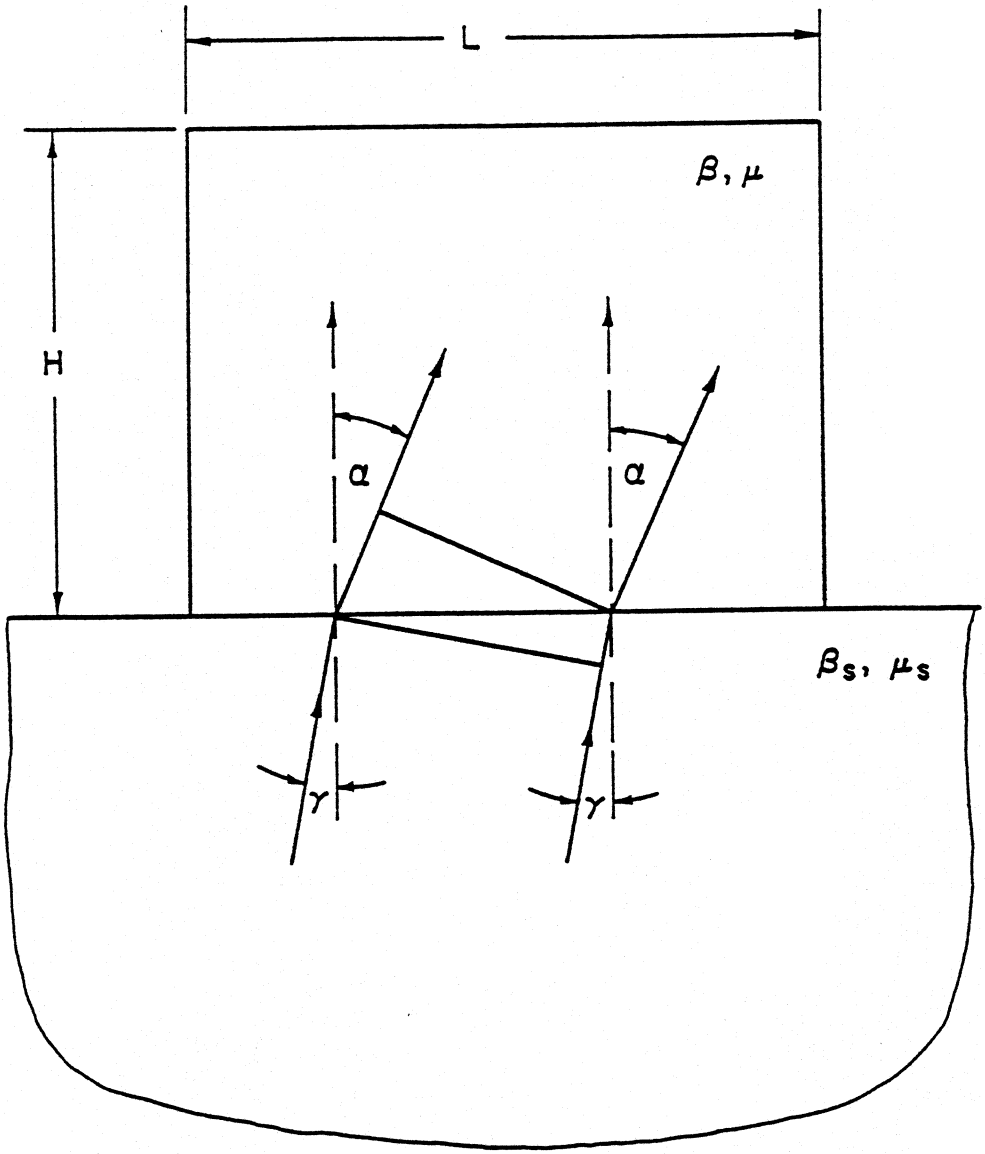

Figure 5.3.1 Refraction of a plane earthquake wave at the interface between the half-space and the building, modeled as a homogeneous, two-dimensional, elastic plate.

for the case of Love waves in a layer, that the energy transmitted from the layer into the half-space, during half period, goes back into the layer during the other half period, and that the resultant energy that enters the half-space during the time of one period of motion is zero. A similar situation occurs in our case too.

The phenomenon of no transfer of energy into the building when the phase velocity of excitation c is greater than the equivalent shear wave velocity of the building can also be explained using the semi-infinite models described in Chapter III. The prescribed displacement at $z = H$ represents a one-dimensional wave propagating with velocity c in the x-direction. According to the Hygens-Fresnel principle in optics, every point of the layer at $z = H$ acts as a point source of a wave of frequency ω and there is phase delay between them, as shown in Figure 5.3.2. The wave front of the wave in the plate is the envelope of the wave fronts of the elementary waves originated from the point sources having the same phase. Let us consider two points on the wave front passing through the points B and C. The point source at B will have the same phase as the point source at A after time $t = \bar{AB}/c$, where $\bar{AB}$ denotes the distance between the points A and B. During the same time the wave from the source at A will travel distance $\bar{AC} = \beta t$, which after substituting the t becomes

$$\bar{AC} = \frac{\beta}{c}\bar{AB} \quad .$$

Then, the angle between the normal N to the line $z = H$ and the direction of propagation of the wave in the plate can be calculated as follows:

$$\sin\alpha = \frac{\beta}{c} \quad . \tag{5.3.2}$$

α will have real values only if $c \geq \beta$, and only then, energy will be transmitted from the body forcing the motion of the plate into the plate.

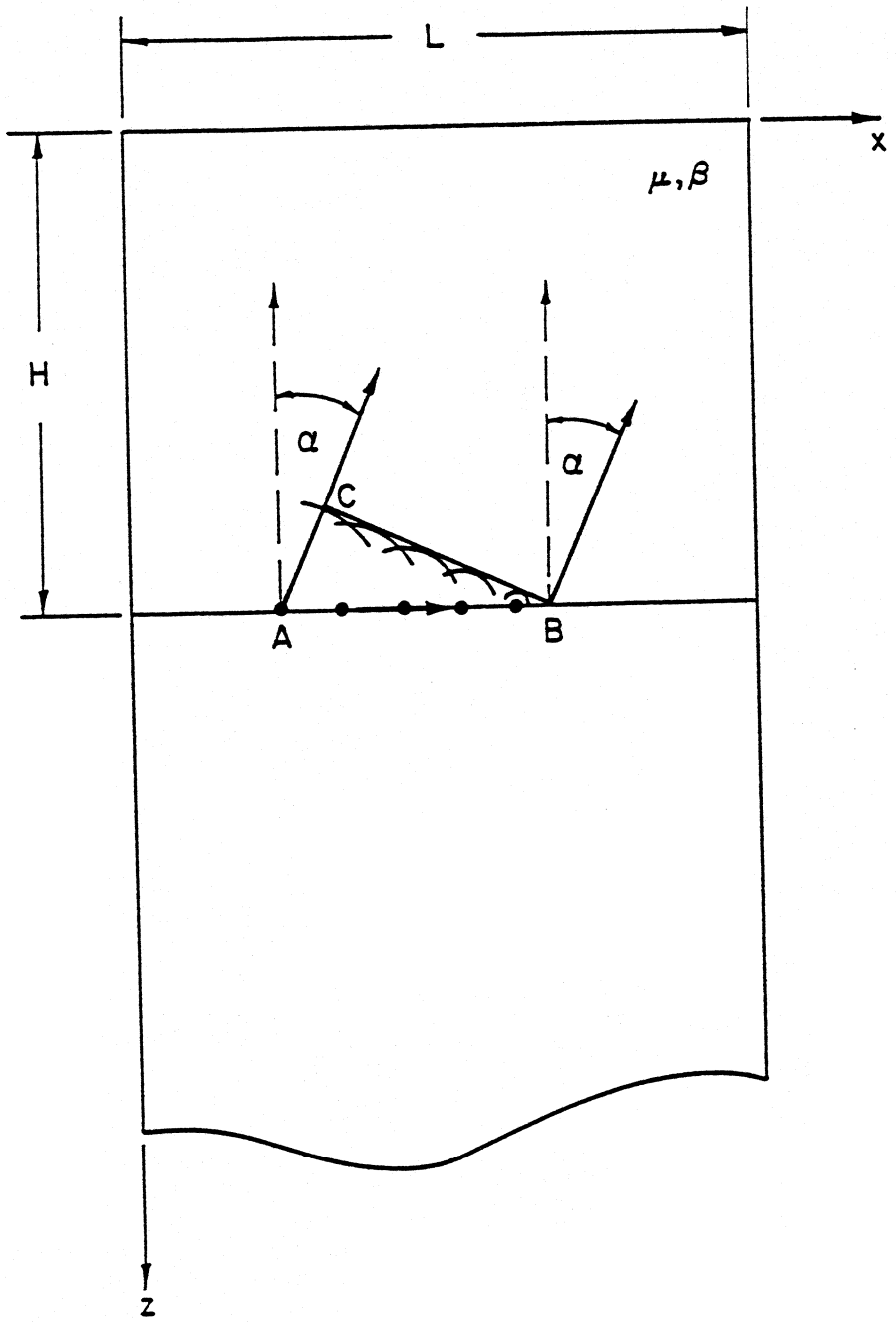

Figure 5.3.2 An illustration of the transfer of wave energy from the ground into the building for homogeneous building modeled as an elastic semi-infinite layer with displacement $e^{i\omega(t-\frac{x}{c})}$ at $z = H$.

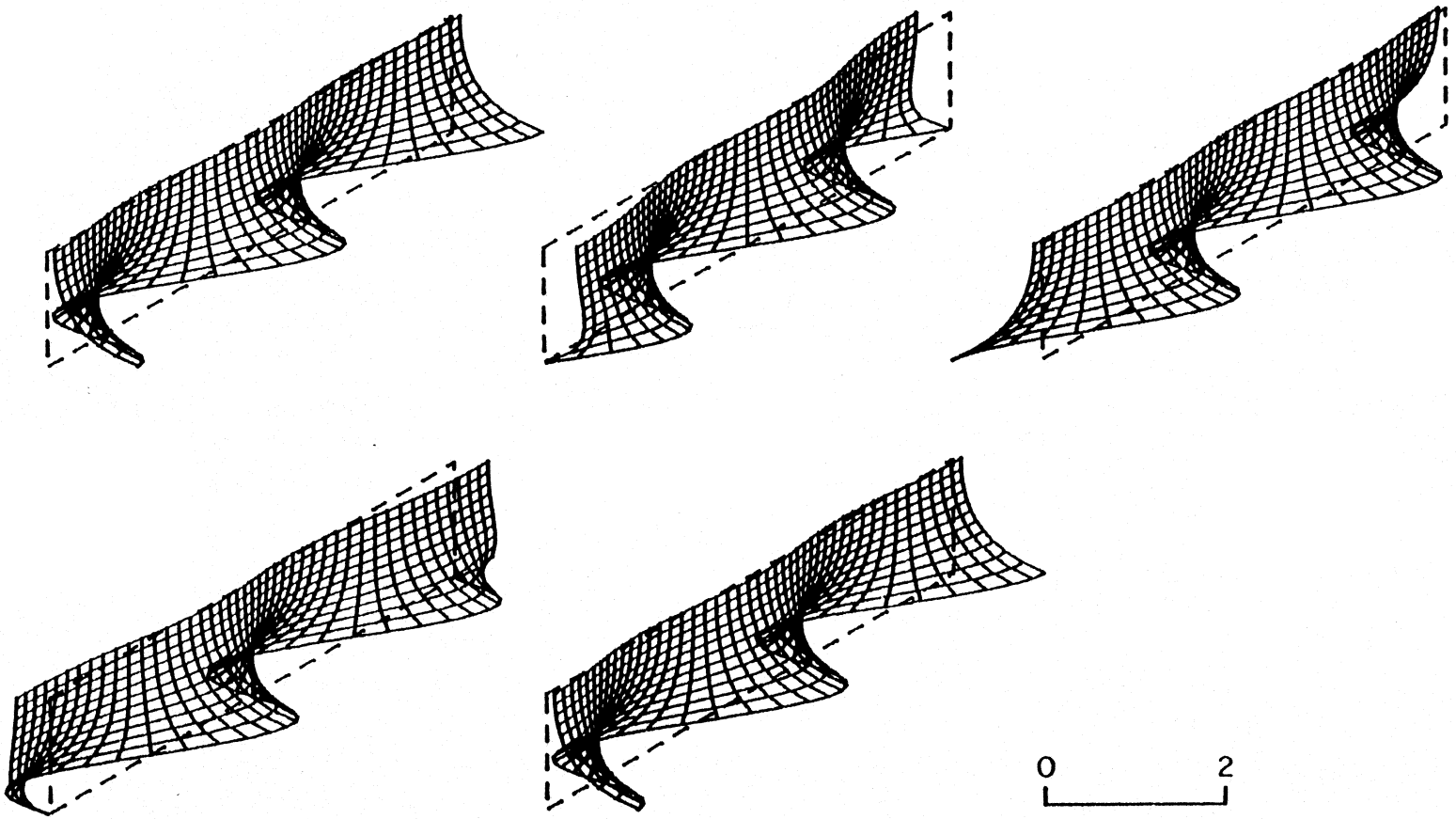

Figure 5.3.3 Displacement response of a long building ($H/L = 0.25$), represented by the homogeneous model, for propagating SH-waves ($\eta = 2$ and $c/\beta = 0.05$), at times $t = 0, T/4, T/2, 3T/4$ and T. The wave energy does not "enter" into the building, as can be seen from the exponential nature of the displacements along vertical lines.

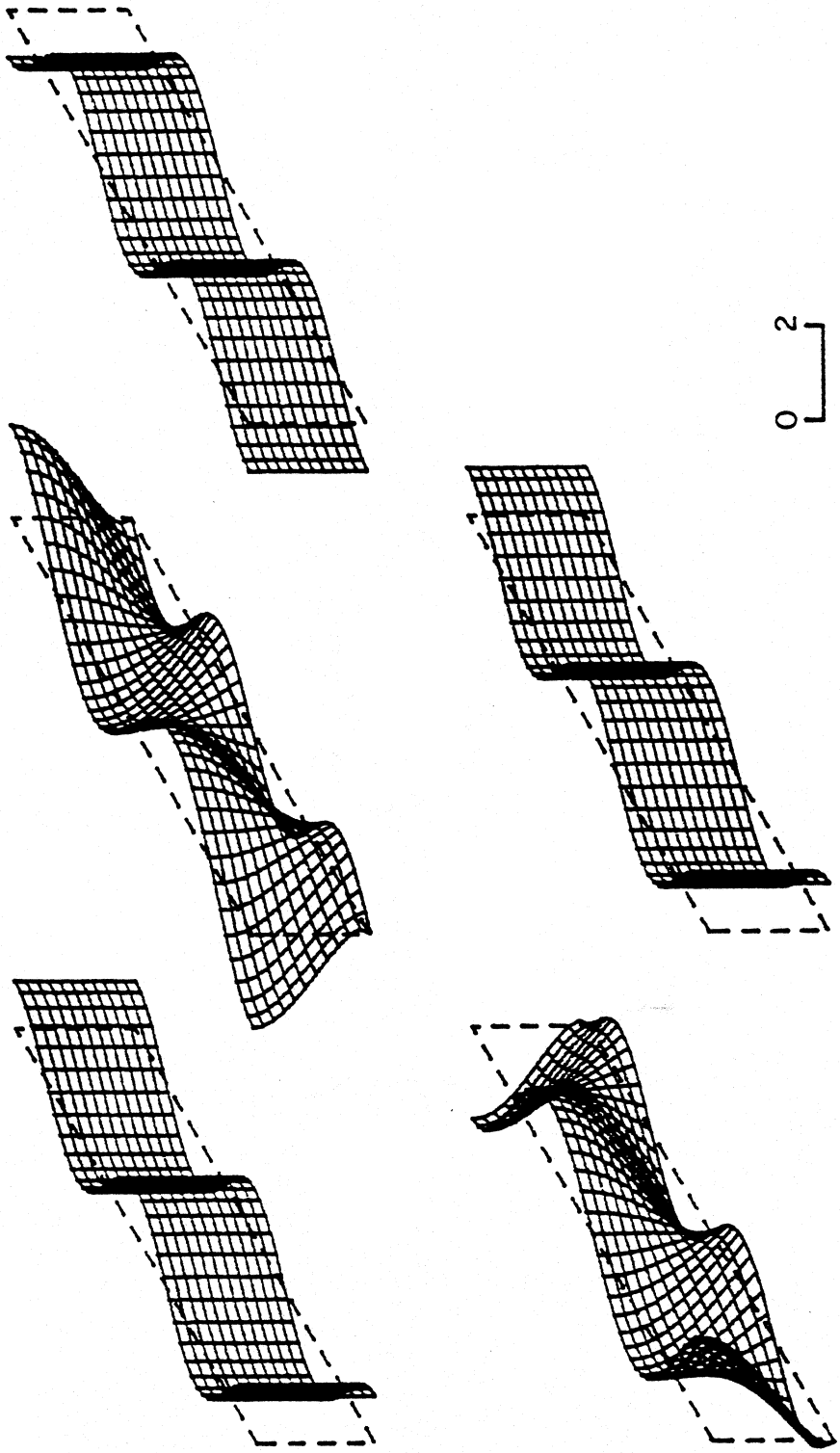

Figure 5.3.4 Displacement response of a long building ($H/L = 0.25$), represented by the homogeneous model, for propagating SH-waves at its base ($\eta = 2$ and $c/\beta = 1$), at times $t = 0, T/4, T/2, 3T/4$ and T. In this example the wave energy "enters" into the building.

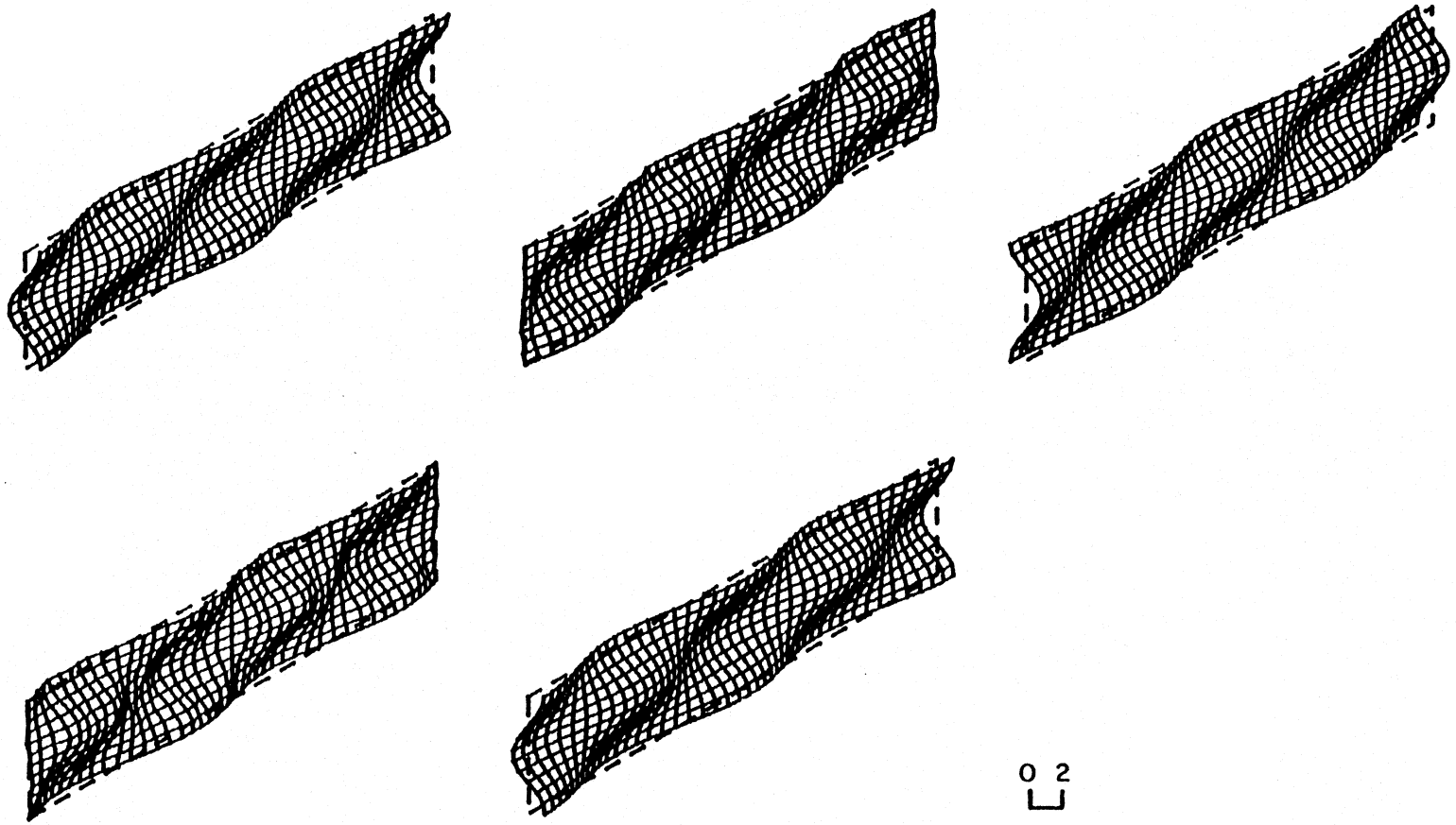

Figure 5.3.5 Displacement response of a long building ($H/L = 0.25$), represented by the homogeneous model, for propagating SH-waves at its base ($\eta = 2$ and $c/\beta = 20$), at times $t = 0, T/4, T/2, 3T/4$ and T. The wave energy "enters" into the building.

Figures 5.3.3, 5.3.4 and 5.3.5 illustrate the dependence of the transfer of energy into the building on the ratio c/β. They represent the displacements of a vertical cross-section of a long building ($H/L = 0.25$) at times equal to $0, T/4, T/2, 3T/4$ and T, where T is the period of the incident wave motion. The amplitude of the incident wave is 0.5, (i.e. the amplitude of surface displacement is 1.0), and the scale in this and in all the subsequent figures is in the same units as the displacement of the incident wave. From now one, this convention will hold for all figures of this type throughout this work. The homogeneous model described in Section 3.2 has been used to represent the building and these figures show the results for the ratios $c/\beta = 0.05, 1$ and 20, respectively and for $\eta = 2$. The figures show that when $c/\beta = 0.05$ the "hyperbolic" modes are dominant in the displacement. The displacement is the largest at the base and exponentially decays towards the top of the building (Figure 5.3.3). When $c/\beta = 1$ is can be seen from the figures that the "harmonic" modes are dominant in the displacement and that energy is entering this building. When $c/\beta = 20$ even the direction of propagation of the transmitted wave can be recognized from the displacement pattern.

5.4 Excitation of Symmetric and Anti-Symmetric Modes of Vibration

The variety of modes, symmetric as well as anti-symmetric with respect to the center of the building, are used to represent the displacement response, for almost any base excitation. Thus for seismic densign of large buildings it is important to understand how the passage of seismic waves excites different modes of response.

In the discussion of the analytical expressions for the displacement response of the homogeneous model in Section 3.2.2 it was shown that, in general, all the modes of vibration are excited. Both symmetric and anti-symmetric modes (with respect to $x = L/2$) contribute to the overall displacement even when the wave number ω/c of the

input motion equals the wave number k_x of one of the modes. However, when the waves arrive vertically at the base of the building, i.e. $\omega/c = 0$, only the first symmetric mode is excited and the problem becomes one-dimensional. This means that the "traditional" analysis of the response of buildings to strong ground motion neglects the fact that the higher x modes of vibration participate in the response of the building.

In section 3.2.2, the resonant frequencies ω_{nk} were defined as frequencies at which the displacement of the homogeneous plate becomes infinite. Realistic buildings possess damping, and therefore the more realistic continuous model would be made of visco-elastic medium. The effect of the damping can be added to the theory of the undamped model as a "perturbation" that will change, but not significantly, the resonant frequencies and the Fourier coefficients of the expansion of the displacement. At the resonant frequencies such a model will experience finite, but still large displacements, that can lead to large forces in the structure.

The frequency content of the earthquake waves is continuous and extends from 0 Hz and practically up to 30 or 40 Hz. High frequencies are present in the Fourier spectrum of the earthquake source, but will have small amplitudes by the time they reach a building.

In Figure 5.4.1 the resonant frequencies corresponding to the first 6 modes in the x-direction and the first 3 modes in the y-direction ($n = 0, 1, \ldots, 5$ and $k = 0, 1$ and 2), in the range 0-60 Hz, have been shown for a "long" building (L=100 m, H=25m) and for a "high" building (L=50 m, H=150 m). For the "long" building the resonant frequencies corresponding to $k = 0$ and $n = 0, \ldots, 5$ and $k = 1$ and $n = 0, \ldots, 4$ fall in this range. For the "high" building the case for $k = 0$ and $n = 0, \ldots, 3$, $k = 1$ and $n = 0, \ldots, 3$, and $k = 2$ and $n = 0, \ldots, 2$ are shown.

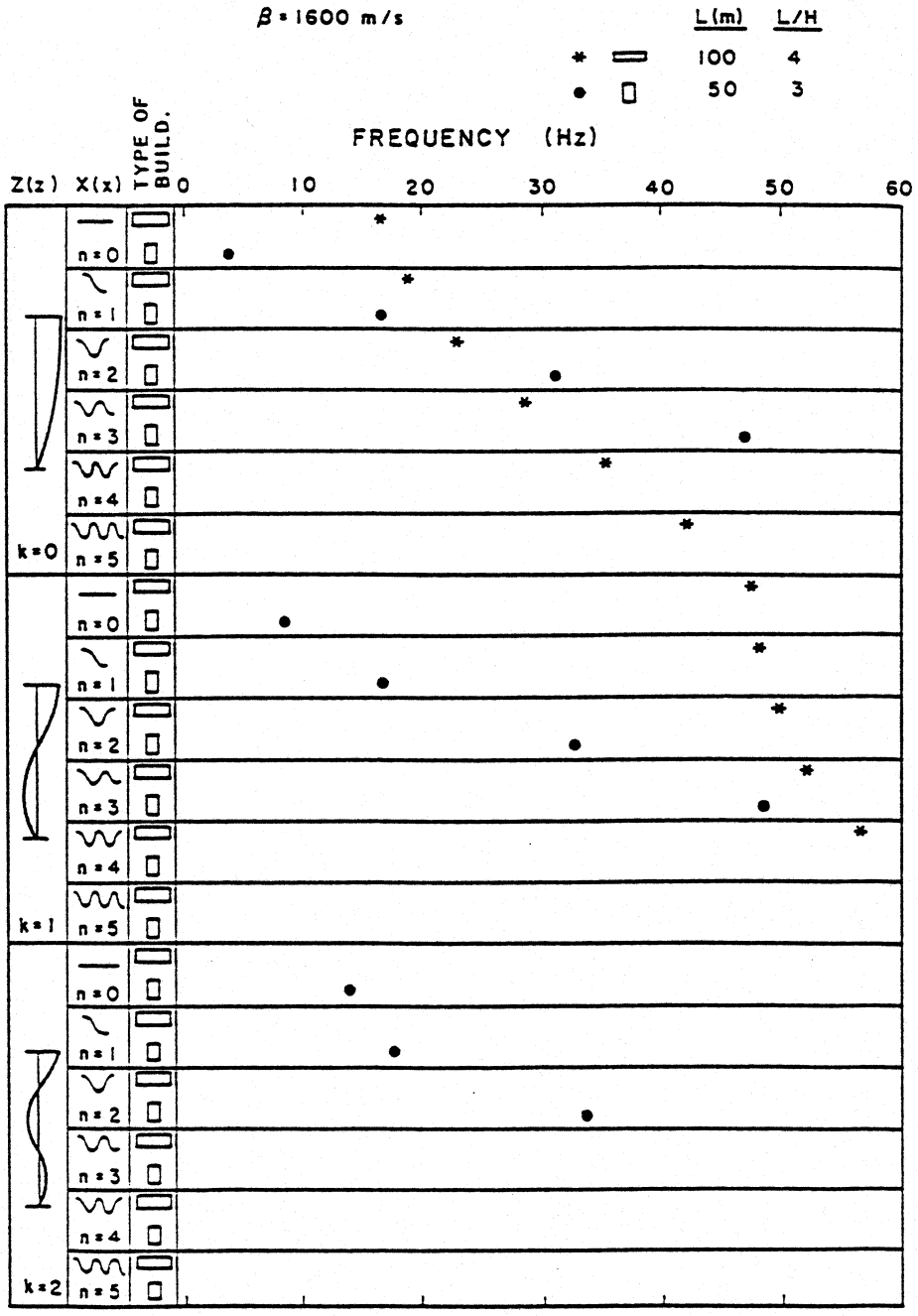

Figure 5.4.1 The resonant frequencies for the first few modes of a long and low, and of a long and high building ($H/L = 0.25$ and 3, respectively), represented by the homogeneous model, in the range between 0 and 60 Hz.

The building will vibrate with all frequencies that are in the range of significant amplitudes of the Fourier spectrum of the excitation, including the resonant frequencies. The contribution of the resonant frequencies to the displacement will depend on the amplitude of the Fourier spectrum of the excitation at that frequency and on the coefficients of the expansion $C_n^*(\omega, c)$. The displacements and the stresses at the resonant frequencies corresponding to the higher modes in x $(n \geq 1)$ can be very large, even larger than the ones corresponding to the first mode in x $(n = 0)$ and that are expected by the one-dimensional analysis. For design purposes, however, the one-dimensional models of the buildings are commonly used. This means that the buildings may not be designed for some loads that may occur during their life.

In Figures 5.4.2 through 5.4.5 examples of the displacement response of the homogeneous model to monochromatic waves passing underneath it have been shown. In each figure the out of plane displacement of a vertical cross-section of the "building" has been shown at five consecutive times: $t = 0, T/4, T/2$, $3T/4$ and T, where T is the period of the input wave. Figure 5.4.2 corresponds to the one-dimensional case, because of the small value of the dimensionless length η. Energy is being transmitted into the building, which can be expected because $c/\beta > 1$, but no anti-symmetric modes in x are excited, as seen from the figure.

Figures 5.4.3, 5.4.4 and 5.4.5 correspond to $\eta = 1$ and $c/\beta = 1$. It can be seen well from these figures how the contribution of the different modes changes, as the wave passes under the "building." At time $t = 0, T/2$ and T only one of the symmetric modes in x contributes to the displacement, and that is the one that has the wave number equal to ω/c. At time $t = T/4$ and $3T/4$ only antisymmetric modes in x contribute to the displacement, and moreover, the displacement at these two moments is larger than the displacement during $t = 0$, $t = T/2$ and $t = T$. The values of the stresses τ_{xy} and τ_{zy}

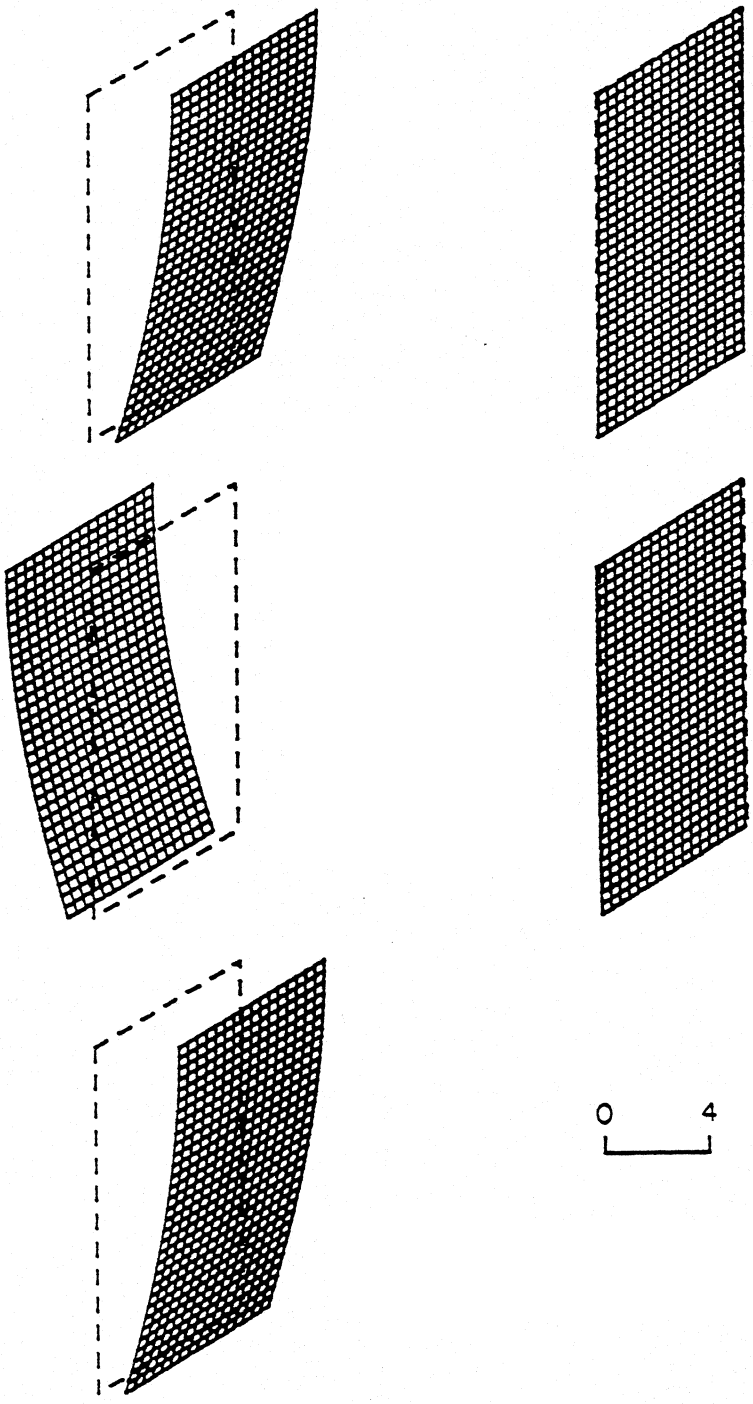

Figure 5.4.2 Displacement response of a long and high building ($H/L = 2$), represented by the homogeneous model, for nearly vertically incident SH-waves ($\eta = 0.01$ and $c/\beta = 10$), at times $t = 0, T/4, T/2, 3T/4$ and T. The anti-symmetric modes are not excited, as can be seen from the displacement patterns, because the wavelength of the incident waves along the x-axis is long compared to L.

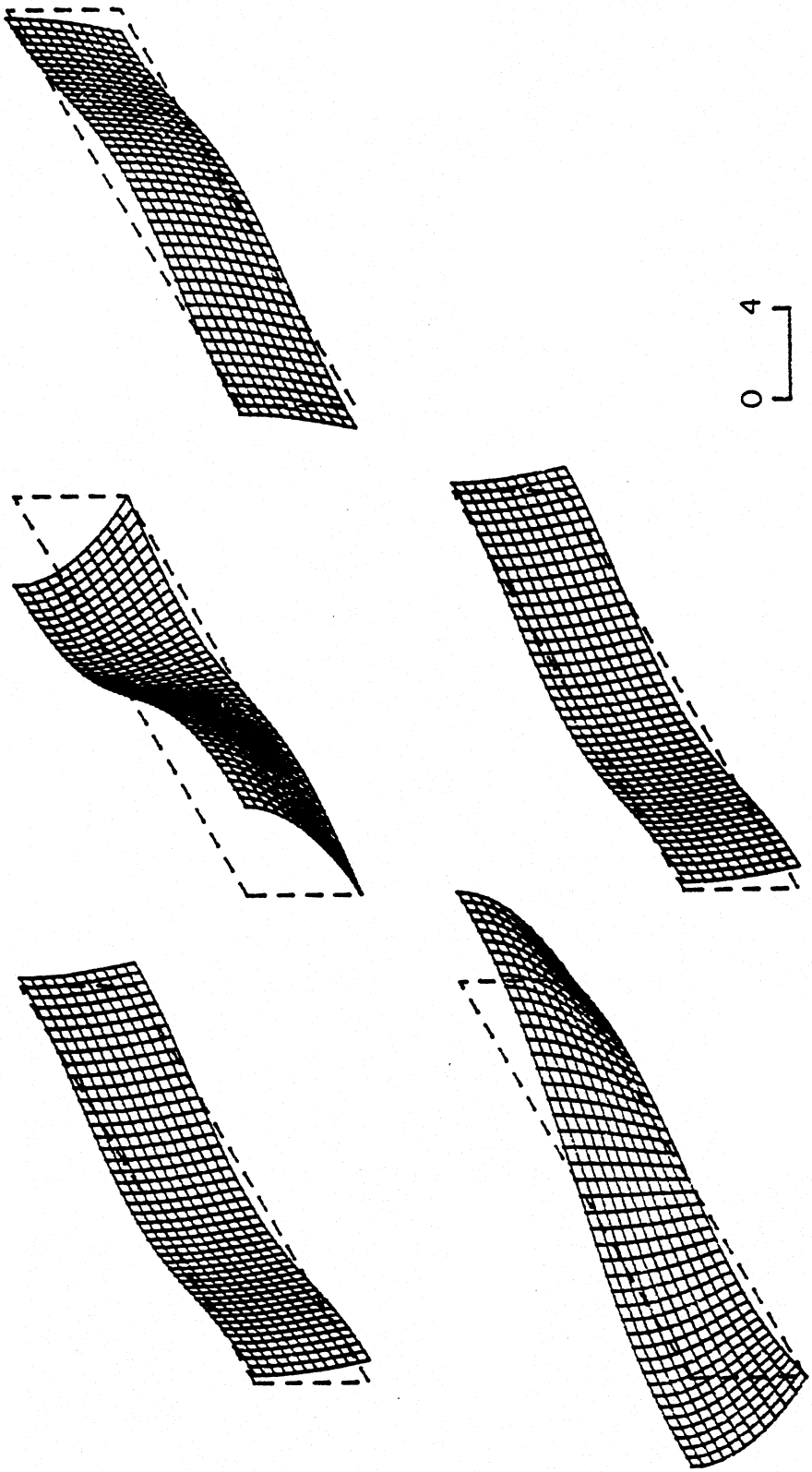

Figure 5.4.3 Displacement response of a long building $(H/L = 0.25)$, represented by the homogeneous model, for propagating SH-waves $(\eta = 1$ and $c/\beta = 1)$, at times $t = 0, T/4, T/2, 3T/4$ and T. Anti-symmetric modes of vibration are seen to contribute to the overall response.

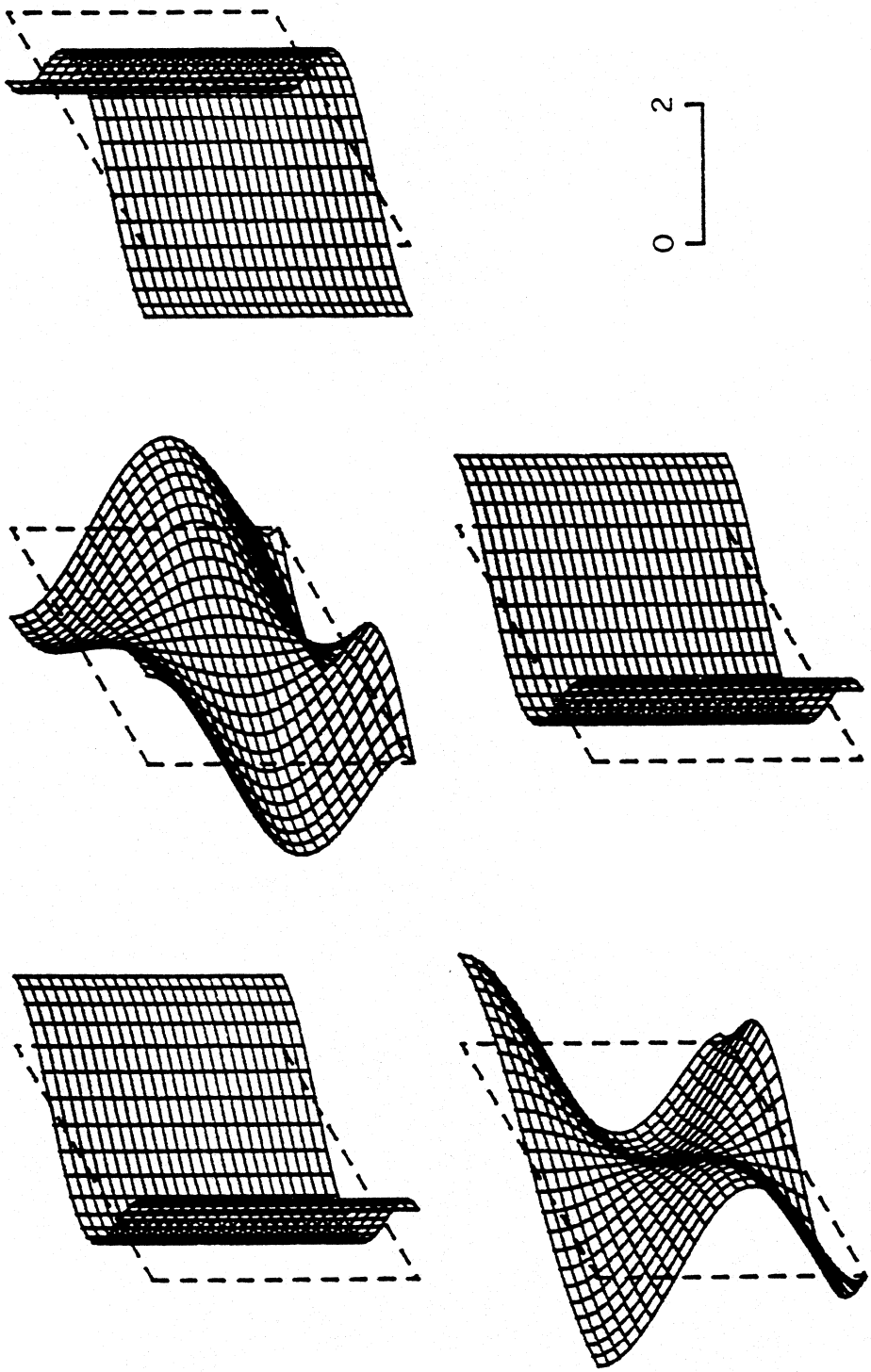

Figure 5.4.4 Displacement response of a building with comparable length and height ($H/L = 1$), represented by the homogeneous model, for propagating SH-waves ($\eta = 1$ and $c/\beta = 1$), at times $t = 0, T/4, T/2, 3T/4$ and T. Anti-symmetric modes of vibration contribute to the overall response.

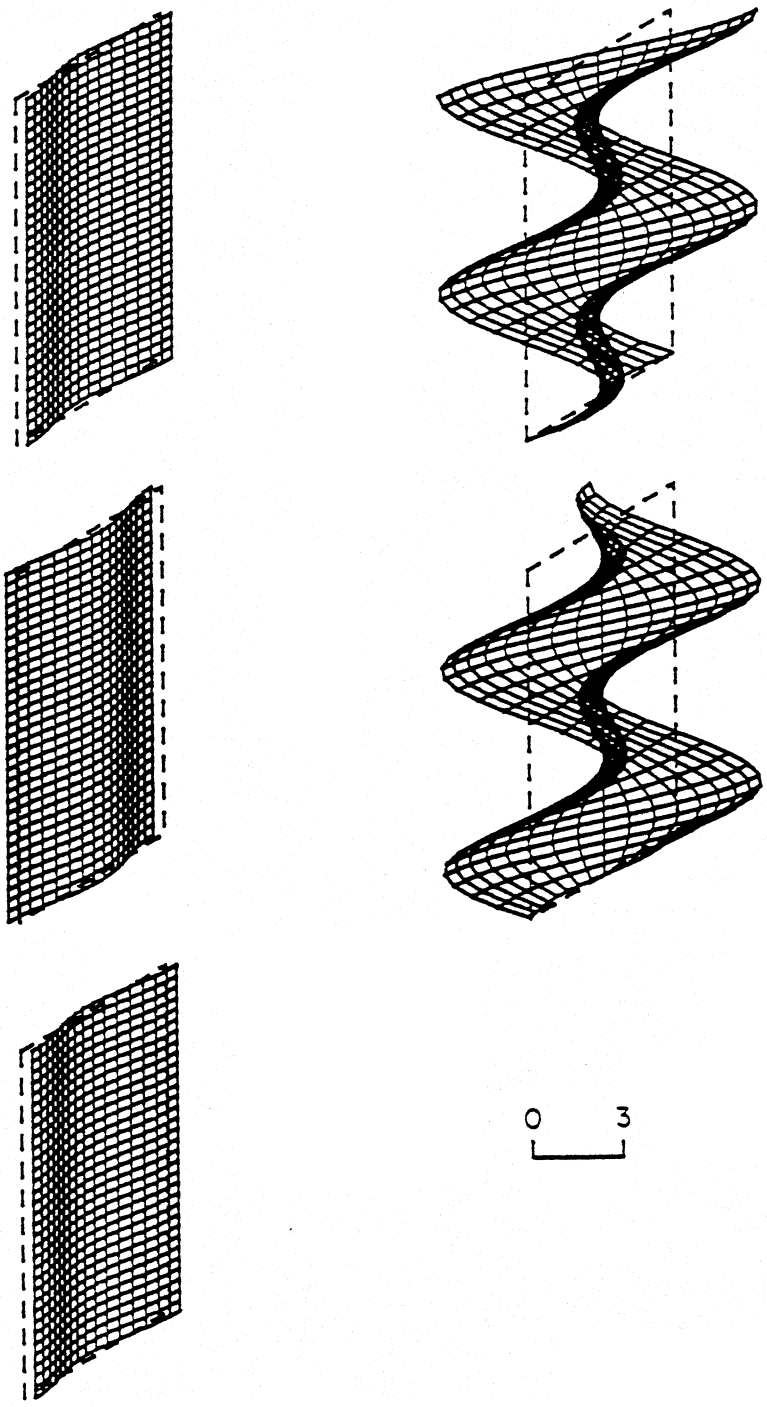

Figure 5.4.5 Displacement repsonse of a long and tall building ($H/L = 2$), represented by the homogeneous model, to propagating SH-waves ($\eta = 1$ and $c/\beta = 1$), at times $t = 0, T/4, T/2, 3T/4$ and T. Anti-symmetric modes of vibration are excited.

are also larger, because of the more "sudden" changes of the slope of the displacement patterns. It can be concluded that in the cases represented by these three figures, the anti-symmetric modes may be important for the response analysis of this building.

5.5 Discontinuities within the Structure

Major stiffness discontinuities within the building will change the distribution of the response amplitudes and the patterns of the displacement response of the building to the incident ground motion.

The analysis which was done in Chapter III showed that the mode shapes and their resonant frequencies are different for the homogeneous model and for the models with major vertical or horizontal stiffness discontinuities. This in turn changes the displacement amplitudes at certain frequencies of input ground motion and alters the contributions of different modes to the overall response. These discontinuities also may redistribute the stress concentrations throughout the building.

5.5.1 Buildings with Shear Walls at Two Ends

The displacement response of a building with shear walls at two ends (Figure 3.1.2b) and represented by the model in Figure 3.3.1, has been analyzed for incident monochromatic SH waves with $\eta = 0.01, 0.05, 0.1., 1$ and 2 (where $\eta = L/cT$, and T and c are the period and the horizontal phase velocity of the input ground motion). The values of the other parameters were: c/β_2=0.05, 1, 20 and 100; $\ell_1/L = \ell_1/L = 0.1$; and $H/L = .25, 1$ and 2. Three ratios of the shear wave velocites were chosen $\beta_i/\beta_1 = 2, 4$ and 10, $i = 1, 3$ (see Figure 3.3.1).

Selected examples of the response of these buildings are illustrated in Figures 5.5.1a through 5.5.7b. These figures again show the displacements of the vertical cross-section of the building at times $t = 0, T/4, T/2, 3T/4$ and T. The excitation is such that at time $t = 0$ the displacement of the base of the building is $\cos \frac{\omega x}{c}$.

Figures 5.5.1a, 5.5.2a and 5.5.3a are examples of the displacements of the buildings with symmetrically distributed stiffness ($\beta_1/\beta_2 = \beta_3/\beta_2 = 4$) to a wave with essentially vertical incidence ($\eta = 0.01, c/\beta_2 = 100$). The height to length ratios in these examples are 0.25, 1 and 2, respectively. For comparison, the displacements of these buildings, without the shear walls and for the same ground excitation are presented in Figures 5.5.1b, 5.5.2b and 5.5.3b, respectively.

It can be seen from Figures 5.5.1a, 5.5.2b and 5.5.3b how the shear walls confine the motion of the lateral sides of the building, and make it vibrate almost as a "membrane," fixed at three sides. The displacements are nearly symmetric in the horizontal direction (because of the nearly symmetric excitation and the symmetric distribution of the stiffness). Displacements increase away from the shear walls and are largest in the center at $x = L/2$. In the vertical direction, the displacement is largest on the top when $H/L = 0.25$ and in the inside of the building when $H/L = 1$ and 2. For the chosen frequency of the ground motion ($\frac{\omega L}{\beta_2} = 2\pi$ in all these three examples) the number of nodes and anti-nodes in the vertical direction depends on the ratio H/L.

Because of the small η, the displacements of the ground in the above three examples may be approximated by $\Delta e^{i\omega t}$ ($\Delta = 1$ in our case). The response of the corresponding buildings without discontinuities is almost symmetric in the x-direction and one dimensional models in the z-direction would be appropriate for the response analysis. On the

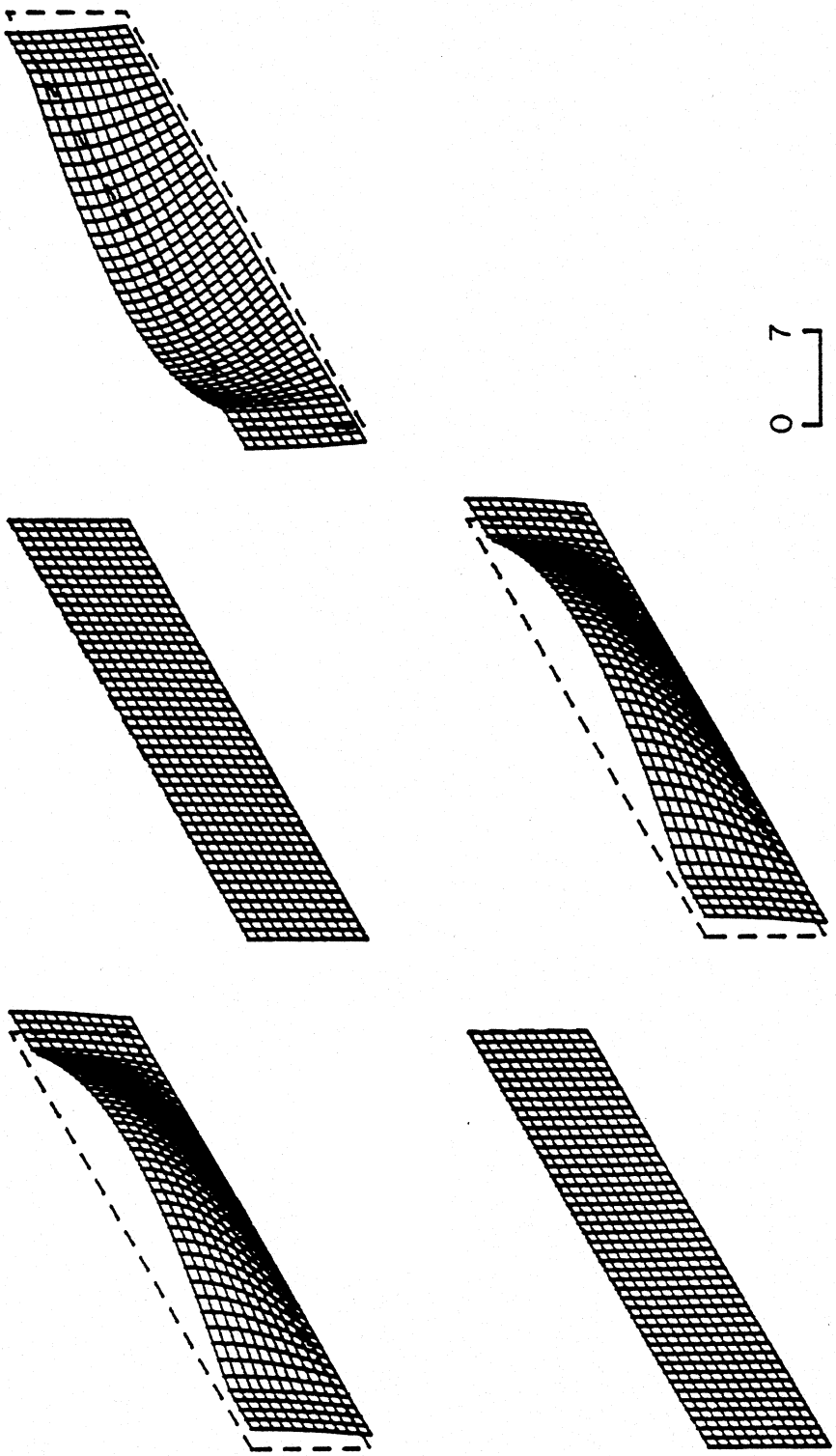

Figure 5.5.1a Displacement response of a long building $(H/L = 0.25)$ with shear walls at its ends $(\ell_1/L = \ell_1/L = 0.1$ and $\beta_1/\beta_2 = \beta_3/\beta_2 = 4)$ for nearly vertically incident SH-waves ($\eta = 0.01$ and $c/\beta_2 = 100$) at times $t = 0, T/4, T/2, 3T/4$ and T.

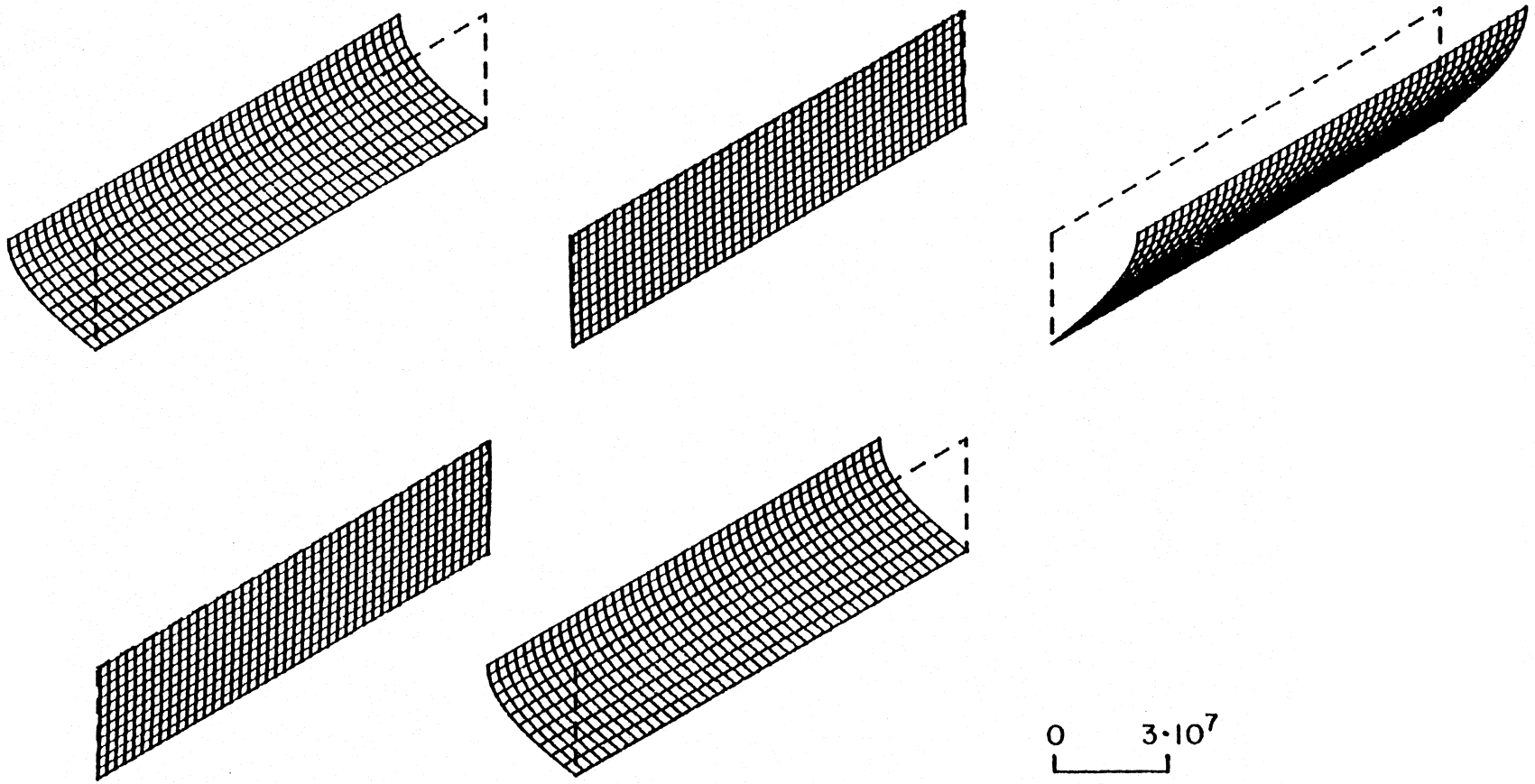

Figure 5.5.1b Displacement response of the building in Figure 5.5.1a without the shear walls and for the same incident ground motion at times $t = 0, T/4, T/2, 3T/4$ and T. The shear walls constrain the response amplitudes as can be seen from the comparison of this and Figure 5.5.1a.

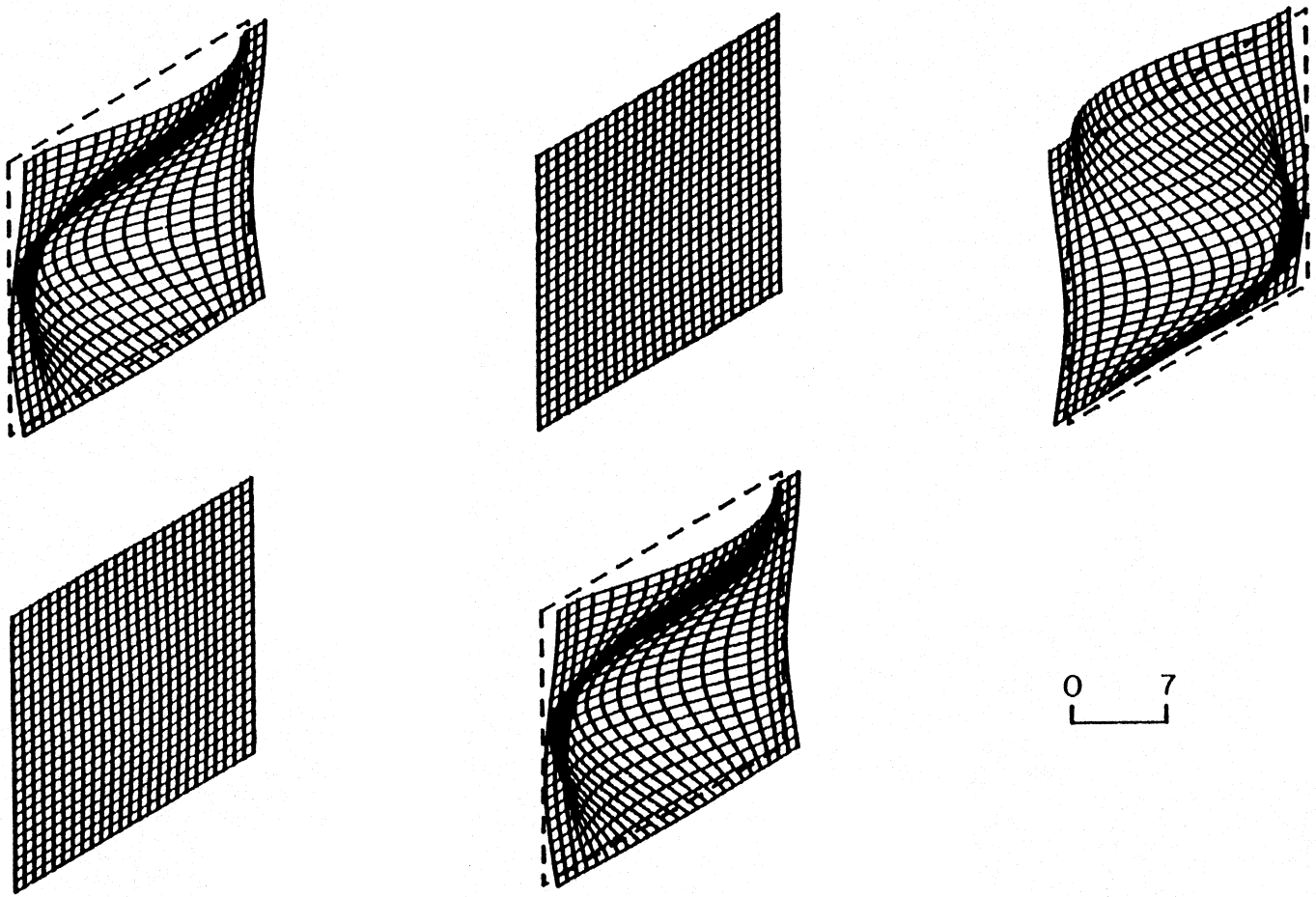

Figure 5.5.2a Displacement response of a long building with comparable length and height $(H/L = 1)$, and with shear walls at its ends $(\ell_1/L = \ell_3/L = 0.1$ and $\beta_1/\beta_2 = \beta_3/\beta_2 = 4)$ for nearly vertically incident SII-waves $(\eta = 0.01, c/\beta_2 = 100)$, at times $t = 0, T/4, T/2, 3T/4$ and T.

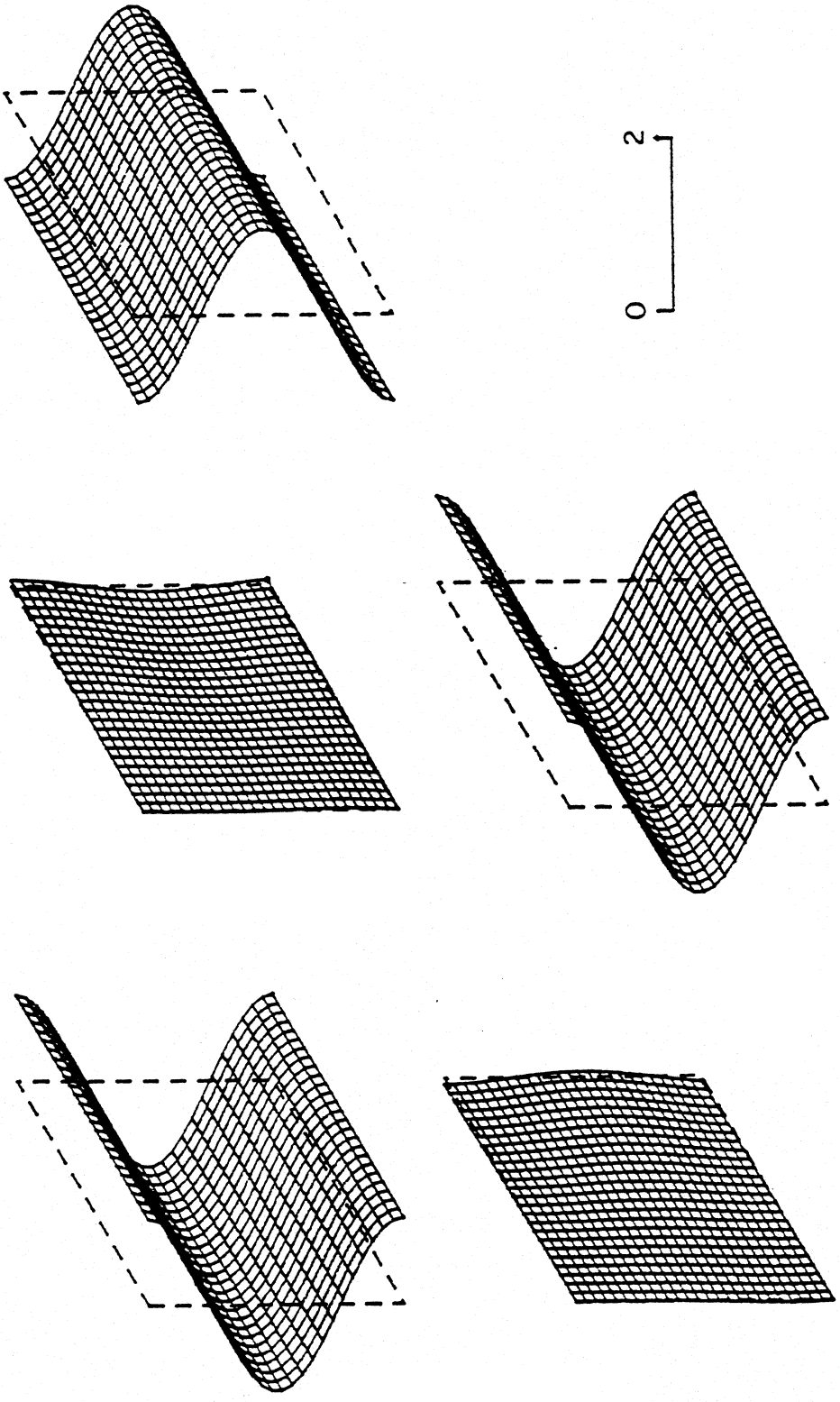

Figure 5.5.2b Displacement response of the building shown in Figure 5.5.2a but here without the shear walls and for the same ground motion. The shear walls constrain the displacements at the ends, as can be seen from the comparison.

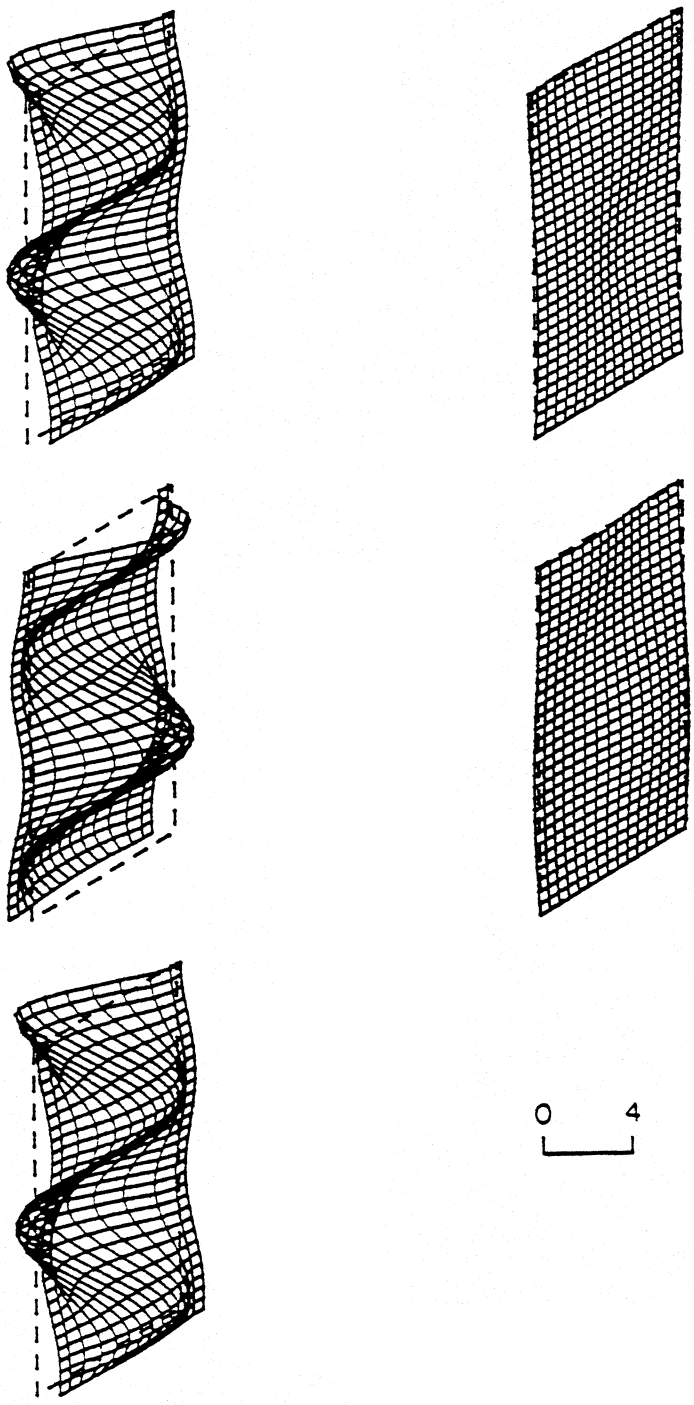

Figure 5.5.3a Displacement response of a long and tall building ($H/L = 2$), and with shear walls at its ends ($\ell_1/L = \ell_3/L = 0.1$ and $\beta_1/\beta_2 = \beta_3/\beta_2 = 4$) for nearly vertically incident SH-wave ($\eta = 0.01$, $c/\beta_2 = 100$), at times $t = 0, T/4, T/2, 3T/4$ and T.

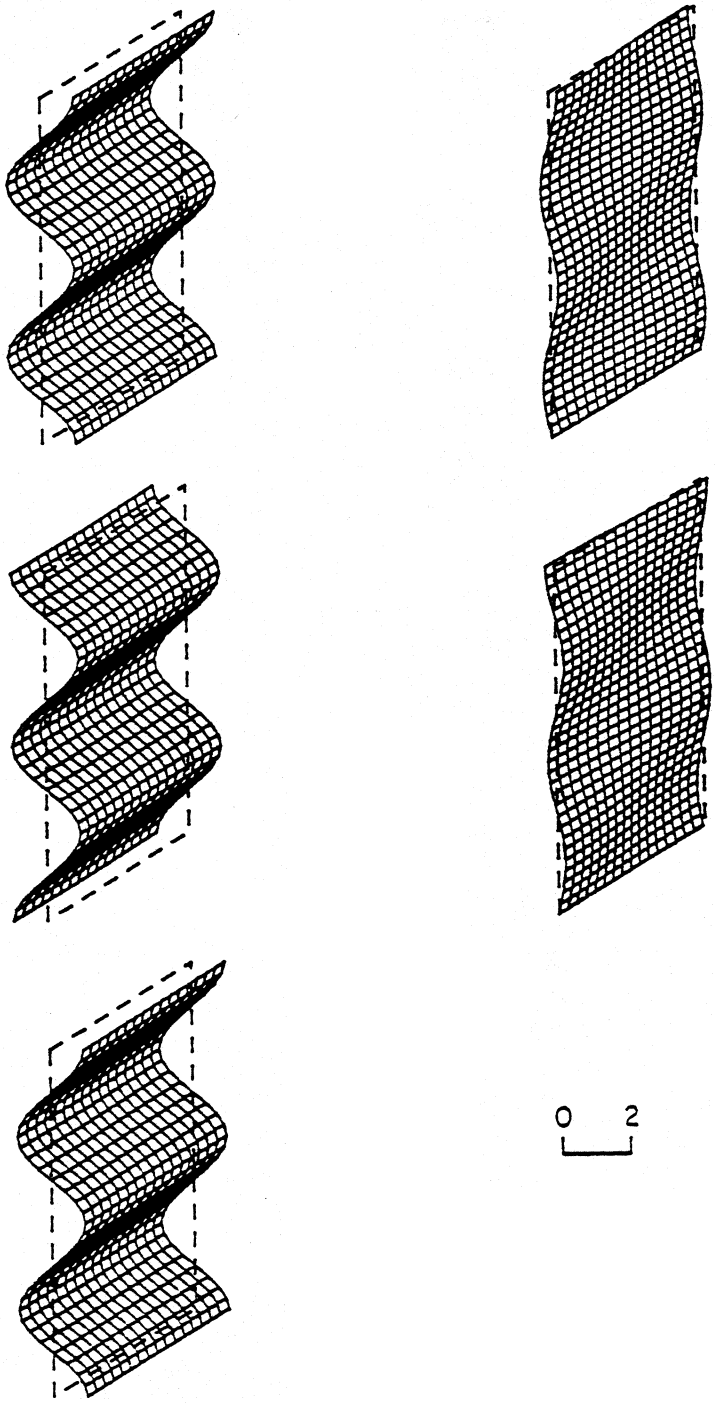

Figure 5.5.3b Displacement response of the building in Figure 5.5.3a but here without the shear walls and for the same ground motion. The shear walls constrain the displacements at the ends of the building, as can be seen from the comparison with Figure 5.5.3a.

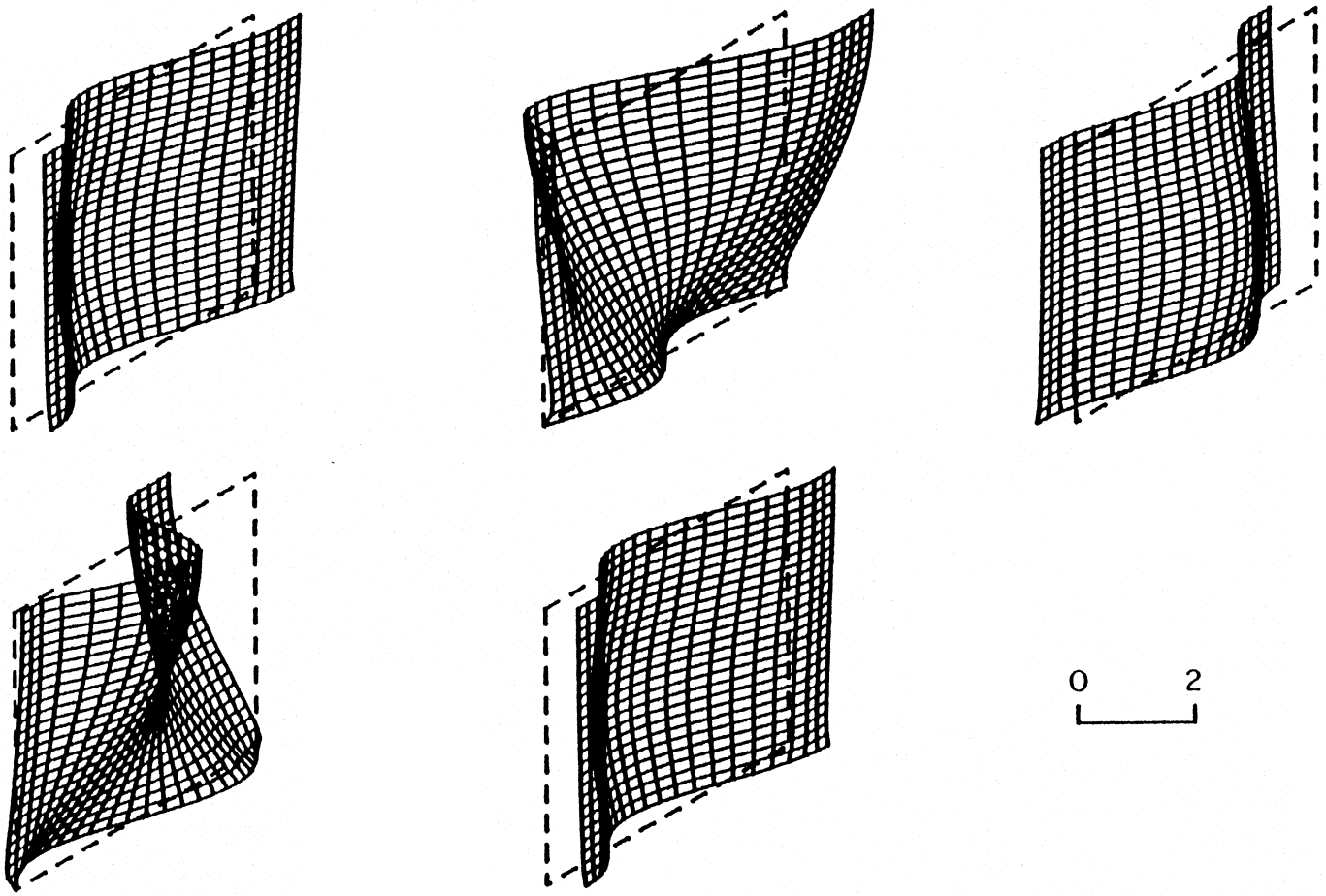

Figure 5.5.4a Displacement response of a long building with height comparable to its length ($H/L = 1$), and with shear walls of different stiffnesses at its ends ($\ell_1/L = \ell_3/L = 0.1$ and $\beta_1/\beta_2 = 10$ and $\beta_3/\beta_2 = 4$), for propagating SH-waves ($\eta = 1$, and $c/\beta_2 = 1$), at times $t = 0, T/4, T/2, 3T/4$ and T. The non-symmetrical distribution of stiffness causes the whipping of the "downstream" end of the building.

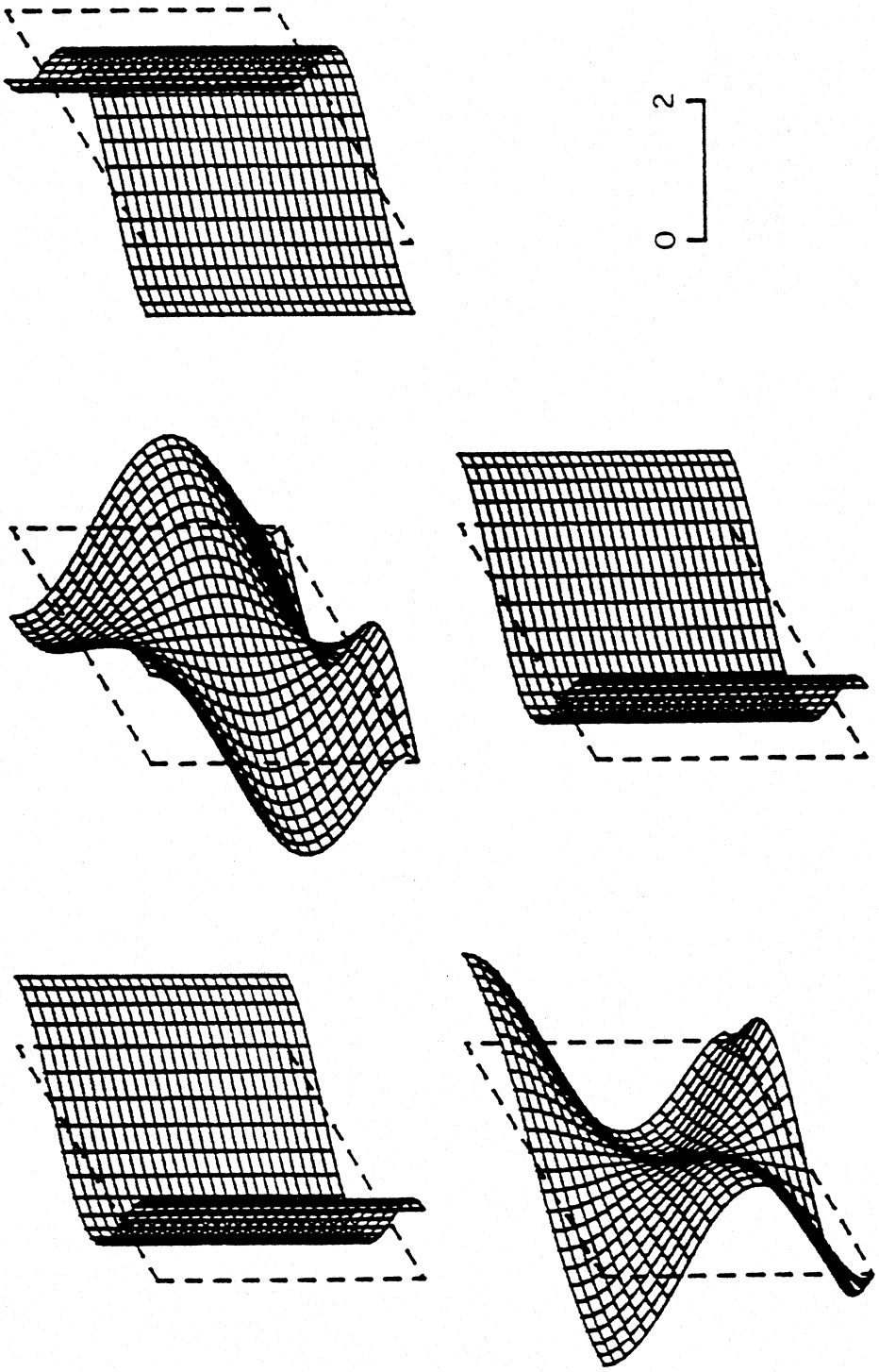

Figure 5.5.4b Displacement response of the building in Figure 5.5.4a without the shear walls and for the same base motion.

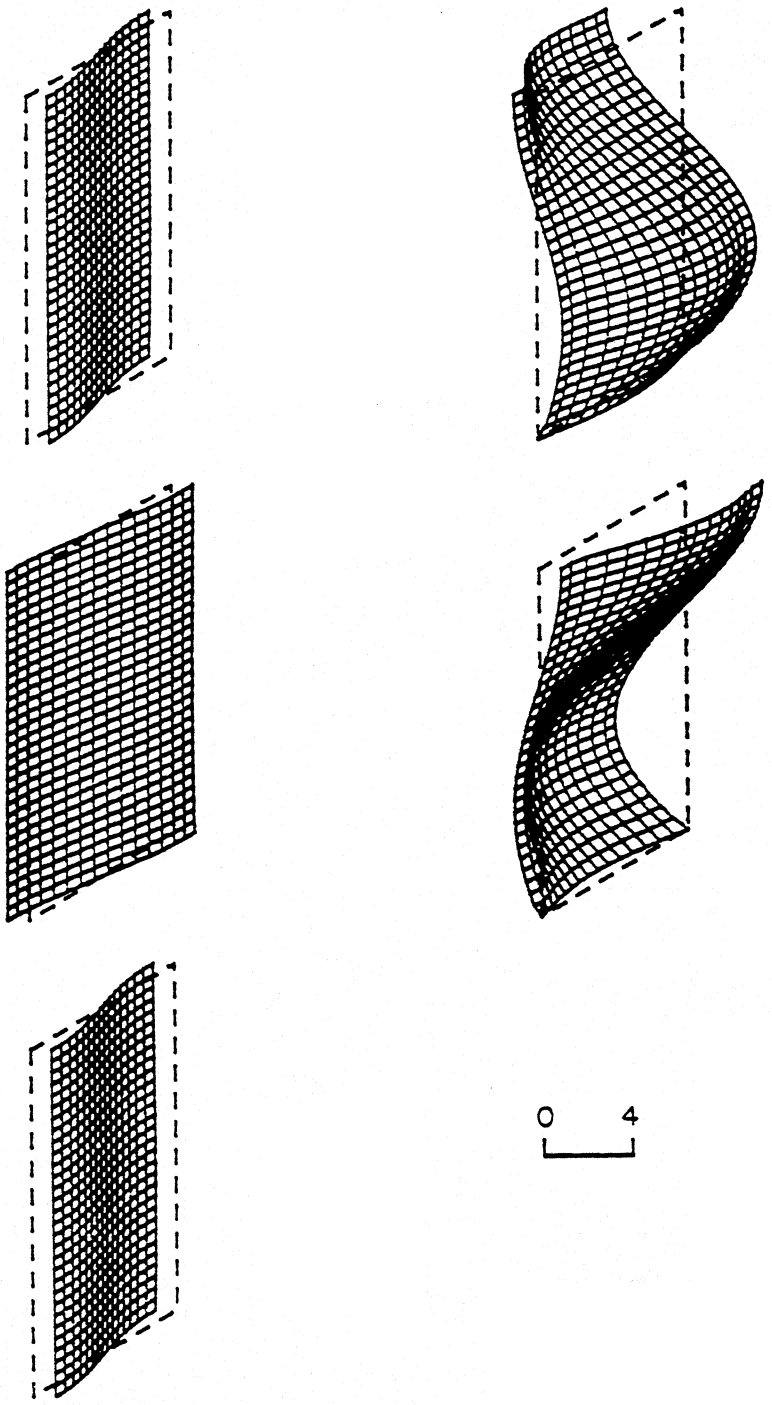

Figure 5.5.5a Displacement response of a long and tall building ($H/L = 2$) with shear walls of different stiffness at its ends ($\ell_1/L = \ell_3/L = 0.1$ and $\beta_1/\beta_2 = 10$ and $\beta_3/\beta_2 = 4$), for propagating SH-waves ($\eta = 0.5$, and $c/\beta_2 = 1$), at times $t = 0, T/4, T/2, 3T/4$ and T. The non-symmetrical distribution of the stiffness causes whipping of its "downstream" end.

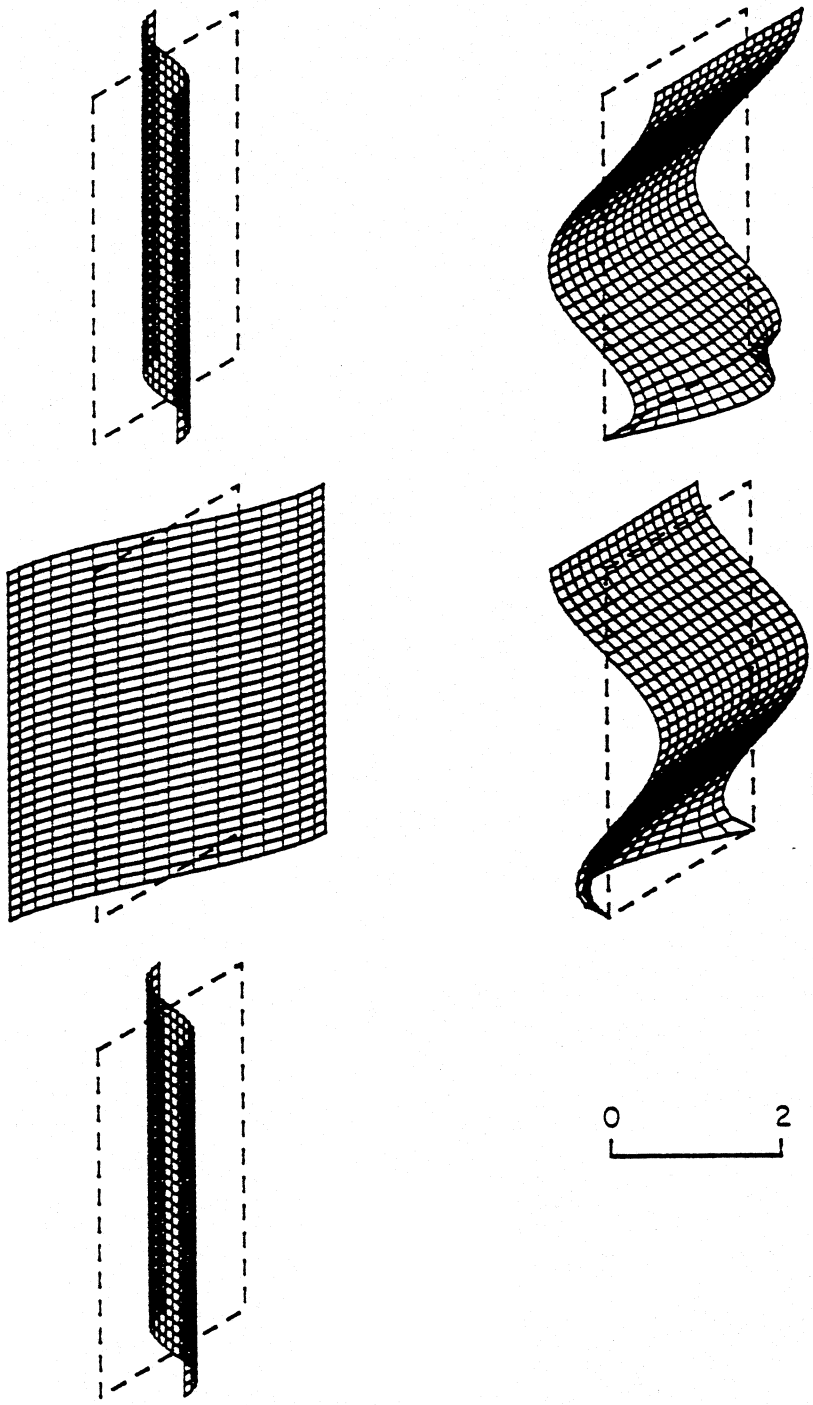

Figure 5.5.5b Displacement response of the building in Figure 5.5.5a without the shear walls and for the same ground motion.

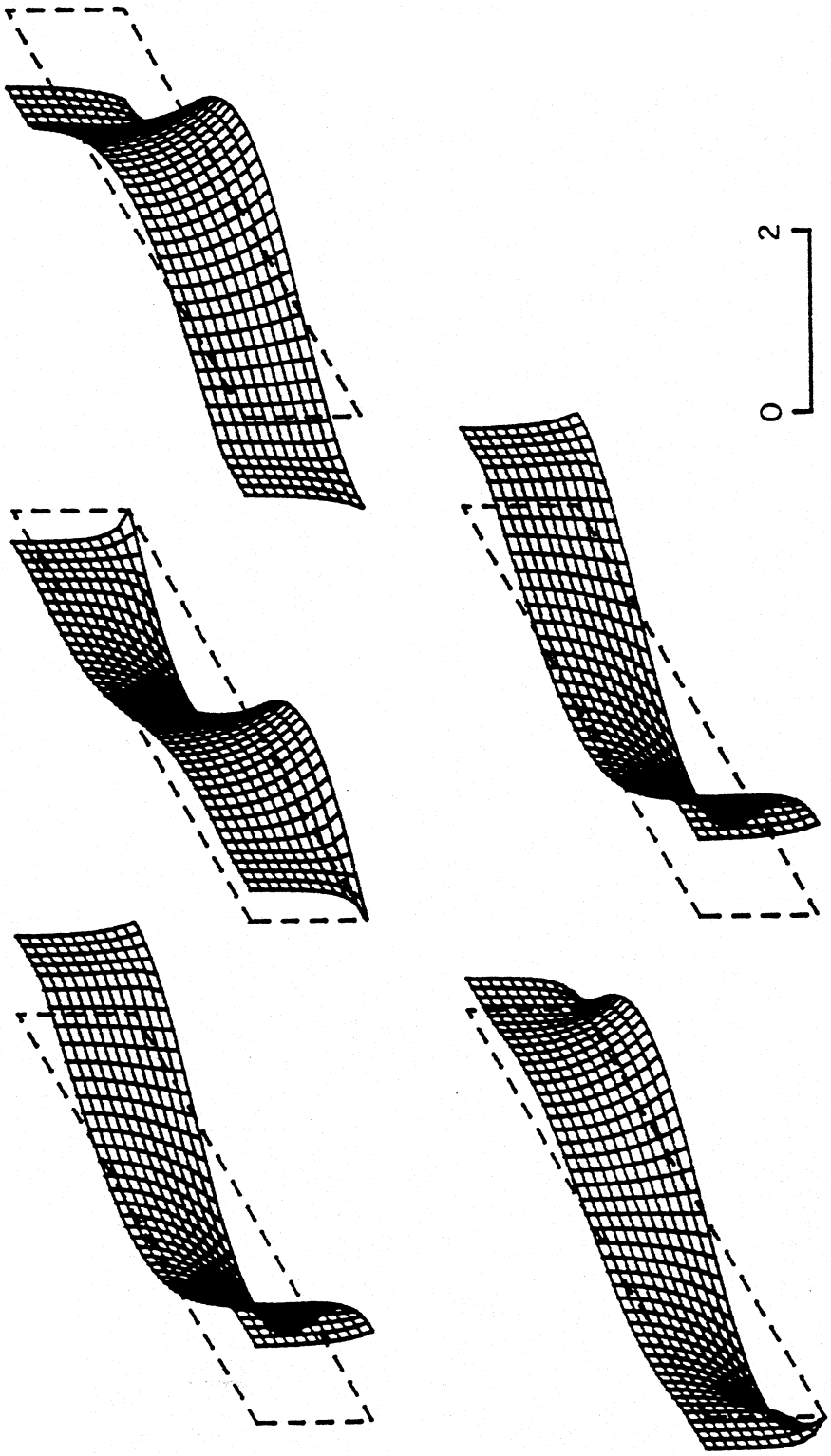

Figure 5.5.6a Displacement response of a long and low building ($H/L = 0.25$) with shear walls at its ends ($\ell_1/L = \ell_3/L = 0.1$ and $\beta_1/\beta_2 = \beta_3/\beta_2 = 4$), for propagating SH-waves ($\eta = 1$, and $c/\beta_2 = 0.05$), at times $t = 0, T/4, T/2, 3T/4$ and T.

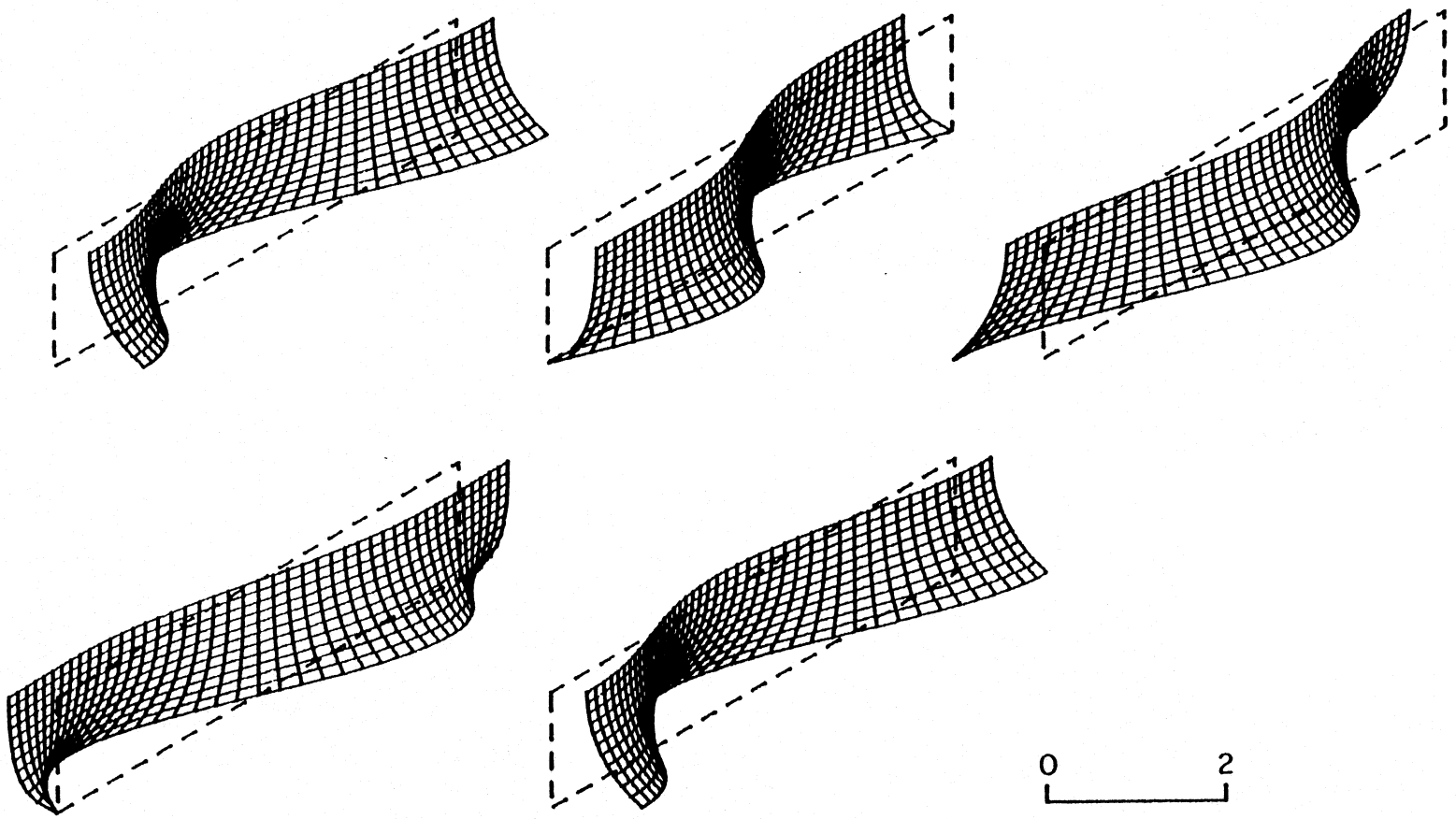

Figure 5.5.6b Displacement response of the building in Figure 5.5.6a, without the shear walls and for the same ground motion. Even when the wave energy does not propagate into the building, the shear walls still decrease the relative displacements.

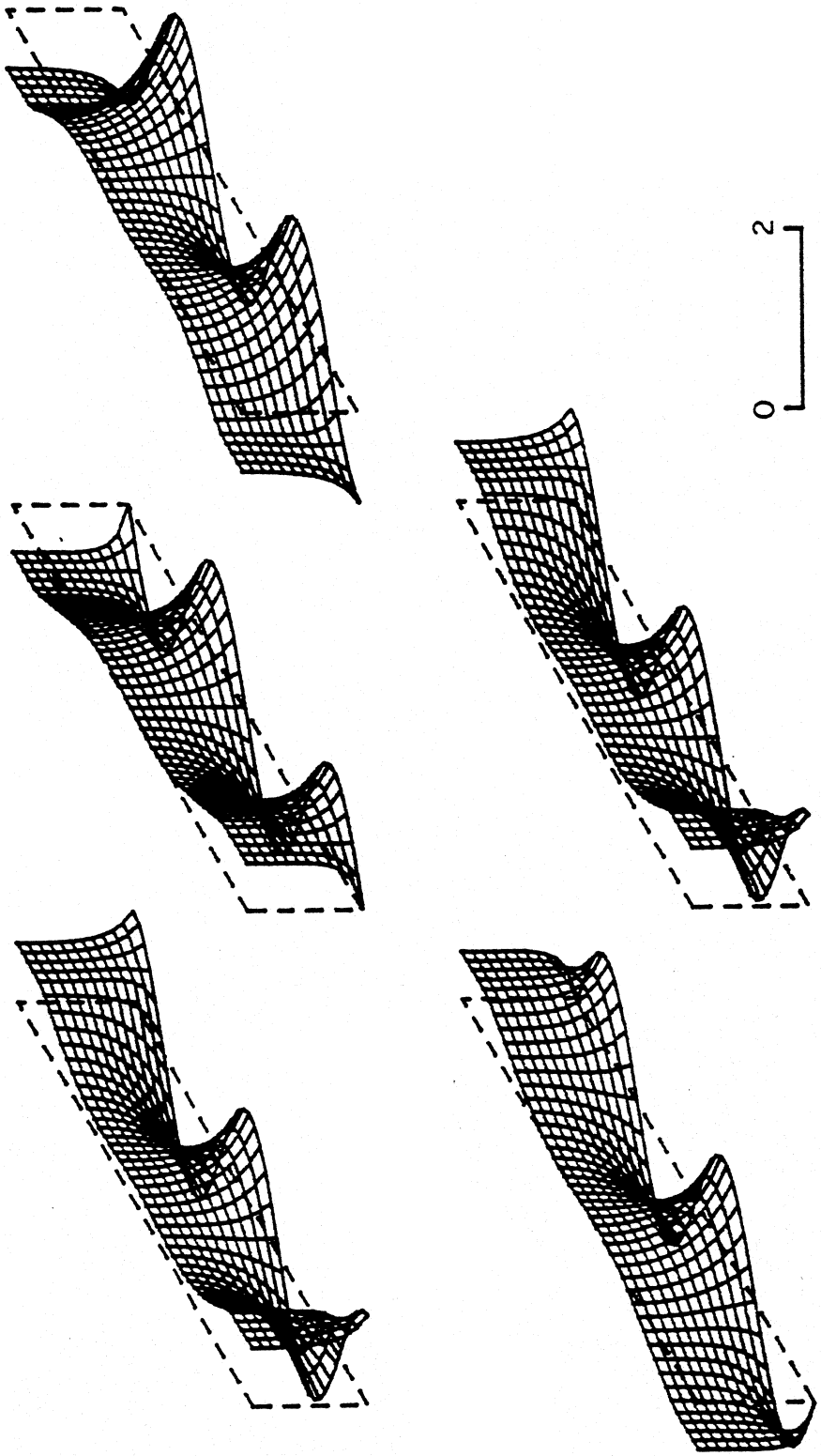

Figure 5.5.7a Displacement response of a long and low building ($H/L = 0.25$) with shear walls at its ends ($\ell_1/L = \ell_3/L = 0.1$ and $\beta_1/\beta_2 = \beta_3/\beta_2 = 4$), for propagating waves ($\eta = 2$, and $c/\beta_2 = 0.05$), at times $t = 0, T/4, T/2, 3T/4$ and T.

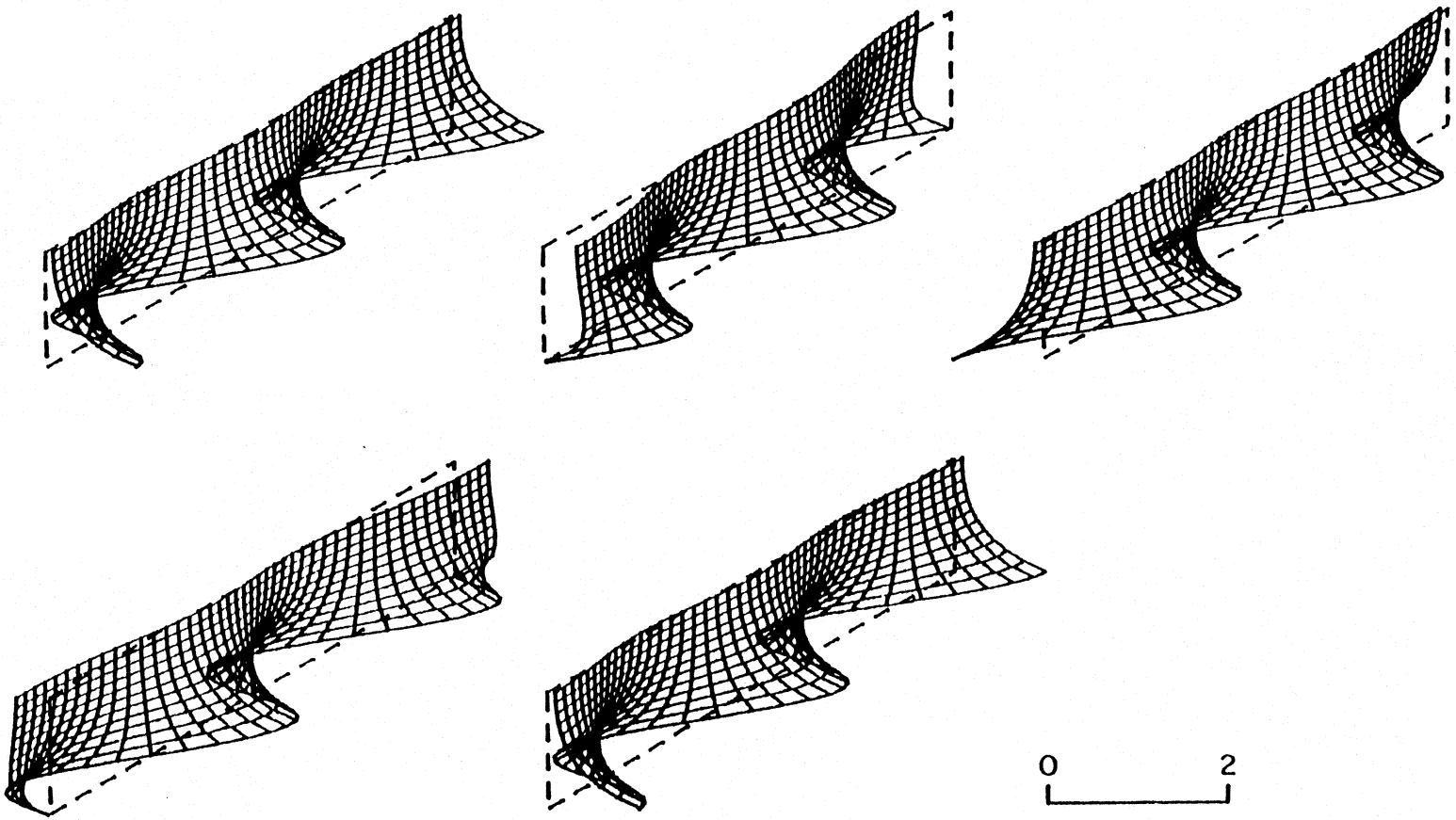

Figure 5.5.7b Displacement response of the building in Figure 5.5.7a but without the shear walls, and for the same ground motion. Although the wave energy does not propagate into the building, the shear walls still decrease the relative displacements in their vicinity.

other hand, the presence of the shear walls makes the two-dimensional aspect of the analysis important and the higher dimensional representation is necessary for a more realistic analysis.

When the two end shear walls do not have the same stiffness, the displacement pattern may become very anti-symmetrical. Figures 5.5.4a and 5.5.5a, for example, illustrate the resulting phenomenon of "whipping" of the "down stream" side ($x = \ell_1 + \ell_2 + \ell_3$, see Figure 3.3.1) of the building at the loaction of the "softer" shear wall. The excitation in both cases is a propagating wave in the positive x-direction, with $\eta = 1$ and $c/\beta_2 = 1$. The ratios of the shear wave velocities in the buildings are $\beta_1/\beta_2 = 10$ and $\beta_3/\beta_2 = 4$. The relative thicknesses of the shear walls are $\ell_1/L = \ell_3/L = .1$ and the height to length ratios are $H/L = 1$ and 2, respectively (see Figure 3.3.1). Figures 5.5.4b and 5.5.5b illustrate the displacement of the same buildings but without the end shear walls and for the same ground motion. Comparison with the homogeneous model displacements shows that the stiffer shear wall is "holding" the building as if it were supported at that side. The "softer" shear wall allows whipping of the opposite side of the building and the displacement pattern resembles the displacement of a thin plate, fixed at two sides.

The effect of "whipping" cannot be so clearly detected by the one-dimensional analysis, which can include only the effects of torsional stiffness excentricity. It is not desirable for it to occur in response of real buildings. It can be avoided by designing the shear walls with comparable stiffnesses.

In all illustrations above, the selected incident ground motion was such that the energy was transmitted into the building ($c/\beta_1 \geq 1$). Figures 5.5.6a and 5.5.7a show examples when the energy is not transmitted into the building ($c/\beta_1 = 0.05$) and the displacement of the building follows an exponential function in the vertical direction. Both

figures illustrate a "long" building ($H/L = 0.25$) with shear walls of relative thickness $\ell_1/L = \ell_3/L = 0.1$ and with relative shear wave velocities $\beta_1/\beta_2 = \beta_3/\beta_2 = 4$. The dimensionless wave length η takes on the values of 1 and 2, respectively. The accompanying Figures 5.5.6b and 5.5.7b illustrate the displacements of the building, without the shear walls and for the same incident ground motions. It can be concluded that in these two cases the shear walls decrease slightly the relative displacements of the buildings.

5.5.2 Buildings with Central Core

Some buildings are designed in such a way that the elevator cores also provide the lateral stiffness. For example, the Millikan Library at Caltech in Pasadena, Figure 5.5.8, (Trifunac, 1972) has two shear walls to carry the horizontal forces in the N-S direction and the central core to carry the horizontal forces in the E-W direction. The question "what is the best location (distribution) and relative stiffness of the shear walls and of elevator cores" is of considerable interest for the designer of buildings with large horizontal dimensions.

Buildings with a central core of width $0.2L$, where L is the length of the building, and with shear wave velocity four times bigger than the shear wave velocity of the surrounding parts of the building (Figure 3.1.3c), will be analyzed in this section. The model in Figure 3.3.1, also described in section 3.3, was selected to represent the building models with central core considered in this section. Plane monochromatic SH waves with different angles of incidence will represent the ground motion.

The analyses show that the central core stiffens the building and constrains its displacements only in the close vicinity to the core walls. Moreover, it may cause complicated displacement patterns that give rise to horizontal stresses that otherwise might not

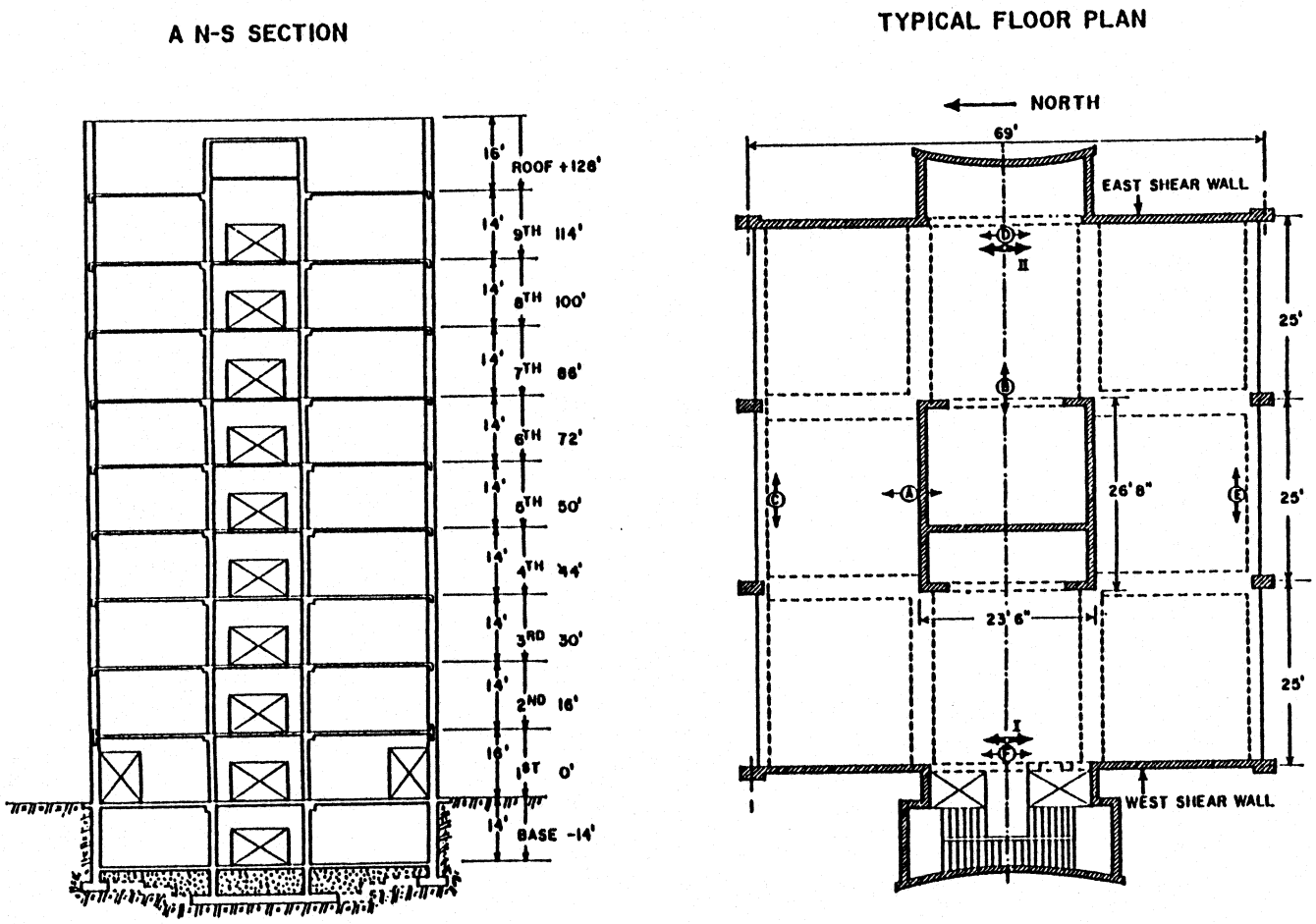

Figure 5.5.8 A NS section and a typical floor plan of the Millican Library at Caltech in Pasadena (after Trifunac, 1972).

be present in the floor slabs. This can happen even when the motion at the base has as simple form as $\Delta e^{i\omega t}$, as illustrated by Figures 5.5.9a amd 5.5.10a ($\Delta = 1, \omega L/\beta_1 = 4\pi$, or $\eta = 0.01, c/\beta_1 = 200$, amplitude of the vertically incident wave $= 1/2$, and $H/L = 0.25, 1$, respectively). For comparison, Figures 5.5.9b and 5.5.10b illustrate the displacement of the buildings without the central core and excited by the same ground motion. While the displacements of the homogeneous buildings, for long incident waves, depend mainly on the z-coordinate, giving rise mainly to the variation of stresses, the displacements of the buildings with the central cores are highly dependent on the x-coordinate. The core separates the two "soft" parts of the buildings and those vibrate independently, like two plates supported at two adjacent sides, with the free sides allowed to whip.

The complicated displacement patterns, the presence of the horizontal stresses and the whipping of the "unsupported" sides are undesirable. To constrain the motion of the "soft" parts, the designer might add shear walls at the ends. Also he might replace the central core by two shear elements (shear walls, or elevator cores) placed between the center and the ends of the building so as to constrain both the ends and the center of the building. In section 5.5.1 examples were shown (Figures 5.5.1a, 5.5.2a and 5.5.3a) that the displacement of the central part of the building may be large if the building has only the shear walls at the ends.

The central core rises the equivalent stiffness of the whole building, and thus increases its resonant frequencies. In the examples in Figures 5.5.9 and 5.5.10, the frequency of the ground motion ($\omega L/\beta_1 = 4\pi$) is closer to the resonant frequencies of the higher modes in the z direction when the buildings do not have the central core.

The central core reduces the displacements of the building, but mainly close to the core, i.e. close to the center of the building. Therefore, it modifies only the displacements of

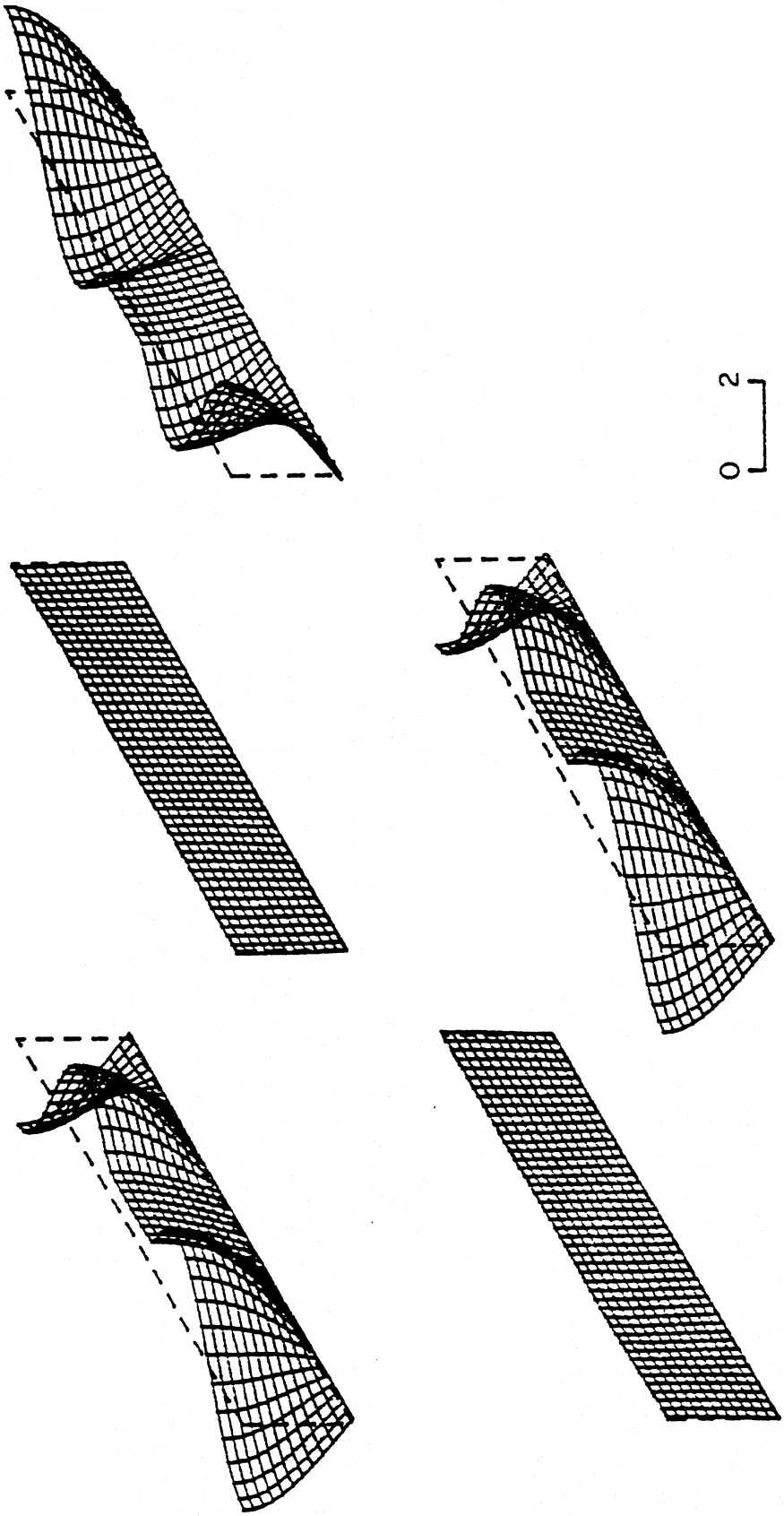

Figure 5.5.9a Displacement response of a long and low building ($H/L = 0.25$) with central core ($\ell_1/L = \ell_3/L = 0.4$ and $\beta_2/\beta_1 = \beta_2/\beta_3 = 4$), for nearly vertically incident SH-wave ($\eta = 0.01$, and $c/\beta_1 = 200$), at times $t = 0, T/4, T/2, 3T/4$ and T.

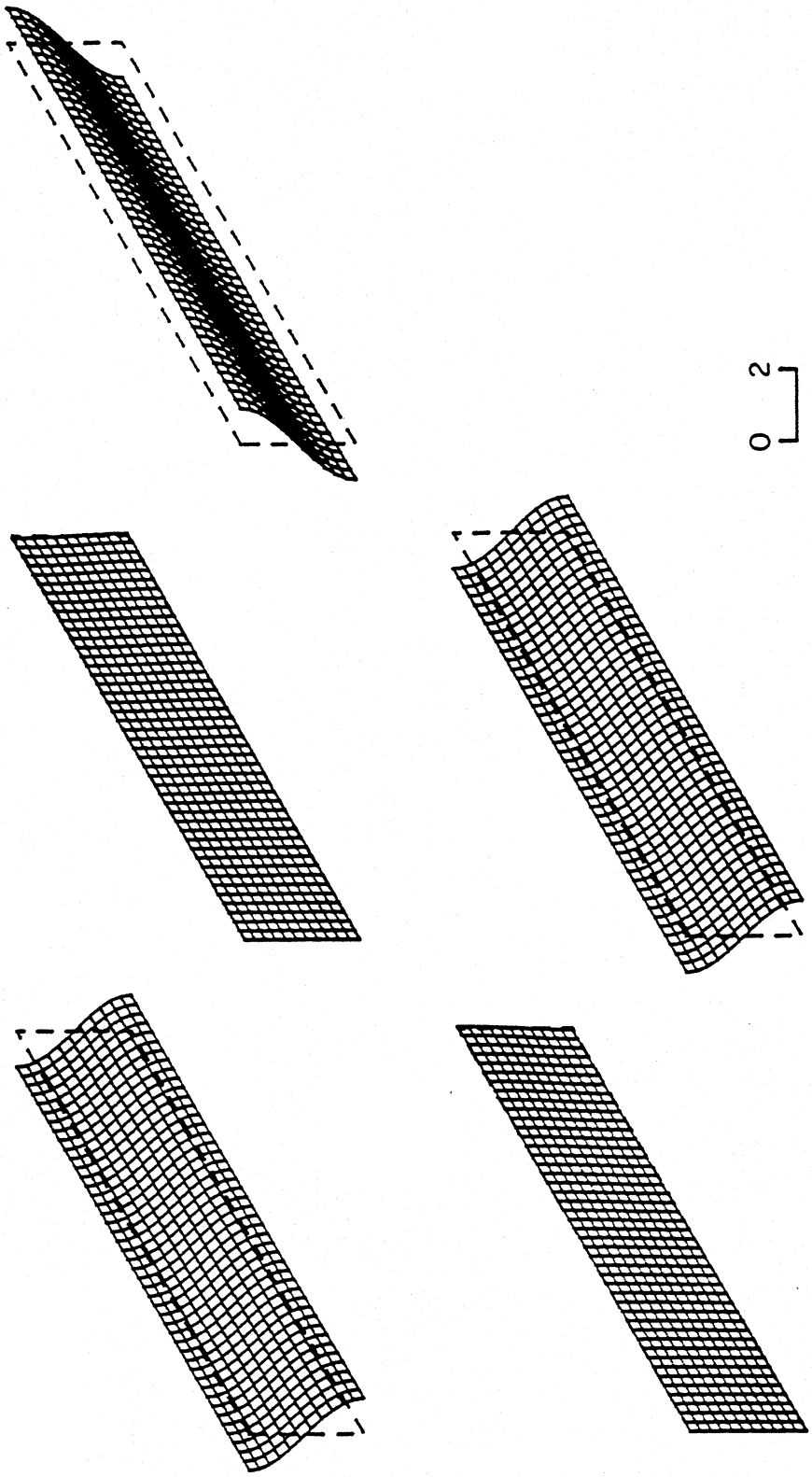

Figure 5.5.9b Displacement response of the building in Figure 5.5.9a without the central core and for the same ground motion. The central core restrains the displacements near the middle of the building only, while its ends continue to deform.

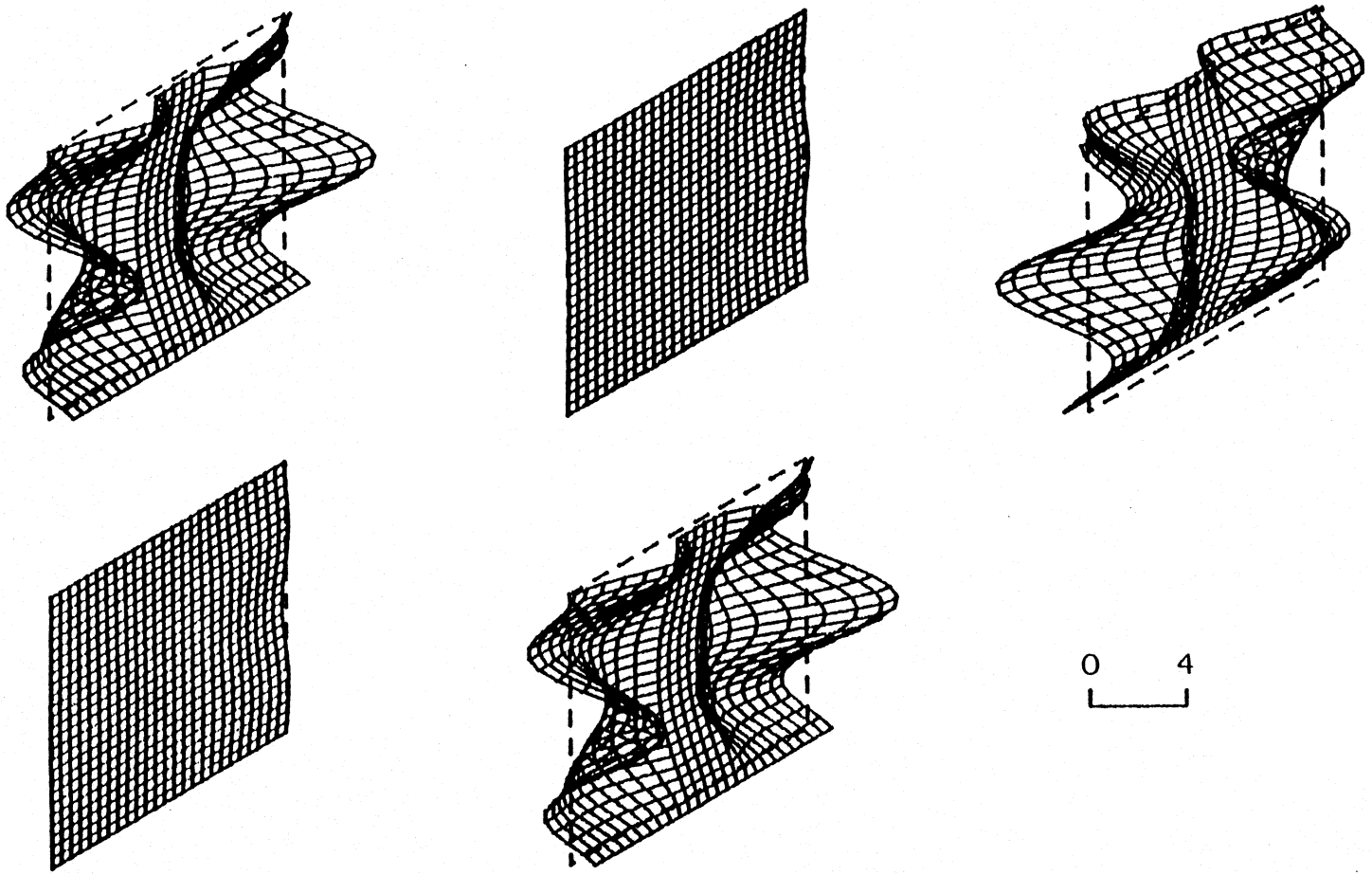

Figure 5.5.10a Displacement response of a building with height comparable to its length ($H/L = 1$), and with a central core ($\ell_1/L = \ell_3/L = 0.4$ and $\beta_2/\beta_1 = \beta_2\beta_3 = 4$), for a nearly vertically incident SH-wave ($\eta = 0.01$, and $c/\beta_1 = 200$), at times $t = 0, T/4, T/2, 3T/4$ and T.

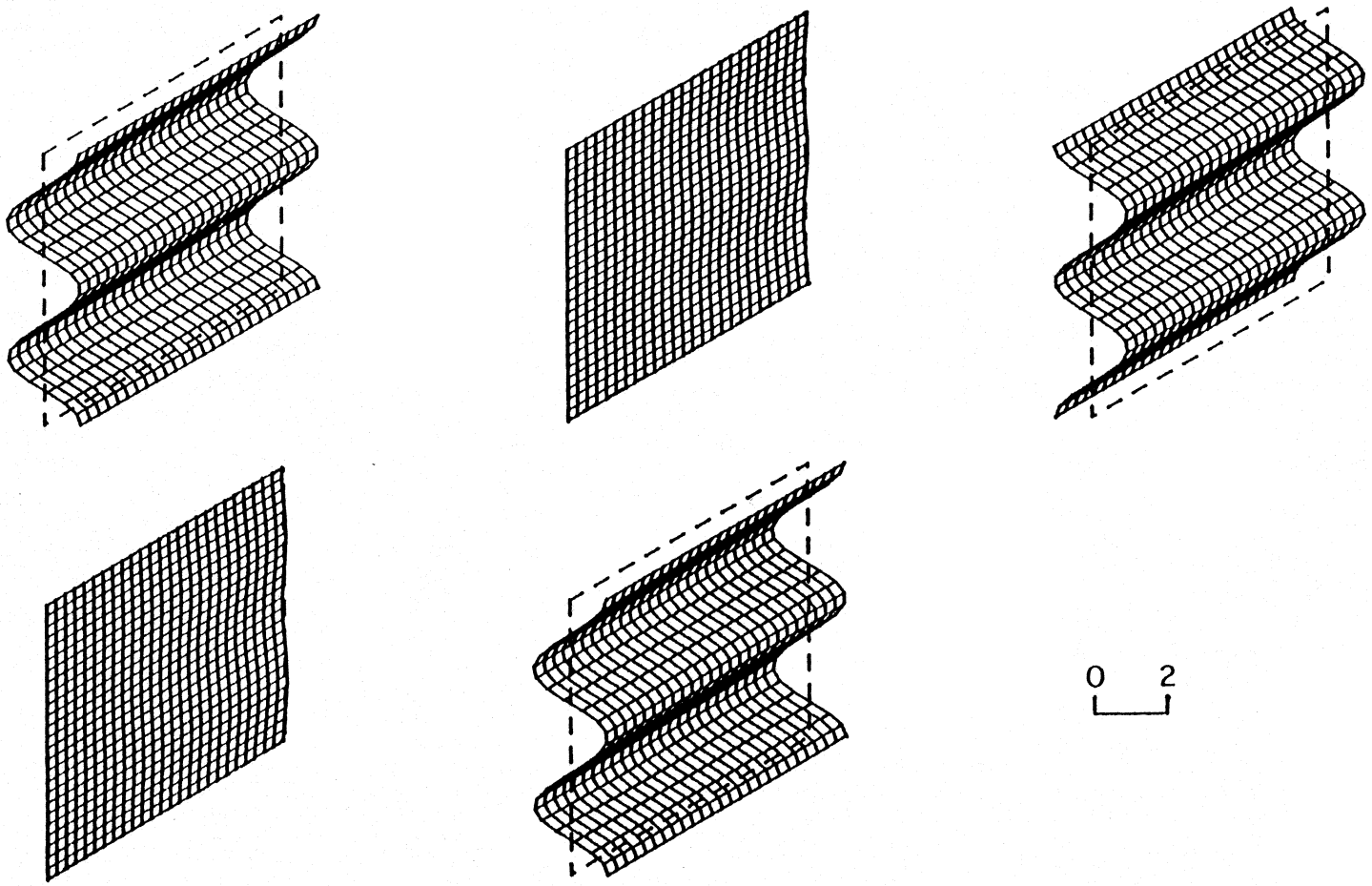

Figure 5.5.10b Displacement response of the building in Figure 5.5.10a but here without the central core and for the same ground motion. The core restrains the motions of the central part of the building only, while the ends continue to deform.

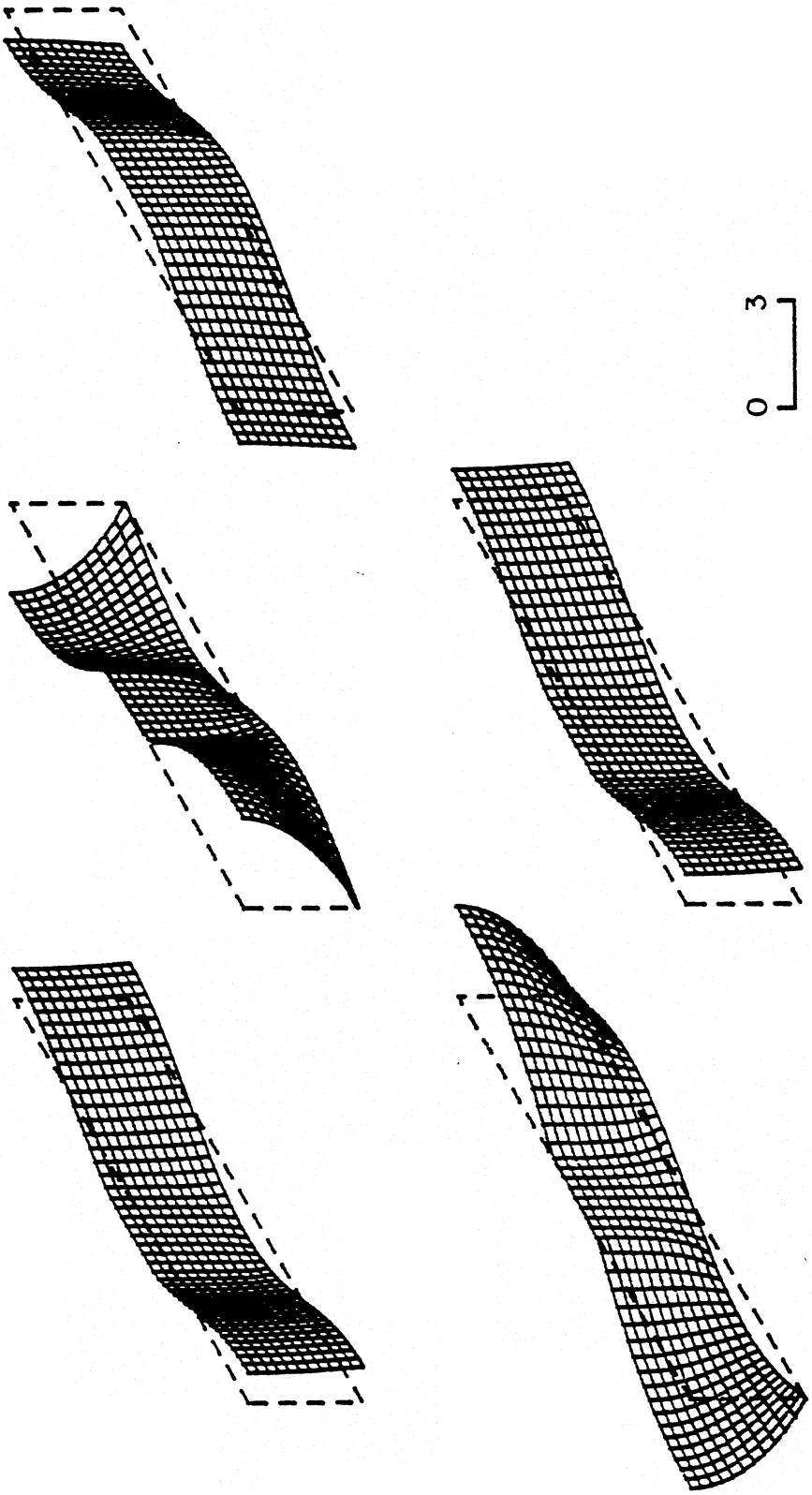

Figure 5.5.11a Displacement response of a long and low building ($H/L = 0.25$) with central core ($\ell_1/L = \ell_3/L = 0.4$ and $\beta_2/\beta_1 = \beta_2/\beta_3 = 4$), for a propagating SH-wave ($\eta = 1$, and $c/\beta_1 = 1$), at times $t = 0, T/4, T/2, 3T/4$ and T.

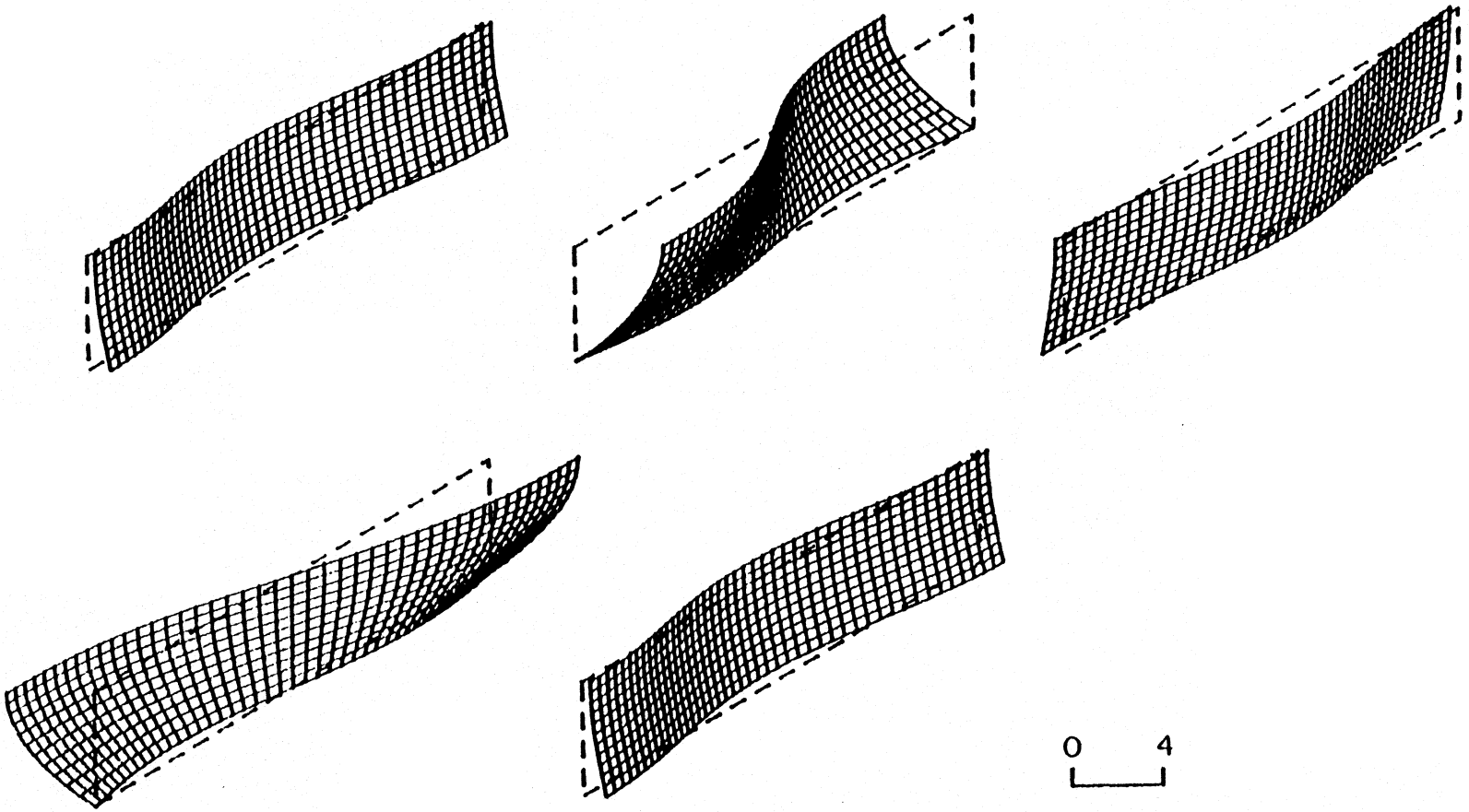

Figure 5.5.11b Displacement response of the building in Figure 5.5.11a without the central core and for the same ground motion. The central core does not restrain the anti-symmetric displacements, as can be seen from the figures.

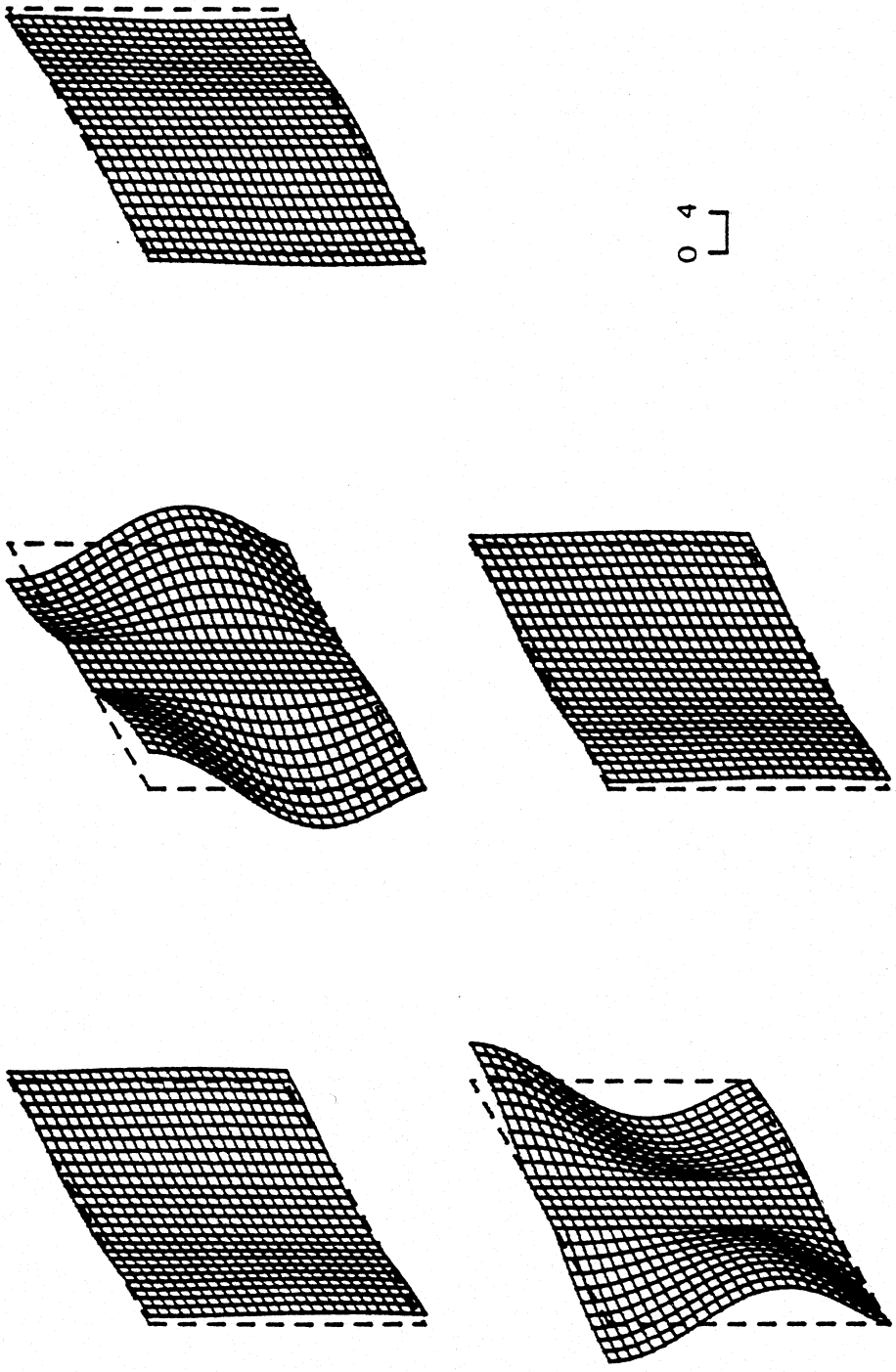

Figure 5.5.12a Displacement response of a long building, with height comparable to its length ($H/L = 1$) and with central core ($\ell_1/L = \ell_3/L = 0.4$ and $\beta_2/\beta_1 = \beta_2/\beta_3 = 4$), for a propagating SH-wave ($\eta = 1$, and $c/\beta_1 = 1$), at times $t = 0, T/4, T/2, 3T/4$ and T.

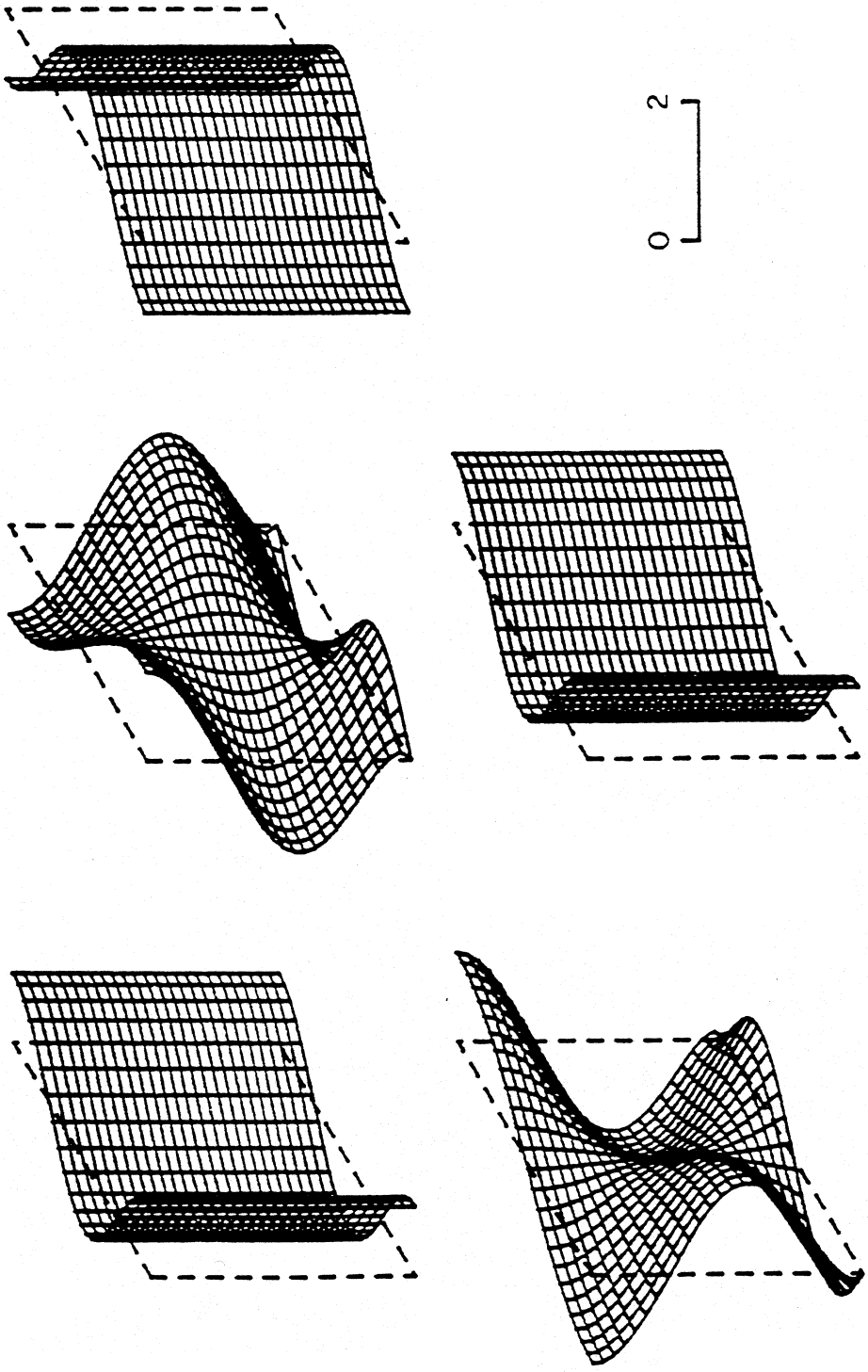

Figure 5.5.12b Displacement response of the building in Figure 5.5.12a but here without the core and for the same ground motion. The central core does not restrain the anti-symmetric displacements.

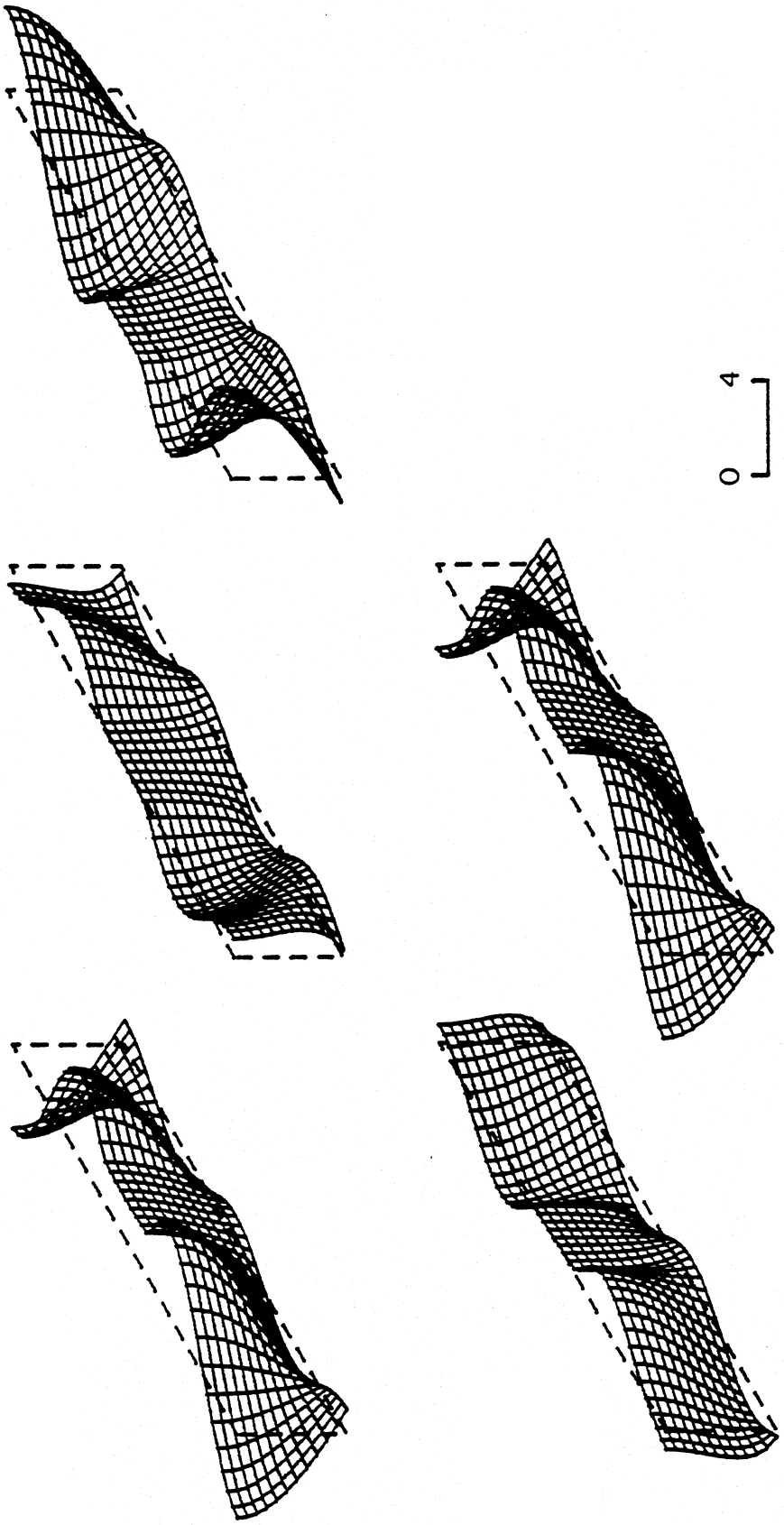

Figure 5.5.13a Displacement response of a long and low building ($H/L = 0.25$) with central core ($\ell_1/L = \ell_3/L = 0.4$ and $\beta_2/\beta_1 = \beta_2/\beta_3 = 4$), for a propagating SH-wave ($\eta = 2$, and $c/\beta_1 = 1$), at times $t = 0, T/4, T/2, 3T/4$ and T.

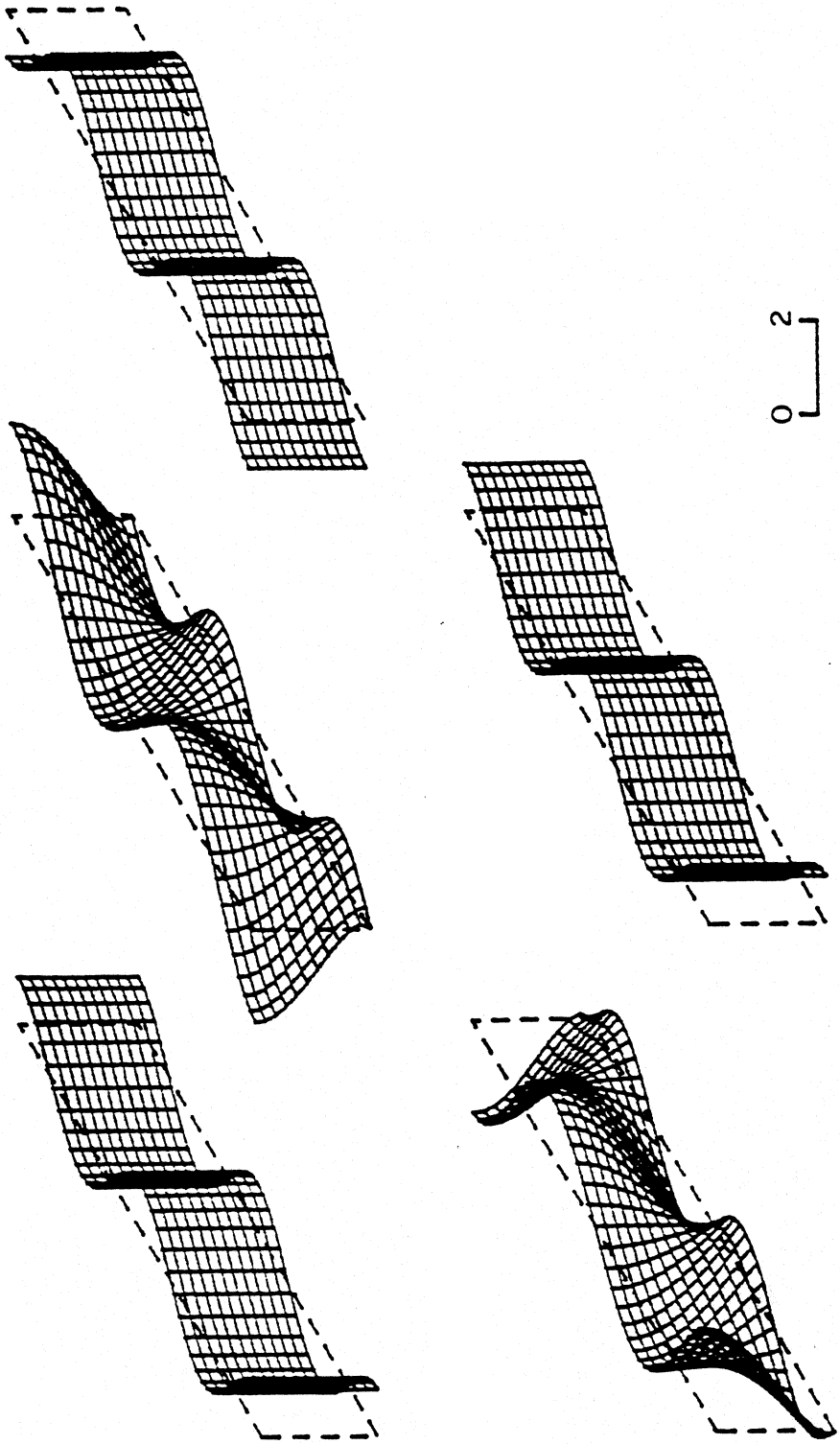

Figure 5.5.13b Displacement response of the building in Figure 5.5.13a but here without the core and for the same ground motion. The core restrains only the symmetric displacements in the x-direction and close to the center only (Figure 5.5.13a).

the symmetric modes. The anti-symmetric modes in x pass through zero at $x = L/2$. This is illustrated by Figures 5.5.11, 5.5.12 and 5.5.13. The first two show the displacements of the building with and without the core when $\eta = 1$ and $c/\beta_1 = 1$ for $H/L = 0.25$ and 1, respectively, and the third one when $\eta = 2, c/\beta_1 = 1$ and $H/L = 0.25$. The width of the core and its relative shear wave velocity compared to the main part of the building are the same as the previous examples in this section.

5.5.3 Buildings with "Soft" First Floor

Because of the architectural requirements, many buildings have the ground or the ground and the first floors with stiffness which is smaller than the stiffness of the upper floors. These are the buildings that typically have stores or various passages on the first floor, and therefore one finds there many "walls" and partitions made of glass instead of concrete or masonry. An example of such a building is the former Imperial County Services Building in El Centro (Kojić et al., 1984), shown in Figures 2.3.5 and 2.3.6. Above the second floor the building had shear walls at the east and west ends, while at the first floor it had only four concrete panels. This reduced the resistance of the first floor in the N-S direction. During the Imperial Valley, California earthquake of 1979 the columns of the first floor experienced very large displacements in the E-W direction and were badly damaged. The upper part of the building experienced much smaller deformations. The building was instrumented and according to the recorded motions during this earthquake, the upper part of the building vibrated like a "rigid" box placed over flexible columns.

Using the ray theory representation of seismic wave propagation, the transfer of the energy of SH waves from the ground into the building can be analyzed for the layered building model as in Figure 5.5.14. In this figure β_1, β_2 and β_s are the shear wave velocities of the upper part of the building, of the first floor and of the soil, respectively. γ is the

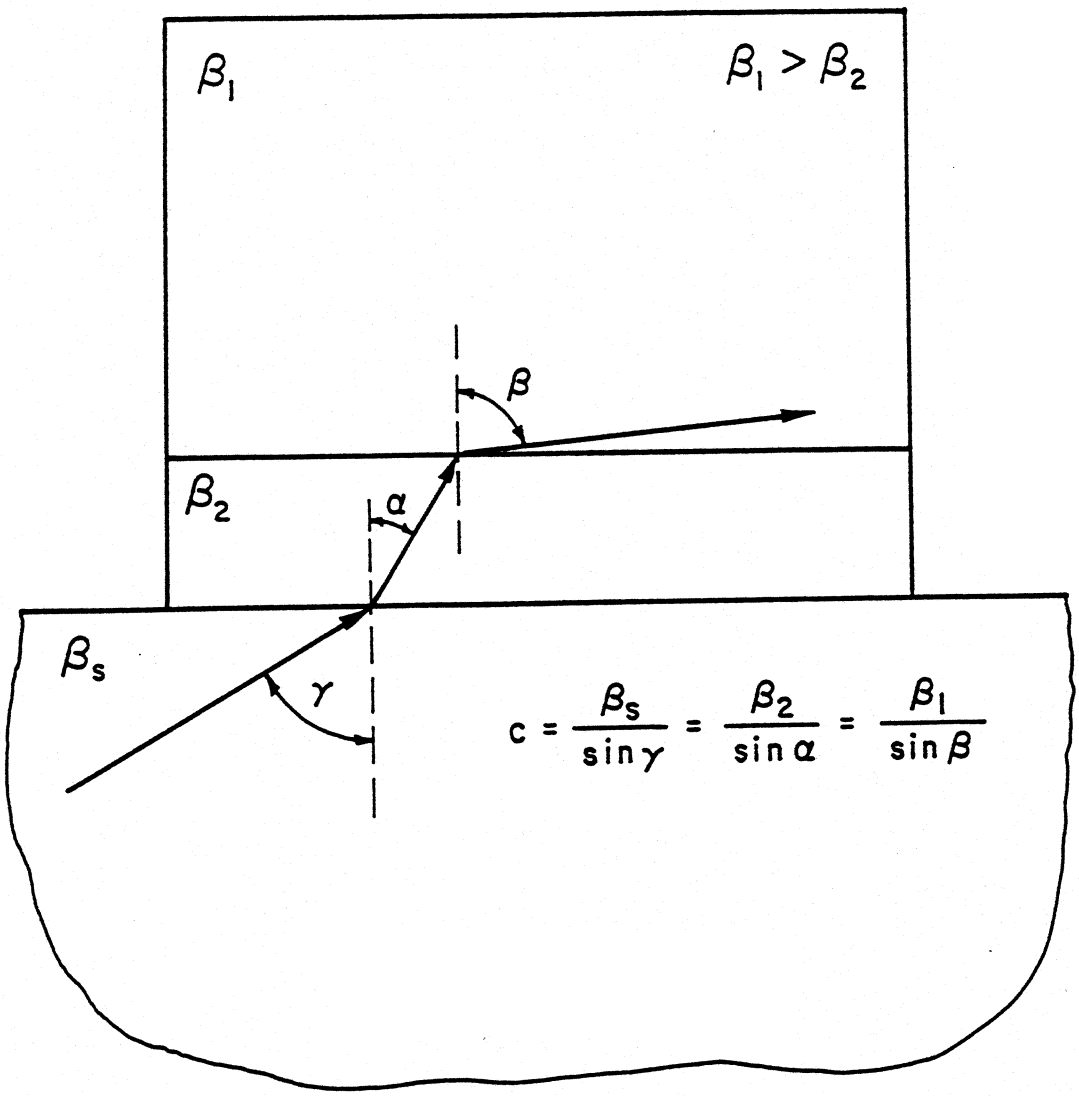

Figure 5.5.14 An illustration of the transfer of the wave energy from the ground into a building with a soft first floor.

incident angle, α and β are the angles of refraction in the "soft" and in the "hard" layers, respectively. Then, according to the Snell's law, the following relations must be satisfied

$$c = \frac{\beta_s}{\sin\gamma} = \frac{\beta_2}{\sin\alpha} = \frac{\beta_1}{\sin\beta} \quad . \tag{5.5.1}$$

The angle α will be real, i.e. the wave energy will be transmitted into the soft layer only if $c/\beta_2 \geq 1$, as it has been explained earlier in section 5.3. If $c/\beta_1 < 1$ then, α will be pure imaginary and thus β will also be pure imaginary (since $\beta_1 > \beta_2$) and the wave energy will not be transmitted into the building. If $c/\beta \geq 1$, whether the wave energy will or will not be transmitted into the upper part depends on the value of the ratio β_2/β_1. The energy will be transmitted into the upper part of the building only if $c/\beta_1 = (c/\beta_2)(\beta_2/\beta_1) \geq 1$. When $c/\beta_1 < 1$, the displacements in the "hard" layer will be exponentially decaying towards the top of the building, and it will vibrate as a "rigid box" welded to the vibrating "soft" first floor.

In this work the model in Figure 3.4.2 and the representation of the displacement by a series in terms of the eigenfunctions of the model (section 3.3) have been used to calculate the response of the building with a "soft" first floor. In the discussion in section 3.4 it was mentioned that for the fundamental mode ($n = 0$ in equation 3.4.4) the wave numbers in the z-direction $k_{z,0}^{(i)}, i = 1,2$ are always real in both media. For the higher modes, they can be real or imaginary, depending on the frequency of the ground motion. Then, there is some N_1 such that all the shape functions in the z-direction $Z_n(z)$ for $n > N_1$ will be hyperbolic functions in the upper part of the building. There is another number $N_2 \geq N_1$ such that for $n \geq N_2$ $Z_n(z)$ will be hyperbolic functions in both media. The energy will be transmitted into the "soft" layer only through the modes for which $n \leq N_2$ and into the upper part of the building only through the modes for which $n \leq N_1$.

Figure 5.5.15a illustrates the displacements of a building with a soft first floor when energy is not transmitted into both the "soft" first floor or into the upper part of the building. The ground motion at the base is a wave of amplitude 1, propagating with phase velocity c in the horizontal direction, and with $\eta = L/cT = 0.5$. The height to length ratio of the building is 1 and the height of the first floor is 25 percent of the total height of the building. The energy does not propagate through the first floor because $c/\beta_2 = 0.05 < 1$, and through the upper part of the building because $c/\beta_1 = (c/\beta_2)(\beta_2/\beta_1) = 0.0125 < 1$. It can be seen from the figure that the building vibrates with "hyperbolic" modes in the z-direction. Figure 5.5.15b illustrates the displacement of a homogeneous building, with the equivalent shear wave velocity, β, the same as the shear wave velocity of the first floor of the building in Figure 5.5.15a, and subjected to the same ground motion ($\eta = 0.5, c/\beta = 0.05$). It can be seen from these two figures that by increasing of the stiffness of the upper floors (Figures 5.1.15a) decreases the relative displacements of the upper part of the building, but increases the relative displacements of the first floor.

The parts "a" of the Figures 5.5.16, 5.5.17 and 5.5.18 illustrate the cases when the energy propagates through the first floor, but does not propagate into the upper floors of the building. The buildings in these figures vibrate with modes that are harmonic functions in the first floor and hyperbolic functions at upper floors. In all three figures the base motion is a propagating wave in the positive x-direction with $c/\beta_2 = 1$. The chosen values of η and H/L are 1, 2 and 4, and 2, 0.25 and 0.25, respectively. The height of the first floor is 0.25 H in all three figures. The ratios β_1/β_2 are 4, 2 and 2, respectively. The parts "b" of these figures illustrate the displacement response of a homogeneous building with equivalent shear wave velocity $\beta = \beta_2$ and subjected to the same base motion as in part "a". There is a significant difference between the displacement patterns in parts "a" and parts "b" of the figures. In all the figures the relative displacements of the upper

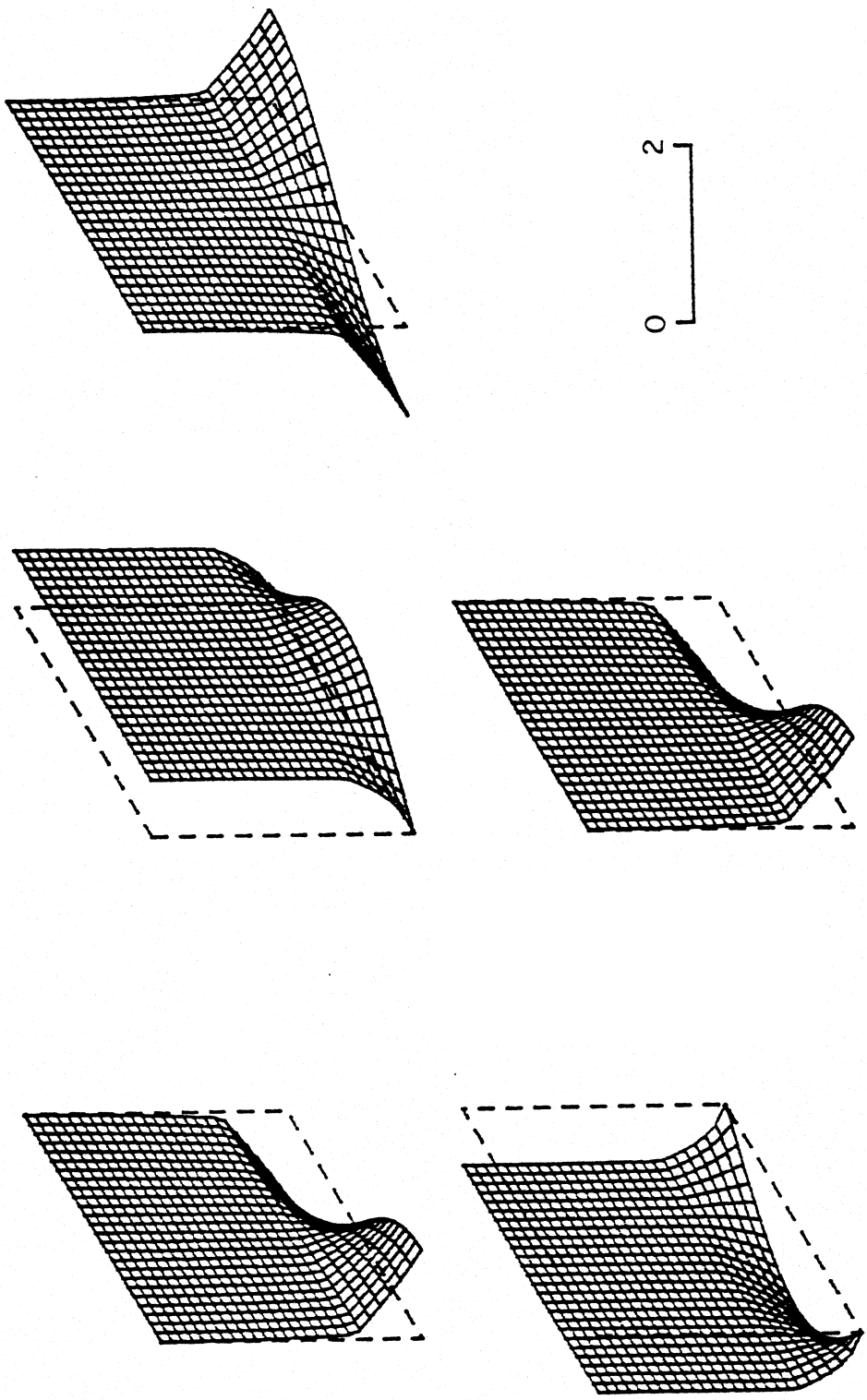

Figure 5.5.15a isplacement response of a long building, with height comparable to its length ($H/L = 1$) and with a soft first floor ($h_2/H = 0.25$ and $\beta_2/\beta_1 = 0.25$), for a propagating SII-wave ($\eta = 0.5$ and $c/\beta_2 = 0.05$), at times $t = 0, T/4, T/2, 3T/4$ and T. The wave energy does not "enter" into the building, as can be seen from the exponential displacements along the vertical.

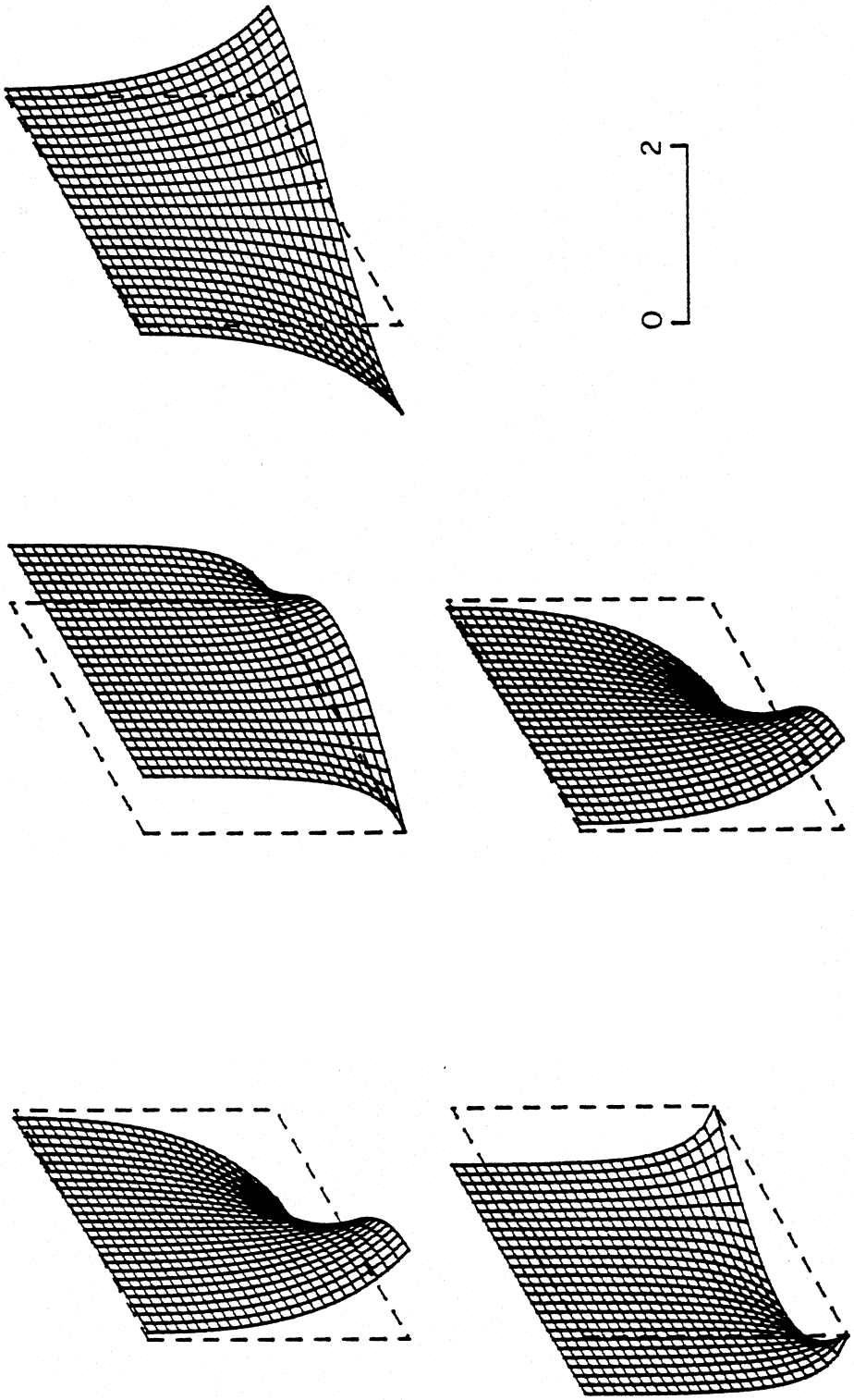

Figure 5.5.15b Displacement respone of a "homogeneous" building of same size as the building in Figure 5.5.15a, with shear wave velocity same as the shear wave velocity of the first floor of the building in Figure 5.5.15a and subjected to the same ground motion.

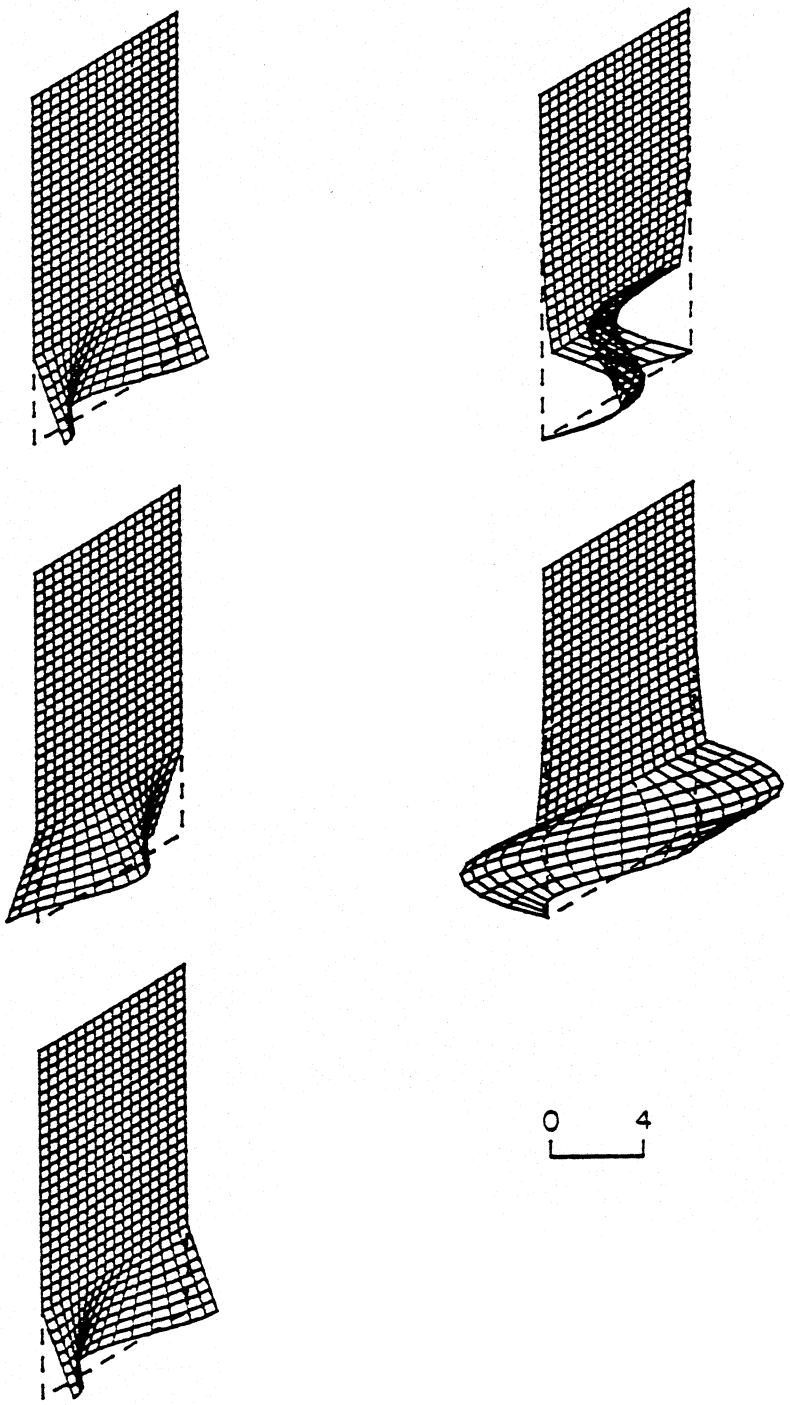

Figure 5.5.16a Displacement response of a long and tall building ($H/L = 2$), with a soft first floor ($h_2/H = 0.25$ and $\beta_2/\beta_1 = 0.25$), for a propagating wave ($\eta = 1$ and $c/\beta_2 = 1$), at times $t = 0, T/4, T/2, 3T/4$ and T. The wave energy "enters" only into the first floor, but not into the upper floors of the building.

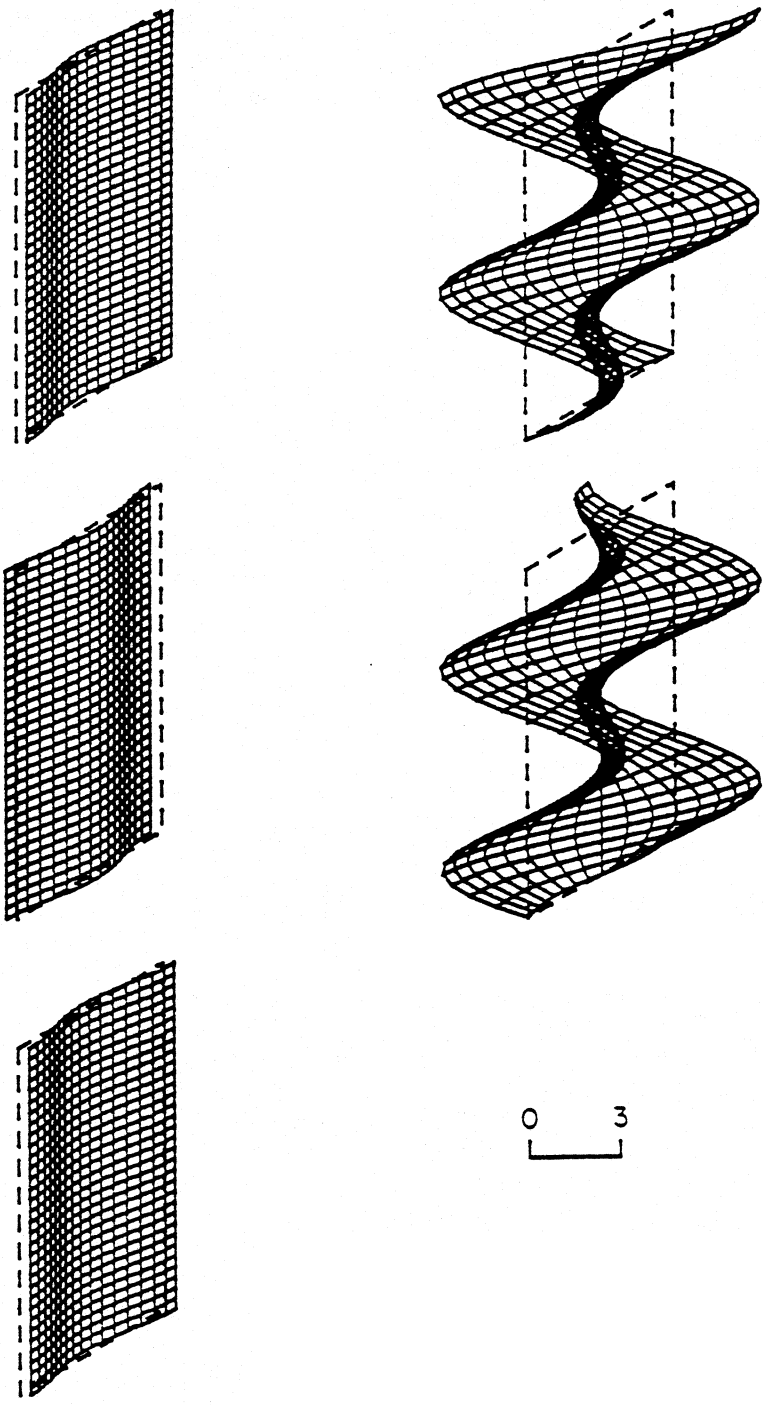

Figure 5.5.16b Displacement response of a "homogeneous" building, of same size as the building in Figures 5.5.16a with same shear wave velocity as in the first floor of the buillding in Figure 5.5.16a for the same ground motion. The wave energy propagates through the whole building.

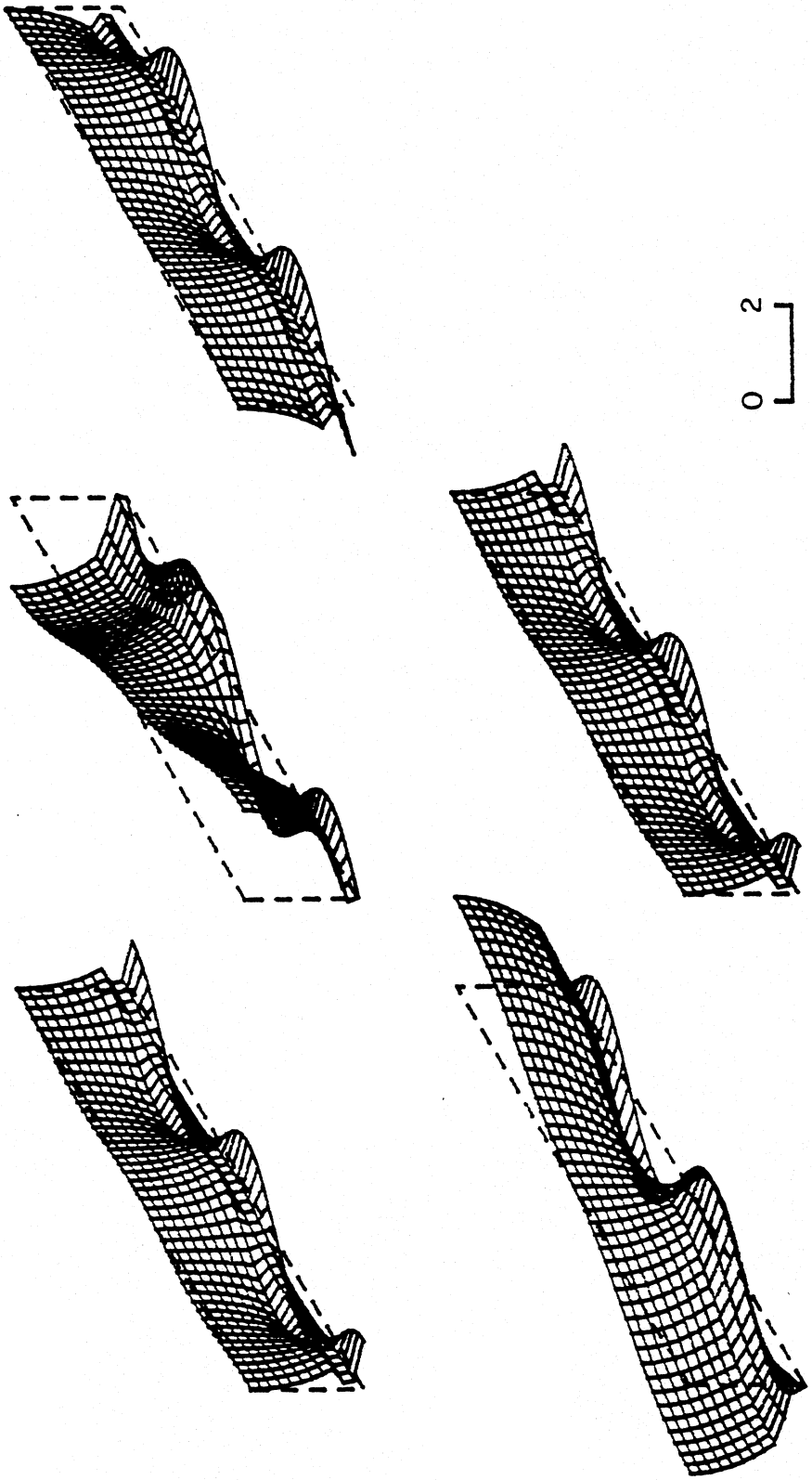

Figure 5.5.17a isplacement response of a long and low building ($H/L = 0.25$) with a soft first floor ($h_2/H = 0.25$ and $\beta_2/\beta_1 = 0.5$), for a propagating SH-wave ($\eta = 2$ and $c/\beta_2 = 1$), at times $t = 0, T/4, T/2, 3T/4$ and T. The wave energy propagates only through the first floor, which acts here as an "isolator" for the upper part of the building.

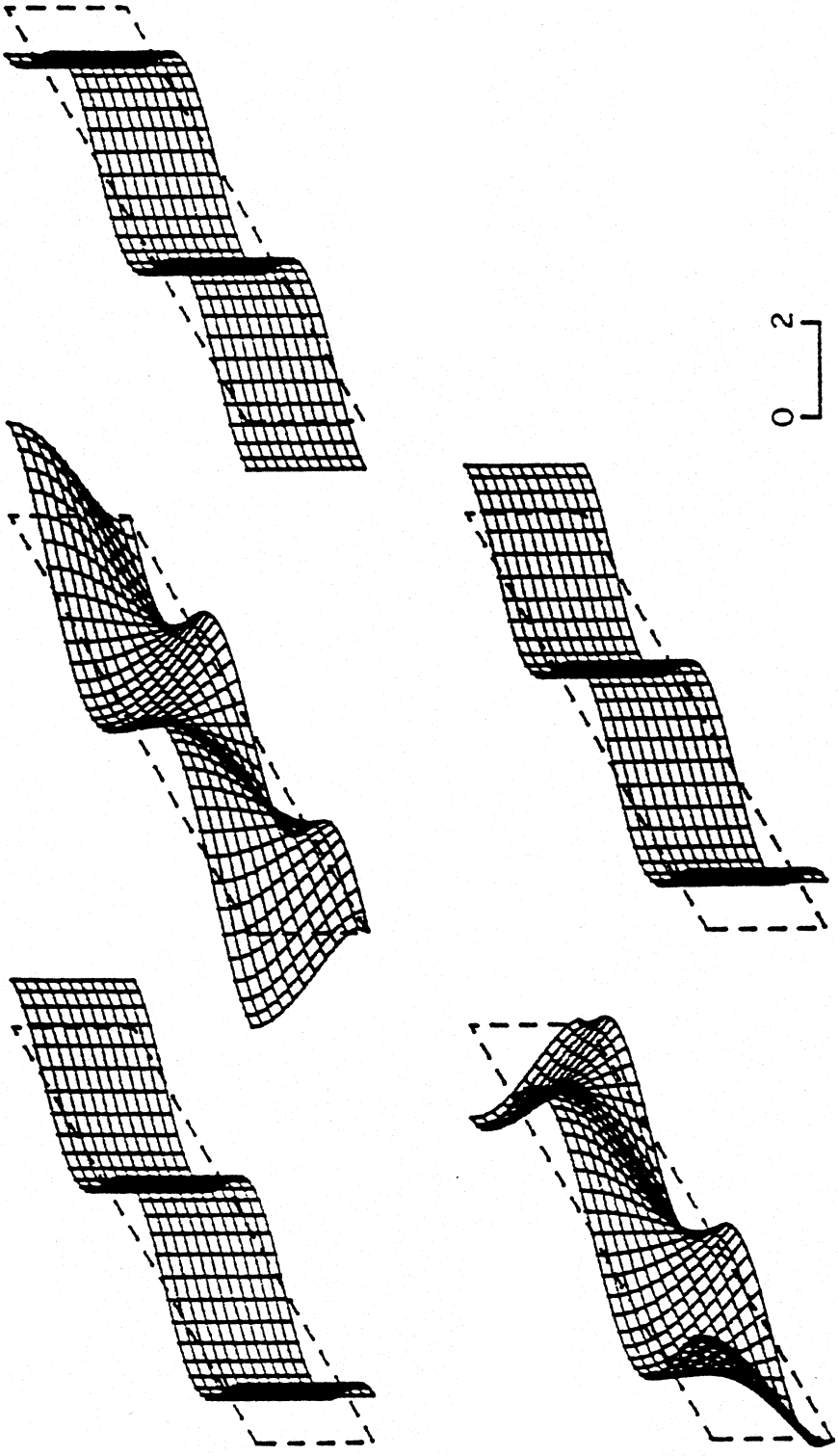

Figure 5.5.17b Displacement response of a "homogeneous" building of the same size, and with shear wave velocity same as in the soft first floor of the building in Figure 5.5.17a, and subjected to the same ground motion. The wave energy propagates through the whole building.

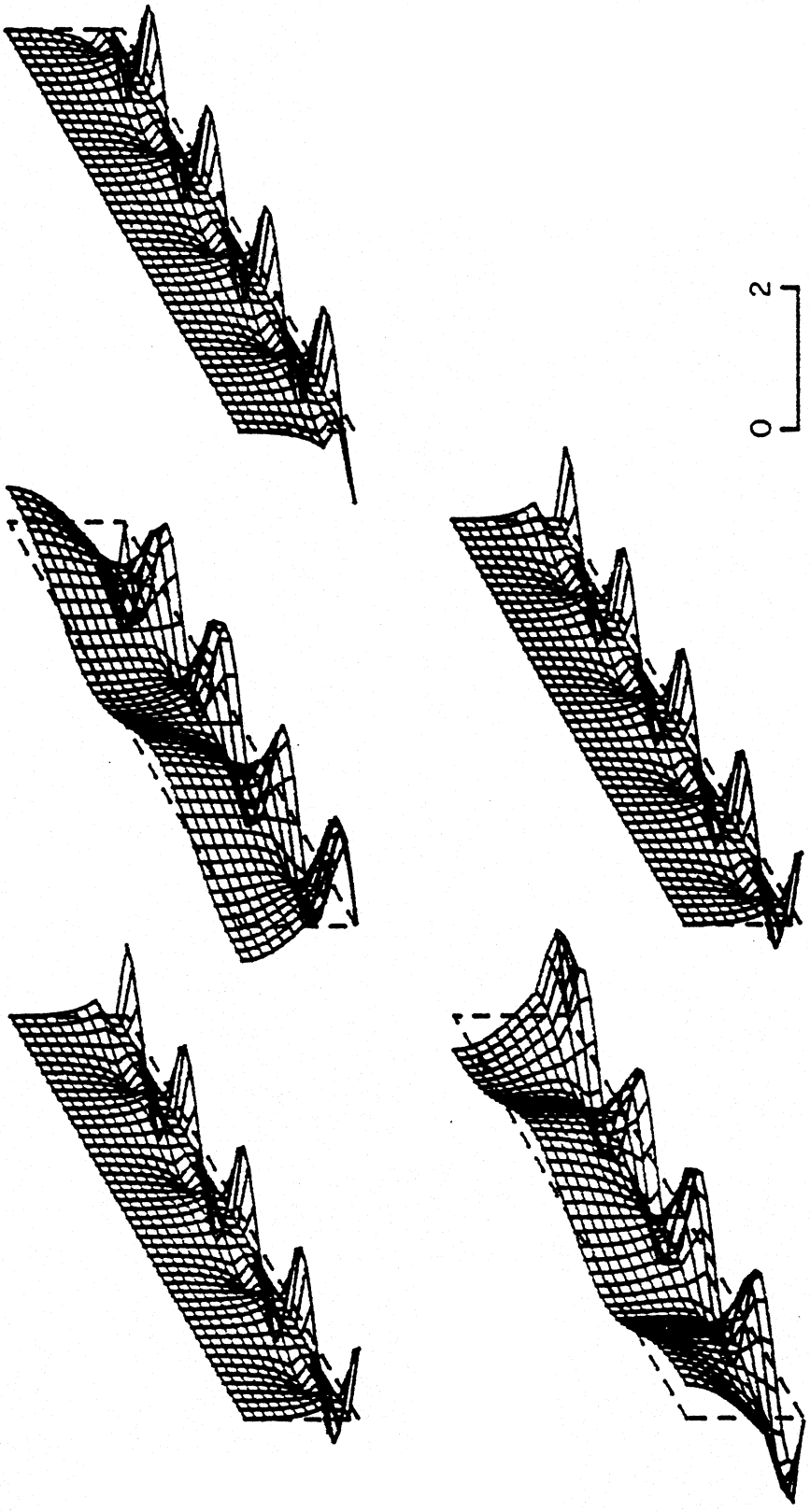

Figure 5.5.18a Displacement response of a long and low building ($H/L = 0.25$) with a soft first floor ($h_2/H = 0.25$ and $\beta_2/\beta_1 = 0.5$), for a propagating SH-wave ($\eta = 4$ and $c/\beta_2 = 1$), at times $t = 0, T/4, T/2, 3T/4$ and T. The wave energy propagates only through the first floor, which acts as an "isolator" for the upper part of the building.

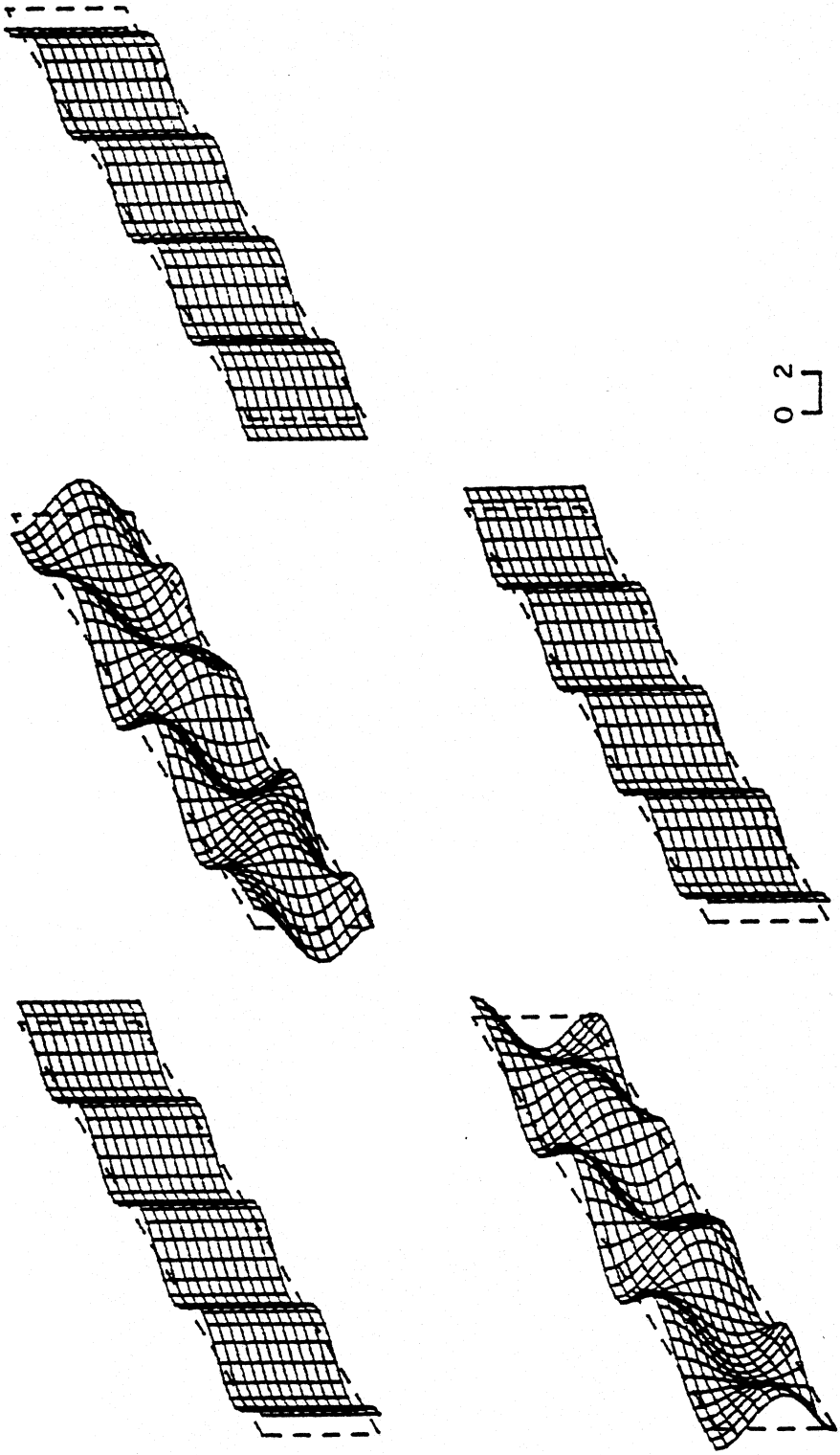

Figure 5.5.18b Displacement response of a "homogeneous" building of same size, for the same ground motion, and with shear wave velocity same as the shear wave velocity of the first floor of the building in Figure 5.5.18a. The wave energy propagates through the whole building.

parts of the buildings with the soft floor are small, smaller than the displacements of the corresponding "homogeneous" buildings. However, the "soft" first floor experiences large displacements and its columns and shear walls become candidates for where the failure of the building may occur.

Figure 5.5.16a shows large "torsional" vibrations of the first floor, while the upper part of the building hardly moves. The first floor vibrates as if it were supported at its upper edge.

For higher value of η ($\eta = 2$) and for the "long" buildings ($H/L = 0.25$) e.g. Figure 5.5.17a, the whole upper part of the building rotates almost as a rigid body. This causes large overall torsional deformations and stresses in the first floor.

The upper part of the "long" building in Figure 5.5.18a ($\eta = 4$) deforms as the wave propagates under the building. However, it illustrates vibrations with modes in x which do not coinside with the wave length of the ground motion causing this vibration.

Figures 5.5.19a and 5.5.20a illustrate the displacements of buildings, with "soft" first floors, when the waves propagate into the buildings. In both figures $\eta = .1, c/\beta_2 = 20, \beta_1/\beta_2 = 2$ and the height of the first floor is $0.25H$. The first building is a "tall" building ($H/L = 2$) while the second building has height comparable to its length ($H/L = 1$). The waves that enter the first floor propagate along the direction which is 2.87° off the vertical while the waves that enter the upper part propagate in the direction which is 5.72° off the vertical ($\sin\alpha = \beta_2/c, \sin\beta = \beta_1/c = (\beta_2/c)(\beta_1/\beta_2)$). The buildings vibrate with modes that are harmonic functions both in the first floor and in the upper part of the buildings. In these cases the soft first floor does not act as an "isolator" for the upper part of the building. Parts "b" of these figures illustrate the displacement of the corresponding homogeneous model, as in the previous examples.

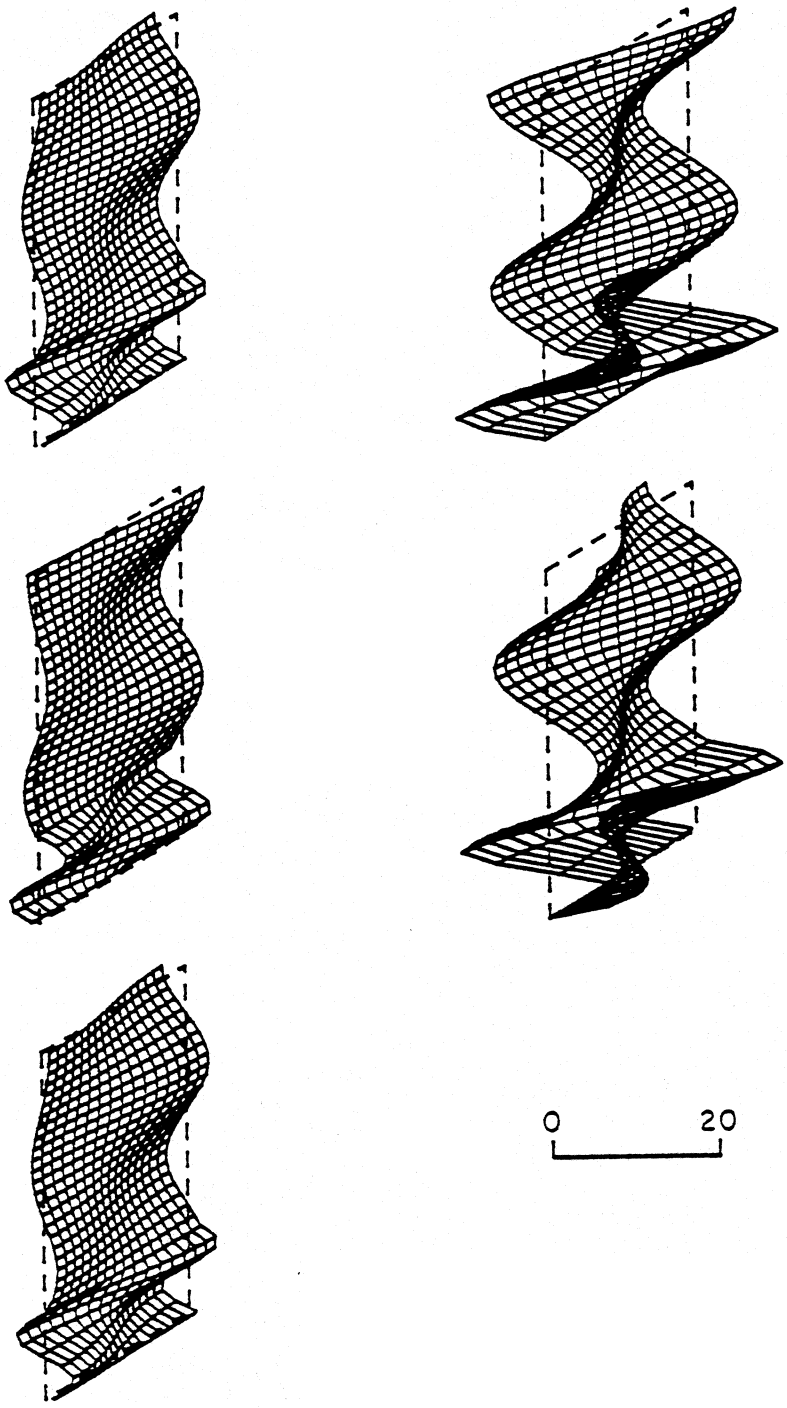

Figure 5.5.19a Displacement response of a tall building ($H/L = 2$) with a soft first floor ($h_2/H = 0.25$ and $\beta_2/\beta_1 = 0.5$), for a nearly vertically incident SH-wave ($\eta = 0.1$ and $c/\beta_2 = 20$), at times $t = 0, T/4, T/2, 3T/4$ and T. The wave energy propagates through the whole building when the incident wave arrives nearly vertically.

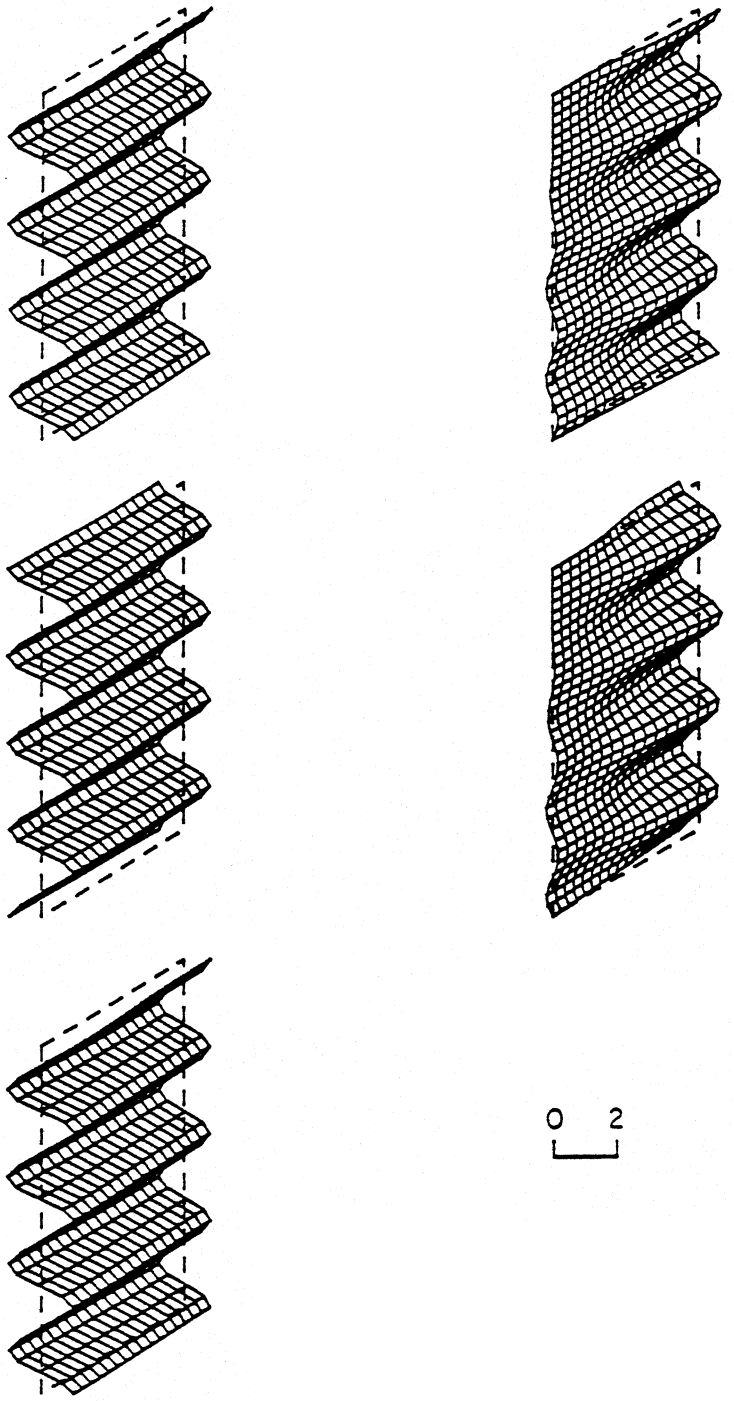

Figure 5.5.19b Displacement response of a "homogeneous" building of same size and for the same ground motion, but with shear wave velocity same as the shear wave velocity of the first floor of the building in Figure 5.5.19a. The wave energy propagates through the entire building.

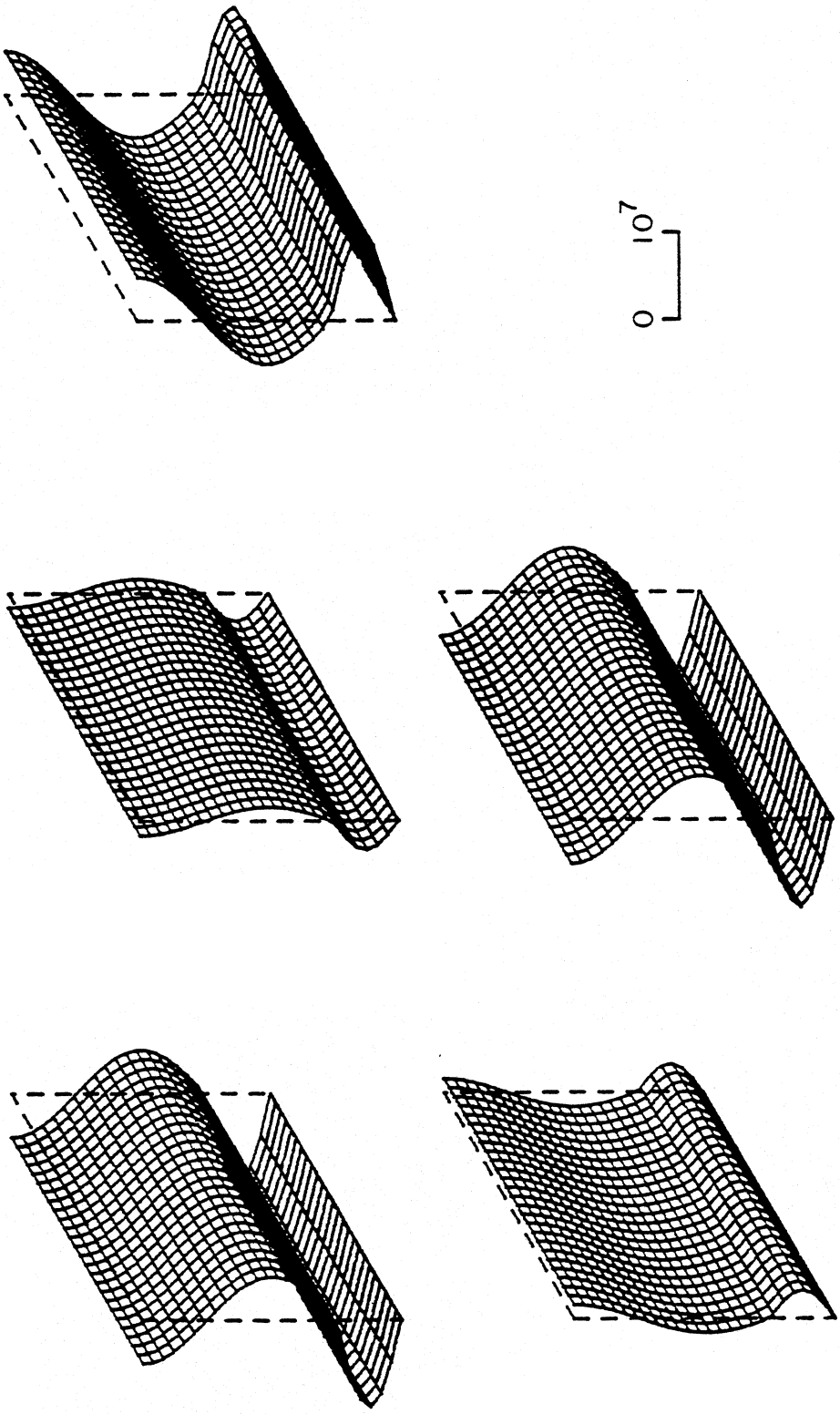

Figure 5.5.20a Displacement response of a building with height comparable to its length ($H/L = 1$) and with a soft first floor ($h_2/H = 0.25$ and $\beta_2/\beta_1 = 0.5$), for a nearly vertically incident SH-wave ($\eta = 0.1$ and $c/\beta_2 = 20$), at times $t = 0, T/4, T/2, 3T/4$ and T. The wave energy propagates through the whole building when the incident wave is arriving nearly vertically.

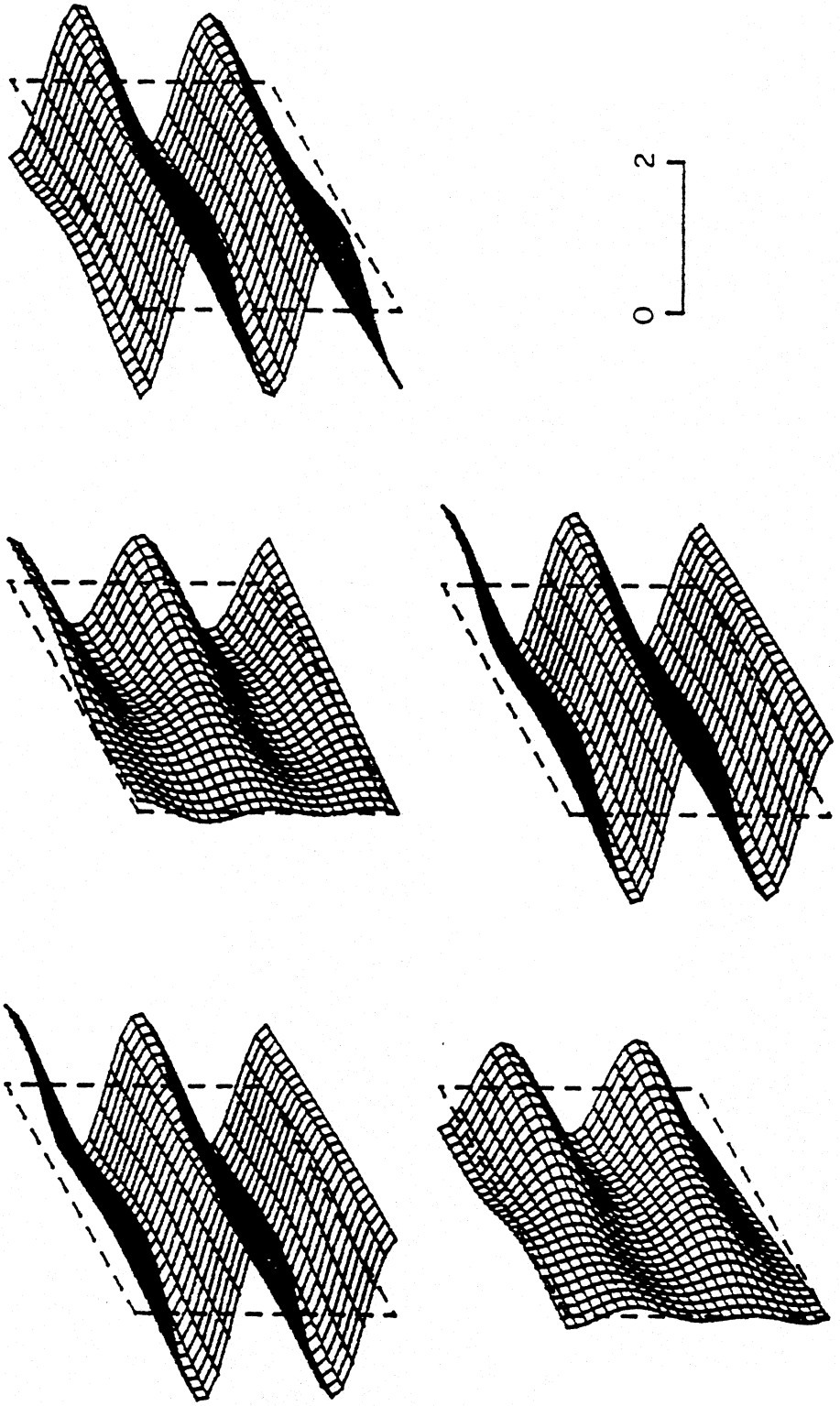

Figure 5.5.20b Displacement response of a "homogeneous" building of same size and for the same ground motion, but with shear wave velocity same as in the first floor of the building in Figure 5.5.20a. The wave energy propagates through the whole building.

5.6 Response of the Building Placed over Soil with Vertical Discontinuity in the Material Properties

The response of a homogeneous model placed over the half-space with a monochromatic vertical discontinuity in the material properties and excited by plane SH waves (Chapter IV, Section 4.3.1) has been analyzed and selected results are presented and discussed in this section. The medium on the left hand side of the discontinuity is "softer" than the medium to the right, and the incident waves are traveling from "soft" towards "hard" medium in all the cases which are presented here.

The following range of the dimensionless input parameters has been considered: $0.5 \leq \eta \leq 2$, $0.05 \leq c/\beta \leq 10$, $0.5 \leq \beta/\beta_L \leq 20$ and $0.025 \leq \beta_L/\beta_R \leq 0.3$, where, as mentioned in Chapter IV, c_L is the phase velocity of waves in the x-direction in the "soft" medium and β, β_L and β_R are the shear wave velocities in the building, the medium on the left and the medium on the right of the discontinuity, respectively. The choice of the above ratios of the shear wave velocities is based on the assumption that the smallest value of the shear wave velocity of soil is 50 m/s (e.g. San Francisco Bay Area, Mexico City), that typically the shear wave velocity of a very "soft" soil is 100-150 m/s (e.g. in Los Angeles Area it is 250-300 m/s), that the shear wave velocity of "rock" is 1500-2000 m/s and that the typical shear wave velocity in the building is of the order of 800 m/s.

Analysis in terms of dimensionless parameters showed that the condition for transmission of the wave motion through the discontinuity and into the "hard" medium, i.e. for real phase velocities in the horizontal direction in the medium on the right side of the discontinuity, is

$$\left(\frac{c_L}{\beta}\right)^2 \left(\frac{\beta}{\beta_L}\right)^2 \leq 1 + \left(\frac{c_L}{\beta}\right)^2 \left(\frac{\beta}{\beta_L}\right)^2 \left(\frac{\beta_L}{\beta_R}\right)^2 \tag{5.6.1}$$

and it does not depend on the dimensionless length η.

The motions in the "building" have been calculated for the following location of the "building" relative to the discontinuity: (1) buildilng entirely situated on the "soft" medium, (2) building lying partly on "soft" and partly on "hard" soil and (3) building entirely situated on the "hard" medium (Figure 4.3.4). Figures 5.6.1 through 5.6.7 represent the out of plane displacements of the vertical cross-section of the homogeneous model at five different equally spaced times during one period, T, of ground motion (i.e. at times $0, T/4, T/2, 3T/4$ and T). If one visualizes the horizontally propagating wave in the direction of the positive x-axis and with the wave length $\lambda = c_L T$, for "0" its displacement under the building is $v(x) = \cos \frac{2\pi x}{\lambda}$, for "$T/4$" it is $v(x) = \cos \frac{2\pi(x+\lambda/4)}{\lambda}$ and so on.

Figures 5.6.1, 5.6.2 and 5.6.3 represent displacements of the model when it is entirely placed on the "soft" medium, and the distance between the discontinuity and the closest point of the building is 0.2 L, when $\beta/\beta_L = 0.5$ and 2 and for $\beta_L/\beta_R = 0.025$. Figure 5.6.1 corresponds to $\eta = 0.5$ and $c_L/\beta = 5$, Figure 5.6.1 is for $\eta = 1$ and $c_L/\beta = 1$, and Figure 5.6.3 for $\eta = 2$ and $c_L/\beta = 1$. In all these cases the model is excited by essentially standing waves in the "soft" medium due to nearly complete reflection of incident waves from the discontinuity ($\beta_R/\beta_L = 40$). This can be concluded also from the fact that there are points at the base of the model for which the displacements are very small or zero at all times. These points correspond to the nodes of the standing waves in the soil and around them the torsional excitations of the plate take place. The points on the base that lie on the anti-nodes have the largest amplitudes during the cycle. From Figure 5.6.1 it can be seen, for example, that when $\eta = 0.5$ the torsional mode (the first anti-symmetric mode) is dominant. The position of this node depends on the position of the plate with respect to the discontinuity.

Analysis shows that when the building is partly situated on both the "soft" and the "hard" soil, the displacement amplitudes and patterns depend mostly on the values of

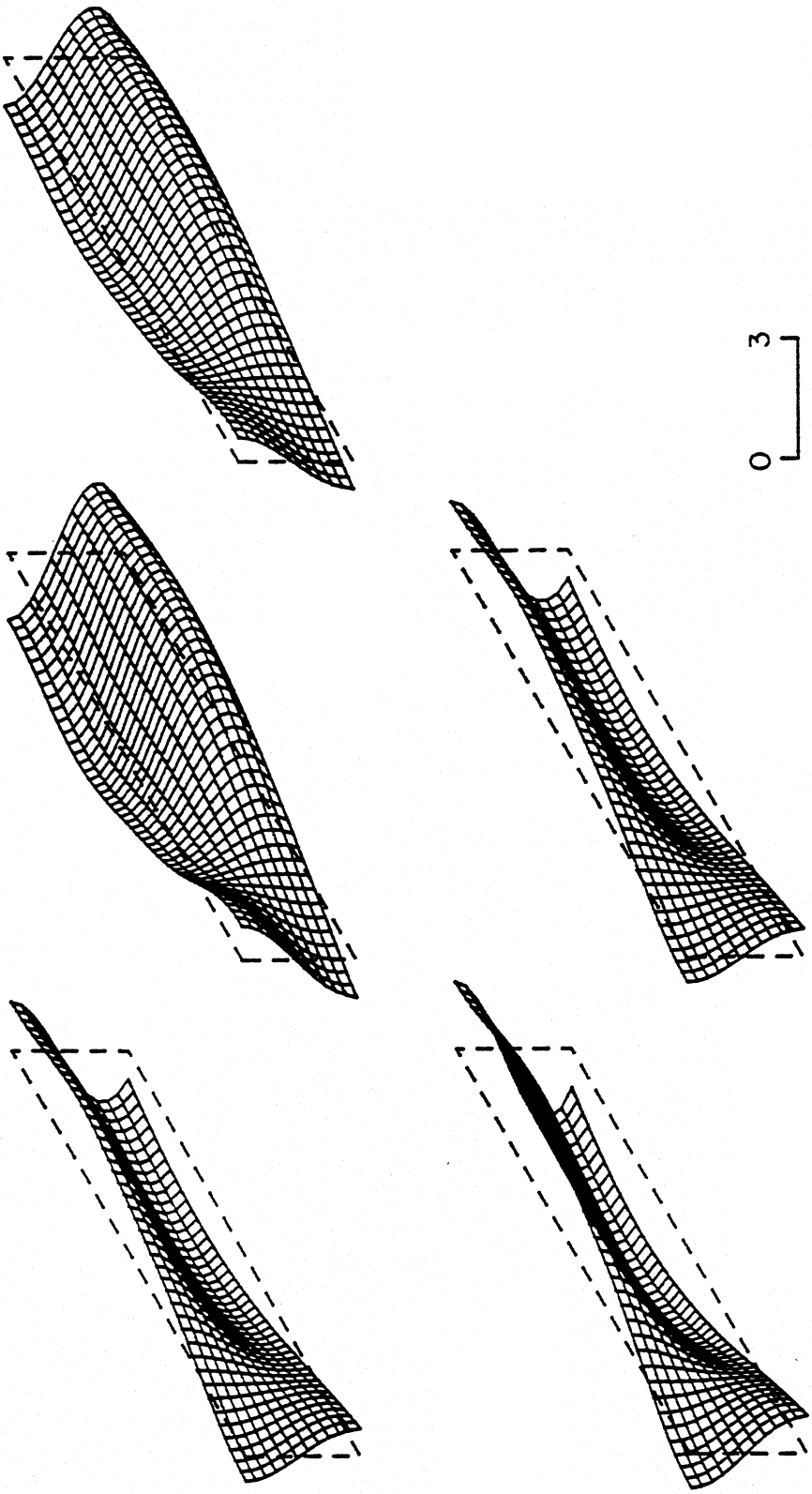

Figure 5.6.1 Displacement response of a long and low building ($H/L = 0.25$) placed over the "soft" soil in front of the vertical discontinuity in the soil ($\beta/\beta_L = 0.5$, $\beta_L/\beta_R = 0.025$ and $d/L = 1.2$) for incident SII-waves in the soft medium ($\eta = 0.5$ and $c_L/\beta = 5$), at times $t = 0, T/4, T/2, 3T/4$ and T. The building is practically "sitting" on a standing wave with wave length equal to twice the length of the building.

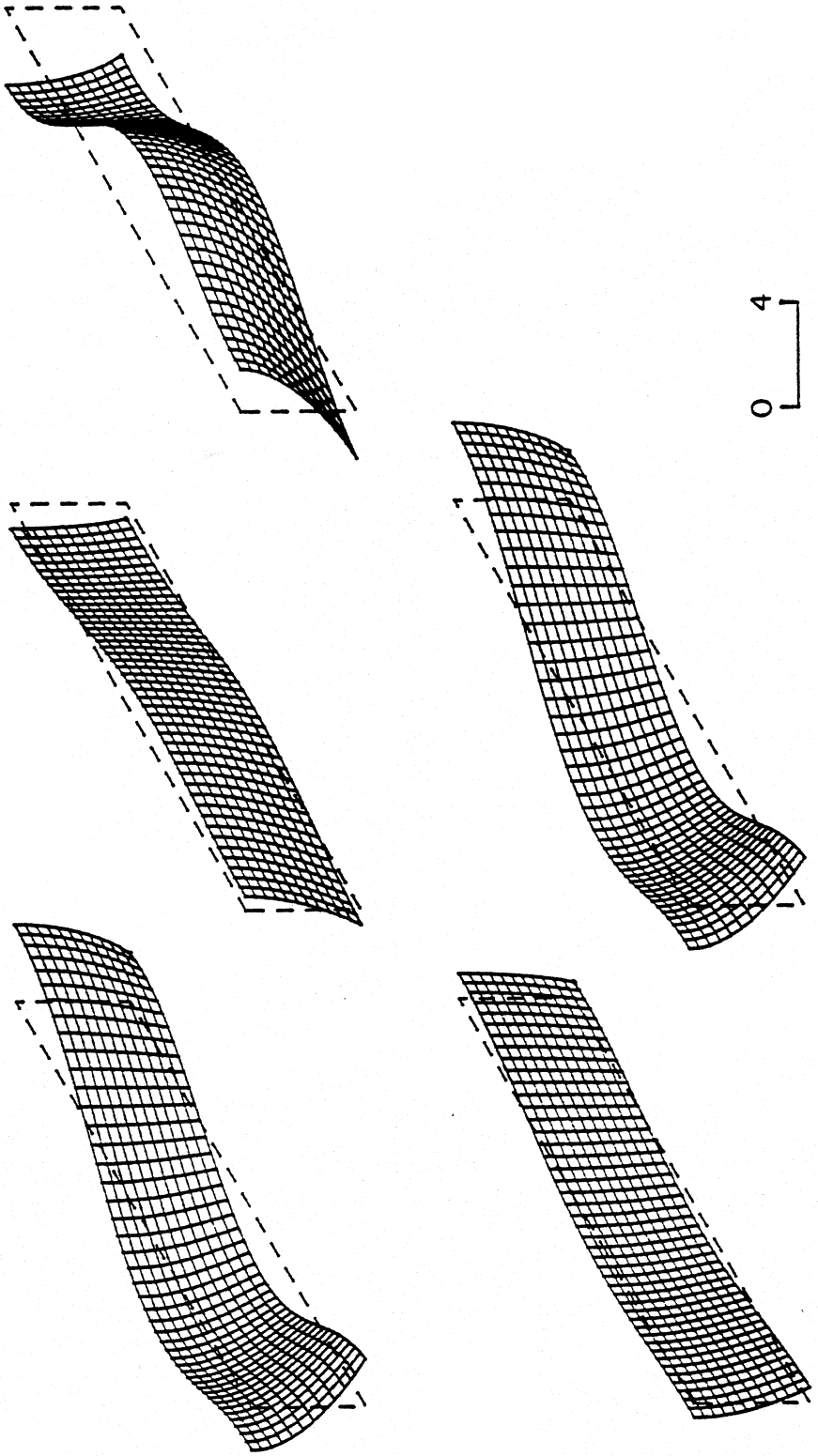

Figure 5.6.2 Displacement response of a long and low building ($H/L = 0.25$) placed over the "soft" soil in front of the vertical discontinuity ($\beta/\beta_L = 2$, $\beta_L/\beta_R = 0.025$ and $d/L = 1.2$) for incident waves in the "soft" medium ($\eta = 1$ and $c_L/\beta = 1$), at times $t = 0, T/4, T/2, 3T/4$ and T. The building is practically "sitting" on a standing wave with wave length equal to the length of the building.

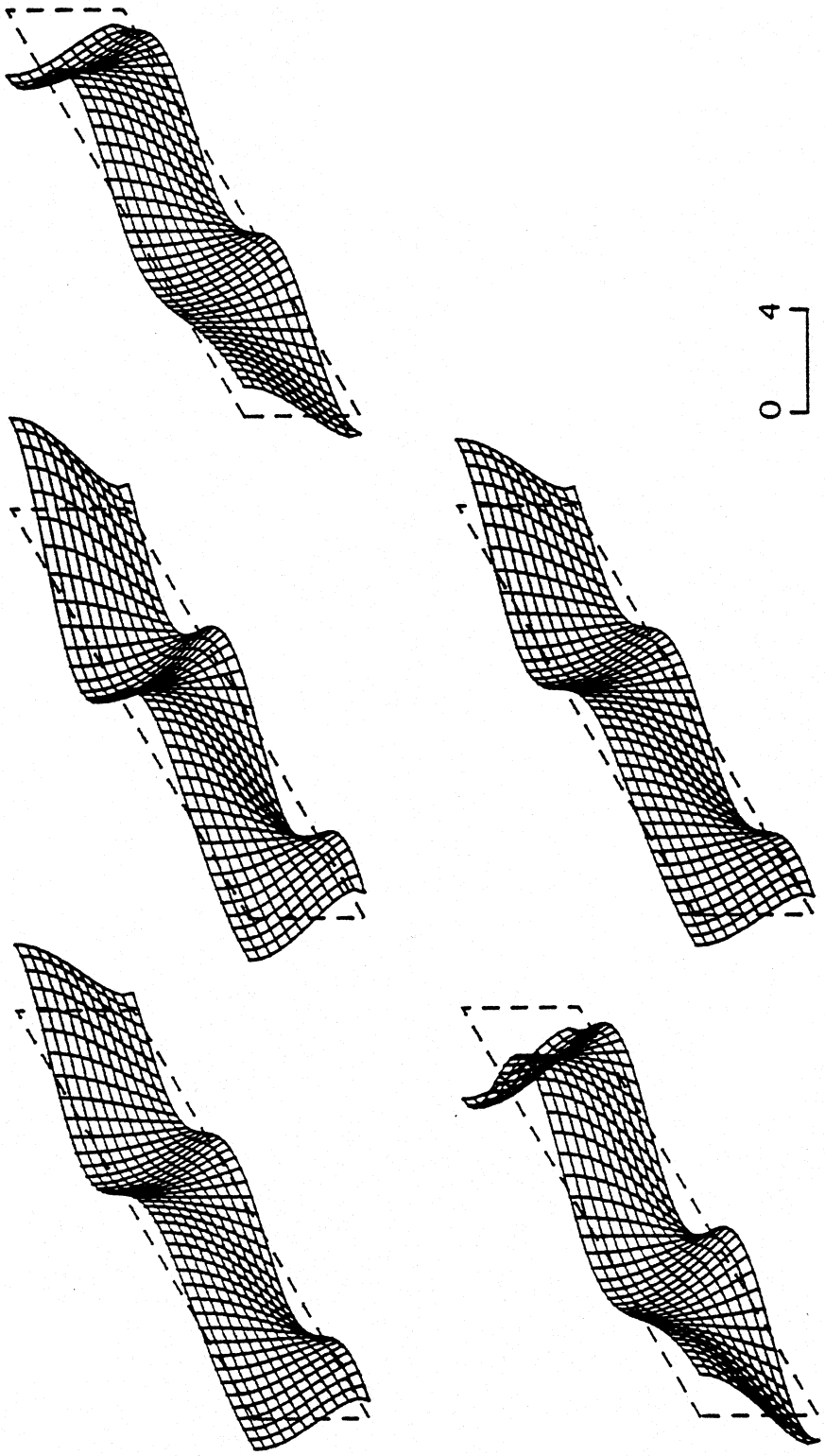

Figure 5.6.3 Displacement response of a long and low building ($H/L = 0.25$) placed over the "soft" soil in front of the vertical interface with the "hard" soil ($\beta/\beta_L = 2$, $\beta_L/\beta_R = 0.025$ and $d/L = 1.2$) for incident SII-waves in the soft medium ($\eta = 2$ and $c_L/\beta = 1$), at times $t = 0, T/4, T/2, 3T/4$ and T. The building is practically "sitting" on a standing wave with wave length equal to half of the length of the building.

$\eta = L/c_L T = L/\lambda_{x,L}$ and $c_L/\beta = \beta_L/\beta \sin\gamma$ (see Figure 5.3.1), and little on the values of β/β_L and β_L/β_R, i.e. because the phase velocity in the building in vertical direction becomes pure imaginary. $\lambda_{x,L}$ is the x-wave length of the incident waves in the medium on the left. Figures 5.6.4 through 5.6.6 illustrate the displacement of the model situated so that 70 percent of the base lies on "soft" soil and 30 percent on "hard" soil.

In Figure 5.6.4 $\eta = 2$, $c_L/\beta = 0.05$, $\beta/\beta_L = 20$ and $\beta_L/\beta_R = 0.025$. The phase velocity in the horizontal direction in the "harder" soil is real, but the wave that is transmitted through the discontinuity has very small amplitude. Also, the energy does not propagate into the building through the interface with the "soft" soil, because the value of $c_L/\beta < 1$ i.e. because the phase velocity in the building in the vertical direction becomes pure imaginary. In the "hard" soil $c_R/\beta > 1$. Yet, the hard soil does not excite large displacements of the building, because of the very small ground displacements in this medium.

Figures 5.6.5 and 5.6.6 correspond to $\eta = 0.5, c_L/\beta = 5$, $\beta/\beta_L = 0.5$ and $\beta_L/\beta_R = 0.025$ and to $\eta = 2$, $c_L/\beta = 10$, $\beta/\beta_L = 0.5$ and $\beta_L/\beta_R = 0.3$, respectively. The phase velocity c_R in the "hard" medium is pure imaginary in both cases, meaning that through the interface with the "hard" soil these buildings are excited by periodic displacements with exponentially decaying amplitudes towards the right end of the buildings. The left portion of the building ($x \leq d$ see Figure 4.3.4b) is excited mostly by the standing waves. The number of the standing wave nodes there depends on η. In both figures the part of the building that is in contact with the "soft" medium exhibits larger displacements compared to the part over the "hard" soil. The reason for this is the fact that the waves transmitted into the building from the "soft" soil are traveling nearly vertically through the building. The angle α (see Figures 5.3.1 and 5.3.2) is equal to 11.54° and 5.74° for $\eta = 0.5$ and $\eta = 2$, respectively.

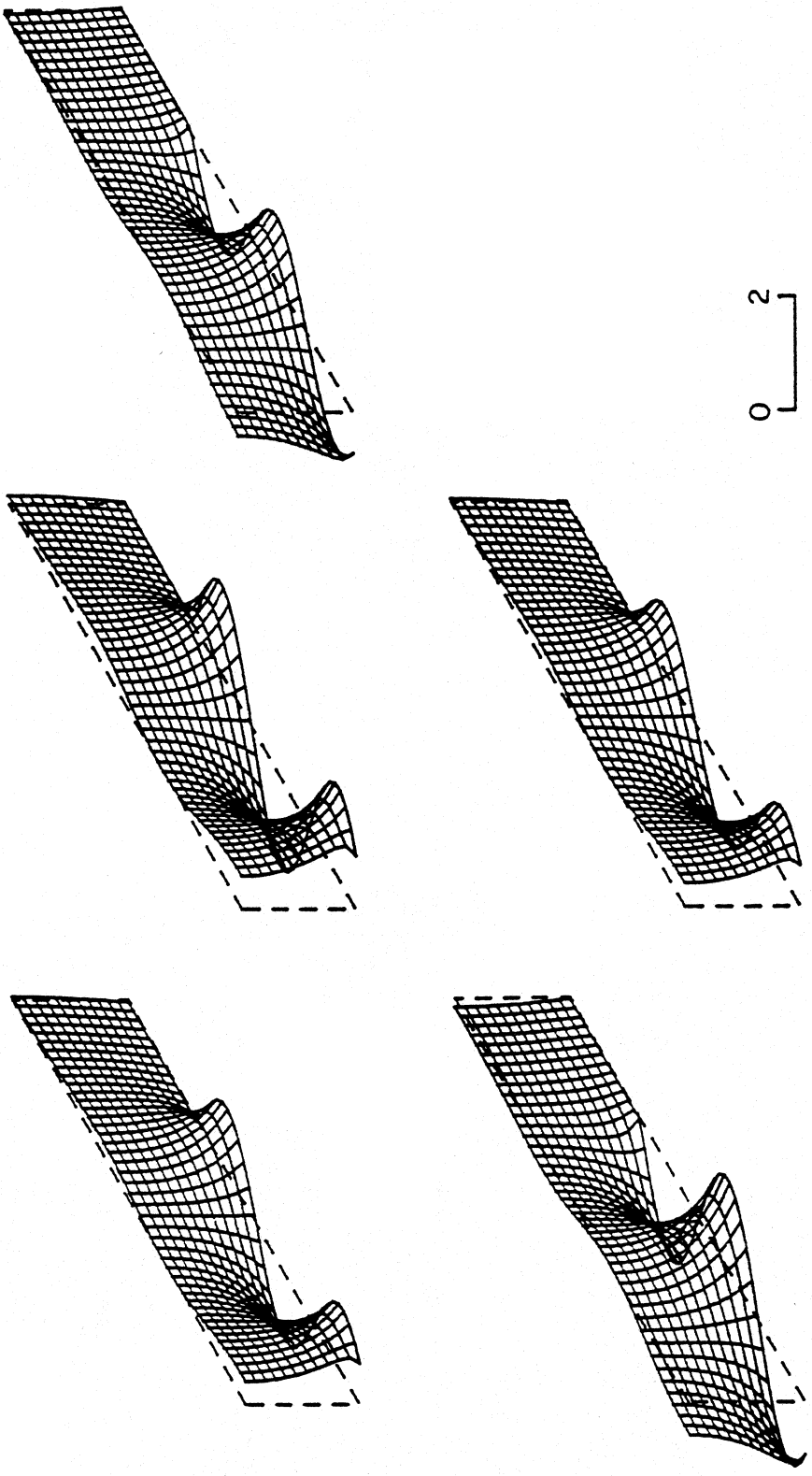

Figure 5.6.4 Displacement response of a long building ($H/L = 0.25$) placed over the vertical interface between the "soft" and "hard" soils ($\beta/\beta_L = 20$, $\beta_L/\beta_R = 0.025$ and $d/L = 0.7$) for incident SH-wave in the soft medium ($\eta = L/c_L T = 2$ and $c_L/\beta = 0.05$), at times $t = 0, T/4, T/2, 3T/4$ and T. The displacement in the "hard" soil is a propagting wave, but with small amplitudes. The wave energy does not propagate into the building because c_L/β and c_R/β are less than 1.

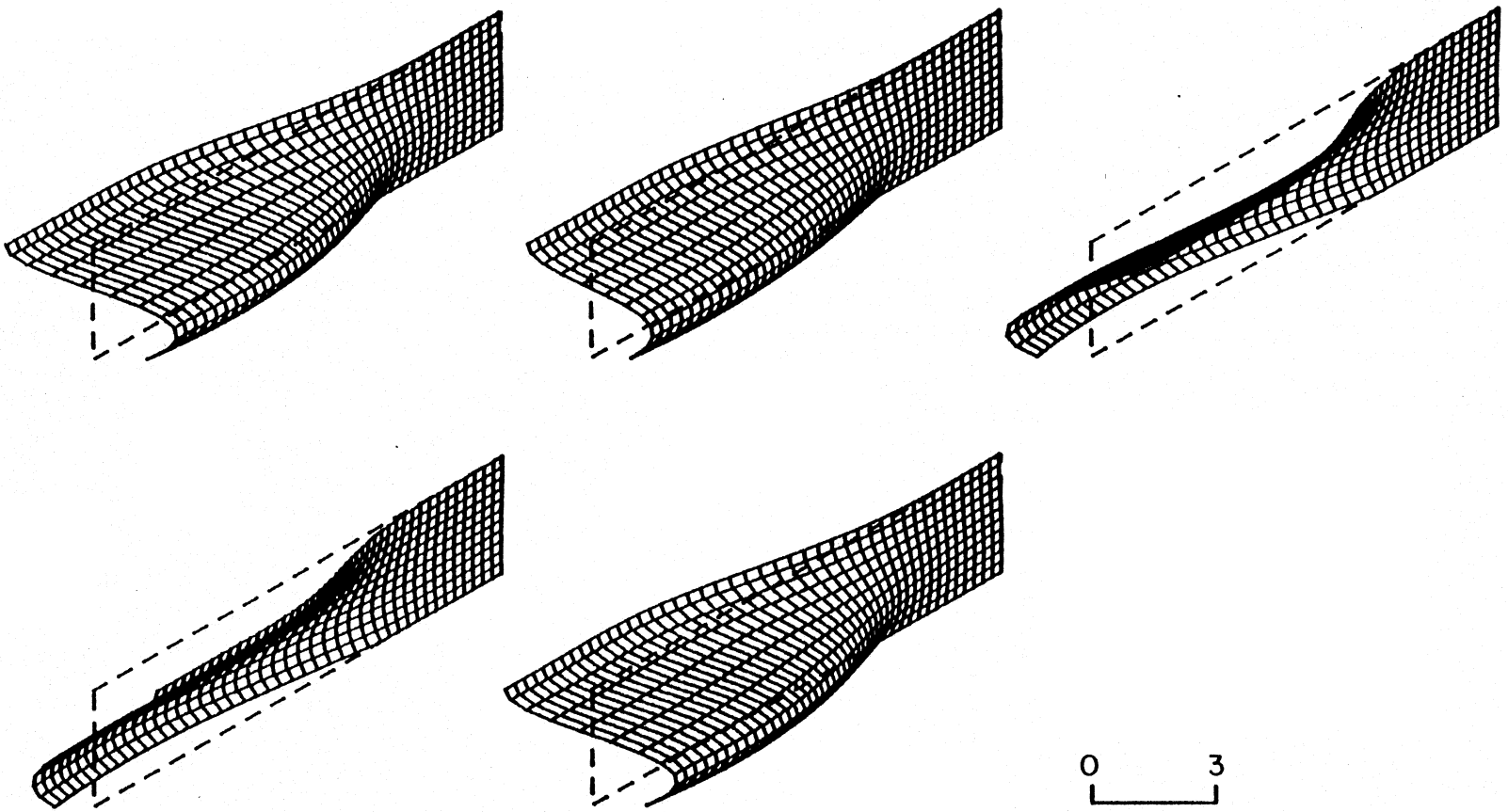

Figure 5.6.5 Displacement response of a long building ($H/L = 0.25$) placed over the vertical interface between the "soft" and "hard" soils ($\beta/\beta_L = 0.5$, $\beta_L/\beta_R = 0.025$ and $d/L = 0.7$) for incident SH-wave in the soft medium ($\eta = 0.5$ and $c_L/\beta = 5$), at times $t = 0, T/4, T/2, 3T/4$ and T. The wave energy propagates nearly vertically into the building through the interface with the "soft" soil only. The part of the building that is sitting over the "hard" soil has displacement amplitudes practically equal to zero.

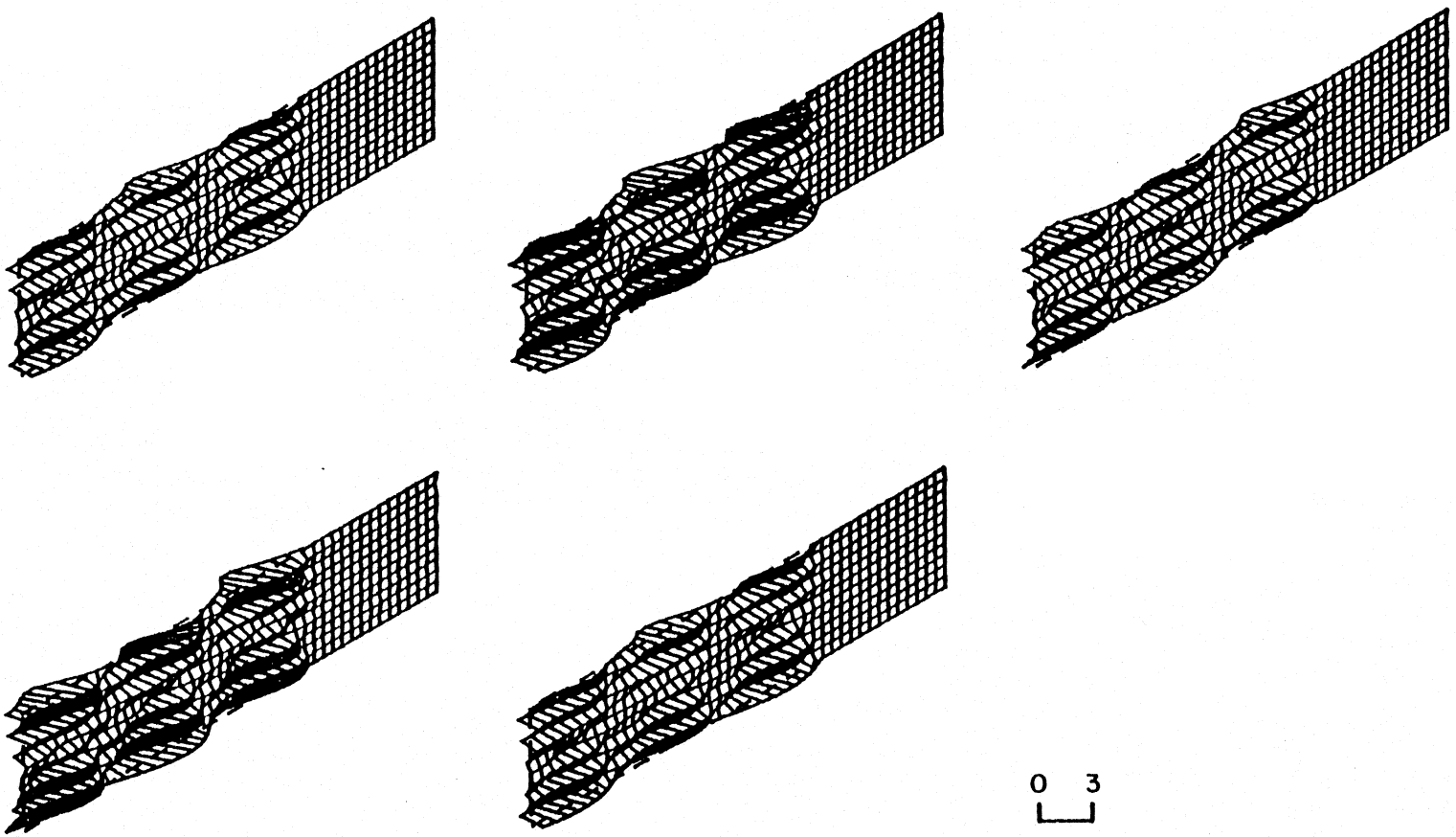

Figure 5.6.6 Displacement response of a long building ($H/L = 0.25$) placed over the vertical discontinuity in the soil ($\beta/\beta_L = 0.5$, $\beta_L/\beta_R = 0.3$ and $d/L = 0.7$) for incident SH-wave in the "soft" soil ($\eta = 2$ and $c_L/\beta = 10$), at times $t = 0, T/4, T/2, 3T/4$ and T. The wave energy propagates nearly vertically into the building through the interface with the "soft" soil. The part of the building that is sitting over the "hard" soil has displacement amplitudes practically equal to zero.

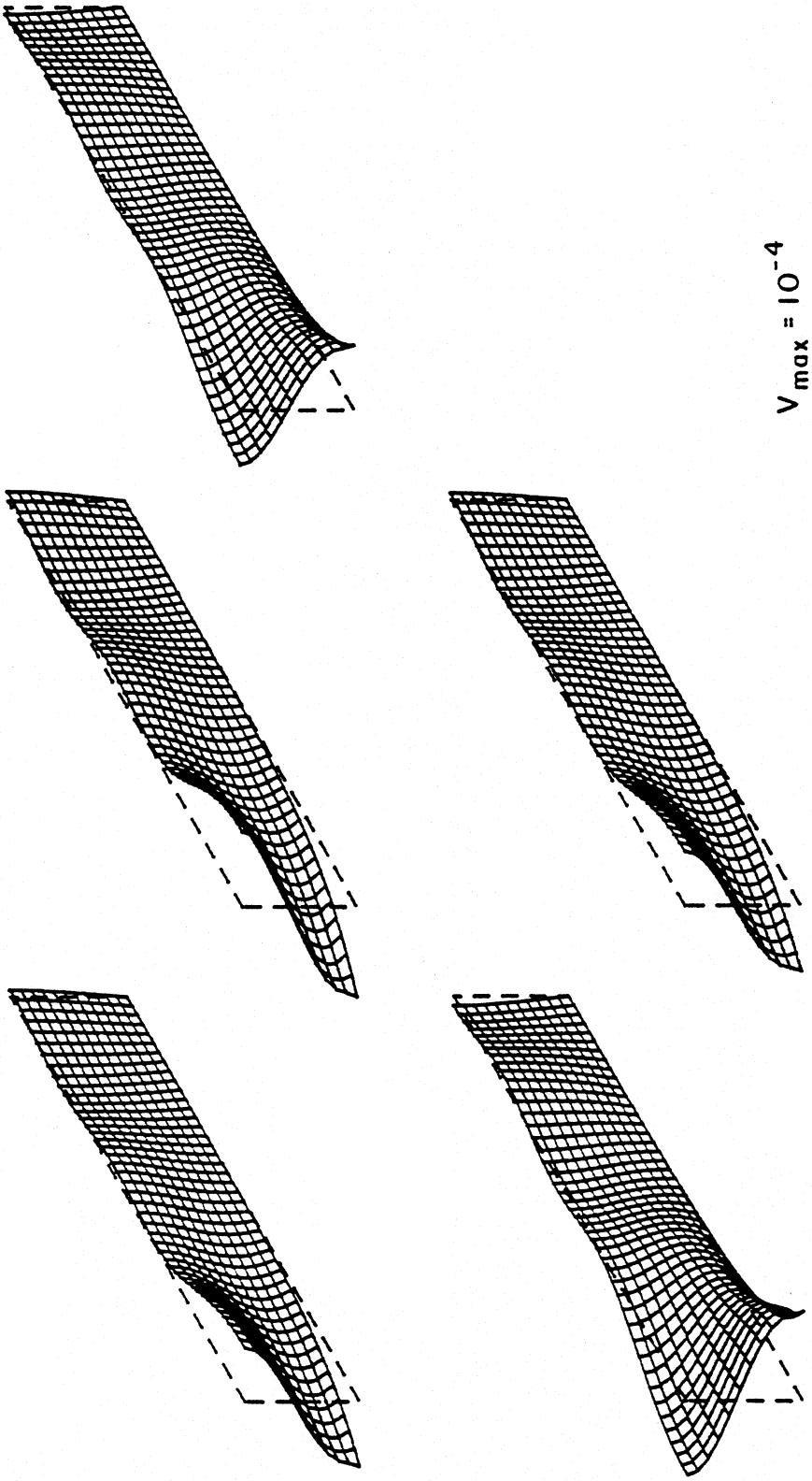

Figure 5.6.7 Displacement response of a long building $(H/L = 0.25)$, placed on the "hard" soil behind the vertical discontinuity in the soil $(\beta/\beta_L = 0.5,\ \beta_L/\beta_R = 0.025$ and $d/L = -0.2)$, for exponential displacements along the x-axis in the hard medium that result from the incident SH-wave in the soft medium $(\eta = 0.5$ and $c_L/\beta = 5)$, at times $t = 0, T/4, T/2, 3T/4$ and T.

Figure 5.6.7 illustrates a building which is entirely over the "hard" soil. The distance $d = -0.2L$ (see Figure 4.3.4c), and the phase velocity c_R is pure imaginary. The building is excited by the base displacement $f(x)e^{i\omega t}$, where $f(t)$ is an exponential function, decreasing with x. The parameters of the input wave are $\eta = 0.5$ and $c_L/\beta = 5$. The shear wave velocity ratios are $\beta/\beta_L = 0.5$ and $\beta_L/\beta_R = .025$. The displacements of the plate are small because of the small displacements of the soil. However, the interesting feature of this example is that only one side of the building is vibrating (near $x = 0$), in the region where the ground is having the largest amplitudes, with the right part of the building essentially remaining still. It is seen that two types of structural response can occur also when the discontinuity is within the building ($d = 0.7$ see Figures 5.6.5 and 5.6.6) and motions are larger and periodic in the area of "soft" soil. In both Figures 5.6.5 and 5.6.6 the waves enter the building nearly vertically ($\alpha = 11.54°$ and $\alpha = 5.74°$, respectively), through the contact with the "soft" soil.

CHAPTER VI
CONCLUSIONS

The principal observations and findings of this study as discussed in the preceeding sections, can be summarized as follows.

Two-dimensional models of buildings are more representative than the one-dimensional models because of the possibility they give 1) to apply a more realistic excitation to the building model and 2) to investigate and understand the variety of physical phenomena in their response. The models used in this work abound in new phenomena that cannot be seen from the one-dimensional models, and at the same time are simple enough to allow an analytical form of the solution. The advantage of the analytical form of the solution is that it is easier to see and to understand the influence of certain parameters on the overall response characteristics.

It has been shown that a building will vibrate not only with harmonic modes, but also with hyperbolic modes in the vertical direction, having exponentially decaying amplitude towards the top of the building. The number of harmonic modes, with which a building can vibrate, is finite. The hyperbolic modes are not associated with propagation of the wave energy into the building and the phenomenon of resonance occurs only for the harmonic modes. One dimensional models can vibrate only with harmonic modes.

The two-dimensional analysis shows that the transfer of energy from the ground into the building depends on the phase velocities with which the ground motion propagates. Energy will propagate into the building only when $c/\beta \geq 1$, where c is the phase velocity in the horizontal direction of the ground motion and β is the equivalent shear wave velocity of the building. In one-dimensional models of buildings the ground motion representation always has infinite phase velocities in the horizontal direction. This corresponds

to vertically incident waves, and under those conditions the energy always propagates into the building. The fact that the wave energy is not always transmitted into the building is of considerable practical importance. A soft layer under the building will reduce the phase velocities of the incident ground motion and can eventually make the ratio $c/\beta < 1$. Another way of reducing c is by chanelling the ground motion to arrive at the building site nearly horizontally. This way much of the wave energy may be prevented from propagating into the building.

The waves that are propagating in the horizontal direction excite the building to vibrate with a variety of symmetric and anti-symmetric modes of vibration, even when the building is perfectly symmetric. The one dimensional theory neglects all the higher modes, and the one-dimensional model vibrates only with the first symmetric mode that has a constant displacement in the horizontal direction. The current typical design practices consider 5 to 10 percent accidental torsion of the building and thus the torsional response because of the excentricity of the building only. Typically the buildings are not designed for the rotational excitation which is associated with strong ground motion. Gupta and Trifunac (1987), using a probabilistic approach, investigated the contributions of this torsional excitation to the earthquake response of simple symmetric buildings and concluded that the rotation of the ground should be considered in the design of buildings. Such rotational excitation is a good representation of the rotational characteristics of the ground motion only when the wave length of the seismic waves is long compared to the in-plan dimensions of the building. The two dimensional models used in this work do not put any limitations on the wave lengths of the input wave motion. The problem has been solved exactly and can be used in future work to determine the precision of the method of Gupta and Trifunac (1987), for example.

If the building is on long and inhomogeneous soil and near a vertical discontinuity in the material properties of the soil, which partially reflects the incoming waves, the building will be excited in part by the standing waves. In that case the points of the base of the building that are standing on the nodes of the standing wave will experience large torsional excitation. This does not happen if the displacement of the base is a propagating wave. If the building is long and partly sitting on "soft" soil and partly on "hard" soil it may happen that the building vibrates asymmetrically because of the large ground displacements in the "soft" soil and very small displacements in the hard soil. When the wave that has been transmitted into the building through the contact with the soft soil propagates nearly vertically through the building, it may happen that only the part of the building on the "soft" soil vibrates and the other part of the building is relatively quiet. Only the two-dimensional analysis can meaningfully be used to understand the response of such buildings.

Major discontinuities within the building will change its modes of vibrations its resonant frequencies and many general characteristics of the response. It was concluded that shear walls placed symmetrically near or at the ends constrain the displacements of the ends and reduce the horizontal "whipping" that could happen otherwise. The central core constrains only the displacements of the symmetric modes and does not change much the anti-symmetric mode-shapes. Thus, in general, it should be more desirable to design the shear resisting elements close to the ends of a building. When a building with soft first floor is excited by the propagating waves it may happen that the wave energy propagates only into the soft part and not into the upper parts of the building. The columns of the first floor, then, may experience very large displacements which are difficult to accomodate in design, but the overall consequences may be advantageous for the upper part of the

building. For nearly vertical incidence, the wave energy will propagate always into the whole building.

REFERENCES

1. Achenbach, J. D. (1973). "Wave Propagtion in Elastic Solids," North-Holland Publishing Company - Amsterdam, London, American Elsevier Publishing Company, Inc. - New York.

2. Akademia Nauk SSSR (1987). "Volnovie Protcesi v Konstrukciah Zdanii pri Seizmitcheskiih Vozdeistviah," edited by V. A. Krivelev, "Nauka," Moskwa, (in Russian).

3. Courant, R. and D. Hilbert (1953). "Methods of Mathematical Physics," Volume I, A Wiley Interscience Publication, John Wiley and Sons, New York, Chichester, Brisbane, Toronto, Singapore.

4. Grimmet, G. R. and D. R. Stirzaker (1985). "Probability and Random Processes," Clerendon Press, Oxford.

5. Gupta, I. D. and M. D. Trifunac (1987). "A Note on Contribution of Torsional Excitation to Earthquake Response of Simple Symmetric Builidngs," Earthquake Engineering and Engineering Vibration, Vol. 7, No. 3.

6. Hildebrand, F. B. (1964). "Advanced Calculus for Applications," Prentice-Hall, Inc., Englewood Cliffs, New Jersey.

7. Hudson, J. A. (1961). "The Total Internal Reflection of SH Waves," The Geophysical Journal of the Royal Astronomical Society, Vol. 6, 509-31

8. Kashefi, J. and M. D. Trifunac (1986). "Investigation of Earthquake Response of Simple Bridge Structure," University of Southern California, Dept. of Civil Engineering Report No. CE 86-02, Los Angeles.

9. Kojic, S., M. D. Trifunac and J. C. Anderson (1984). "A Postearthquake Response Analysis of the Imperial County Services Building in El Centro," University of Southern California, Dept. of Civil Engineering Report No. CE 84-02, Los Angeles.

10. Lee, V. W. and M. D. Trifunac (1985). "Torsional Accelerograms," International Journal of Earthquake Engineering and Soil Dynamics, Vol. 4, No. 3, 132-139.

11. Meirovitch, L. (1975). "Elements of Vibration Analysis," McGraw-Hill Book Company, New York.

12. Moeen-Vaziri, N. and M. D. Trifunac (1986). "Investigation of Scattering and Diffraction of Plane Seismic Waves through Two Dimensional Inhomogeneities," University of Southern California, Dept. of Civil Engineering Report No. CE-03, Los Angeles.

13. Moslem, K. and M. D. Trifunac (1987). "Spectral Amplitudes of Strong Earthquake Accelerations Recorded in Buildings," Soil Dynamics and Earthquake Engineering, Vol. 6, No. 2, Los Angeles.

14. Sato, R. (1961). "Love Waves Propagated Across Transitional Zone," Japanese Journal of Geophysics, Vol. 2, 117-134.

15. Trifunac, M. D. (1971a). "Surface Motion of a Semi-Cylindrical Alluvial Valley for Incident Plane SH Waves," Bull. Seism. Soc. Amer., Vol. 61, No. 6, 1755-1770.

16. Trifunac, M. D. (1971b). "A Method for Synthesizing Realistic Strong Ground Motion," Bull. Seism. Soc. Amer., Vol. 61, No. 6, 1739-1753.

17. Trifunac, M. D. (1972a). "Tectonic Stresses and Source Mechanism of the Imperial Valley, California Earthquake of 1940," Bull. Seism. Soc. Amer., Vol. 62, 1283-1302.

18. Trifunac, M. D. (1972b). "Comparison Between Ambient and Forced Vibration Experiments," Earthquake Engineering and Structural Dynamics, Vol. 1, 133-150.

19. Tzenov, L. (1981). "Vliane na dlzinata na konstruktsiite vrhu natovaranie," Bulgarian Academy of Sciences, Theoretical and Applied Mechanics, Sofia, Year XII, No. 2, (in Bulgarian).

20. Tzenov, L. and Boncheva, H. (1979). "Dlgi v plan sgradi s ogled seizmichnoto im osiguriavanie," Bulgarian Academy of Sciences, Bulgarian Geophysical Journal, Vol. V, No. 4, Sofia, (in Bulgarian).

21. Werner, S. D., L. C. Lee, H. L. Wong and M. D. Trifunac (1977). "An Evaluation of the Effects of Traveling Seilsmic Waves on the Three- Dimensional Response of Structures," Agbabian Associates, El Segundo, California, Report No. R-7720-4514.

22. Wong, H. L. (1979). "Diffraction of P, SV and Rayleigh Waves by Surface Topographies," University of Southern California, Dept. of Civil Engineering Report No. CE 79-05, Los Angeles.

APPENDIX A

FACTOR f IN THE EQUATION (2.3.3b)

The bending stiffness k in the y-direction of a rectangular column made of reinforced concrete is

$$k = \frac{12 E_c I_{y,r}}{h^3} \quad , \tag{A.1}$$

where $I_{y,r}$ is the area moment of inertia of the entire section for bending about an axis perpendicular to y. Therefore, the factor f in equation (2.3.3b) is

$$f = \frac{I_{y,r}}{I_y} \quad , \tag{A.3}$$

where I_y is the area moment of inertia of the concrete section only.

Let A_s and A'_s be the areas of the tension and compression steel, respectively, and let these two areas be equal. One can also assume that the concrete and the steel are perfectly elastic, both in tension and in compression, so that the mutual axis is in the center of the cross-section.

The area moment of inertia of the reinforced cross-section is equal to the area moment of inertia of the transformed cross-section, when the steel has been replaced by concrete, but of area E_s/E_c times bigger than the actual area of the steel. E_s/E_c is the ratio of the Young's moduli of elasticity of the steel and of the concrete. The area moment of inertia of the transformed section $I_{y,tr}$ is approximately equal to

$$I_{y,tr} = I_y + 2A_s \frac{E_s}{E_c} d_s^2 \quad , \tag{A.4}$$

where d_s is the distance from the neutral exis to the reinforcing bars. In equation (A.4) it has been assumed that the diameters of the steel bars are small compared to the size of the cross-section.

Having in mind that $I_y = ab^3/12$, the factor f becomes

$$f = 1 + 24\frac{A_s}{ab}\frac{E_s}{E_c}\left(\frac{d_s}{b}\right)^2 \quad . \tag{A.5}$$

For example, if A_s is equal to 3 percent of the total area of the cross-section, if $E_s/E_c = 8$ and if $d_s = 0.4b$, then $f \approx 2$.

APPENDIX B

ORTHOGONALITY OF THE EIGENFUNCTIONS IN X-DIRECTION FOR THE MODEL WITH VERTICAL DISCONTINUITIES

The eigenfunctions in the x-direction, $X_n(x)$, of the model with vertical discontinuities of the material properties, are discussed in section 3.3 (the model is illustrated in Figure 3.3.1) and can be written in the following form:

$$X_n(x) = \begin{cases} X_n^{(1)}(x) & L_0 \le x < L_1 \\ X_n^{(2)}(x) & L_1 \le x < L_2 \\ X_n^{(3)}(x) & L_2 \le x < L_3 \end{cases} \qquad n = 0, 1, \ldots \tag{B.1}$$

where $L_0 = 0, L_1 = 1, L_2 = \ell_1 + \ell_2, L_3 = \ell_1 + \ell_2 + \ell_3 = L$, and ℓ_1, ℓ_2 and ℓ_3 are as shown in Figure 3.3.1.

All eigenfunctions $X_n(x)$, and consequently the functions $X_n^{(j)}(x) \quad j = 1, 2, 3$, satisfy the following differential equation:

$$X_n^{(j)''} + (k_j^2 - k_{z,n}^2) X_n^{(j)} = 0 \quad \begin{matrix} j = 1, 2, 3 \\ n = 0, 1, \ldots \end{matrix} \quad , \tag{B.2}$$

where $k_j = \omega/\beta_j$ is the wave number in the j-th layer, $k_{z,n}$ is the wave number in the z-direction of the n-th mode, and $X_n^{(j)''}(x)$ stands for the second derivative of $X_n^{(j)}(x)$. $k_{z,n}$ is the same in all the layers and its allowable values are the eigenvalues of the problem. The boundary and the continuity conditions to be satisfied are

$$X_n^{(1)'}(L_0) = X_n^{(3)'}(L_3) = 0, \quad n = 0, 1, \ldots \tag{B.3}$$

$$X_n^{(j)}(L_j) = X_n^{(j+1)}(L_j), \quad j = 1, 2\ , \quad n = 0, 1, \ldots \tag{B.4}$$

and

$$\mu_j X_n^{(j)}(L_j) = \mu_{j+1} X_n^{(j+1)}(L_j), \quad j = 1, 2, \quad n = 0, 1, \ldots \quad , \tag{B.5}$$

where μ_j is the shear modulus of the j-th layer.

If the equation (B.3), written for the n-th mode, is multiplied with $X_m^{(j)}$, and the same equation, written for the m-th mode is multipled by $X_n^{(j)}$, the following equations are obtained:

$$X_m^{(j)} X_n^{(j)''} + (k_j^2 - k_{z,n}^2) X_m^{(j)} X_n^{(j)} = 0 \qquad j = 1,2,3 \tag{B.6}$$

and

$$X_n^{(j)} X_m^{(j)''} + (k_j^2 - k_{z,m}^2) X_n^{(j)} X_m^{(j)} = 0 \qquad j = 1,2,3 \tag{B.7}$$

By subtracting equation (B.7) from the equation (B.6) it follows that

$$X_m^{(j)} X_n^{(j)''} - X_n^{(j)} X_m^{(j)''} = (k_{z,n}^2 - k_{z,m}^2) X_n^{(j)} X_m^{(j)} \qquad j = 1,2,3 \quad . \tag{B.8}$$

Multiplying each of the equations (B.8) by μ_j, then integrating each side from L_{j-1} to L_j, and at the end summing up the three equations, results in

$$\begin{aligned} &\sum_{j=1}^{3} \left(X_m^{(j)} \mu_j X_n^{(j)'} \Big|_{L_{j-1}}^{L_j} - X_n^{(j)} \mu_j X_m^{(j)'} \Big|_{L_{j-1}}^{L_j} \right) = \\ &(k_{z,n}^2 - k_{z,m}^2) \sum_{j=1}^{3} \int_{L_{j-1}}^{L_j} \mu_j X_n^{(j)} X_m^{(j)} dx \qquad j = 1,2,3 \quad . \end{aligned} \tag{B.9}$$

The left-hand-side of equation (B-9) is equal to zero because of the conditions (B.3), (B.4) and (B.5). The sum on the right-hand-side of the equation (B.9), by definition, equals the weighted inner product $(X_n, X_m)_w$, defined in section 3.3 by the equations (3.3.7) and (3.3.8). Substituting this in the equation (B.9) it follows that

$$(k_{z,n}^2 - k_{z,m}^2)(X_n, X_m)_w = 0 \quad . \tag{B.10}$$

If $m \neq n$, $k_{z,n}^2 - k_{z,m}^2 \neq 0$ and therefore $(X_n, X_n)_w$ must be equal to zero. When $m = n$, $(X_n, X_n)_w$ is always greater than zero, because the eigenfunctions $X_n(x)$ are not identically equal to zero on the interval $[0, L]$. This proves the orthogonality of the set of the functions $\{X_n(x)\}_{n=0}^{\infty}$.

APPENDIX C

ANALYTICAL EXPRESSIONS FOR THE COEFFICIENTS $C_n, n = 0, 1, \ldots$ IN THE EQUATION (3.3.11a)

Following the definition of the weighted inner product, in equation (3.3.9), with respect to which the eigenfunctions in the x-direction $X(x)$ of the model with the vertical discontinuities are orthogonal, the inner products $(e^{i\omega\frac{x}{c}}, X_n)_w$ and (X_n, X_m) are

$$\begin{aligned}(e^{i\omega\frac{x}{c}}, X_n)_w = \mu_1 &\int_0^{\ell_1} e^{-i\frac{\omega}{c}x}\cos k_{x,n}^{(1)}x\,dx \\ &+ \mu_2\int_{\ell_1}^{\ell_1+\ell_2} e^{-i\frac{\omega}{c}x}(A_n^{(2)}\cos k_{x,n}^{(2)}x + B_n^{(2)}\sin k_{x,n}^{(2)}x)dx \qquad (C.1)\\ &+ \mu_3 A_n^{(3)}\int_{\ell_1+\ell_2}^{L} e^{-i\frac{\omega}{c}x}\cos k_{x,n}^{(3)}(x-L)dx \quad ,\end{aligned}$$

and

$$\begin{aligned}(X_n, X_n)_w = \mu_1 &\int_0^{\ell_1} \cos^2 k_{x,n}^{(1)}x\,dx \\ &+ \mu_2\int_{\ell_1}^{\ell_1+\ell_2} (A_n^{(2)}\cos k_{x,n}^{(2)}x + B_n^{(2)}\sin k_{x,n}^{(2)}dx)^2 dx \qquad (C.2)\\ &+ \mu_3\int_{\ell_1+\ell_2}^{L} \left(A_n^{(3)}\right)^2\cos^2 k_{x,n}^{(3)}(x-L)dx \quad .\end{aligned}$$

All the integrals in the above equations can be evaluated analytically. The coefficients C_n are then given by the ratios of the two inner products, i.e.

$$C_n = \frac{\left(e^{-i\frac{\omega}{c}x}, X_n\right)_w}{(X_n, X_n)_w} \qquad n = 0, 1, \ldots \quad . \qquad (C.3)$$

APPENDIX D

PROOF THAT THE WAVE NUMBERS IN THE x-DIRECTION IN THE "SOFTEST" LAYER OF THE MODEL WITH VERTICAL DISCONTINUITIES ARE ALWAYS REAL

Suppose that the wave number in the x-direction in the "softest" layer is imaginary for the k-th mode. Then, because of the relationship given in equation (3.3.6), the x-wave numbers in the other layers are also imaginary. The sine and the cosine functions of the form $\sin k_{x,k}^{(i)} a$ and $\cos k_{x,k}^{(i)} a$, where $i = 1, 2, 3$, and a is some length, which appear in the shape function $X_k(x)$, will change into $i \sinh |k_{x,k}^{(i)}| a$ and $\cosh |k_{x,k}^{(i)}| a$, respectively.

Substituting in the frequency equation (3.3.8) the expression for $A_k^{(3)}$ (from equation (3.3.7c)), and comparing the terms multiplying $A_k^{(2)}$ and $B_k^{(2)}$ on the left and on the right hand side of the equation, it follows that the following two equations must be simultaneously satisfied:

$$\frac{\mu_2 k_{x,k}^{(2)}}{\mu_3 k_{x,k}^{(3)}} \tanh |k_{x,k}^{(2)}|(\ell_1 + \ell_2) = \tanh |k_{x,k}^{(3)}| \ell_3 \qquad (D.1)$$

and

$$\frac{\mu_2 k_{x,k}^{(2)}}{\mu_3 k_{x,k}^{(3)}} \coth |k_{x,k}^{(2)}|(\ell_1 + \ell_2) = \tanh |k_{x,k}^{(3)}| \ell_3 \quad . \qquad (D.2)$$

Because the hyperbolic functions are not periodic, equations (D.1) and (D.2) cannot be simultaneously satisfied, and therefore the imaginary x-wave numbers for the k-th mode in the layers do not satisfy the frequency equation. This means that imaginary x-wave numbers are not allowed in the softest layer.

APPENDIX E

THE COEFFICIENTS $C_n, n = 0, 1, \ldots,$ IN THE EQUATIONS (3.2.4a,b) WHEN η IS VERY SMALL

Expanding $\sin \frac{\omega L}{c}$ and $\cos \frac{\omega L}{c}$ in Taylor's series around zero, the coefficients $C_n, n = 0, 1, \ldots,$ in the equations (3.2.14a,b) will have the following form:

$$C_o = \frac{1}{\frac{\omega L}{c}} \left[\frac{\omega L}{c} + \frac{1}{6} \left(\frac{\omega L}{c} \right)^3 + \cdots i \left(1 - \frac{1}{2} \left(\frac{\omega L}{c} \right)^2 + \cdots - 1 \right) \right] \qquad (E.1a)$$

and

$$\begin{aligned} C_n = 2 \frac{\frac{\omega L}{c}}{\left(\frac{\omega L}{c}\right)^2 - (n\pi)^2} \{ (-1)^n \left(\frac{\omega L}{c} + \frac{1}{6} \left(\frac{\omega L}{c} \right)^3 + \cdots \right) \\ + \left[(-1)^n \left(1 - \frac{1}{2} \left(\frac{\omega L}{c} \right)^2 + \cdots \right) - 1 \right] \} \quad n = 1, 2, \ldots \quad . \end{aligned} \qquad (E.1b)$$

Since $\omega L/C = 2\pi\eta$, and neglecting the terms in the above equations that are $o(\eta)$, the coefficients C_n $n = 0, 1, \ldots$ will become

$$C_o = 1 - \frac{i}{2} \frac{\omega L}{c} \qquad (E.2a)$$

and

$$C_n = \begin{cases} 0 & , n \text{ even} \\ \frac{4}{L} i \frac{\frac{\omega}{c}}{\left(\frac{n\pi}{L}\right)^2} & , n \text{ odd} \end{cases} \quad . \qquad (E.2b)$$

APPENDIX F

ANALYTICAL EXPRESSIONS FOR THE COEFFICIENTS $C_n, n = 0, 1, \ldots$, OF THE EXPANSION OF THE DISPLACEMENT AT THE BASE OF THE HOMOGENEOUS MODEL, PLACED OVER THE HALF-SPACE WITH A VERTICAL DISCONTINUITY

The displacement $f(x)$ at the base of the building, placed on the surface of the half-space with a vertical discontinuity at $x = d$, Figure 4.3.4, for an incident SH wave as in Figure 4.3.3, for the different positions of the building relative to the discontinuity, was given in equations (4.3.14), (4.3.15) and (4.3.16). The coefficients $C_n, n = 0, 1, \ldots$, of the expansion of $f(x)$ in terms of the basis $X_n(x)_{n=0}^{\infty}$, where $X_n(x)$ are the eigenfunctions in the x-direction of the homogeneous model, equation (3.2.5), were defined to be

$$C_n = \frac{(f(x), X_n(x))}{(X_n(x), X_n(x))} \quad . \tag{F.1}$$

The inner product in the above equation was defined by the equation (3.2.10). Applying this definition to the denominator of the equation (F.1) gives

$$(X_n(x), X_n(x)) = \int_0^L \cos^2 \frac{n\pi}{L} x \, dx = \frac{L}{2} \quad , \tag{F.2}$$

If the building is entirely situated on the left side of the discontinuity, i.e. $L \leq d$

$$(f(x), X_n(x)) = \int_0^L \left(A_0 e^{-i\frac{\omega}{c_L}x} + A_1 e^{i\frac{\omega}{c_L}x} \right) \cos \frac{n\pi}{L} x \, dx \quad . \tag{F.3}$$

If the building is "sitting" on the discontinuity, i.e. $L \geq d > 0$, then

$$\begin{aligned} (f(x), X_n(x)) = &\int_0^d \left(A_0 e^{-i\frac{\omega}{c_L}x} + A_1 e^{i\frac{\omega}{c_L}x} \right) \cos \frac{n\pi}{L} x \, dx + \\ &+ \int_d^L A_2 e^{-i\frac{\omega}{c_R}x} \cos \frac{n\pi}{L} x \, dx \, . \end{aligned} \tag{F.4}$$

And, if the building is entirely situated on the right side of the discontinuity, i.e. $d \leq 0$,

$$(f(x), X_n(x)) = \int_0^L A_2 e^{-i\frac{\omega}{c_R}x} \cos\frac{n\pi}{L}x \, dx \quad . \tag{F.5}$$

The integrals in equations (F.3), (F.4) and (F.5) can be evaluated analytically.